Pau Amaro Seoane

# Dynamics of dense star-gas systems
# BHs and their precursors

HEIDELBERG, 2004

Referees:

Prof. Dr. Rainer Spurzem (Th. Astroph.)
Prof. Dr. Josef Fried (Obs. Astroph.)
Prof. Dr. Matthias Bartelmann (Th. Astroph., Cosmology)
Prof. Dr. H-G Dosch (Th. Physics)

Day of oral examination:

23rd July 2004

## Clàusula de bon ús

Queda absolutament prohibida la utilització, recerca i desenvolupament, de manera directa o indirecta, de qualsevol de les aportacions científiques pròpies de l'autor que es presenten en aquesta memòria, per part de qualsevol exèrcit del món o per part de qualsevol grup armat, per a qualsevol ús militar i per a qualsevol altre ús que atempte contra els drets humans o contra el medi ambient, si no és amb el permís escrit de totes les persones del món.

## Good use right

It is strictly prohibited to use, to investigate or to develop, in a direct or indirect way, any of the scientific contributions of the author contained in this work by any army or armed group in the world, for military purposes and for any other use which is against human rights or the environment, unless a written consent of all the persons in the world is obtained.

## Zusammenfassung

Diese Thesis umfasst mehrere Aspekte theoretischer Stellardynamik in Sternhaufen, sowohl in analytischer als auch in numerischer Hinsicht. Wir versuchen, Licht auf Phänomene zu werfen, welche zur Zeit in allen Galaxietypen beobachtet werden, einschließlich AGNs und Quasare, welche zu den mächtigsten Objekten des Universums zählen. Die Wechselwirkungen zwischen einem Sternsystem und einem zentralen schwarzen Loch führen zu einer Menge interessanter Phänomene. Die von uns verwendete Methode ermöglicht eine Betrachtung leicht einsichtiger Aspekte ohne jegliches Rauschen, welches die Teilchen-Methoden mit sich bringen. Wir untersuchen die wichtigsten physikalischen Prozesse, die in der Entwicklung eines sphärischen Sternhaufens ablaufen, etwa Selbstanziehungskraft, Zwei-Körper-Relaxation etc sowie die Wechselwirkung mit einem schwarzen Loch und die Funktion des Massenspektrums. Wir beschäftigen uns jedoch nicht nur mit diesem Thema alleine, sondern auch mit einer Analyse supermassiver Sterne. Wie diese Sterne die Aktivitäten der Quasare durch Sternakkretion und Energiestrom antreiben ist eine der Fragen, die hierbei aufkommen. Wir gehen auch anderen Fragen nach, etwa jener nach der noch nicht verstandenen Entwicklung eines solchen Objektes und seiner Wechselwirkung mit dem ihn umgebendem Sternsystem. Dies ist ein Kernpunkt der Astrophysik, da diese Objekte als Vorläufer von supermassiven schwarzen Löchern betrachtet werden können.

## Abstract

This thesis embraces several aspects of theoretical stellar dynamics in clusters, both analytically and numerically. We try to elucidate the phenomena currently observed in all types of galaxies, including AGNs and quasars, some of the most powerful objects in the universe. The interactions between the stellar system and the central black hole give rise to a lot of interesting phenomena. The scheme we employ enables a study of clean-cut aspects without any noise that particle methods suffer from. We study the most important physical processes that are readily available in the evolution of a spherical cluster, like self-gravity, two-body relaxation etc, the interaction with a central black hole and the role of a mass spectrum. Not only embark we upon this subject, but we set about an analysis on super-massive stars. How these stars could power the quasar activity by star accretion and energy flows is one of the questions that arises. We undertake other questions, such as the uncertain evolution of such an object and its interaction with the surrounding stellar system. This is of crucial importance in astrophysics, for these objects could be regarded as super-massive black holes progenitors.

Antonio Amaro Pita, my father, never could see finished this work, because he passed away in November of last year. It is very difficult to write these lines, because I miss him a lot. He lived intensively, much more than all people I know. He squeezed the nice things out of life until the very last drop and then he decided to go away and carry on with the fun somewhere else because here it was damned boring for him.

When my father died, Marc Freitag, who was in the north of America, wrote:

*En Pennsylvanie c'est un automne magnifique avec des arbres qui deviennent très rouges avant de se depouiller totalement. J'imagine qu'il est normal que les grands arbres, devenus vieux, soient terassés par le vent... Cela n'enlève rien a la beauté de la forêt*.

There is death because there is life, and there is life because there is death. My father died, and so will I someday; this is not a reason to be upset, it is just the flowing of life. It steals us the surface of the sand and allows us to walk in the new surface and leave our prints. Sabine is now pregnant and I hope our child will be as full of life as his grandfather was and able to enjoy every second of his new life, just as my father did.

Iste traballo está adicado a il

# STRUCTURE OF THE THESIS

**hen he was in this plight, Ino daughter of Cadmus, also called Leucothea, saw him. She had formerly been a mere mortal, but had been since raised to the rank of a marine goddess. Seeing in what great distress Ulysses now was, she had compassion upon him, and, rising like a sea-gull from the waves, took her seat upon the raft. "My poor good man," said she, "why is Poseidon so furiously angry with you? He is giving you a great deal of trouble, but for all his bluster he will not kill you. You seem to be a sensible person, do then as I bid you; strip, leave your raft to drive before the wind, and swim to the Phaecian coast where better luck awaits you. And here, take my veil and put it round your chest; it is enchanted, and you can come to no harm so long as you wear it. As soon as you touch land take it off, throw it back as far as you can into the sea, and then go away again." With these words she took off her veil and gave it him. Then she dived down again like a sea-gull and vanished beneath the dark blue waters. But Odysseus did not know what to think. "Alas," he said to himself in his dismay, "this is only some one or other of the gods who is luring me to ruin by advising me to will quit my raft. At any rate I will not do so at present, for the land where she said I should be quit of all troubles seemed to be still a good way off. I know what I will do- I am sure it will be best- no matter what happens I will stick to the raft as long as her timbers hold together, but when the sea breaks her up I will swim for it; I do not see how I can do any better than this.**

***Odyssey, Homer (Book V)***

Odysseus clearly distrusted the benevolence of the goddess. And his resolution was quite clear: neither to accept the advice nor the favours of superhuman origin until tragedy be imminent. While the ship remained whole, he would not dare leave it... despite the clear help that (whichever) gods offered. Perhaps because Leucothea had once been mortal? This did not seem to be the reason, in my view. Odysseus, one of the first western heroes of whom we have written evidence, did not rely at all on the gods who favoured him.

Alone, wet, cold, in a feeble boat that could not guarantee him the necessary cover against the wrath of another god, in the middle of the night, battling the fearsome waves that carried him directly to the reefs, Odysseus looks at the piece of sail that the goddess gave him with which he will have to reach the cost, still far away. Perhaps because he is a hero, he arrives there where many do not. Those who, desperate, would blindly have heeded the advice of gods. He, on the contrary, proceeds *rationally*. Odysseus will not pay attention to the advice of gods until his chances be clearly doomed, until his ship disintegrates, taken by the rage of the sea, and he has nothing to lose. Then, and only then, he will abandon the chunk of wood in which he finds himself at the mercy of the storm, and he would launch himself into the water with the hope that the madness of the seagull-goddess be true.
Naturally, as the reader can guess, either because he is familiar with Homer's work or sufficiently savvy to be irrational and see it, Odysseus reaches the shore.

I read this passage a couple of years ago, when I was still studying in València. It impressed me to see that a mythological greek hero, maybe *the* mythological greek hero could think in such a rational way and only leave his last shelter when all other possibilities were ruled out. I interpreted it like a knowing wink of Homer to us, poor mortals. When I started my PhD I felt a bit like Odysseus. Only a couple of months ago I decided to trust the veil and now, safe in the cost, I resolved to include this text here.

# Chapter 1

# Motivation

## 1.1 What is this all about? First words

MASSIVE objects avoiding light to escape from it is a concept that goes back to the 18th century, when John Michell (1724 – 1793), an English natural philosopher and geologist overtook Laplace with the idea that a very massive object could be able to stop light escaping from it thanks to its overwhelming gravity. Such an object would be *black*, that is, invisible, precisely because of the lack of light (Michell, 1784; Schaffer, 1979). He wrote:

> *"If the semi-diameter of a sphere of the same density as the sun is in the proportion of five hundred to one, and by supposing light to be attracted by the same force in proportion to its mass with other bodies, all light emitted from such a body would be made to return towards it, by its own proper gravity.*"

Even thought we shall sift through this concept oftentimes in the work to be presented along the next chapters, it appears to be necessary to give an initial, short overview of the problem's subject we shall tackle in this thesis.

A "black hole"[1] embraces the observation of phenomena which are associated with matter accretion on to it, for we are not able to directly observe it. Emission of electromagnetic radiation, accretion discs and emerging jets are some, among others, evidences we have for the existence of such massive dark objects, lurking at the centre of galaxies.

On the other hand, spectroscopic and photometric studies of the stellar and gas dynamics in the inner regions of local spheroidal galaxies and prominent bulges give us the certainty that nearly all galaxies should harbour a central massive dark object, with a tight relationship between its mass and the mass or

[1] This term was first employed by John Archibald Wheeler (b. 1911), an American theoretical physicist

the velocity dispersion of the host galaxy spheroidal component (as we will see ahead). Nonetheless, even though we should mention that we do not dispose of any direct evidence that such massive dark objects are black holes, alternative explanations are sorely constrained (see, for instance, Kormendy 2003).
Super-massive black holes are ensconced at the centre of *active galaxies*. What we understand with *active* is a galaxy in which we can find an important amount of emitted energy which cannot be attributed to its "normal" components. AGNs, as they are usually denominated, have the powerhouse for their observed phenomena in a compact region in the centre.

We will embark in the next chapters on an analytical and numerical study of the dynamics of stellar systems harbouring a central massive object in order to extract the dominant physical processes and their parameter dependences like dynamical friction and mass accretion.
This chapter is devoted to a general description of the scenario with which we shall deal with. Firstly, we give a short bird's-eye view of active galactic nuclei in order to clearly exhibit the boundaries of our problem and then, secondly, we will give an extending to the present time summary on the possible nature of the central dark object and its possible origin and formation.

## 1.2 What are AGNs and what makes them interesting?

The expression "active galactic nucleus" of a galaxy (AGN henceforth) is referred to the energetic phenomena occurring at the central regions of galaxies which cannot be explained in terms of stars, dust or interstellar gas. The released energy is emitted across most of the electromagnetic spectrum, UV, X-rays, as infrared, radio waves and gamma rays. Such objects have big luminosities ($10^4$ times that of a typical galaxy) coming from tiny volumes ($\ll 1\mathrm{pc}^3$); in the case of a typical Seyfert galaxy the luminosity is about $\sim 10^{11}\, L_\odot$ ($L_\odot = 3.83 \cdot 10^{33}$ erg/s is the luminosity of the sun), whilst for a typical quasar it is brighter by a factor 100 or even more; actually they can emit as much as some thousand galaxies like our Milky-Way. They are thus the most powerful objects in the universe. There is a connexion between young galaxies and the creation of active nuclei, because this luminosity can strongly vary with the red-shift.

Anticipating something on which we will elaborate a bit ahead, nowadays one explains (although this is still not accepted ubiquitously [2]) the generation of energy resorting to matter accreting on to a super-massive black hole in the range of mass $\mathscr{M}_\bullet \sim 10^{6-10}\mathrm{M}_\odot$ (where $\mathscr{M}_\bullet$ is the black hole mass). In this process, angular momentum flattens the structure of the in-falling material to a so-called *accretion disc*. It is frequent to observe jets, which may be arising from the accretion disc (see Fig. 1.1), although we do not dispose of direct direct observations that corroborate this. Accretion is a very efficient channel

[2] For some alternative and interesting schemes, see Ginzburg and Ozernoy (1964) for spinars, Arons et al. (1975) for clusters of stellar mass BHs or neutron stars and Terlevich (1989) for *warmers*: massive stars with strong mass-loss spend a significant amount of their He-burning phase to the left of the ZAMS on the HR diagram. The ionisation spectrum of a young cluster of massive stars will be strongly influenced by extremely hot and luminous stars

of turning matter into energy. Whereas nuclear fusion reaches only a few percent, accretion can breeze in almost 50% of the mass-energy of a star into energy.

Being a bit more punctilious, we should say that hallmarks for AGNs are the frequency of their electromagnetic emission frequencies, observed from $\lesssim 100$ MHz (as low frequency radio sources) to $\gtrsim 100$ MeV (which corresponds to $\sim 2 \cdot 10^{22}$ Hz gamma ray sources). Giant jets give the upper size of manifest activity $\lesssim 6$ Mpc $\sim 2 \cdot 10^{25}$ cm [3], and the lower limit is given by the covered distance by light in the shortest X-ray variability times, which is $\sim 2 \cdot 10^{12}$ cm.

As regards the size, and resorting again to Fig. (1.1), we can envisage this as a radial distance from the very centre of the AGN where, ostensibly, a SMBH is harboured, and the different observed features of the nucleus. From the centre outwards, we have first a UV ionising source amidst the optical continuum region. This, in turn, is enclosed by the emission line clouds (NLR, BLR [4]) and the compact radio sources and these betwixt another emitting region etc.

The radiated power at a certain frequency per *dex* [5] frequency ranges from $\sim 10^{39}$ erg/s (radio power of the MW) to $\sim 10^{48}$ erg/s, the emitted UV power of the most powerful, high-redshifted quasars. Such broad frequencies and radius ranges for emission makes us to duly note that they are far out of thermal equilibrium. This manifests in two ways: first, smaller regions are hotter; second, components of utterly different temperature can exist together, even though components differ in one or two orders of magnitude in size.

### 1.2.1 Outstanding features of AGNs

We have to somehow specify what we mean with the term AGN. For this scope we should name the observable phenomena which are used to detect them; on the other hand, nevertheless, AGNs can be noticed in many ways, but this does not mean that all of them partake the same features. In fact, an AGN "picks up" some of these defining qualities to be such an object.

**Very small angular size** If we have optical images of the host galaxy, the nucleus happens to be a very bright point with a flux that can touch or even surpass the rest one of the host galaxy. In Fig. (1.2) we can see an example of this: NGC 1566, a nearby AGN (Jarrett et al., 2003).

**Radio astronomical observations** were the first proof for the existence of non-stellar activity in external galaxies. Early observations revealed that many bright radio sources have the shape of two lobes with a galaxy situated at half the distance (see Fig. 1.3). Even though radio astronomical techniques are powerful, they might be misguiding, since the radio band never accounts for more than $\sim 1\%$ of

[3] If we do not take into account the ionising radiation on intergalactic medium
[4] See subsection 1.2.2
[5] A "unit" in the logarithmic axis

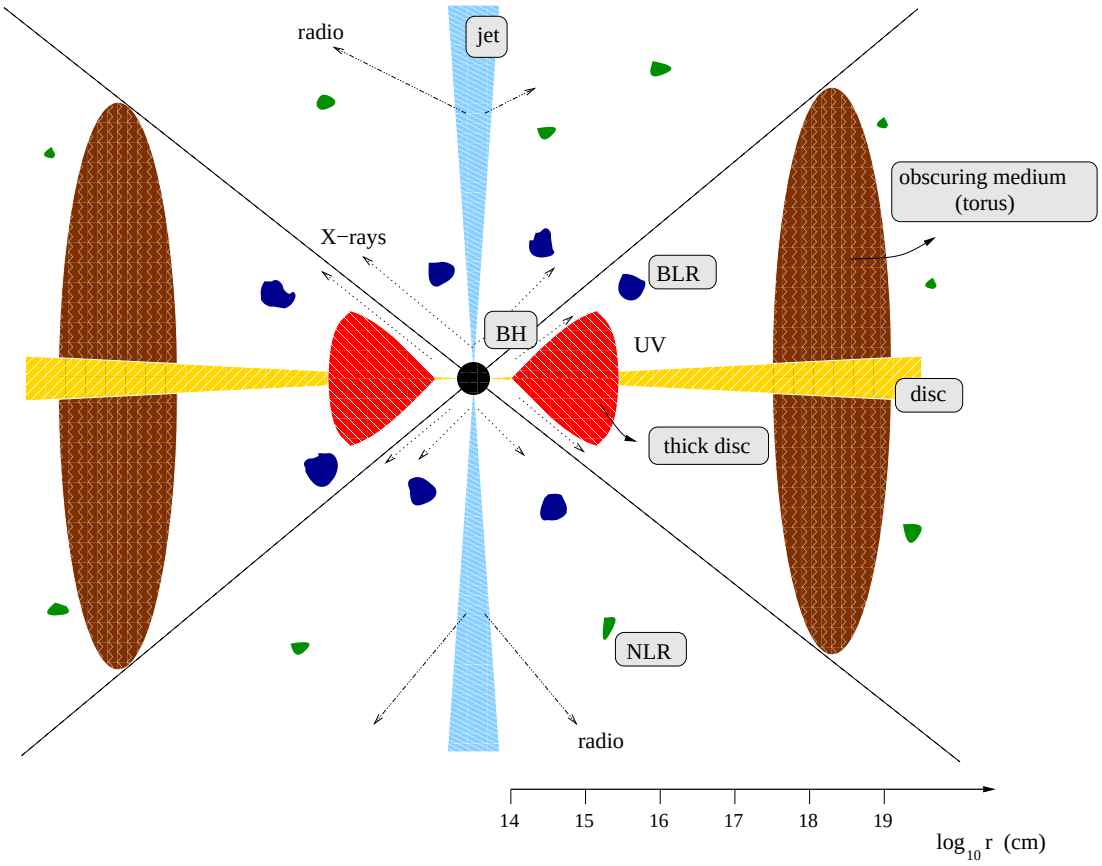


Fig. 1.1: Unified model of an AGN. A relativistic jet is only to be found in radio-loud sources. In the vicinity of the central BH we may find a flared-up disc due to X-rays.

the bolometric luminosity; to boot, less biased surveys bore witness that the most AGNs emit a much smaller portion of their total power in the radio.

**High luminosity** This can run in the case of an AGN from about 1% of a typical galaxy up to $\sim 10^4$ times as great. Of course these limits are not completely fixed, for there can be "hidden" a huge population with lower, non observable luminosities; another possible reason for the incapacity of observation is relativistic beaming, or obscuration, due to thick dust extinction, which can misguide our measurements. Compared with the galaxy spectra, an AGN continuum spectra looks stunningly different. The energy flux per logarithmic bandwidth produces a spectrum far broader compared with that of a galaxy. In comparison with a galaxy, AGNs give out in the radio band a fraction of bolometric luminosity that is about an order of magnitude greater, and the corresponding in the x-ray band is between three and four larger.

Fig. 1.2: NGC 1566 (Jarrett et al., 2003)

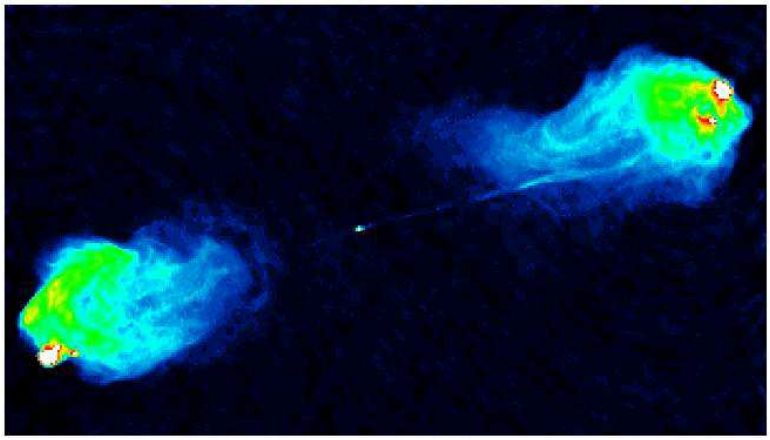

Fig. 1.3: Cygnus A at 6 cm wavelength (Perley et al., 1984). The total extent of this source is $\sim 120$ kpc

**Variability** is often said to be a distinctive characteristic of AGNs; this is relative for, even though the most of them can be seen to vary in the optical band, the typical amplitude over time-scales is frequently 10%. There is no a fixed time-scale on which AGNs vary, and therefore it is hard to measure their amplitude of variability. We can find a subgroup of these objects that can be observed to vary even from night to night, and cumulative changes of factors of hundred have happened over year time-scales. In Fig. (1.4) we can see an example of this rapid variation (Pian et al., 1997).

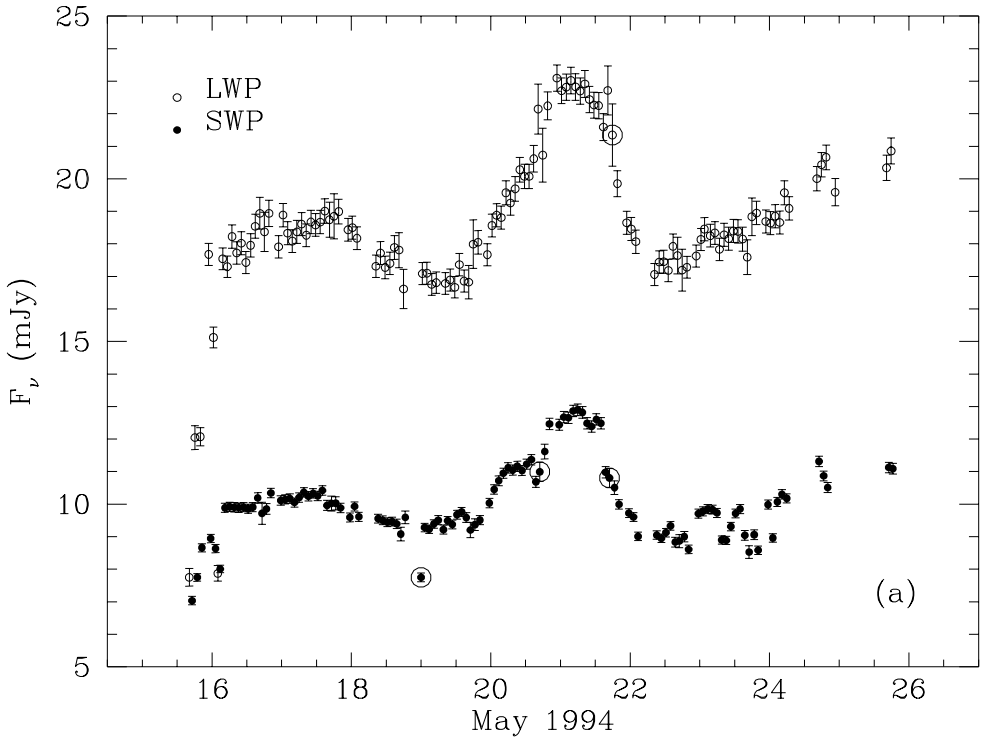


Fig. 1.4: Two ultraviolet light curves for PKS 2155-304. The open circles show the continuum flux at 2800 Å; the filled ones at 1400 Å. We can see that within one day changes of several tens of percent occurred

**Polarisation** Like in the case of galaxies, even though stars are in itself unpolarised, the light we observe is by and large polarised by about 0.5% because of interstellar dust transmission polarisation. As for the AGNs, they are also polarised, linearly and with a fractional polarisation of between 0.5-$-$ 2%. We find a minority that is much more polarised, frequently $\sim$ 10%. We have a strong variation on both the magnitude and the direction of the polarisation for those objects that are strongly polarised and have strongly variable total flux. Nonetheless, variability does have bounds, for circular polarisation has never been detected.

**Emission lines** This draws our attention, for it is easy and productive to study them. On the contrary to most of galaxies, these are very prominent for this kind of objects. The observed emission lines are stereotypic from one AGN to the other; almost at all times we observe Ly$\alpha$, the Balmer lines, the $C_{\rm IV}$ 1549 doublet etc. Oftentimes is seen the FeK$\alpha$ x-ray line near 6.4 KeV.

### 1.2.2 AGN taxonomy

To key out the sub-variety of AGNs we are talking about we have several terms. Whether or not the distinctions is beneficial is something we could call into question, but we have to know it if we want to follow "the conversation". A deep description of all AGNs nomenclatures with their typical characteristics is beyond the scope of this work. Here we just want to give a general idea of the vast variety of AGNs and main features. We have different ways of categorisation, depending on by which criteria we want to classify. Some of the terms are self-explanatory; like, for instance *radio loud* or *radio quiet*. OVV is the acronym for *Optically Violently Variable*, for in the optic band we have very rapid and large amplitude variability, as the name itself reveals. Others are coined terms; *Quasar* is simply the pronounced form of "QSR" (*Quasi-Stellar Radio source*), but after a time the meaning changed and evolved to "generic AGN"; nowadays it has nothing to do with the radio luminosity. In fact, for instance, very low luminosity AGNs are called *micro-quasars*. Some terms bring up the name of the first people that identified the class: Carl Seyfert remarked the first *Seyfert galaxies*, and they were split up later into two types, depending on the existence or not of broad wings in the emission lines. In an equal manner, Fanaroff and Riley pointed out a distinction in luminosity and morphology among the radio galaxies, and so they were named *FR galaxies* after them. We find also far-out histories in the nomenclature of AGNs: The type *BL Lac Objects* were initially identified as variable stars in the Lacerta constellation and, thus, they were named "BL Lac". The term *Blazar* springs up from the fact that the power output of the classes OVV and BL Lac "blazes" dramatically and was thought to unify them, because they are very similar.

In table 1.1 (taken from Krolik 1999) an object is said to be point-like if an optical point source can be seen. By broad-band we mean that there is a comparable luminosity in the infrared, optical and x-ray bands. The existence in the optical and ultraviolet spectra of lines several thousand (hundred) km/s in width is meant with broad-lines (narrow-lines). By radio we understand that for the object the fraction of luminosity emitted in the radio is relatively large, perhaps $\sim 10^{-3}$ of the bolometric. The members of a class should vary by an order of magnitude or more in the optical band over a human time life for the variable entrance and for polarisation the optical light should be at least a few percent linearly polarised. In the table we have added the subdivision *LINERs*, which stands for "Low-Ionisation Nuclear Emission Region" (Heckman, 1980), but this category is on the verge of activity; it is not clear whether or not these galaxies are really active.

This classification allows us to arrange the types in a three-dimensional parameter space, since we find that we have the groups radio-loud against radio-quiet, strong variable against all the others and narrow emission lines against broad emission lines. We can display a three-parameter space in which we locate each of the types of AGNs (after Krolik 1999), as we can see in Fig. (1.5).

### 1.2.3 The unified model

After a study of almost 20 years, as we commented at the beginning of this chapter, a unification scheme for AGNs has appeared in the community. According to it, a well-mannered AGN should have the following identifying characteristics (see Fig 1.1),

| Type | Point-like | Broad-band | Broad lines | Narrow lines | Radio | Variable | Polarised |
|---|---|---|---|---|---|---|---|
| Radio-loud quasars | yes | yes | yes | yes | yes | some | some |
| Radio-quiet quasars | yes | yes | yes | yes | weak | weak | weak |
| Broad line radio galaxies (FR2 only) | yes | yes | yes | yes | yes | weak | weak |
| Narrow line radio galaxies (FR1 and FR2) | no | no | no | yes | yes | no | no |
| OVV quasars | yes | yes | yes | yes | yes | yes | yes |
| BL Lac objects | yes | yes | no | no | yes | yes | yes |
| Seyferts type 1 | yes | yes | yes | yes | weak | some | weak |
| Seyferts type 2 | no | yes | no | yes | weak | no | some |
| LINERs | no | no | no | yes | no | no | no |

Table 1.1: The AGN taxonomy

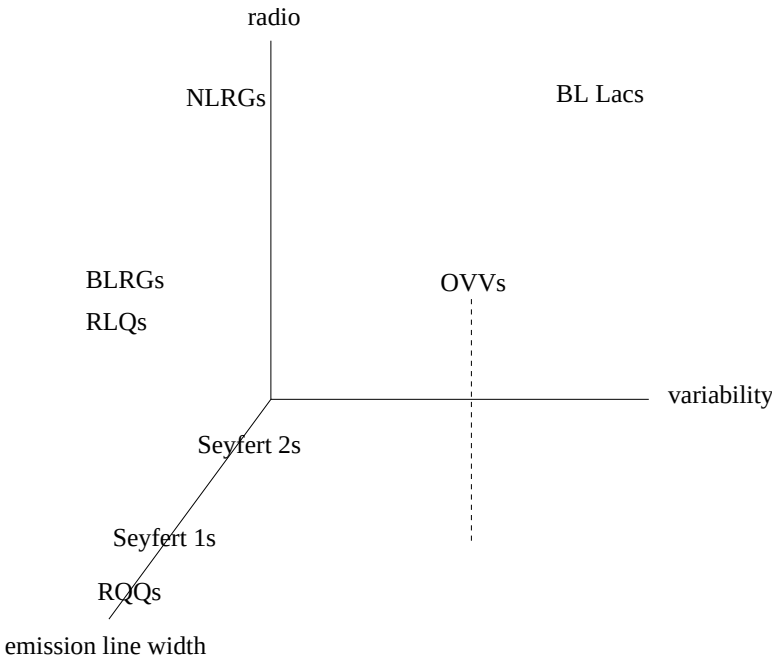


Fig. 1.5: Classification of AGNs in a three-dimensional parameter space

**Super-massive black hole** – in the range of $10^{6-10}\,M_{\odot}$

**Accretion disc and corona** – heated by magnetic and/ or viscous processes with optical radiation though soft X-ray energy

**Broad line region** – with high velocity gas

**Narrow line region** – corresponding to lower velocity gas

**Obscuring medium** – which can adopt a torus form or another geometry. This has the characteristic, as its names pinpoints, of hiding the broad-line region from some directions owing to its material (dust). It is located at about 10 – 100 pc between the smaller inner region from which the broad emission lines come from and the more external zone where the narrow emission lines emerge

**Relativistic jet** – emerging at distances of about $\sim 100\,\mathscr{R}_{\rm Schw}$ (Schwarzschild radius) of the BH. The extension of these objects can be out to tens of hundreds of parsecs or even Mpc

Excluding intrinsic variances in BH's differentia, like $\mathscr{M}_{\bullet}$, ionisation parameter, size, density, luminosity etc, the unification model properties (except for, maybe, relativistic jets) stay staunch to all AGNs. In conformity with it, many of the main observational characteristics that we have described before are due to orientation and are not intrinsic differences. The galaxy appears as a Seyfert 2 or NLRG at the regions where the obscuring medium stops the direct view of the central parts. Facing the AGN, as we look into the inner regions and it appears as Seyfert 1s or, in radio-loud, BLRGs to radio-loud quasars and at inferior luminosities, BL Lacs.

### 1.2.4 Appraising $\mathscr{M}_\bullet$

A direct consequence of the paradigm of SMBHs at the centre of ancient galaxies to explain the energy emitted by quasars is that relic SMBHs should inhabit at least a fraction of present-day galaxies (Rees, 1990). This conclusion was first made quantitative by Sołtan (1982) and has recently be revisited in more detail and in the light of recent observations by Yu and Tremaine (2002).
In a system of luminosity $L$ with a lifetime $T_{\rm lum}$, if $\varepsilon$ is the conversion of matter to energy (accretion) efficiency, one should expect that in the system, an amount of material $LT_{\rm lum}/\varepsilon c^2$ has been gathered at some place, where c is the light velocity. We are referring to the central super-massive black hole, harboured by the host galaxy. We will give a description of such an object in the next section and pore over it in the next chapters.
If we are capable of determining $T_{\rm lum}$ and $\varepsilon$, we will have a rough idea of what $\mathscr{M}$ is. Usually, for $\varepsilon$ one can prove that $\varepsilon \sim 1/10$ is a suitable value (McCray, 1979). Assuming that the lobes are powered by the central engine, we have that, for Cyg A, with a lobe separation of 80 kpc, $T_{\rm lum} \sim 4 \cdot 10^7$ yr and, so, $\mathscr{M}_\bullet \sim 10^8 {\rm M}_\odot$. If we do not have at our disposal double radio sources, we can reckon in a different way: if the lifetime of the galaxy is $\sim 10^{10}$ yr and 1% of galaxies are active and they all go through activity phases, $T_{\rm lum} \sim 10^8$ yr; this means that, for the more luminous sources ($L \geq 10^{47}$ erg/s), $\mathscr{M}_\bullet \sim 10^{10} {\rm M}_\odot$. On the other hand, if we had resorted to the luminosity per unit volume from quasars from observations, we would have found out that, since this gives the energy output per unit volume over the age of the universe, the mass density of "recycled" material is consistent with an average dead mass of $10^8 {\rm M}_\odot$. A number of independent deductions leads to a similar result (Frank et al., 2002).

## 1.3 Massive black holes and their possible progenitors

### 1.3.1 (Super-) massive black holes

The quest for the source of the luminosities of $L \approx 10^{12} {\rm L}_\odot$ produced on such small scales, jets and other properties of quasars and other types of active galactic nuclei led in the 60's and 70's to a thorough research that hint to the inkling of "super-massive central objects" harboured at their centres. These were suggested to be the main source of such characteristics (Lynden-Bell, 1967; Lynden-Bell and Rees, 1971a; Hills, 1975). Lynden-Bell (1969) showed that the release of gravitational binding energy by stellar accretion on to a SMBH could be the primary powerhouse of an AGN (Lynden-Bell, 1969).
In the last decade, observational evidences have been accumulating that strongly suggest that massive BHs are indeed present at the centre of most galaxies, with a significant spheroidal component. Mostly thanks to the *HST*, the kinematics in present-day universe of gas or stars has been measured in the central parts of tens of nearby galaxies. In almost all cases [6], proper modelling of the measured motions requires the presence of a central compact dark object with a mass of a few $10^6$ to $10^9 {\rm M}_\odot$ (Ferrarese et al., 2001; Gebhardt et al., 2002; Pinkney et al., 2003; Kormendy, 2003, and references therein). Note, however, that the conclusion that such an object is indeed a BH rather than a cluster of smaller dark objects (like

[6] With, notably, the possible exception of M33 (Gebhardt et al., 2001; Merritt et al., 2001)

neutron stars, brown dwarves etc) has only been reached for two galaxies. The first one is the Milky Way itself at the centre of which the case for a 3–4 $\times 10^6 M_\odot$ MBH has been clinched, mostly through ground-based IR observations of the fast orbital motions of a few stars (Ghez et al., 2003; Schödel et al., 2003). The second case is NGC4258, which passes a central Keplerian gaseous disc with $H_2O$ MASER strong sources allowing high resolution VLBI observations down to 0.16 pc of the centre (Miyoshi et al., 1995; Herrnstein et al., 1999; Moran et al., 1999).

In any case, it is nowadays largely accepted that the central dark object required to explain kinematics data in local active and non-active galaxies is an MBH. The large number of galaxies surveyed has allowed to study the demographics of the MBHs and, in particular, look for correlations with properties of the host galaxy. The most remarkable ones are the fact that the MBH has a mass which is roughly about 0.1% of the stellar mass of the spheroidal component of the galaxy and that the mass of the BH, $\mathscr{M}_\bullet$, correlates even more tightly with the velocity of this component. These facts certainly strike a close link between the formation of the galaxy and the massive object harboured at its centre.

Of particular importance are the following channels for interactions between stars and the DCO (assumed to be a MBH).

The centre-most part of a galaxy, its *nucleus* consist of a cluster of a few $10^7$ to a few $10^8$ stars surrounding the DCO, with a size of a few pc. The nucleus is naturally expected to play a major role in the interaction between the DCO and the host galaxy. In the nucleus, stellar densities in excess of $10^6\,\mathrm{pc}^{-3}$ and relative velocities of order a few 100 to a few $1000\,\mathrm{km\,s}^{-1}$ are reached. In these exceptional conditions and unlike anywhere else in the bulk of the galaxy, collisional effects come into play. These include 2-body relaxation, i.e. mutual gravitational deflections, and genuine contact collisions between stars.

Stars can produce gas to be accreted on to the MBH, through normal stellar evolution, collisions or disruptions of stars by the strong central tidal field. When the massive central object acts on the gravity of a body, a star, the *tidal forces* set in and the difference of gravitational forces can prodigally vary between the diametrically separated points of the star. The result is that the star will be altered in its shape, from its initial approximately spherical architecture to an ellipsoidal one, splitted into two lobes, since the volume remains the same. In the end, as tidal forces increase, the star will be *tidally disrupted*. See section 4.13. In Fig. (1.6) we give an intuitive image of this scenario, where distortions due to gravitational-lens have not been taken into consideration. In Fig. (1.7), on the left we show a Chandra x-ray image of J1242-11 with a scale of 40 arcsec on a side. This Fig. pinpoints one of the most extreme variability events ever detected in a galaxy. One plausible explanation for the extreme brightness of the ROSAT source could be accretion of stars on to a super-massive black hole. On the right we have its optical companion piece, obtained with the 1.5 m Danish telescope at ESO/La Silla. The right circle indicates the position of the Chandra source in the centre of the brighter galaxy.

These processes may contribute significantly to the mass of the MBH (Murphy et al., 1991; Freitag and Benz, 2002). Tidal disruptions trigger phases of bright accretion that may reveal the presence of a MBH in an otherwise quiescent, possibly very distant, galaxy (Hills, 1975; Gezari et al., 2003).

On the other hand, stars can be swallowed whole if they are kicked directly through the horizon or are captured by emission of gravitational waves (GWs). The later process is one of the main targets of the

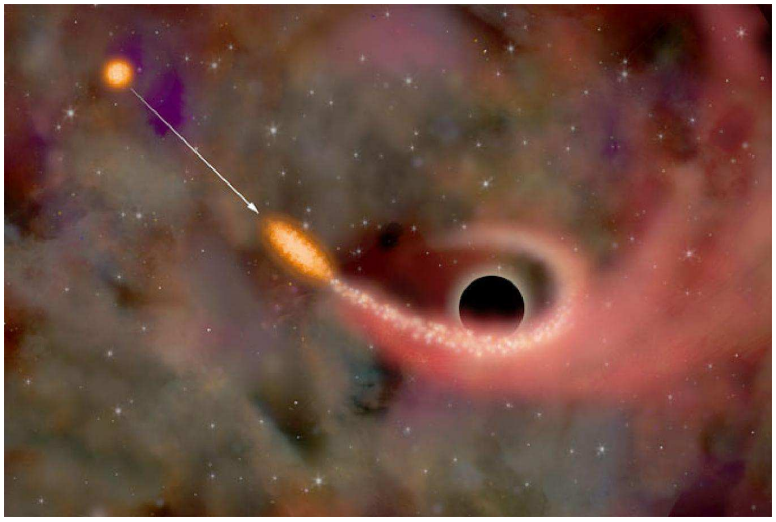

Fig. 1.6: Schematic representation of the tidal disruption process. As the star approaches the central BH, tidal forces act on it and tear it apart. Illustration credit M. Weiss

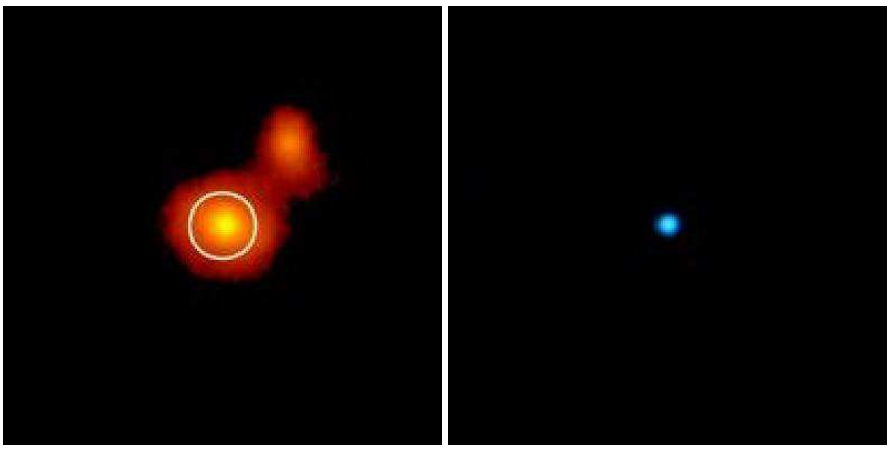

Fig. 1.7: Optical and x-ray images of RX J1242-11. Credits: ESO/MPE/S.Komossa (left) and NASA/CXC/MPE/S.Komossa et al.(right)

future space-borne GW antenna, LISA (Laser Interferometer Space Antenna).

For a spherical nucleus in dynamical equilibrium, only collisional effects can bring stars on to the "loss-cone", i.e. the very elongated orbits which allow close interaction between a star and the DCO (Amaro-Seoane and Spurzem, 2001).

So far, galactic nuclei have been modelled as isolated spherical clusters (i.e. Murphy et al. (1991);

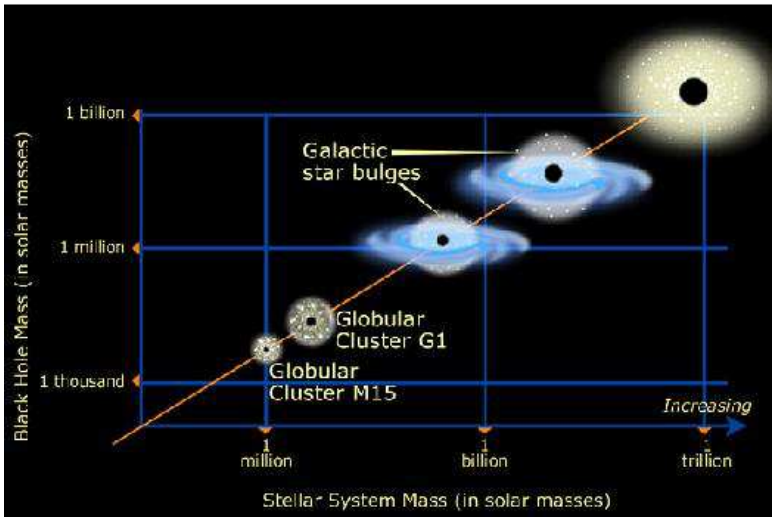


Fig. 1.8: Extension of galactic correlations to smaller systems

Freitag and Benz (2002)). However, non-spherical structures such as triaxial bulges, bars or stellar discs are common on scales of 100-1000 pc, and also the nucleus itself may be non-spherical. E.g. it could be rotating, as a result of a merger with another nucleus (Milosavljević and Merrit, 2001) or due to dissipative interactions between the stars and a dense accretion disc (Rauch, 1995). The influence of non-sphericity at small and intermediate scales on the structure and evolution of the nucleus has been little explored but it could boost the estimates of capture and disruption rates by orders of magnitudes Merritt and Poon, M. Y. (2003).

### 1.3.2 Intermediate mass black holes

If one extends the relations we mentioned above to smaller stellar systems, one could expect that globular clusters host so-called *intermediate-mass black holes*, i.e. BHs whose mass is in the range of $10^2$–$10^4 M_\odot$ (see, for illustration, Fig. 1.8).
After having been suggested in the 70's to explain the x-ray sources observed in globular clusters, later discovered to be stellar-mass binaries, this possibility has recently be revived by two lines of observations. First IMBHs may explain the ultra-luminous x-ray sources (ULXs) that are present in regions of strong stellar formation in interacting galaxies and hence suggesting a link with young "super stellar clusters" (SSC), although ULXs are typically not found at the centre of luminous SSCs. On IMBHs and their possible link to ULXs, see the review by Miller and Colbert (2003). Second, recent *HST* observations of the stellar kinematics at the centre of M15 around the Milky Way and G1 around M31 have been interpreted as indications of the presence of an IMBH in both clusters (van der Marel et al., 2002; Gerssen et al., 2002, 2003; Gebhardt et al., 2002). However, in the case of M15, the mass

of the point masses required by the observations is compatible with zero and *N*–body models have been made of both clusters that lack a central IMBH but are compatible with the observations (Baumgardt et al., 2003a,b) . We note that scenarios have been proposed that would quite naturally explain the formation of an IMBH at the centre of a stellar cluster, through run-away stellar collisions, provided that the relaxation time is short enough and that very massive stars ($10^2 M_\odot < M_\star < 10^4 M_\odot$) evolve into IMBH (Ebisuzaki et al., 2001; Portegies Zwart and McMillan, 2002; Rasio et al., 2003).
The theoretical study of the structure and evolution of a stellar cluster (galactic nucleus or globular cluster) harbouring a central MBH started 30 years ago. However, due to the complex nature of the problem which includes many physical processes and span a huge range of time and length scales, our understanding of such systems is still incomplete and, probably, subjected to revision. As in many fields of astrophysics, analytical computations can only been applied to highly idealised situations and only a very limited variety of numerical methods have been developed so far that can tackle this problem.

## 1.4 Super-massive stars: Possible SMBHs progenitors?

Since it became clear relatively early that most super-massive black holes cannot be formed fast enough from stellar mass seed black holes in nuclei (Duncan and Shapiro 1982, 1983, but see also Lee 1995 for a somewhat differing view), they must have been formed during the galaxy formation process directly, which is linked to cosmological boundary conditions. Rees (1984) argued that galactic nuclei in their formation process inevitably produce a dense core consisting of a star-gas system or a cluster of compact stellar evolution remnants, both ultimately collapsing to a super-massive black hole.
The concept of central super-massive stars (*SMS*s henceforth) ($\mathscr{M} \geq 5 \times 10^4 M_\odot$) [7] embedded in dense stellar systems was suggested as a possible explanation for high- energy emissions phenomena occurring in AGN and quasars (Hara, 1978; Vil'Koviskii, 1978), such as X-ray emissions (Bahcall and Ostriker, 1975). *SMS*s and super-massive black holes (SMBHs) are two possibilities to explain the nature of these SMOs, and the super-massive stars may be an intermediate step towards the formation of these (Rees, 1984): Stoner and Ptak (1984) argued that a $10^6 M_\odot$ central gas cloud may be a possible source of energy emission of some Seyfert galaxies. For a more up-to-date documentation on the formation of such an *SMS* see Quinlan and Shapiro (1990) (and references therein). On the other hand, such a system is interesting not just because it generalises the BH accretion problem to a massive central gas cloud, but also because such clouds can be the massive BH progenitors or a possible stock-point to the gas being piled up at the centres of GN. Nowadays we know that post-Newtonian instabilities make the lifetime of the star lay in the range $10^5 - 10^6$ yr (Fuller et al., 1986). On the other hand, the active phenomena related to QSOs and giant radio sources have a lifetime of about $\sim 10^8$ yr. This limit caused the idea that accretion on super-massive BH could be the engine of these phenomena (Hills, 1975; Lynden-Bell, 1969; Salpeter, 1964; Lynden-Bell and Rees, 1971b).

[7] Very massive stars are usually defined in the related literature to be stars so massive that at some point they collapse on an electron-positron pair instability; according to Bond et al. (1984); Woosley and Weaver (1982); Zeldovich and Novikov (1971), this is the situation of a star whose mass is larger than $\sim 100 M_\odot$ but less than $5 \times 10^4 M_\odot$. Stars even more massive will collapse on the general relativistic gravitational instability before they start burning H (Chandrasekhar, 1964; Hoyle and Fowler, 1963); here we denominate such objects after them as *super-massive stars*, *SMS*s.

Finally, the stability of compact dense star clusters was examined (Zel'Dovich and Podurets, 1966; Quinlan and Shapiro, 1990). All these papers as a common feature conclude that, provided the central object, star cluster, *SMS* or a mixture of both, becomes smaller than a certain critical radius, it is able to undergo catastrophic collapse in a dynamical time scale due to an instability caused by Post-Newtonian relativistic corrections of hydrostatic equilibrium. The question, however, whether and how that final unstable state can be reached, is much less clear. Angular momentum of the protogalaxy or its dark matter halo, self-enrichment during the dissipative collapse providing opacity through lines which prevents collapse as compared to radiation driven expansion, and star-gas interactions heating the central massive gas object could all at least for some time prevent the ultimate collapse. Given the complex physical nature of the interstellar matter, star formation, and stellar interactions alone this is a complicated question and the conditions under which a super-massive object can form in a spherical, isolated star-forming and collapsing gas cloud, rotating or not, has to our knowledge never been exhaustively studied and answered. Some pioneering approaches were however done by Spitzer and Saslaw (1966); Spitzer and Stone (1967); Colgate (1967); Langbein et al. (1990); Quinlan and Shapiro (1987); Sanders (1970). The question has gained even more complexity, since we now know that the baryonic matter of galaxies collapses in their dominating dark halo, and that most galaxies and their dark haloes experience merging with other dark haloes and large and small galaxies during the hierarchical gravitational structure formation (Diaferio et al., 1999; Kauffmann et al., 1999a,b).

The general idea of how these *SMS*s have formed is that of massive clusters collapse and coalescence nearby the galactic centre. According to Begelman and Rees (1978), a dense cluster of $1M_{\odot}$ main sequence stars forms a cloud of about $10^5 - 10^6 M_{\odot}$. When the post-Newtonian instability occurs we can have either a nuclear explosion, a collapse to BH, fragmentation or a collapse to a BH "seed". (Rees, 1984) studies the possible runaway evolution for active GN and includes a scheme in which the *SMS* formation and fate are given (see Fig. 1.9). Fuller et al. (1986) find for their *SMS*s sample that the collapse, bounce, expansion and/or explosion are homologous. They attribute this to the fact that the adiabatic index is so close to $4/3$ (and the polytropic index $n = 3$). Goldreich and Weber (1980) claim that such a configuration is scale invariant and that it is essentially right at the Jeans mass so that collapse or expansion will remain self-similar.

This has led to another type of study of black hole statistics. As we explained in the last section, the black hole masses are well correlated with the bulge masses of their mother galaxies. As a matter of fact, these correlations support the idea that black hole formation is linked to galaxy formation.

The detailed physics and parameters describing how these processes work in a self-consistent model of black hole formation, however, are much less understood. This means that we, poor mortals, lack any idea of what are the signatures of the black hole formation process in the morphology and kinematics of the innermost core and cusp regions, and to what extent they survive the merging history. Brave attempts to advance modelling in that domain (Rauch, 1999) demonstrate in our view more the problems which still prevail originating from the large dynamical range of the problem and the complexity of the treatment of relaxation in a stellar system, rather than that they provide much reliable new insight.

Galaxy merging poses another serious problem due to the possibility that it can lead to two or more black holes in one nucleus, and the structure and kinematics is critically dependent on the evolution and

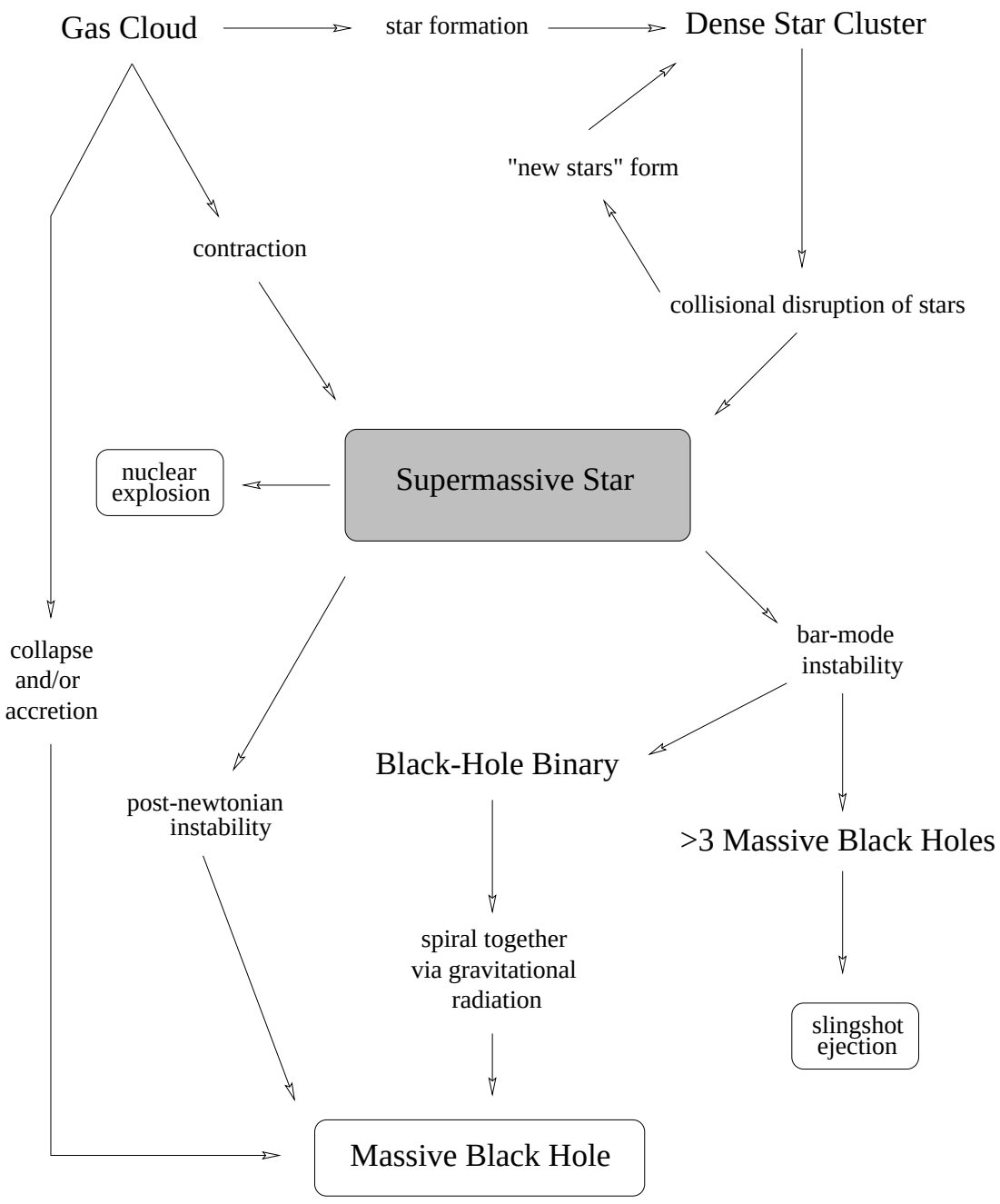


Fig. 1.9: Schematic diagram for the *SMS* formation and fate (source Rees 1984)

possible gravitational radiation merger of the resulting black hole binary. The most direct approach to study the dynamical evolution of a system containing a large number of stars is the so-called "direct" $N$-body methods in which the trajectories of $N$ particles are explicitly integrated by computing all $N(N-1)/2$ forces at each time step. With present-day hardware and software, one is limited to $N$ considerably smaller than $10^6$ and rescaling the results to larger number of stars ($10^7 - 10^8$ for a galactic nucleus) presents intractable difficulties as soon as many different physical processes are at play (relaxation, collision, interaction with the central MBH).
This is the only available possibility here using special GRAPE supercomputers (Makino, 1997; Makino and Ebisuzaki, 1996). The use of a GRAPE computer for such simulations is particularly well suited because, as a built-in feature, the list of the 50 closest neighbours is returned for each particle, which permits an easy local density estimation Burkert (2000).
The principle behind GRAPE systems is to hardwire on a special purpose chip the most time consuming part of an $N$-body simulation : the calculation of the accelerations between the particles. The remainder is calculated on a normal computer which serves as host to the accelerator board(s) containing the special purpose chips. The history of the GRAPE project (short for GRAvity PipE) is detailed in a book by Makino and Taiji (1998), and more information is available on the GRAPE project website [8] at the University of Tokyo.
Another possibility are general purpose supercomputers, or a suitable hybrid method between direct and approximate $N$-body codes (Hemsendorf et al., 2001). From these models it is yet unclear how fast in the real system dynamical friction, stochastic three-body interactions and external perturbations work together to produce eventually a single black hole again.
On the other hand, due to the ever increasing observational capabilities with ground and space based telescopes we get more and more detailed dynamical and photometric data of the structure of stellar systems around black holes. Therefore, we find it worthwhile to reconsider with present day numerical possibilities and increased knowledge about galaxy formation and evolution a detailed study of the evolution of dense star clusters, with gas, forming an *SMS* and its further evolution.
Furthermore, independently on the importance of the role of an *SMS* in the process of formation of SMBHs, these objects have recently drawn the general attention, for they could be good candidates for detection by proposed space-based gravitational wave detectors like LISA (the Laser Interferometer Space Antenna). LISA would be very sensitive to long wavelengths and low frequency radiation. Thus, *SMS*s are among the most probable sources (see, for instance Thorne 1995).

## 1.5 Time-scales

We introduce in this subsection some useful time-scales to which we will refer often throughout this thesis; namely *the crossing time*, *the relaxation time* and *the dynamical time*. These three time-scales allow us to delimit our physical system.

[8] `http://grape.c.u-tokyo.ac.jp/grape`

### 1.5.1 The relaxation time

Chandrasekhar (1942) defined a time-scale which stems from the 2-body small-angle encounters and gives us a typical time for the evolution of a stellar system.
This relaxation time could be regarded as an analogy of the shock time of the gas dynamics theory, by telling us when a particle (a star) has forgotten its initial conditions or, expressed in another way, when the local thermodynamical equilibrium has been reached. Then we can roughly say that the most general idea is that this is the time over which the star "forgets" its initial orbit due to the series of gravitational tugs caused by the passing-by stars. After a relaxation time the system has lost all information about the initial orbits of all the stars. This means that the encounters alter the star orbit from that one it would have followed if the distribution of matter were smooth. Therewith can we regard *the relaxation time* as the time interval required for the velocity distribution to reach the Maxwell-Boltzmann form.
In galactic nuclei the relaxation time is (Chandrasekhar, 1942; Larson, 1970),

$$t_{\rm relax} = \frac{9}{16\sqrt{\pi}} \frac{\sigma^3}{G^2 m \rho \ln(\gamma N)}. \tag{1.1}$$

In this expression $G$ is the gravitational constant, $\rho$ the mean stellar mass density, $\sigma$ the local 1D velocity dispersion, $N = \frac{4}{3}\pi n_c r_c^3$ the total particle number and $\gamma$ a parameter of order unity whose exact value cannot be defined easily and depends on the initial model and the anisotropy. We will elaborate on this in the next chapters.

### 1.5.2 The crossing time

As the name suggests, this is the required time for a star to pass through the system, to *cross* it. Obviously, its value is given by the ratio between space and velocity,

$$t_{\rm cross} = \frac{R}{v}, \tag{1.2}$$

where $R$ is the radius of the physical system and $v$ the velocity of the star crossing it.
For instance, in a star cluster it would be:

$$t_{\rm cross} = \frac{r_{\rm h}}{\sigma_{\rm h}}; \tag{1.3}$$

where $r_{\rm h}$ is the radius containing 50 % of the total mass and $\sigma_{\rm h}$ is a typical velocity taken at $r_{\rm h}$. One denominates it *velocity dispersion* and is introduced by the statistical concept of root mean square (RMS) dispersion; the *variance* $\sigma^2$ gives us a measure for the dispersion, or scatter, of the measurements within the statistical population, which in our case is the star sample,

$$\sigma^2 = \frac{1}{N}\sum_{i=1}^{N}(x_i - \mu_a)^2.$$


Fig. 1.10: Definition of the collision time

Where $x_i$ are the individual stellar velocities and $\mu_a$ is the arithmetic mean,

$$\mu_a \equiv \frac{1}{N}\sum_{i=1}^{N} x_i.$$

If Virial equilibrium prevails, we have $\sigma_\mathrm{h} \approx \sqrt{GM_\mathrm{h}/r_\mathrm{h}}$, then we get the dynamical time-scale

$$t_\mathrm{dyn} \approx \sqrt{\frac{r_\mathrm{h}^3}{GM_\mathrm{h}}} \approx \frac{1}{\sqrt{G\rho_\star}}, \tag{1.4}$$

where $\rho_\star$ is the mean stellar density.
On the contrary to the gas dynamics, the thermodynamical equilibrium time-scale $t_\mathrm{relax}$ in a stellar system is large compared with the crossing time $t_\mathrm{cross}$. In a homogeneous, infinite stellar system, we expect in the limit $t \to \infty$ some kind of stationary state to be established. The decisive feature for such a Virial equilibrium is how quick a perturbation of the system will be smoothed down.
The dynamical time in Virial equilibrium is (cf e.g. Spitzer, 1987):

$$t_\mathrm{dyn} \propto \frac{\log(\gamma N)}{N} \cdot t_\mathrm{relax} \ll t_\mathrm{relax}. \tag{1.5}$$

If we have perturbations in the system because of the heat conduction, star accretion on the BH, etc. a new Virial equilibrium will be established within a $t_\mathrm{dyn}$, which is short. This means that we get again a Virial-type equilibrium in a short time. This situation can be considered not far from a Virial-type equilibrium. We say that the system *changes in a quasi-stationary way*.

### 1.5.3 Collision time

$t_\mathrm{coll}$ is defined as the mean time which has passed when the number of stars within a volume $V = \Sigma \cdot v_\mathrm{rel} \cdot \triangle t$ is one (see Fig. 1.10), where $v_\mathrm{rel}$ is the relative velocity at infinity of two colliding stars.

Computed for an average distance of closest approach $\bar{r}_{\rm min} = \frac{2}{3} r_\star$, this time is

$$n_\star V(t_{\rm coll}) = 1 = n_\star \Sigma v_{\rm rel}\, t_{\rm coll}. \tag{1.6}$$

And so,

$$t_{\rm coll} = \frac{m_\star}{\rho_\star \Sigma \sigma_{\rm rel}}, \tag{1.7}$$

with

$$\Sigma = \pi \bar{r}^2_{\rm min}\left(1 + \frac{2Gm_\star}{\bar{r}_{\rm min}\sigma^2_{\rm rel}}\right); \tag{1.8}$$

$\sigma^2_{\rm rel} = 2\sigma^2_\star$ is the stellar velocity dispersion and $\Sigma$ a collisional cross section with gravitational focusing

## 1.6 Intention of this thesis

This work comprises several aspects of theoretical stellar dynamics in clusters, whether globular clusters or galactic nuclei, both analytically and numerically. The relevance of computer simulations in current astrophysics is well-known and clear, for it is the only way we have to establish (at least in tendency) what we should expect from an analytic point of view. Also, questions for which we are not able to develop an exact mathematical model are tackled thanks to these methods. Astronomy is a science that, at the beginning, was purely observational. We have rarely the chance to access direct measurements of what we would like to analyse. In our discipline, creating models that enable us to evaluate the physical system exposed to study -although in a way that is more or less idealised according to the method to which we resort- is crucial. The work presented here is consecrated to two different aspects that involve massive black holes in globular clusters and galactic nuclei.

As we have seen, the formation of most super-massive black holes (SMBHs) cannot be explained from accretion of stars on to seed black holes in nuclei, since the process is unlikely to be fast enough. It has been argued that galactic nuclei in their formation process produce a dense core consisting of a star-gas system or a cluster of compact stellar remnants. In both cases the system may ultimately collapse to a SMBH. Dense super-massive star-gas composite objects have been regarded as a transient progenitor of a SMBH. Provided that the central object (a star cluster, *SMS* or a mixture of both) becomes smaller than a certain critical radius, it will collapse in a dynamical time scale due to an instability caused by Post-Newtonian relativistic corrections of hydrostatic equilibrium. However, it is not clear at all whether and how this final unstable state can be reached. Due to the complex physical nature of the interstellar matter, star formation and stellar interactions, this is a rather complicated question. The conditions under which a supermassive object can form in a spherical, isolated, star-forming and collapsing gas cloud -rotating or not- has never been exhaustively studied. In parallel with my work on stellar clusters containing an SMBH, together with an intense analytical study and description of such an *SMS* (**chapter 3**), I worked on its numerical implementation into the anisotropic model. For that aim, I take into account the transfer of radiation in a spherically symmetric moving medium allowing for the contributions which are of the order of the flow velocity divided by the velocity of light, the thermal energy equation and the

turbulent energy equation. The interaction between stars (collisions) and star gas (drag force between stars and gas, loss-cone etc) and post-Newtonian corrections are also considered. How these *SMS*s could power the quasar activity by star accretion and energy flows is one of the main questions that could be answered thanks to this method that is in a very advanced state of development, even though not yet fully implemented into the numerical program. Here we give an exhaustive analytical description of such a physical configuration in **chapter 2**. I have made also a semi-analytical study of the influence of accretion of stars on to an *SMS* harboured at the centre of the galactic nucleus (see **chapter 4**).
For the analysis of star clusters with a central BH, I employed an anisotropic model that solves numerically moment equations of the full Fokker-Planck equation with Boltzmann-Vlasov terms on the left- and interaction (collisional) terms on the right-hand side of the equations. The cluster is modelled like a self-gravitating, conducting gas sphere. In this method, all quantities of interest are accessible as smooth functions of the radius and time. In **chapter 2** there is a detailed description of the approach.
This enables a detailed study of clean-cut aspects of the dynamics without any noise that particle methods suffer from. This model allows us to study the most important physical processes that are present in the evolution of a spherical cluster, like self-gravity, two-body relaxation, stellar evolution, collisions, binary stars etc and, undoubtedly, the interaction with a central BH and the role of a mass spectrum. I have performed calculations to follow the joint evolution of a spherical star cluster with a central BH making feasible anisotropy in order to check for the reliability of the method. I include here the study of the growth of the central BH due to star accretion at its tidal disruption radius thanks to a diffusion model to treat loss-cone physics. The core collapse is studied in detail in a self-consistent manner, as well as the post-collapse evolution of the surrounding stellar cluster. The results are in good agreement with classical literature about this subject (**chapter 5**). The current new version of the program enables the analysis of the effects of an a (discretised) stellar mass spectrum and stellar evolution. Using it, I present also more realistic models of dense clusters and give a description of mass segregation in these systems with and without a central BH (**chapter 6**).

## 1.7 Literature of chapter 1


Amaro-Seoane, P. and Spurzem, R. (2001). The loss-cone problem in dense nuclei. *MNRAS*, 327:995–1003.

Arons, J., Kulsrud, R. M., and Ostriker, J. P. (1975). A multiple pulsar model for quasi-stellar objects and active galactic nuclei. *apj*, 198:687–705.

Bahcall, J. N. and Ostriker, J. P. (1975). Massive black holes in globular clusters. *nat*, 256:23.

Baumgardt, H., Hut, P., Makino, J., McMillan, S., and Portegies Zwart, S. (2003a). On the Central Structure of M15. *ApJ Lett.*, 582:L21–L24.

Baumgardt, H., Makino, J., Hut, P., McMillan, S., and Portegies Zwart, S. (2003b). A Dynamical Model for the Globular Cluster G1. *ApJ Lett.*, 589:L25–L28.

Begelman, M. C. and Rees, M. J. (1978). The fate of dense stellar systems. *MNRAS*, 185:847–860.

Bond, J. R., Arnett, W. D., and Carr, B. J. (1984). The evolution and fate of Very Massive Objects. *apj*, 280:825–847.

Burkert, A. (2000). The Structure and Evolution of Weakly Self-interacting Cold Dark Matter Halos. *ApJ Lett.*, 534:143–146.

Chandrasekhar, S. (1942). Principles of stellar dynamics. *Physical Sciences Data*.

Chandrasekhar, S. (1964). The Dynamical Instability of Gaseous Masses Approaching the Schwarzschild Limit in General Relativity. *apj*, 140:417.

Colgate, S. A. (1967). Stellar coalescence and the multiple supernova interpretation of quasi-stellar sources. *ApJ*, 150:163.

Diaferio, A., Kauffmann, G., Colberg, J. M., and White, S. D. M. (1999). Clustering of galaxies in a hierarchical universe - III. Mock redshift surveys. *mnras*, 307:537–552.

Duncan, M. J. and Shapiro, S. L. (1982). Star clusters containing massive, central black holes. IV - galactic tidal fields. *ApJ*, 253:921–938.

Duncan, M. J. and Shapiro, S. L. (1983). Monte carlo simulations of the evolution of galactic nuclei containing massive, central black holes. *ApJ*, 268:565–581.

Ebisuzaki, T., Makino, J., Tsuru, T. G., Funato, Y., Portegies Zwart, S., Hut, P., McMillan, S., Matsushita, S., Matsumoto, H., and Kawabe, R. (2001). Missing Link Found? The "Runaway" Path to Supermassive Black Holes. *ApJ Lett.*, 562:L19–L22.

Ferrarese, L., Pogge, R. W., Peterson, B. M., Merritt, D., Wandel, A., and Joseph, C. L. (2001). Supermassive Black Holes in Active Galactic Nuclei. I. The Consistency of Black Hole Masses in Quiescent and Active Galaxies. *ApJ Lett.*, 555:79–82.

Frank, J., King, A., and Raine, D. J. (2002). *Accretion Power in Astrophysics: Third Edition*. Accretion Power in Astrophysics: Third Edition, by Juhan Frank, Andrew King, and Derek J. Raine. Cambridge University Press, 2002, 398 pp.

Freitag, M. and Benz, W. (2002). A new monte carlo code for star cluster simulations: II. central black hole and stellar collisions. *A&A*, 394:345–374.

Fuller, G. M., Woosley, S. E., and Weaver, T. A. (1986). The evolution of radiation-dominated stars. I - Nonrotating supermassive stars. *apj*, 307:675–686.

Gebhardt, K., Lauer, T. R., Kormendy, J., Pinkney, J., Bower, G., Green, R., Gull, T., Hutchings, J. B., Kaiser, M. E., Nelson, C. H., Richstone, D., and Weistrop, D. (2001). M33: A galaxy with no supermassive black hole. *AJ*, 122:2469–2476.

Gebhardt, K., Rich, R. M., and Ho, L. C. (2002). A $20000 M_{\odot}$ Black Hole in the Stellar Cluster G1. *ApJ Lett.*, 578:41–45.

Gerssen, J., van der Marel, R. P., Gebhardt, K., Guhathakurta, P., Peterson, R. C., and Pryor, C. (2002). Hubble Space Telescope Evidence for an Intermediate-Mass Black Hole in the Globular Cluster M15. II. Kinematic Analysis and Dynamical Modeling. *AJ*, 124:3270–3288.

Gerssen, J., van der Marel, R. P., Gebhardt, K., Guhathakurta, P., Peterson, R. C., and Pryor, C. (2003). Addendum: Hubble Space Telescope Evidence for an Intermediate-Mass Black Hole in the Globular Cluster M15. II. Kinematic Analysis and Dynamical Modeling. *AJ*, 125:376–377.

Gezari, S., Halpern, J. P., Komossa, S., Grupe, D., and Leighly, K. M. (2003). Follow-Up Hubble Space Telescope/Space Telescope Imaging Spectroscopy of Three Candidate Tidal Disruption Events. *apj*, 592:42–51.

Ghez, A. M., Duchêne, G., Matthews, K., Hornstein, S. D., Tanner, A., Larkin, J., Morris, M., Becklin, E. E., Salim, S., Kremenek, T., Thompson, D., Soifer, B. T., Neugebauer, G., and McLean, I. (2003). The First Measurement of Spectral Lines in a Short-Period Star Bound to the Galaxy's Central Black Hole: A Paradox of Youth. *ApJ Lett.*, 586:L127–L131.

Ginzburg, V. and Ozernoy, L. M. (1964). *Sov. Phys. JETP*, 20:489.

Goldreich, P. and Weber, S. V. (1980). Homologously collapsing stellar cores. *apj*, 238:991–997.

Hara, T. (1978). Evolution of a super-massive star in a dense stellar system. *Progress of Th. Phys.*, 60:711–723.

Heckman, T. M. (1980). An optical and radio survey of the nuclei of bright galaxies - Activity in normal galactic nuclei. *aap*, 87:152–164.

Hemsendorf, M., Sigurdsson, S., and Spurzem, R. (2001). Binary black holes in galactic centres. *EAS Publications Series, Volume 1. Active galactic nuclei in their cosmic environment. JENAM 99, Toulouse, France, September 7-9, 1999. Ed. by B. Rocca-Volmerange and H. Sol. Les Ulis: EDP Sciences, ISBN 2-86883-563-5, 2001, p. 173*, 1:173.

Herrnstein, J. R., Moran, J. M., Greenhill, L. J., Diamond, P. J., Inoue, M., Nakai, N., Miyoshi, M., Henkel, C., and Riess, A. (1999). A geometric distance to the galaxy ngc 4258 from orbital motions in a nuclear gas disk. *Nat*, 400:539–541.

Hills, J. G. (1975). Possible power source of Seyfert galaxies and QSOs. *Nat*, 254:295–298.

Hoyle, F. and Fowler, W. A. (1963). On the nature of strong radio sources. *mnras*, 125:169.

Jarrett, T. H., Chester, T., Cutri, R., Schneider, S. E., and Huchra, J. P. (2003). The 2MASS Large Galaxy Atlas. *aj*, 125:525–554.

Kauffmann, G., Colberg, J. M., Diaferio, A., and White, S. D. M. (1999a). Clustering of galaxies in a hierarchical universe - I. Methods and results at z=0. *mnras*, 303:188–206.

Kauffmann, G., Colberg, J. M., Diaferio, A., and White, S. D. M. (1999b). Clustering of galaxies in a hierarchical universe - I. Methods and results at z=0. *mnras*, 303:188–206.

Kormendy, J. (2003). The Stellar-Dynamical Search for Supermassive Black Holes in Galactic Nuclei. In Ho, L., editor, *"Coevolution of Black Holes and Galaxies", Carnegie Observatories, Pasadena*. astro-ph/0306353.

Krolik, J. H. (1999). *Active galactic nuclei: from the central black hole to the galactic environment*. Princeton University Press.

Langbein, T., Fricke, K. J., Spurzem, R., and Yorke, H. W. (1990). Interactions between stars and gas in galactic nuclei. *aa*, 227:333–341.

Larson, R. B. (1970). A method for computing the evolution of star clusters. *MNRAS*, 147:323.

Lee, H. M. (1995). Evolution of galactic nuclei with 10-m_ black holes. *MNRAS*, 272:605–617.

Lynden-Bell, D. (1967). Statistical mechanics of violent relaxation in stellar systems. *MNRAS*, 136:101.

Lynden-Bell, D. (1969). Galactic Nuclei as Collapsed Old Quasars. *nat*, 223:690.

Lynden-Bell, D. and Rees, M. J. (1971a). On quasars, dust and the galactic centre. *MNRAS*, 152:461.

Lynden-Bell, D. and Rees, M. J. (1971b). On quasars, dust and the galactic centre. *mnras*, 152:461.

Makino, J. (1997). Merging of Galaxies with Central Black Holes. II. Evolution of the Black Hole Binary and the Structure of the Core. *apj*, 478:58.

Makino, J. and Ebisuzaki, T. (1996). Merging of Galaxies with Central Black Holes. I. Hierarchical Mergings of Equal-Mass Galaxies. *apj*, 465:527.

Makino, J. and Taiji, M. (1998). *Scientific simulations with special-purpose computers : The GRAPE systems*. Scientific simulations with special-purpose computers : The GRAPE systems /by Junichiro Makino & Makoto Taiji. Chichester ; Toronto : John Wiley & Sons, c1998.

McCray, R. (1979). *Spherical accretion onto supermassive black holes*, pages 227–239. Active galactic nuclei. (A79-50785 22-90) Cambridge, Cambridge University Press, 1979, p. 227-239. NSF-supported research.

Merritt, D., Ferrarese, L., and Joseph, C. L. (2001). No Supermassive Black Hole in M33? *Science*, 293:1116–1119.

Merritt, D. and Poon, M. Y. (2003). Chaotic Loss Cones, Black Hole Fueling and the M-Sigma Relation. *ArXiv Astrophysics e-prints*.

Michell, J. (1784). On the Means of Discovering the Distance, Magnitude, & c. of the Fixed Stars, in Consequence of the Diminution of the Velocity of Their Light, in Case Such a Diminution Should be Found to Take Place in any of Them, and Such Other Data Should be Procured from Observations, as Would be Farther Necessary for That Purpose. By the Rev. John Michell, B. D. F. R. S. In a Letter to Henry Cavendish, Esq. F. R. S. and A. S. *Philosophical Transactions Series I*, 74:35–57.

Miller, M. C. and Colbert, E. J. M. (2003). Intermediate-Mass Black Holes. preprint, astro-ph/0308402.

Milosavljević, M. and Merrit (2001). Formation of Galactic Nuclei. *ApJ*, 563:34–62.

Miyoshi, M., Moran, J., Herrnstein, J., Greenhill, L., Nakai, N., Diamond, P., and Inoue, M. (1995). Evidence for a black-hole from high rotation velocities in a sub-parsec region of ngc4258. *Nat*, 373:127.

Moran, J. M., Greenhill, L. J., and Herrnstein, J. R. (1999). Observational Evidence for Massive Black Holes in the Centers of Active Galaxies. *Journal of Astrophysics and Astronomy*, 20:165.

Murphy, B. W., Cohn, H. N., and Durisen, R. H. (1991). Dynamical and luminosity evolution of active galactic nuclei - models with a mass spectrum. *ApJ*, 370:60–77.

Perley, R. A., Dreher, J. W., and Cowan, J. J. (1984). The jet and filaments in Cygnus A. *apjl*, 285:L35–L38.

Pian, E., Urry, C. M., Treves, A., Maraschi, L., Penton, S., Shull, J. M., Pesce, J. E., Grandi, P., Kii, T., Kollgaard, R. I., Madejski, G., Marshall, H. L., Wamsteker, W., Celotti, A., Courvoisier, T. J.-L., Falomo, R., Fink, H. H., George, I. M., and Ghisellini, G. (1997). Multiwavelength Monitoring of the BL Lacertae Object PKS 2155-304 in 1994 May. II. The IUE Campaign. *apj*, 486:784.

Pinkney, J., Gebhardt, K., Bender, R., Bower, G., Dressler, A., Faber, S. M., Filippenko, A. V., Green, R., Ho, L. C., Kormendy, J., Lauer, T. R., Magorrian, J., Richstone, D., and Tremaine, S. (2003). Kinematics of 10 Early-Type Galaxies from Hubble Space Telescope and Ground-based Spectroscopy. *ApJ*, 596:903–929.

Portegies Zwart, S. F. and McMillan, S. L. W. (2002). The Runaway Growth of Intermediate-Mass Black Holes in Dense Star Clusters. *ApJ*, 576:899–907.

Quinlan, G. D. and Shapiro, S. L. (1987). The collapse of dense star clusters to supermassive black holes - binaries and gravitational radiation. *ApJ*, 321:199–210.

Quinlan, G. D. and Shapiro, S. L. (1990). The dynamical evolution of dense star clusters in galactic nuclei. *ApJ*, 356:483–500.

Rasio, F. A., Freitag, M., and Gürkan, M. A. (2003). Formation of Massive Black Holes in Dense Star Clusters. In Ho, L., editor, *"Coevolution of Black Holes and Galaxies", Carnegie Observatories, Pasadena*. astro-ph/0304038.

Rauch, K. P. (1995). Dynamical evolution of star clusters around a rotating black hole with an accretion disc. *MNRAS*, 275:628–640.

Rauch, K. P. (1999). Collisional stellar dynamics around massive black holes in active galactic nuclei. *ApJ*, 514:725–745.

Rees, M. J. (1984). "black hole models for active galactic nuclei". *ARA&A*, 22:471–506.

Rees, M. J. (1990). 'dead quasars' in nearby galaxies? *Science*, 247:817–823.

Salpeter, E. E. (1964). Accretion of Interstellar Matter by Massive Objects. *apj*, 140:796–800.

Sanders, R. H. (1970). The effects of stellar collisions in dense stellar systems. *ApJ*, 162:791.

Schödel, R., Ott, T., Genzel, R., Eckart, A., Mouawad, N., and Alexander, T. (2003). Stellar Dynamics in the Central Arcsecond of Our Galaxy. *ApJ*, 596:1015–1034.

Schaffer, S. (1979). Michell, John and Black Holes. *Journal for the History of Astronomy*, 10:42.

Sołtan, A. (1982). Masses of quasars. *MNRAS*, 200:115–122.

Spitzer, L., J. and Saslaw, W. C. (1966). On the evolution of galactic nuclei. *ApJ*, 143:400.

Spitzer, L. (1987). *Dynamical evolution of globular clusters*. Princeton University Press.

Spitzer, L. J. and Stone, M. E. (1967). On the evolution of galactic nuclei. II. *ApJ*, 147:519.

Stoner, R. E. and Ptak, R. L. (1984). Evidence for Supermassive Stars in Three Seyfert-I Nuclei from Variability in IUE Spectra. *baas*, 16:988.

Terlevich, R. (1989). Active galactic nuclei without black-holes. In *Evolutionary Phenomena in Galaxies*, pages 149–158.

Thorne, K. S. (1995). Gravitational Radiation. In *Seventeeth Texas Symposium on Relativistic Astrophysics and Cosmology*, page 127.

van der Marel, R. P., Gerssen, J., Guhathakurta, P., Peterson, R. C., and Gebhardt, K. (2002). Hubble Space Telescope Evidence for an Intermediate-Mass Black Hole in the Globular Cluster M15. I. STIS Spectroscopy and WFPC2 Photometry. *AJ*, 124:3255–3269.

Vil'Koviskii, É. Y. (1978). Interaction of galaxies with central objects, and the activity of galaxy nuclei. *Soviet Astronomy*, 22:385.

Woosley, S. E. and Weaver, T. A. (1982). Theoretical Models for Supernovae. In *NATO ASIC Proc. 90: Supernovae: A Survey of Current Research*, page 79.

Yu, Q. and Tremaine, S. (2002). Observational constraints on growth of massive black holes. *MNRAS*, 335:965–976.

Zeldovich, Y. B. and Novikov, I. D. (1971). *Relativistic astrophysics. Vol.1: Stars and relativity*. University of Chicago Press.

Zel'Dovich, Y. B. and Podurets, M. A. (1966). The Evolution of a System of Gravitationally Interacting Point Masses. *Soviet Astronomy*, 9:742.

# Chapter 2

# The theoretical model

## 2.1 Introduction

FUNDAMENTALS and principles of the anisotropic gaseous model are presented in this chapter[1] so as to give the description of the numerical approach employed to model stellar clusters, as we shall see in next chapters. We start with a brief description of the mathematical basis which can be regarded as a short summary of the description of kinetic theory in chapter eight of Binney and Tremaine (1987). The reader interested in an in-depth study is addressed to it. On the other hand, we stress on the peculiarities of the approximation we make use of, the so-called local approximation, so as to be aware of the restrictions of our theory and emphasise them. Later, we will give the set of equations describing the system, the interaction terms to be taken into consideration to represent realistic models, like mass exchange by mass loss, heating, loss-cone, exchange of kinetic energy between the stellar system and the interstellar gas via drag forces, etc, to be included in the right-hand terms of this set. Ensuingly we shall make a thoughtfully depiction of the gaseous component in the cluster and their own interaction terms.

## 2.2 The Fokker-Planck equation

The state of a system of $N$ particles with velocities $\mathbf{v} = (\mathbf{v}_i)$ and positions $\mathbf{x} = (\mathbf{x}_i)$ $(i = 1, \ldots N)$ is represented by a point in $6N$-dimensional $\Gamma$-space of positional and velocity variables. The $N$-particle

[1] At the beginnig of each chapter I will give references of published work related to the contents of the chapter. Typically, I will firstly mention the refereed article (if any) and, secondly, contributions to conferences (*proceedings*). As for the chapter under discussion, some sections were used for Amaro-Seoane and Spurzem (2001), Amaro-Seoane and Spurzem (2004) and Spurzem et al. (2003)

distribution $f^{(N)}(\mathbf{x},\mathbf{v},t)$ is defined as the probability to find the system in the volume element $d^3\mathbf{v}d^3\mathbf{x}$ around $\mathbf{x}$ and $\mathbf{v}$ at time $t$. $f^{(N)}$ is normalised as $1 = \int f^{(N)} d^3\mathbf{v}d^3\mathbf{x}$ The evolution of the system is a trajectory in $\Gamma$-space; the evolution of a continuous subspace of systems at $t = t_0$ (initial conditions) can be seen as a flow in $\Gamma$-space, which due to the absence of any dissipation is incompressible, and thus described by a continuity equation in $\Gamma$-space, which is Liouville's equation:

$$\frac{\partial f^{(N)}}{\partial t} + \sum_{i=1}^{N} \Big\{ \frac{\partial}{\partial \mathbf{x}_i} \Big[ f^{(N)} \frac{d\mathbf{x}_i}{dt} \Big] + \frac{\partial}{\partial \mathbf{v}_i} \Big[ f^{(N)} \frac{d\mathbf{v}_i}{dt} \Big] \Big\} = 0. \tag{2.1}$$

Using the definition $d\mathbf{x}_i/dt = \mathbf{v}_i$ and $\partial \mathbf{v}_i/\partial \mathbf{x_i} = 0$, since $\mathbf{v}_i$ and $\mathbf{x}_i$ are independent coordinates, and if the forces are conservative, $d\mathbf{v}_i/dt = -\partial\Phi_i/\partial \mathbf{x}_i$, where $\Phi_i$ is the potential at the position of particle $i$ due to the other particles, we can simplify last equation to

$$\frac{\partial f^{(N)}}{\partial t} + \sum_{i=1}^{N} \Big[ \mathbf{v}_i \cdot \frac{\partial f^{(N)}}{\partial \mathbf{x}_i} - \frac{\partial \Phi_i}{\partial \mathbf{x}_i} \cdot \frac{\partial f^{(N)}}{\partial \mathbf{v}_i} \Big] = 0. \tag{2.2}$$

Here it has been utilised that $d\mathbf{v}_i/dt$ does not depend on $\mathbf{v}_i$ itself, since the potential only depends on the spatial coordinates.
Now we introduce the one-particle distribution function $f^{(1)}(\mathbf{x},\mathbf{v},t)$ as

$$f^{(1)}(\mathbf{x},\mathbf{v},t) = \int f^{(N)}(\mathbf{x}_i,\mathbf{v}_i,t) d^3\mathbf{x_2} \ldots d^3\mathbf{x_N} d^3\mathbf{v_2} \ldots d^3\mathbf{v_N}, \tag{2.3}$$

the two-particle distribution function

$$f^{(2)}(\mathbf{x}_1,\mathbf{x}_2,\mathbf{v}_1.\mathbf{v}_2,t) = \int f^{(N)}(\mathbf{x}_i,\mathbf{v}_i,t) d^3\mathbf{x}_3 \ldots d^3\mathbf{x}_N d^3\mathbf{v}_3 \ldots d^3\mathbf{v}_N \tag{2.4}$$

and the two-particle correlation function $g$ by

$$g(\mathbf{x}_1,\mathbf{x}_2,\mathbf{v}_1.\mathbf{v}_2,t) = f^{(2)}(\mathbf{x}_1,\mathbf{x}_2,\mathbf{v}_1.\mathbf{v}_2,t) - f^{(1)}(\mathbf{x}_1,\mathbf{v}_1,t) f^{(1)}(\mathbf{x}_2,\mathbf{v}_2,t) \tag{2.5}$$

$g$ measures the excess probability of finding a particle at $\mathbf{x}_1$, $\mathbf{v}_1$ due to the presence of another particle at $\mathbf{x}_2$, $\mathbf{v}_2$. Since $f^{(1)}$ is normalised to unity, one has $\rho(\mathbf{x}_2,t) = mN \int f^{(1)}(\mathbf{x}_2,\mathbf{v}_2,t) d\mathbf{v}_2$, where $\rho$ is a mean mass density, and $m$ the individual stellar mass. Assuming that $f^{(N)}$ is symmetric with respect to exchange of particles (i.e. all particles are indistinguishable), and observing that $\Phi_1$ is also symmetric with respect to exchanges of the particles $2,\ldots,N$, one arrives at

$$\frac{\partial f^{(1)}}{\partial t} + \mathbf{v}_1 \cdot \frac{\partial f^{(1)}}{\partial \mathbf{x}_1} - \frac{N-1}{N} \frac{\partial \Phi_1}{\partial \mathbf{x}_1} \cdot \frac{\partial f^{(1)}}{\partial \mathbf{v}_1} =$$

$$-Gm(N-1) \int \frac{\partial}{\partial \mathbf{v}_1} \Big( g(\mathbf{x}_1,\mathbf{x}_2,\mathbf{v}_1.\mathbf{v}_2,t) \Big) \frac{\partial}{\partial \mathbf{x}_1} \Big( |\mathbf{x}_1 - \mathbf{x}_2|^{-1} \Big) d^3\mathbf{x_2} d^3\mathbf{v_2}. \tag{2.6}$$

Now one substitutes $f^{(1)}$ by the more common phase space density $f = f^{(1)}/N$ and drops for simplicity

all subscripts "1". It follows

$$\frac{\partial f}{\partial t}+\mathbf{v}\cdot\frac{\partial f}{\partial \mathbf{x}}-\frac{N-1}{N}\frac{\partial \Phi}{\partial \mathbf{x}}\cdot\frac{\partial f}{\partial \mathbf{v}}=\left(\frac{\delta f}{\delta t}\right)_{\text{enc}} \tag{2.7}$$

If the average particle distance $\bar{d}=1/n^{1/3}$ is bigger than the impact parameter $p_{90}$ related to a $90^o$ deflection, most of the scattering is due to small angle encounters, which change velocity and position of the particle only weakly. So, if we assume that all correlations stem from gravitational two-body scatterings of particles, not from higher order correlations, we have that the Fokker-Planck equation is

$$\begin{aligned}\left(\frac{\delta f}{\delta t}\right)_{\text{enc}} &= -\sum_{i=1}^{3}\left[\frac{\partial}{\partial x_i}\Big(f(\mathbf{x},\mathbf{v})D(\Delta x_i)\Big)+\frac{\partial}{\partial v_i}\Big(f(\mathbf{x},\mathbf{v})D(\Delta v_i)\Big)\right]\\ &+\frac{1}{2}\sum_{i,j=1}^{3}\left[\frac{\partial^2}{\partial x_i\partial x_j}\Big(f(\mathbf{x},\mathbf{v})D(\Delta x_i\Delta x_j)\Big)+\frac{\partial^2}{\partial v_i\partial v_j}\Big(f(\mathbf{x},\mathbf{v})D(\Delta v_i\Delta v_j)\Big)\right.\\ &\left.+\frac{\partial^2}{\partial x_i\partial v_j}\Big(f(\mathbf{x},\mathbf{v})D(\Delta x_i\Delta v_j)\Big)+\frac{\partial^2}{\partial v_i\partial x_j}\Big(f(\mathbf{x},\mathbf{v})D(\Delta v_i\Delta x_j)\Big)\right]\end{aligned} \tag{2.8}$$

Here the convenient notation of diffusion coefficients has been introduced, which contain the integration over the velocity and position changes, as e.g.:

$$D(\Delta v_i):=\int \Delta v_i\Psi(\mathbf{x},\mathbf{v},\Delta\mathbf{x},\Delta\mathbf{v})d^3\,\Delta\mathbf{x}d^3\Delta\mathbf{v}, \tag{2.9}$$

where $\Psi(\mathbf{x},\mathbf{v},\Delta\mathbf{x},\Delta\mathbf{v})\;d^3\Delta\mathbf{x}d^3\Delta\mathbf{v}dt$ is defined as the probability for a star with position $\mathbf{x}$ and velocity $\mathbf{v}$ to be scattered into a new phase space volume element $d^3\Delta\mathbf{x}\;d^3\Delta\mathbf{v}$ located around $\mathbf{x}+\Delta\mathbf{x}$, $\mathbf{v}+\Delta\mathbf{v}$ during the time interval $dt$.

## 2.3 The local approximation

There are two alternative ways of further simplification. One is the orbit average, which uses that any distribution function, being a steady state solution of the collisionless Boltzmann equation, can be expressed as a function of the constants of motion of an individual particle (Jeans' theorem). For the sake of simplicity, it is assumed that all orbits in the system are regular, as it is the case for example in a spherically symmetric potential; thus the distribution function $f$ now only depends on maximally three independent integrals of motion (strong Jeans' theorem). Let us transform the Fokker-Planck equation to a new set of variables, which comprise the constants of motion instead of the velocities $v_i$. Since in a spherically symmetric system the distribution only depends on energy and the modulus of the angular momentum vector $J$, the number of independent coordinates in this example can be reduced from six to two, and all terms in the transformed equation (8) containing derivatives to other variables than $E$ and $J$ vanish (in particular those containing derivatives to the spatial coordinates $x_i$). Integrating the remaining

parts of the Fokker-Planck equation over the spatial coordinates is called orbit averaging, because in our present example (a spherical system) it would be an integration over accessible coordinate space for given $E$ and $J$ (which is a spherical shell between $r_{\min}(E,J)$ and $r_{\max}(E,J)$, the minimum and maximum radius for stars with energy $E$ and angular momentum $J$). Such volume integration is, since $f$ does not depend any more on $x_i$ carried over to the diffusion coefficients $D$, which become orbit-averaged diffusion coefficients.

Orbit-averaged Fokker-Planck models treat very well the diffusion of orbits according to the changes of their constants of motion, taking into account the potential and the orbital structure of the system in a self-consistent way. However, they are not free of any problems or approximations. They require checks and tests, for example by comparisons with other methods, like the one described in the following.

We treat relaxation like the addition of a big non-correlated number of two-body encounters. Close encounters are rare and thus we admit that each encounter produces a very small deflection angle. Thence, relaxation can be regarded as a diffusion process [2].

A typical two-body encounter in a large stellar system takes place in a volume whose linear dimensions are small compared to other typical radii of the system (total system dimension, or scaling radii of changes in density or velocity dispersion). Consequently, it is assumed that an encounter only changes the velocity, not the position of a particle. Thenceforth, encounters do not produce any changes $\Delta\mathbf{x}$, so all related terms in the Fokker-Planck equation vanish. However, the local approximation goes even further and assumes that the entire cumulative effect of all encounters on a test particle can approximately be calculated as if the particle were surrounded by a very big homogeneous system with the local distribution function (density, velocity dispersions) everywhere. We are left with a Fokker-Planck equation containing only derivatives with respect to the velocity variables, but still depending on the spatial coordinates (a local Fokker-Planck equation).

In practical astrophysical applications, the diffusion coefficients occurring in the Fokker-Planck equation are not directly calculated, containing the probability $\Psi$ for a velocity change $\Delta\mathbf{v}$ from an initial velocity $\mathbf{v}$. Since $D(\Delta v_i)$, and $D(\Delta v_i \Delta v_j)$ are of the dimension velocity (change) per time unit, and squared velocity (change) per time unit, respectively, one calculates such velocity changes in a more direct way, considering a test star moving in a homogeneous sea of field stars. Let the test star have a velocity $\mathbf{v}$ and consider an encounter with a field star of velocity $\mathbf{v}_f$. The result of the encounter (i.e. velocity changes $\Delta v_i$ of the test star) is completely determined by the impact parameter $p$ and the relative velocity at infinity $v_{\rm rel} = |\mathbf{v} - \mathbf{v}_f|$; thus by an integration of the type

$$< \Delta \dot{v}_i >_p = 2\pi \int (\Delta v_i)\, v_{\rm rel}\, n_f\, p\, dp, \tag{2.10}$$

the rate of change of the test star velocity due to encounters with $v_{\rm rel}$, in field of stars with particle density $n_f$, averaged over all relevant impact parameters is computed. The integration is normally carried out from $p_0$ (impact parameter for $90^o$ deflection) until $R$, which is some maximum linear dimension of the system under consideration. Such integration generates in subsequent equations the so-called Coulomb

[2] Anyhow, it has been argued that rare deflections with a large angle may play a important role in the vicinity of a BH (Lin and Tremaine, 1980).

logarithm $\ln\Lambda$; we will argue later that it can be well approximated by $\ln(0.11N)$, where $N$ is the total particle number. The diffusion coefficient finally is

$$D(\Delta v_i) = \int <\Delta \dot{v}_i>_p f(\mathbf{v}_f) d^3\mathbf{v}_f, \tag{2.11}$$

where $f(\mathbf{v}_f)$ is the velocity distribution of the field stars. In an equal mass system, $f(\mathbf{v}_f)$ should be equal to the distribution function of the test stars occurring in the Fokker-Planck equation for self-consistency. In case of a multi-mass system, however, $f(\mathbf{v}_f)$ could be different from the test-star distribution, if the diffusion coefficient arising from encounters between two different species of stars is to be calculated. The diffusion coefficients are (for an exact procedure see Appendix 8.A of Binney and Tremaine 1987):

$$\begin{aligned} D(\Delta v_i) = &\quad 4\pi G^2 m_f \ln\Lambda \frac{\partial}{\partial v_i} h(\mathbf{v}) \\ D(\Delta v_i v_j) = &\quad 4\pi G^2 m_f \ln\Lambda \frac{\partial^2}{\partial v_i \partial v_j} g(\mathbf{v}) \end{aligned} \tag{2.12}$$

with the Rosenbluth potentials Rosenbluth et al. (1957)

$$\begin{aligned} h(\mathbf{v}) = &\quad (m+m_f) \int \frac{f(\mathbf{v}_f)}{|\mathbf{v}-\mathbf{v}_f|} d^3\mathbf{v}_f \\ g(\mathbf{v}) = &\quad m_f \int f(\mathbf{v}_f) |\mathbf{v}-\mathbf{v}_f| d^3\mathbf{v}_f \ . \end{aligned} \tag{2.13}$$

With these results we can finally write down the local Fokker-Planck equation in its standard form for the Cartesian coordinate system of the $v_i$:

$$\left(\frac{\delta f}{\delta t}\right)_{\rm enc} = -4\pi G^2 m_f \ln\Lambda \left[ \sum_{i=1}^{3} \frac{\partial}{\partial v_i} \left( f(\mathbf{v}) \frac{\partial h}{\partial v_i} \right) + \frac{1}{2} \sum_{i,j=1}^{3} \frac{\partial^2}{\partial v_i \partial v_j} \left( f(\mathbf{v}) \frac{\partial^2 g}{\partial v_i \partial v_j} \right) \right] \tag{2.14}$$

Note that in Rosenbluth et al. (1957) the above equation is given in a covariant notation, which allows for a straightforward transformation into other curvilinear coordinate systems.

Before going ahead the question is raised, why such approximation can be reasonable, regarding the long-range gravitational force, and the impossibility to shield gravitational forces as in the case of Coulomb forces in a plasma by opposite charges. The key is that logarithmic intervals in impact parameter $p$ contribute equally to the mean square velocity change of a test particle, provided $p \gg p_0$ (see e.g. Spitzer 1987, chapter 2.1). Imagine that on one hand side the lower limit of impact parameters ($p_0$, the $90^o$ deflection angle impact parameter) is small compared to the mean interparticle distance $d$. Let on the other hand side $D$ be a typical radius connected with a change in density or velocity dispersions (e.g. the scale height in a disc of a galaxy), and $R$ be the maximum total dimension of the system. Just to be specific let us assume $D = 100d$, and $R = 100D$. In that case the volume of the spherical shell with radius between $D$ and $R$ is $10^6$ times larger than the volume of the shell defined by the radii $d$ and $D$. Nevertheless the contribution of both shells to diffusion coefficients or the relaxation time is approxi-

mately equal. This is a heuristic illustration why the local approximation is not so bad; the reason is with other words that there are a lot more encounters with particles in the outer, larger shell, but the effect is exactly compensated by the larger deflection angle for encounters happening with particles from the inner shell. If we are in the core or in the plane of a galactic disc the density would fall off further out, so the actual error will be smaller than outlined in the above example. By the same reasoning one can see, however, that the local approximation for a particle in a low-density region, which suffers from relaxation by a nearby density concentration, is prone to failure.
These rough handy examples should illustrate that under certain conditions the local approximation is not a priori bad. On the other hand, it is obvious from our above arguments, that if we are interested in relaxation effects on particles in a low-density environment, whose orbit occasionally passes distant, high-density regions, the local approximation could be completely wrong. One might think here for example of stars on radially elongated orbits in the halo of globular clusters or of stars, globular clusters, or other objects as massive black holes, on spherical orbits in the galactic halo, passing the galactic disc. In these situations an orbit-averaged treatment seems much more appropriate.

## 2.4 A numerical anisotropic model

In this section we introduce the fundamentals of the numerical method we use to model our system. We give a brief description of the mathematical basis of it and the physical idea behind it. The system is treated as a continuum, which is only adequate for a large number of stars and in well populated regions of the phase space. We consider here spherical symmetry and single-mass stars. We handle relaxation in the Fokker-Planck approximation, i.e. like a diffusive process determined by local conditions. We make also use of the hydrodynamical approximation; that is to say, only local moments of the velocity dispersion are considered, not the full orbital structure. In particular, the effect of the two-body relaxation can be modelled by a local heat flux equation with an appropriately tailored conductivity. Neither binaries nor stellar evolution are included at the presented work. As for the hypothesis concerning the BH, see section (5.2).
For our description we use polar coordinates, $r$ $\theta$, $\phi$. The vector $\mathbf{v} = (v_i), i = r, \theta, \phi$ denotes the velocity in a local Cartesian coordinate system at the spatial point $r, \theta, \phi$. For succinctness, we shall employ the notation $u = v_\mathrm{r}$, $v = v_\theta$, $w = v_\phi$. The distribution function $f$, is a function of $r$, $t$, $u$, $v^2 + w^2$ only due to spherical symmetry, and is normalised according to

$$\rho(r,t) = \int f(r,u,v^2+w^2,t)\,du\,dv\,dw. \tag{2.15}$$

Here $\rho(r,t)$ is the mass density; if $m_\star$ denotes the stellar mass, we get the particle density $n = \rho/m_\star$. The Euler-Lagrange equations of motion corresponding to the Lagrange function

$$\mathscr{L} = \frac{1}{2}\left(\dot{r}^2 + r^2\dot{\theta}^2 + r^2\sin^2\theta\,\dot{\phi}^2\right) - \Phi(r,t) \tag{2.16}$$

are the following

$$\begin{aligned} \dot{u} = & -\frac{\partial \Phi}{\partial r} + \frac{v^2+w^2}{r} \\ \dot{v} = & -\frac{uv}{r} + \frac{w^2}{r\tan\theta} \\ \dot{w} = & -\frac{uw}{r} - \frac{vw}{r\tan\theta} \end{aligned} \tag{2.17}$$

And so we get a complete local Fokker-Planck equation,

$$\frac{\partial f}{\partial t} + v_{\rm r}\frac{\partial f}{\partial r} + \dot{v_{\rm r}}\frac{\partial f}{\partial v_{\rm r}} + \dot{v_\theta}\frac{\partial f}{\partial v_\theta} + \dot{v_\varphi}\frac{\partial f}{\partial v_\varphi} = \left(\frac{\delta f}{\delta t}\right)_{FP} \tag{2.18}$$

In our model we do not solve the equation directly; we use a so-called *momenta process*. The momenta of the velocity distribution function $f$ are defined as follows

$$< i,j,k >:= \int_{-\infty}^{+\infty} v_{\rm r}^i v_\theta^j v_\phi^k \, f(r, v_{\rm r}, v_\theta, v_\phi, t)\, dv_{\rm r} dv_\theta dv_\phi; \tag{2.19}$$

We define now the following moments of the velocity distribution function,

$$\begin{aligned} < 0,0,0 >:= & \quad \rho = \int f du dv dw \\ < 1,0,0 >:= & \quad u = \int u f du dv dw \\ < 2,0,0 >:= & \quad p_{\rm r} + \rho u^2 = \int u^2 f du dv dw \\ < 0,2,0 >:= & \quad p_\theta = \int v^2 f du dv dw \\ < 0,0,2 >:= & \quad p_\phi = \int w^2 f du dv dw \\ < 3,0,0 >:= & \quad F_{\rm r} + 3up_{\rm r} + u^3 = \int u^3 f du dv dw \\ < 1,2,0 >:= & \quad F_\theta + up_\theta = \int uv^2 f du dv dw \\ < 1,0,2 >:= & \quad F_\phi + up_\phi = \int uw^2 f du dv dw, \end{aligned} \tag{2.20}$$

where $\rho$ is the density of stars, $u$ is the bulk velocity, $v_{\rm r}$ and $v_{\rm t}$ are the radial and tangential flux velocities, $p_{\rm r}$ and $p_{\rm t}$ are the radial and tangential pressures, $F_{\rm r}$ is the radial and $F_{\rm t}$ the tangential kinetic energy flux (Louis and Spurzem, 1991). Note that the definitions of $p_i$ and $F_i$ are such that they are proportional to the random motion of the stars. Due to spherical symmetry, we have $p_\theta = p_\phi =: p_{\rm t}$ and $F_\theta = F_\phi =: F_{\rm t}/2$. By $p_{\rm r} = \rho\sigma_{\rm r}^2$ and $p_{\rm t} = \rho\sigma_{\rm t}^2$ the random velocity dispersions are given, which are closely related to observable properties in stellar clusters.

$F = (F_\mathrm{r} + F_\mathrm{t})/2$ is a radial flux of random kinetic energy. In the notion of gas dynamics it is just an energy flux. Whereas for the $\theta-$ and $\phi-$ components in the set of Eqs. (2.20) are equal in spherical symmetry, for the $r$ and $t$- quantities this is not true. In stellar clusters the relaxation time is larger than the dynamical time and so any possible difference between $p_\mathrm{r}$ and $p_\mathrm{t}$ may *survive* many dynamical times. We shall denote such differences anisotropy. Let us define the following velocities of energy transport:

$$\begin{aligned} v_\mathrm{r} &= \frac{F_\mathrm{r}}{3p_\mathrm{r}} + u, \\ v_\mathrm{t} &= \frac{F_\mathrm{t}}{2p_\mathrm{t}} + u. \end{aligned} \tag{2.21}$$

In case of *weak* isotropy ($p_\mathrm{r}$=$p_\mathrm{t}$) $2F_\mathrm{r} = 3F_\mathrm{t}$, and thus $v_\mathrm{r} = v_\mathrm{t}$, i.e. the (radial) transport velocities of radial and tangential random kinetic energy are equal.

The Fokker-Planck equation (2.18) is multiplicated with various powers of the velocity components $u$, $v$, $w$. We get so up to second order a set of moment equations: A mass equation, a continuity equation, an Euler equation (force) and radial and tangential energy equations. The system of equations is closed by a phenomenological heat flux equation for the flux of radial and tangential RMS (*root mean square*) kinetic energy, both in radial direction. The concept is physically similar to that of Lynden-Bell and Eggleton (1980). The set of equations is

$$\frac{\partial \rho}{\partial t} + \frac{1}{r^2}\frac{\partial}{\partial r}(r^2 u \rho) = 0$$

$$\frac{\partial u}{\partial t} + u\frac{\partial u}{\partial r} + \frac{GM_\mathrm{r}}{r^2} + \frac{1}{\rho}\frac{\partial p_\mathrm{r}}{\partial r} + 2\frac{p_\mathrm{r} - p_\mathrm{t}}{\rho r} = 0$$

$$\begin{aligned} &\frac{\partial p_\mathrm{r}}{\partial t} + \frac{1}{r^2}\frac{\partial}{\partial r}(r^2 u\, p_\mathrm{r}) + 2\,p_\mathrm{r}\frac{\partial u}{\partial r} + \frac{1}{r^2}\frac{\partial}{\partial r}(r^2 F_\mathrm{r}) \\ &\quad - \frac{2F_\mathrm{t}}{r} = -\frac{4}{5}\frac{(2p_\mathrm{r} - p_\mathrm{t})}{\lambda_A t_\mathrm{relax}} \end{aligned} \tag{2.22}$$

$$\begin{aligned} &\frac{\partial p_\mathrm{t}}{\partial t} + \frac{1}{r^2}\frac{\partial}{\partial r}(r^2 u\, p_\mathrm{t}) + 2\,\frac{p_\mathrm{t} u}{r} + \frac{1}{2r^2}\frac{\partial}{\partial r}(r^2 F_\mathrm{t}) \\ &\quad + \frac{F_\mathrm{t}}{r} = \frac{2}{5}\frac{(2p_\mathrm{r} - p_\mathrm{t})}{\lambda_A t_\mathrm{relax}}, \end{aligned}$$

where $\lambda_A$ is a numerical constant related to the time-scale of collisional anisotropy decay. The value

chosen for it has been discussed in comparison with direct simulations performed with the $N$–body code (Giersz and Spurzem, 1994). The authors find that $\lambda_A = 0.1$ is the physically realistic value inside the half-mass radius for all cases of $N$, provided that close encounters and binary activity do not carry out an important role in the system, what is, on the other hand, inherent to systems with a big number of particles, as this is.
With the definition of the mass $M_\mathrm{r}$ contained in a sphere of radius $r$

$$\frac{\partial M_\mathrm{r}}{\partial r} = 4\pi r^2 \rho, \tag{2.23}$$

the set of Eqs. (2.22) is equivalent to gas-dynamical equations coupled with the equation of Poisson. To close it we need an independent relation, for moment equations of order $n$ contain moments of order $n+1$. For this intent we use the heat conduction closure, a phenomenological approach obtained in an analogous way to gas dynamics. It was used for the first time by Lynden-Bell and Eggleton (1980) but restricted to isotropy. In this approximation one assumes that heat transport is proportional to the temperature gradient,

$$F = -\kappa \frac{\partial T}{\partial r} = -\Lambda \frac{\partial \sigma^2}{\partial r} \tag{2.24}$$

That is the reason why such models are usually also called *conducting gas sphere models*.
It has been argued that for the classical approach $\Lambda \propto \bar{\lambda}^2/\tau$, one has to choose the Jeans' length $\lambda_J^2 = \sigma^2/(4\pi G\rho)$ and the standard Chandrasekhar local relaxation time $t_\mathrm{relax} \propto \sigma^3/\rho$ (Lynden-Bell and Eggleton, 1980), where $\bar{\lambda}$ is the mean free path and $\tau$ the collisional time. In this context we obtain a conductivity $\Lambda \propto \rho/\sigma$. We shall consider this as a working hypothesis. For the anisotropic model we use a mean velocity dispersion $\sigma^2 = (\sigma_\mathrm{r}^2 + 2\sigma_\mathrm{t}^2)/3$ for the temperature gradient and assume $v_\mathrm{r} = v_\mathrm{t}$ (Bettwieser and Spurzem, 1986). Forasmuch as, the equations we need to close our model are

$$\begin{aligned} v_\mathrm{r} - u + \frac{\lambda}{4\pi G\rho\, t_\mathrm{relax}} \frac{\partial \sigma^2}{\partial r} &= 0 \\ v_\mathrm{r} &= v_\mathrm{t}. \end{aligned} \tag{2.25}$$

## 2.5 Interaction terms and implementation of the gaseous component

The set of Eqs. (2.22) describe the stellar cluster without taking into consideration the different interaction processes which may play a role in these systems. Heating, cooling processes, mass exchange between stars and gas by stellar mass loss or disruptive stellar collisions, exchange of kinetic internal energy between the stellar system and the interstellar gas via drag forces, loss-cone processes etc are not included in the equations. Here we will give a description for some interesting phenomena that crop up in the systems we want to study. Chapter 5 is partly devoted to a profound description of a loss-cone

diffusion model.
In parallel with the description of the interaction terms for the stellar component of a cluster, here we will describe the inclusion of an *SMS*in the anisotropic numerical model. For that aim, one should take into account the transfer of radiation in a spherically symmetric moving medium allowing for the contributions which are of the order of the flow velocity divided by the velocity of light, the thermal energy equation and the turbulent energy equation. The equations will be given also "in their logarithmic form" (i.e. in our equations we work with $\ln x$ instead of $x$), ready to include in the gaseous model.
The interaction terms for the *gaseous component* [3] are also described and post-Newtonian corrections are also considered. How these *SMS*scould power the quasar activity by star accretion and energy flows is one of the main questions that could be answered thanks to this method. Therefore we have found of paramount importance to give the set of equations describing this situation.

### 2.5.1 The star component

We now introduce the interaction terms to be added to right hand of the star component equations. This and the next section benefit from the paper by Langbein et al. (1990).

#### Equation of continuity

Langbein et al. (1990) derive the interaction terms to be added to the basic equations of the gaseous model. According to them, the star continuity equation is no longer

$$\frac{\partial \rho_\star}{\partial \mathrm{t}} + \frac{1}{\mathrm{r}^2}\frac{\partial}{\partial \mathrm{r}}(\mathrm{r}^2 \rho_\star \mathrm{u}_\star) = 0, \tag{2.26}$$

but

$$\frac{\partial \rho_\star}{\partial \mathrm{t}} + \frac{1}{\mathrm{r}^2}\frac{\partial}{\partial \mathrm{r}}(\mathrm{r}^2 \rho_\star \mathrm{u}_\star) = \left(\frac{\delta \rho_\star}{\delta \mathrm{t}}\right)_{\mathrm{coll}} + \left(\frac{\delta \rho_\star}{\delta \mathrm{t}}\right)_{\mathrm{lc}}; \tag{2.27}$$

where the right-hand term reflects the time variation of the star's density due to stars interactions (i.e. due to the calculation of the mean rate of gas production by stars collisions) and loss-cone (stars plunging onto the central object).
If $f(v_{\mathrm{rel}})$ is the stellar distribution of relative velocities, then the mean rate of gas production by stellar collisions is

$$\left(\frac{\delta \rho_\star}{\delta \mathrm{t}}\right)_{\mathrm{coll}} = -\int_{|v_{\mathrm{rel}}|>\sigma_{\mathrm{coll}}} \frac{\rho_\star f_{\mathrm{c}}(v_{\mathrm{rel}})}{t_{\mathrm{coll}}} f(v_{\mathrm{rel}}) d^3 v_{\mathrm{rel}} \tag{2.28}$$

[3] One should here not be confused by the terminology. When we talk about the *gaseous model*, we mean the numerical anisotropic model we use to model stellar systems; it is called like that because it is based on moments of the Boltzmann equation with relaxation. The stellar cluster is modelled like a self-gravitating, conducting *gas* sphere, and was first presented in Louis and Spurzem (1991) and Giersz and Spurzem (1994). On the other hand, when we refer to the *gaseous component*, we mean the physical gas in the cluster, which may conform an *SMS*.

In the calculation of equation (14) $f(v_{\rm rel})$ is a Schwarzschild-Boltzmann distribution,

$$f(v_{\rm rel}) = \frac{1}{2\pi^{3/2}\sigma_{\rm r}\sigma_{\rm t}^2}\cdot\exp\left(-\frac{(v_{\rm rel,r}-u_\star)^2}{4\sigma_{\rm r}^2}-\frac{v_{\rm rel,t}^2}{2\sigma_{\rm t}^2}\right) \tag{2.29}$$

As regards $f_{\rm c}$, it is the relative fraction of mass liberated per stellar collision into the gaseous medium. Under certain assumptions given in the initial work of Spitzer and Saslaw (1966), we can calculate it as an average over all impact parameters resulting in $r_{\rm min} < 2r_\star$ and as a function of the relative velocity at infinity of the two colliding stars, $v_{\rm rel}$. Langbein et al. (1990) approximate their result by

$$f_{\rm c}(v_{\rm rel}) = \begin{cases} \left(1+q_{\rm coll}\sqrt{\sigma_{\rm coll}/v_{\rm rel}}\right)^{-1} & v_{\rm rel} > \sigma_{\rm coll} \\ 0 & v_{\rm rel} < \sigma_{\rm coll}, \end{cases}$$

with $q_{\rm coll} = 100$. So, we have that

$$f_{\rm c}(v_{\rm rel}) = \begin{cases} 0.01 & \sigma_{\rm coll} = v_{\rm rel} \\ 0 & \sigma_{\rm coll} > v_{\rm rel}, \end{cases}$$

The first interaction term is

$$\left(\frac{\delta\rho_\star}{\delta {\rm t}}\right)_{\rm coll} = -\rho_\star\frac{{\rm f_c}}{{\rm t_{coll}}}\left[1-{\rm erf}\left(\frac{\sigma_{\rm coll}}{\sqrt{6}\sigma_{\rm r}}\right)\right]\left[1-{\rm erf}\left(\frac{\sigma_{\rm coll}}{\sqrt{6}\sigma_{\rm t}}\right)\right]^2 \tag{2.30}$$

which, for simplification, we re-call like this

$$\left(\frac{\delta\rho_\star}{\delta {\rm t}}\right)_{\rm coll} \equiv -\rho_\star {\rm X_{coll}}. \tag{2.31}$$

Since the evolution of the system that we are studying can be regarded as stationary, we introduce for each equation the "logarithmic variables" in order to study the evolution at long-term. In the other hand, if the system happens to have quick changes, we should use the "non-logarithmic" version of the equations. For this reason we will write at the end of each subsection the equation in terms of the logarithmic variables.

In the case of the equation of continuity, we develop it and divide it by $\rho_\star$ because we are looking for the logarithm of the stars density, $\partial\ln\rho_\star/\partial t = (1/\rho_\star)\partial\rho_\star/\partial t$. The result is:

$$\frac{\partial\ln\rho_\star}{\partial t}+\frac{\partial u_\star}{\partial r}+u_\star\frac{\partial\ln\rho_\star}{\partial r}+\frac{2u_\star}{r} = \frac{1}{\rho_\star}\left(\frac{\delta\rho_\star}{\delta {\rm t}}\right)_{\rm coll}+\frac{1}{\rho_\star}\left(\frac{\delta\rho_\star}{\delta {\rm t}}\right)_{\rm lc} \tag{2.32}$$

**Momentum balance**

The second equation in Eq. (2.22) has the following star interaction terms:

$$\frac{\partial u_\star}{\partial t}+u_\star\frac{\partial u_\star}{\partial r}+\frac{GM_{\rm r}}{r^2}+\frac{1}{\rho_\star}\frac{\partial p_{\rm r}}{\partial r}+2\frac{p_{\rm r}-p_{\rm t}}{\rho_\star r} = \left(\frac{\delta u_\star}{\delta t}\right)_{\rm drag} \tag{2.33}$$

The interaction term is due to the decelerating force at which stars that move inside the gas are subject to. As we shall see, an estimate for the force is given by Eq. (4.6). Explicitely, it is

$$\left(\frac{\delta u_\star}{\delta t}\right)_{\rm drag} = -X_{\rm drag}\frac{1}{\rho_\star}(u_\star - u_{\rm g}) \tag{2.34}$$

where we have introduced the following definition:

$$X_{\rm drag} \equiv -C_D\frac{\pi r_\star^2}{m_\star}\rho_\star\rho_{\rm g}\sigma_{\rm tot}, \tag{2.35}$$

with $\sigma_{\rm tot}^2 = \sigma_{\rm r}^2 + \sigma_{\rm t}^2 + (u_\star - u_{\rm g})^2$

To the end of the calculation of the logarithmic variable version of the equation, we multiply Eq. (2.33) by $\rho_\star r/p_{\rm r}$:

$$\frac{\rho_\star r}{p_{\rm r}}\left(\frac{\partial u_\star}{\partial t} + u_\star\right) + \frac{GM_{\rm r}}{rp_{\rm r}}\rho_\star + \frac{\partial \ln p_{\rm r}}{\partial \ln r} + 2(1 - \frac{p_{\rm t}}{p_{\rm r}}) = -X_{\rm drag}\frac{r}{p_{\rm r}}(u_\star - u_{\rm g}) \tag{2.36}$$

### Radial energy equation

As regards the last but one equation, the interaction terms are:

$$\frac{\partial p_{\rm r}}{\partial t} + \frac{1}{r^2}\frac{\partial}{\partial r}(r^2 u_\star p_{\rm r}) + 2p_{\rm r}\frac{\partial u_\star}{\partial r} + \frac{4}{5}\frac{(2p_{\rm r} - p_{\rm t})}{t_{\rm relax}} + \frac{1}{r^2}\frac{\partial}{\partial r}(r^2 F_{\rm r}) - \frac{2F_{\rm t}}{r} =$$

$$\left(\frac{\delta p_{\rm r}}{\delta t}\right)_{\rm drag} + \left(\frac{\delta p_{\rm r}}{\delta t}\right)_{\rm coll}, \tag{2.37}$$

where

$$\left(\frac{\delta p_{\rm r}}{\delta t}\right)_{\rm drag} = -2X_{\rm drag}\sigma_{\rm r}^2, \left(\frac{\delta p_{\rm r}}{\delta t}\right)_{\rm coll} = -X_{\rm coll}\rho_\star\tilde{\sigma}_{\rm r}{}^2\varepsilon. \tag{2.38}$$

In order to determine $\varepsilon$ we introduce the ratio $k$ of kinetic energy of the remaining mass after the encounter over its initial value (before the encounter); $k$ is a measure of the inelasticity of the collision: for $k = 1$ we have the minimal inelasticity, just the kinetic energy of the liberated mass fraction is dissipated, whereas if $k < 1$ a surplus amount of stellar kinetic energy is dissipated during the collision (tidal interactions and excitation of stellar oscillations). If we calculate the energy loss in the stellar system per unit volume as a function of $k$ we obtain

$$\varepsilon = f_{\rm c}^{-1}[1 - k(1 - f_{\rm c})]. \tag{2.39}$$

We divide by $p_r$ so that we get the logarithmic variable version of the equation. We make also the

following substitution:

$$\begin{aligned} F_{\rm r} = &\quad 3p_{\rm r}v_{\rm r} \\ F_{\rm t} = &\quad 2p_{\rm t}v_{\rm t} \end{aligned} \tag{2.40}$$

The resulting equation is

$$\frac{\partial \ln p_{\rm r}}{\partial t} + (u_\star + 3v_{\rm r})\frac{\partial \ln p_{\rm r}}{\partial r} + 3\left(\frac{\partial u_\star}{\partial r} + \frac{\partial v_{\rm r}}{\partial r}\right) + \frac{2}{r}\left(u_\star + 3v_{\rm r} - 2v_{\rm t}\frac{p_{\rm t}}{p_{\rm r}}\right) + \frac{4}{5}\frac{2-\frac{p_{\rm t}}{p_{\rm r}}}{t_{\rm relax}} = \frac{1}{p_{\rm r}}\left(\frac{\delta p_{\rm r}}{\delta t}\right)_{\rm drag} + \frac{1}{p_{\rm r}}\left(\frac{\delta p_{\rm r}}{\delta t}\right)_{\rm coll} \tag{2.41}$$

**Tangential energy equation**

To conclude the set of equations of the star component with the interaction terms, we have the following equation:

$$\frac{\partial p_{\rm t}}{\partial t} + \frac{1}{r^2}\frac{\partial}{\partial r}(r^2 u_\star p_{\rm t}) + 2\frac{p_{\rm t}u_\star}{r} - \frac{4}{5}\frac{(2p_{\rm r} - p_{\rm t})}{t_{\rm relax}} + \frac{1}{r^2}\frac{\partial}{\partial r}(r^2 F_{\rm t}) + \frac{2F_{\rm t}}{r} = \left(\frac{\delta p_{\rm t}}{\delta t}\right)_{\rm drag} + \left(\frac{\delta p_{\rm t}}{\delta t}\right)_{\rm coll}, \tag{2.42}$$

where

$$\left(\frac{\delta p_{\rm t}}{\delta t}\right)_{\rm drag} = -2X_{\rm drag}\sigma_{\rm t}^2, \ \left(\frac{\delta p_{\rm t}}{\delta t}\right)_{\rm coll} = -X_{\rm coll}\rho_\star \tilde{\sigma_{\rm t}}^2 \varepsilon. \tag{2.43}$$

We follow the same path like in the last case and so we get the following logarithmic variable equation:

$$\frac{\partial \ln p_{\rm t}}{\partial t} + (u_\star + 2v_{\rm t})\frac{\partial \ln p_{\rm t}}{\partial r} + \frac{\partial}{\partial r}(u_\star + 2v_{\rm t}) + \frac{4}{r}(u_\star + 2v_{\rm t}) - \frac{4}{5}\frac{2\frac{p_{\rm r}}{p_{\rm t}} - 1}{t_{\rm relax}} = \frac{1}{p_{\rm t}}\left(\frac{\delta p_{\rm t}}{\delta t}\right)_{\rm drag} + \frac{1}{p_{\rm t}}\left(\frac{\delta p_{\rm t}}{\delta t}\right)_{\rm coll} \tag{2.44}$$

### 2.5.2 The gaseous component

In this section we give the set of equations corresponding to the gaseous component as for their right hand interaction terms.

**Equation of continuity**

For the *SMS* the equation of continuity looks as follows:

$$\frac{\partial \rho_{\rm g}}{\partial t} + \frac{1}{\rm r^2}\frac{\partial}{\partial r}({\rm r}^2 \rho_{\rm g} u_{\rm g}) = \left(\frac{\delta \rho_{\rm g}}{\delta t}\right)_{\rm coll} \tag{2.45}$$

where, for the mass conservation, we have that, obviously,

$$\left(\frac{\delta\rho_{\rm g}}{\delta t}\right)_{\rm coll} = -\left(\frac{\delta\rho_{\star}}{\delta t}\right)_{\rm coll} \tag{2.46}$$

We follow the same procedure as for the star continuity equation to get the equation in terms of the logarithmic variables:

$$\frac{\partial \ln\rho_{\rm g}}{\partial t} + \frac{\partial u_{\rm g}}{\partial r} + u_{\rm g}\frac{\partial \ln\rho_{\rm g}}{\partial r} + \frac{2u_{\rm g}}{r} = \frac{1}{\rho_{\rm g}}\left(\frac{\delta\rho_{\rm g}}{\delta {\rm t}}\right)_{\rm coll} \tag{2.47}$$

The interaction term is in this case

$$\frac{1}{\rho_{\rm g}}\left(\frac{\delta\rho_{\rm g}}{\delta {\rm t}}\right) = \frac{1}{\rho_{\rm g}}\left(-\frac{\delta\rho_{\star}}{\delta {\rm t}}\right) = -\frac{\rho_{\star}}{\rho_{\rm g}}X_{\rm coll} \tag{2.48}$$

**Momentum balance**

We modify equation number (2.9) of Langbein et al. (1990) in the following way:

$$\frac{\partial(\rho_{\rm g}u_{\rm g})}{\partial t} = u_{\rm g}\frac{\partial\rho_{\rm g}}{\partial t} + \rho_{\rm g}\frac{\partial u_{\rm g}}{\partial t}; \tag{2.49}$$

we substitute this equality in their equation, divide by $\rho_{\rm g}$ ($u_{\rm g}$ is the variable in our code) and make use of the equation of continuity for the gas component. Thus, we get the following expression:

$$\frac{\partial u_{\rm g}}{\partial t} + u_{\rm g}\frac{\partial u_{\rm g}}{\partial r} + \frac{GM_{\rm r}}{r^2} + \frac{1}{\rho_{\rm g}}\frac{\partial p_{\rm r}}{\partial r} - \frac{4\pi}{c}\kappa_{\rm ext}H = \left(\frac{\delta u_{\rm g}}{\delta t}\right)_{\rm coll} \tag{2.50}$$

To get the interaction term we use the mass and momentum conservation:

$$\left(\frac{\delta\rho_{\rm g}}{\delta t}\right)_{\rm coll} + \left(\frac{\delta\rho_{\star}}{\delta t}\right)_{\rm coll} = 0$$

$$\left(\frac{\delta(\rho_{\rm g}u_{\rm g})}{\delta t}\right)_{\rm coll} + \left(\frac{\delta(\rho_{\star}u_{\star})}{\delta t}\right)_{\rm coll} = 0. \tag{2.51}$$

We know that

$$\left(\frac{\delta u_{\star}}{\delta t}\right)_{\rm coll} = 0, \tag{2.52}$$

thus,

$$\left(\frac{\delta(\rho_{\rm g}u_{\rm g})}{\delta t}\right)_{\rm coll} = u_{\star}\rho_{\star}X_{\rm coll} = \rho_{\rm g}\left(\frac{\delta u_{\rm g}}{\delta t}\right)_{\rm coll} + u_{\rm g}X_{\rm coll}\rho_{\star}. \tag{2.53}$$

Therefore, the resulting interaction term is

$$\left(\frac{\delta u_{\rm g}}{\delta t}\right)_{\rm coll} = \frac{\rho_{\star}}{\rho_{\rm g}}X_{\rm coll}(u_{\star} - u_{\rm g}) \tag{2.54}$$

In the case of the stellar system

$$F = \frac{1}{2}(F_{\rm r} + F_{\rm t}) = \frac{5}{2}\rho_\star v_\star \tag{2.55}$$

By analogy, we now introduce $F_{\rm rad}$ in this way

$$\frac{F_{\rm rad}}{4\pi} = H = \frac{5}{2}p_{\rm g}v_{\rm g}, \tag{2.56}$$

where $v_{\rm g}$ is per gas particle.

$$v_{\rm g} = \frac{2}{5}\frac{H}{p_{\rm g}} \tag{2.57}$$

As means to write the equation in its "logarithmic variable version", we multiply the equation by $\rho_{\rm g} r/p_{\rm g}$, as we did for the corresponding momentum balance star equation and replace $H$ by $5/2 p_{\rm g} v_{\rm g}$,

$$\frac{\rho_{\rm g} r}{p_{\rm g}}\left(\frac{\partial u_{\rm g}}{\partial t} + u_{\rm g}\frac{\partial u_{\rm g}}{\partial r}\right) + \frac{GM_{\rm r}}{r p_{\rm g}}\rho_{\rm g} + \frac{\partial \ln p_{\rm g}}{\partial \ln r} - \frac{5}{2}\frac{\kappa_{\rm ext}}{c}\rho_{\rm g} r v_{\rm g} = \frac{r}{p_{\rm g}}\rho_\star X_{\rm coll}(u_\star - u_{\rm g}) \tag{2.58}$$

**Radiation transfer**

We extend here and improve the work done by Langbein et al. (1990) by resorting to a more detailed description of the radiation transfer (Castor, 1972).
Consider a radiation field; we place a surface element $d\sigma$ with a surface normal **n**, see Fig. (2.1); the radiation energy which passes through $d\sigma$ per unit time at angle $\theta$ to **n** within a small range of solid angle $d\omega$ given by the directional angles $\theta$ and $\phi$ is

$$dE = I_\nu(\theta,\phi)\mu d\nu d\sigma d\omega \tag{2.59}$$

where $\mu = \cos\theta$.
The radiation intensity $I_\nu(\theta,\phi)$ is defined as the amount of energy that passes through a surface normal to the direction ($\theta$,$\phi$) per unit solid angle (1 steradian) and unit frequency range (1 Hz) in one second. The intensity of the total radiation is given by integrating over all frequencies,

$$I = \int_0^\infty I_\nu d\nu \tag{2.60}$$

The three radiation moments (the moments of order zero, one and two) are defined by:

$$\begin{aligned} J = &\int_0^\infty J_\nu d\nu = \int_0^\infty d\nu \frac{1}{2}\int_{-1}^{+1} I_\nu d\mu \\ H = &\int_0^\infty H_\nu d\nu = \int_0^\infty d\nu \frac{1}{2}\int_{-1}^{+1} I_\nu \mu d\mu \\ K = &\int_0^\infty K_\nu d\nu = \int_0^\infty d\nu \frac{1}{2}\int_{-1}^{+1} I_\nu \mu^2 d\mu, \end{aligned} \tag{2.61}$$

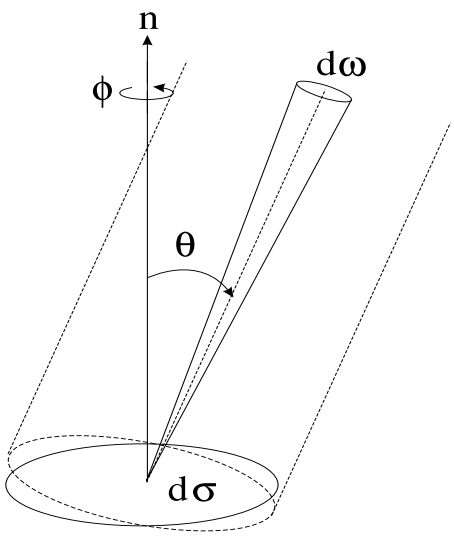


Fig. 2.1: Radiation intensity definition

The moment of order zero is related to the density of energy of the field of radiation $E_{\rm rad}$, the moment of order one to the flux of radiation $F_{\rm rad}$ and the moment of order one to the radiation pressure $p_{\rm rad}$,

$$\begin{aligned} E_{\rm rad} &= \frac{4\pi}{c} J \\ F_{\rm rad} &= 4\pi H \\ p_{\rm rad} &= \frac{4\pi}{c} K \end{aligned} \tag{2.62}$$

The transfer of radiation in a spherically symmetric moving medium is considered taking into account the contributions which are of the order of the flow velocity divided by the velocity of light; we include also the variation from the centre up to the atmosphere of the Eddington factor $f_{\rm Edd} = K/J$, where $K$ and $J$ are the radiation moments; $f_{\rm Edd}$ is obtained from a numerical solution of the equation of radiation transfer in spherical geometry Yorke (1980). We get the radiation transfer equations by re-writing the frequency-integrated moment equations from Castor (1972):

$$\frac{1}{c}\frac{\partial J}{\partial t} + \frac{\partial H}{\partial r} + \frac{2H}{r} - \frac{J(3f_{\rm Edd}-1)}{cr} u_{\rm g} - \frac{J(1+f_{\rm Edd})}{c}\frac{\partial \ln \rho_{\rm g}}{\partial t} = \kappa_{\rm abs}(B-J) \tag{2.63}$$

$$\frac{1}{c}\frac{\partial H}{\partial t}+\frac{\partial(Jf_{\rm Edd})}{\partial r}+\frac{J(3f_{\rm Edd}-1)}{r}-\frac{2u_{\rm g}}{cr}H-\frac{2}{c}\frac{\partial\ln\rho_{\rm g}}{\partial t}H= -\kappa_{\rm ext}\rho_{\rm g}H \tag{2.64}$$

In the equations $\kappa_{\rm abs}$ and $\kappa_{\rm ext}$ are the absorption and extinction coefficients per unit mass

$$\kappa_{\rm abs}=\frac{\rho_{\rm g}\Lambda(T)}{B},\ \kappa_{\rm ext}=\rho_{\rm g}(\kappa_{\rm abs}+\kappa_{\rm scatt}), \tag{2.65}$$

$\Lambda(T)$ is the cooling function, $B$ the Planck function and $\kappa_{\rm scatt}$ the scattering coefficient per unit mass. We have made use of $\partial M_{\rm r}/\partial r=4\pi^2\rho$, $f_{\rm Edd}=K/J$, and the Kirchhoff's law, $B_\nu=j_\nu/\kappa_\nu$ ($j_\nu$ is the emission coefficient), so that the right-hand terms in Castor (1972) are the corresponding given here.
We now look for the logarithmic variable version of both equations; for this aim, we divide Eq. (2.63) by $J$ and multiply Eq. (2.64) by $2c/(5p_{\rm g}v_{\rm g})$,

$$\frac{1}{c}\frac{\partial\ln J}{\partial t}+\frac{5}{2J}\frac{\partial}{\partial r}(v_{\rm g}p_{\rm g})+\frac{5}{Jr}p_{\rm g}v_{\rm g}-\frac{3f_{\rm Edd}-1}{cr}u_{\rm g}-(1+f_{\rm Edd}) \frac{1}{c}\frac{\partial\ln\rho_{\rm g}}{\partial t}=\frac{\kappa_{\rm abs}}{J}(B-J) \tag{2.66}$$

$$\frac{\partial\ln v_{\rm g}}{\partial t}+\frac{\partial\ln p_{\rm g}}{\partial t}+\frac{2c}{5}\frac{1}{p_{\rm g}v_{\rm g}}\frac{\partial(Jf_{\rm Edd})}{\partial r}+\frac{2c}{5}\frac{3f_{\rm Edd}-1}{rp_{\rm g}v_{\rm g}}J-\frac{2u_{\rm g}}{r} -2\frac{\partial\ln\rho_{\rm g}}{\partial t}=-c\kappa_{\rm ext}\rho_{\rm g} \tag{2.67}$$

Where we have substituted $H=5p_{\rm g}v_{\rm g}/2$.

### Thermal energy conservation

It is enlightening to construct from Eqs. (2.22) an equation for the energy per volume unit $e=(p_{\rm r}+2p_{\rm t})/2$ which, in the case of an isotropic gas ($p_{\rm r}=p_{\rm t}$) is $e=3p/2$. For this aim we take, for instance, equation (2.37) and in the term $2p_{\rm r}\partial u_\star/\partial r$ we include now a source for radiation pressure, $2(p_{\rm r}+p_{\rm rad})\partial u_\star/\partial r$ and we divide everything by $e$ so that we get the logarithmic variables. The resulting equation is

$$\frac{\partial\ln e}{\partial t}+(u_{\rm g}+3v_{\rm g})\frac{\partial\ln e}{\partial r}+\frac{2}{r}(u_{\rm g}+v_{\rm g})=\frac{1}{e}\left(\frac{\delta e}{\delta t}\right)_{\rm drag}+\frac{1}{e}\left(\frac{\delta e}{\delta t}\right)_{\rm coll} \tag{2.68}$$

The interaction terms for this equation are

$$\left(\frac{\delta e}{\delta t}\right)_{\rm drag}=X_{\rm drag}(\sigma_{\rm r}^2+\sigma_{\rm t}^2+(u_\star-u_{\rm g})^2) \tag{2.69}$$

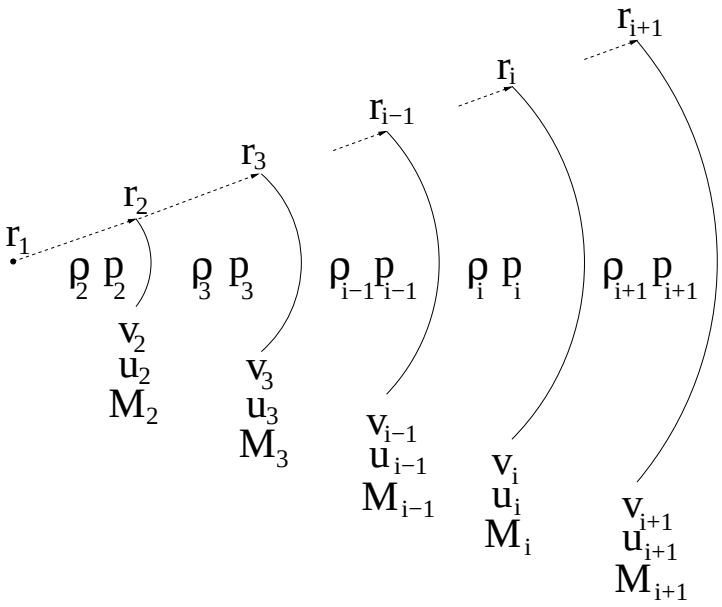


Fig. 2.2: Representation of the logarithmic radial mesh used in the code. With $v$, $p$ we represent both, the radial and tangential components of the velocity and pressure.

$$\left(\frac{\delta e}{\delta t}\right)_{\rm coll} = \frac{1}{2} X_{\rm coll} \rho_\star ((\sigma_{\rm r}+\sigma_{\rm t})^2 \varepsilon + (u_\star - u_{\rm g})^2 - \xi\,\sigma_{\rm coll}^2) \tag{2.70}$$

**Mass conservation**

The mass conservation is guaranteed by

$$\frac{3}{4\pi}\frac{\partial M_{\rm r}}{\partial r^3} = \rho_\star + \rho_{\rm g} \tag{2.71}$$

## 2.6 A mathematical view of our approach

In this subsection, we explain briefly how the gaseous model is solved numerically. We concentrate on aspects of the method not exposed in previous work. This description is therefore complementary to Sec. 2.2 of Giersz and Spurzem (1994). The algorithm used is a partially implicit Newton-Raphson-Henyey iterative scheme (Henyey et al. 1959, see also Kippenhahn and Weigert 1994, Sec. 11.2).
Putting aside the bounding conditions, the set of equations to be solved are Eqs. 2.22 to 2.25. In practice, however, the equations are rewritten using the logarithm of all positive quantities as dependant functions. As explained in Giersz and Spurzem (1994), this greatly improves energy conservation. Formally, one

may write this system as follows

$$\begin{aligned} \frac{\partial x^{(i)}}{\partial t} + f^{(i)}\left(\left\{x^{(j)}, \frac{\partial x^{(j)}}{\partial r}\right\}_{j=1}^{N_{\rm eq}}\right) = 0 \quad \text{for } i = 1\ldots 4 \\ f^{(i)}\left(\left\{x^{(j)}, \frac{\partial x^{(j)}}{\partial r}\right\}_{j=1}^{N_{\rm eq}}\right) = 0 \quad \text{for } i = 5\ldots N_{\rm eq} \end{aligned} \tag{2.72}$$

where the $x^{(i)}$ are the local quantities defining the state of the cluster, i.e.

$$\begin{aligned} \underline{x} &\equiv \left\{x^{(1)}, x^{(2)}, \ldots x^{(N_{\rm eq})}\right\} \\ &\equiv \{\log\rho, u, \log p_{\rm r}, \log p_{\rm t}, \log M_{\rm r}, v_{\rm r}-u, v_{\rm t}-u\}, \end{aligned} \tag{2.73}$$

with $N_{\rm eq} = 7$ in the present application.
To be solved numerically, this set of coupled partial differential equations have to be discretised according to time and radius. Let us first consider time stepping. Let $\Delta t$ be the time step. Assume we know the solution $\underline{x}(t-\Delta t)$ at time $t-\Delta t$ and want to compute $\underline{x}(t)$. For the sake of numerical stability, a partially implicit scheme is used. We adopt the shorthand notations $x^{(i)} \equiv x^{(i)}(t)$ and $y^{(i)} \equiv x^{(i)}(t-\Delta t)$. Time derivation is replaced by finite differences,

$$\frac{\partial x^{(i)}}{\partial t} \to \Delta t^{-1}(x^{(i)} - y^{(i)}). \tag{2.74}$$

In the terms $f^{(i)}$, we replace the $x^{(j)}$ by $\tilde{x}^{(j)}$ which are values intermediate between $y^{(j)}$ and $x^{(j)}$, $\tilde{x}^{(j)} = \zeta x^{(j)} + (1-\zeta)y^{(j)}$, with $\zeta = 0.55$ for stability purpose (Giersz and Spurzem, 1994).
Spatial discretisation is done by defining all quantities (at a given time) on a radial mesh, $\{r_1, r_2, \ldots r_{N_{\rm r}}\}$ with $r_1 = 0$ and $r_{N_{\rm r}} = r_{\rm max}$. A staggered mesh is implemented. While values of $r$, $u$, $v_{\rm t}$, $v_{\rm r}$ and $M_{\rm r}$ are defined at the boundaries of the mesh cells, $\rho$, $p_{\rm t}$ and $p_{\rm r}$ are defined at the centre of each cell, see Fig. 2.2. When the value of a "boundary" quantity is needed at the centre of a cell, or vice-versa, one resort to simple averaging, i.e. $\hat{b}_k = 0.5(b_{k-1} + b_k)$, $\hat{c}_k = 0.5(c_k + c_{k+1})$, if $b$ and $c$ are is border- and centre-defined quantities, and $\hat{b}$, $\hat{c}$ their centre- and border-interpolations, respectively. For all runs presented here, $N_{\rm r} = 300$ and the points $r_2$ to $r_{\rm max}$ are logarithmically equidistant with $r_{\rm max} = 10^4\,$pc and $r_2 \simeq 1.7\times10^{-6}\,$pc. Let us adopt the notation $x_k^{(j)}$ for the value of $x^{(j)}$ at position $r_k$ (or $\hat{r}_k$) and $\Delta r_k \equiv r_k - r_{k-1}$. Then, radial derivatives in the terms $f^{(i)}$ are approximated by finite differences,

$$\frac{\partial x^{(j)}}{\partial r} \to \frac{\tilde{x}_k^{(j)} - \tilde{x}_{k-1}^{(j)}}{\Delta r_k} \tag{2.75}$$

if the derivative has to be evaluated at a point where $x_k$ is defined (centre or border of a cell), or

$$\frac{\partial x^{(j)}}{\partial r} \rightarrow \frac{\hat{\tilde{x}}_k^{(j)} - \hat{\tilde{x}}_{k-1}^{(j)}}{\Delta r_k} = \frac{\tilde{x}_{k+1}^{(j)} - \tilde{x}_{k-1}^{(j)}}{2\Delta r_k} \tag{2.76}$$

otherwise. As an exception we use upstream differencing in $\partial u/\partial r$ for the second equation in set 2.22, i.e. the difference quotient is displaced by half a mesh point upstream to improve stability.
By making the substitutions for $\partial x^{(j)}/\partial t$ and $\partial x^{(j)}/\partial r$ in the set of differential equations 2.72, one obtains, at each mesh point $r_k$, a set of $N_{\mathrm{eq}}$ non-linear algebraic equations linking the new values to be determined, $\underline{x}_{k-1}$ and $\underline{x}_k$, to the "old" ones, $\underline{y}_{k-1}$ and $\underline{y}_k$, which are known,

$$\begin{gathered} \mathscr{F}_k^{(i)}\left(\underline{x}_{k-1}, \underline{x}_k | \underline{y}_{k-1}, \underline{y}_k\right) = 0 \\ i = 1 \ldots N_{\mathrm{eq}},\ k = 1 \ldots N_{\mathrm{r}}. \end{gathered} \tag{2.77}$$

Note that the structure of the equations is the same at all mesh points, except $k = 1$ and $k = N_{\mathrm{r}}$. In particular, terms $k-1$ do not appear in $\mathscr{F}_1^{(i)}$. Also, one has to keep in mind that only the $\underline{x}_{k-1}$ and $\underline{x}_k$ are unknown; the $\underline{y}_{k-1}$ and $\underline{y}_k$ play the role of fixed parameters in these equation (as do the $\Delta r_k$). If one defines a $(N_{\mathrm{eq}} \times N_{\mathrm{r}})$-dimension vector $\mathscr{X}^*$ whose component $N_{\mathrm{eq}}(k-1)+i$ is $x_k^{(i)}$, one can write the system of $N_{\mathrm{eq}} \times N_{\mathrm{r}}$ equations as $\mathscr{F}^*(\mathscr{X}^*) = 0$, i.e.

$$\mathscr{F}^*(\mathscr{X}^*) \equiv \begin{pmatrix} \mathscr{F}_1^{(1)} \\ \mathscr{F}_1^{(2)} \\ \vdots \\ \mathscr{F}_1^{(N_{\mathrm{eq}})} \\ \mathscr{F}_2^{(1)} \\ \vdots \\ \mathscr{F}_2^{(N_{\mathrm{eq}})} \\ \vdots \\ \mathscr{F}_{N_{\mathrm{r}}}^{(1)} \\ \vdots \\ \mathscr{F}_{N_{\mathrm{r}}}^{(N_{\mathrm{eq}})} \end{pmatrix} = \begin{pmatrix} 0 \\ \vdots \\ 0 \end{pmatrix} \text{ with } \mathscr{X}^* \equiv \begin{pmatrix} x_1^{(1)} \\ x_1^{(2)} \\ \vdots \\ x_1^{(N_{\mathrm{eq}})} \\ x_2^{(1)} \\ \vdots \\ x_2^{(N_{\mathrm{eq}})} \\ \vdots \\ x_{N_{\mathrm{r}}}^{(1)} \\ \vdots \\ x_{N_{\mathrm{r}}}^{(N_{\mathrm{eq}})} \end{pmatrix}. \tag{2.78}$$

The system is solved iteratively using Newton-Raphson scheme. If ${\mathscr{X}^*}_{[m]}$ is the approximation to the solution of Eq. 2.78 after iteration $m$, with ${\mathscr{F}^*}_{[m]} \equiv \mathscr{F}^*({\mathscr{X}^*}_{[m]}) \neq 0$, the solution is refined through the relation

$${\mathscr{X}^*}_{[m+1]} = {\mathscr{X}^*}_{[m]} - \left(\frac{\partial \mathscr{F}^*}{\partial \mathscr{X}^*}\right)^{-1} {\mathscr{F}^*}_{[m]} \tag{2.79}$$

where $(\partial\mathscr{F}^*/\partial\mathscr{X}^*)^{-1}$ is the inverse of the matrix of derivatives. The latter, of dimension $(N_{\rm eq}N_{\rm r})\times(N_{\rm eq}N_{\rm r})$, has the following structure

$$\frac{\partial\mathscr{F}^*}{\partial\mathscr{X}^*}=\begin{pmatrix}
\blacksquare & \square_+ & & & & & \\
\square_- & \blacksquare & \square_+ & & & & \\
 & \square_- & \blacksquare & \square_+ & & & \\
 & & \ddots & \ddots & & & \\
 & & \square_{-k} & \blacksquare_k & \square_{+k} & & \\
 & & & \ddots & \ddots & & \\
 & & & \square_- & \blacksquare & \square_+ & \\
 & & & & \square_- & \blacksquare &
\end{pmatrix}. \tag{2.80}$$

In this diagram, each square is a $N_{\rm eq}\times N_{\rm eq}$ sub-matrix. For $2\leq k\leq N_{\rm r}-1$, lines $N_{\rm eq}k-6$ to $N_{\rm eq}k$ of $\partial\mathscr{F}^*/\partial\mathscr{X}^*$ are composed of a group of 3 such $N_{\rm eq}\times N_{\rm eq}$ matrices, $\square_{-k},\blacksquare_k,\square_{+k}$ that span columns $N_{\rm eq}k-13$ to $N_{\rm eq}k+N_{\rm eq}$, while the rest is composed of zeros,

$$\begin{aligned}
\blacksquare_k &= \begin{pmatrix}
\frac{\partial\mathscr{F}_k^{(1)}}{\partial x_k^{(1)}} & \frac{\partial\mathscr{F}_k^{(1)}}{\partial x_k^{(2)}} & \cdots & \frac{\partial\mathscr{F}_k^{(1)}}{\partial x_k^{(N_{\rm eq})}} \\
\vdots & & & \vdots \\
\frac{\partial\mathscr{F}_k^{(N_{\rm eq})}}{\partial x_k^{(1)}} & \frac{\partial\mathscr{F}_k^{(N_{\rm eq})}}{\partial x_k^{(2)}} & \cdots & \frac{\partial\mathscr{F}_k^{(N_{\rm eq})}}{\partial x_k^{(N_{\rm eq})}}
\end{pmatrix} \\
\square_{\pm k} &= \begin{pmatrix}
\frac{\partial\mathscr{F}_k^{(1)}}{\partial x_{k\pm1}^{(1)}} & \frac{\partial\mathscr{F}_k^{(1)}}{\partial x_{k\pm1}^{(2)}} & \cdots & \frac{\partial\mathscr{F}_k^{(1)}}{\partial x_{k\pm1}^{(N_{\rm eq})}} \\
\vdots & & & \vdots \\
\frac{\partial\mathscr{F}_k^{(N_{\rm eq})}}{\partial x_{k\pm1}^{(1)}} & \frac{\partial\mathscr{F}_k^{(N_{\rm eq})}}{\partial x_{k\pm1}^{(2)}} & \cdots & \frac{\partial\mathscr{F}_k^{(N_{\rm eq})}}{\partial x_{k\pm1}^{(N_{\rm eq})}}
\end{pmatrix}.
\end{aligned} \tag{2.81}$$

We can see this more explicitely,

$$\frac{\partial \mathscr{F}^*}{\partial \mathscr{X}^*} = \begin{pmatrix}
\frac{\partial \mathscr{F}_1^1}{\partial x_1^1} & \cdots & \frac{\partial \mathscr{F}_1^1}{\partial x_1^{N_{\rm eq}}} & \frac{\partial \mathscr{F}_1^1}{\partial x_2^1} & \cdots & \frac{\partial \mathscr{F}_1^1}{\partial x_2^{N_{\rm eq}}} & 0 & \cdots & & & & 0 \\
\vdots & & & & & \vdots & \vdots & & & & & \vdots \\
\frac{\partial \mathscr{F}_1^{N_{\rm eq}}}{\partial x_1^1} & \cdots & \frac{\partial \mathscr{F}_1^{N_{\rm eq}}}{\partial x_1^{N_{\rm eq}}} & \frac{\partial \mathscr{F}_1^{N_{\rm eq}}}{\partial x_2^1} & \cdots & \frac{\partial \mathscr{F}_1^{N_{\rm eq}}}{\partial x_2^{N_{\rm eq}}} & 0 & \cdots & & & & 0 \\
\frac{\partial \mathscr{F}_2^1}{\partial x_1^1} & \cdots & \frac{\partial \mathscr{F}_2^1}{\partial x_1^{N_{\rm eq}}} & \frac{\partial \mathscr{F}_2^1}{\partial x_2^1} & \cdots & \frac{\partial \mathscr{F}_2^1}{\partial x_2^{N_{\rm eq}}} & \frac{\partial \mathscr{F}_2^1}{\partial x_3^1} & \cdots & \frac{\partial \mathscr{F}_2^1}{\partial x_3^{N_{\rm eq}}} & 0 & \cdots & 0 \\
\vdots & & & & & & & & \vdots & \vdots & & \vdots \\
\frac{\partial \mathscr{F}_2^{N_{\rm eq}}}{\partial x_1^1} & \cdots & \frac{\partial \mathscr{F}_2^{N_{\rm eq}}}{\partial x_1^{N_{\rm eq}}} & \frac{\partial \mathscr{F}_2^{N_{\rm eq}}}{\partial x_2^1} & \cdots & \frac{\partial \mathscr{F}_2^{N_{\rm eq}}}{\partial x_2^{N_{\rm eq}}} & \frac{\partial \mathscr{F}_2^{N_{\rm eq}}}{\partial x_3^1} & \cdots & \frac{\partial \mathscr{F}_2^1}{\partial x_3^{N_{\rm eq}}} & 0 & \cdots & 0 \\
\cdots & & & & & & & & & & & \\
\cdots & & & & & & & & & & & \\
0 & \cdots & & & 0 & \frac{\partial \mathscr{F}_{N_{\rm r}}^1}{\partial x_{N_{\rm r}-1}^1} & \cdots & \frac{\partial \mathscr{F}_{N_{\rm r}}^1}{\partial x_{N_{\rm r}-1}^{N_{\rm eq}}} & \frac{\partial \mathscr{F}_{N_{\rm r}}^1}{\partial x_{N_{\rm r}}^1} & \cdots & \frac{\partial \mathscr{F}_{N_{\rm r}}^1}{\partial x_{N_{\rm r}}^{N_{\rm eq}}} \\
\vdots & & & & \vdots & \vdots & & & & & & \vdots \\
0 & \cdots & & & 0 & \frac{\partial \mathscr{F}_{N_{\rm r}}^{N_{\rm eq}}}{\partial x_{N_{\rm r}-1}^1} & \cdots & \frac{\partial \mathscr{F}_{N_{\rm r}}^{N_{\rm eq}}}{\partial x_{N_{\rm r}-1}^{N_{\rm eq}}} & \frac{\partial \mathscr{F}_{N_{\rm r}}^{N_{\rm eq}}}{\partial x_{N_{\rm r}}^1} & \cdots & \frac{\partial \mathscr{F}_{N_{\rm r}}^{N_{\rm eq}}}{\partial x_{N_{\rm r}}^{N_{\rm eq}}}
\end{pmatrix}$$

More schematically, to have an overview of the structure,

$$\frac{\partial \mathscr{F}^*}{\partial \mathscr{X}^*} = \left(\begin{array}{c} \\ \\ \\ \\ \\ \\ \\ \\ \\ \\ \\ \end{array}\right.$$

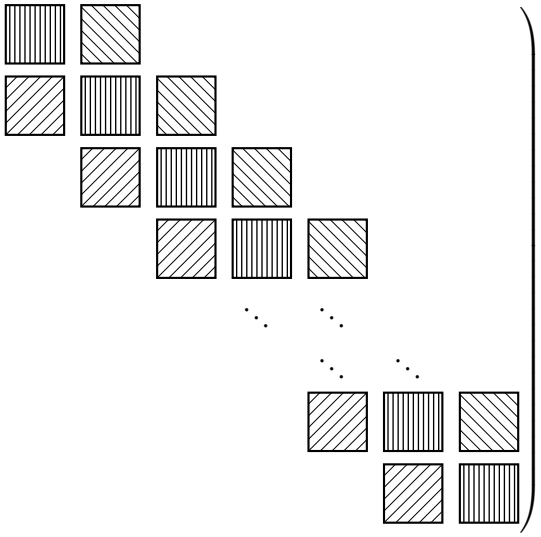

$$\left.\begin{array}{c} \\ \\ \\ \\ \\ \\ \\ \\ \\ \\ \\ \end{array}\right)$$

The Heyney method is a way to take advantage of the special structure of matrix $\partial \mathscr{F}^*/\partial \mathscr{X}^*$ to solve system (2.79) efficiently, with a number of operation scaling like $\mathscr{O}(N_{\rm r})$ rather than $\mathscr{O}(N_{\rm r}^3)$ as would be the case if one uses a general-purpose matrix inversion scheme[4]. Setting $\mathscr{B}^* \equiv -\mathscr{F}^*_{[m]}$ and $\mathscr{W}^* \equiv$

[4]Memory usage is also reduced, scaling like $\mathscr{O}(N_{\rm r})$ rather than $\mathscr{O}(N_{\rm r}^2)$.

${\mathscr{X}^*}_{[m+1]} - {\mathscr{X}^*}_{[m]}$, Eq. (2.79) is equivalent to

$$\left(\frac{\partial \mathscr{F}^*}{\partial \mathscr{X}^*}\right) \mathscr{W}^* = \mathscr{B}^* \tag{2.82}$$

with $\mathscr{W}^*$ the unknown vector. We further decompose vectors $\mathscr{W}^*$ and $\mathscr{B}^*$ into $N_{\text{eq}}$–dimensional sub-vectors, each one representing the values at a given mesh points,

$$\mathscr{W}^* = \begin{pmatrix} \mathscr{W}_1 \\ \mathscr{W}_2 \\ \vdots \\ \mathscr{W}_k \\ \vdots \\ \mathscr{W}_{N_{\text{r}}} \end{pmatrix}. \tag{2.83}$$

Then, the system (2.83) can be written as a set of coupled $N_{\text{eq}}$–dimensional vector equations,

$$\begin{array}{rrrr} & \blacksquare_1 \mathscr{W}_1 & + \square_{+1} \mathscr{W}_2 & = \mathscr{B}_1 \\ \square_{-k} \mathscr{W}_{k-1} & + \blacksquare_k \mathscr{W}_k & + \square_{+k} \mathscr{W}_{k+1} & = \mathscr{B}_k \\ \square_{-N_{\text{r}}} \mathscr{W}_{N_{\text{r}}-1} & + \blacksquare_{N_{\text{r}}} \mathscr{W}_{N_{\text{r}}} & & = \mathscr{B}_{N_{\text{r}}}. \end{array} \tag{2.84}$$

The algorithm operates in two passes. First, going from $k = 1$ to $N_{\text{r}}$, one defines recursively a sequence of $N_{\text{eq}}$–vectors $\mathscr{V}_k$ and $(N_{\text{eq}} \times N_{\text{eq}})$–matrices $\mathfrak{M}_k$ through

$$\begin{aligned} \mathscr{V}_1 &= (\blacksquare_1)^{-1} \mathscr{B}_1 \\ \mathfrak{M}_1 &= (\blacksquare_1)^{-1} \square_{+1} \\ \mathscr{V}_k &= (\blacksquare_k - \square_{-k} \mathfrak{M}_{k-1})^{-1} (\mathscr{B}_k - \square_{-k} \mathscr{V}_{k-1}) \\ \mathfrak{M}_k &= (\blacksquare_k - \square_{-k} \mathfrak{M}_{k-1})^{-1} \square_{+k} \qquad 2 \leq k \leq N_{\text{r}}. \end{aligned} \tag{2.85}$$

$\mathfrak{M}_{N_{\text{r}}}$ is not defined. In the second pass, the values of the unknown $\mathscr{V}_k$ are computed, climbing back from $k = N_{\text{r}}$ to 1, with

$$\begin{aligned} \mathscr{W}_{N_{\text{r}}} &= \mathscr{V}_{N_{\text{r}}} \\ \mathscr{W}_k &= \mathscr{V}_k - \mathfrak{M}_k \mathscr{W}_{k+1} \qquad 1 \leq k \leq N_{\text{r}} - 1. \end{aligned} \tag{2.86}$$

Note that, with this algorithm, only $(N_{\text{eq}} \times N_{\text{eq}})$ matrices have to be inverted. We use Gauss elimination for this purpose because this venerable technique proves to be robust enough to properly deal with the kind of badly conditioned matrices that often appear in this application.

The initial model for the Newton-Raphson algorithm is given by the structure of the cluster at the previous time, ${\mathscr{X}^*}_{[0]}(t) = \mathscr{X}^*(t - \Delta t)$ One iterates until the following convergence criteria are met. Let

us set $\delta x_k^{(i)} \equiv x_k^{(i)}\Big|_{[m+1]} - x_k^{(i)}\Big|_{[m]}$. Then, the condition for logarithmic quantities is

$$\max_{i=1\ldots N_{\rm eq}} \frac{1}{N_{\rm r}} \sum_{k=1\ldots N_{\rm r}} \left(\delta x_k^{(i)}\right)^2 < \varepsilon_1, \tag{2.87}$$

with $\varepsilon_1 = 10^{-6}$. For velocities $(u,\, v_{\rm r} - u,\, v_{\rm t} - u)$, one checks

$$\max_{i=1\ldots N_{\rm eq}} \frac{1}{N_{\rm r}} \sum_{k=1\ldots N_{\rm r}} \left(\frac{\delta x_k^{(i)}}{x_k^{(i)} + \varepsilon_1 w_k}\right)^2 < \varepsilon_2, \tag{2.88}$$

with $\varepsilon_2 = 10^{-3}$ and $w_k = r_k (4\pi G \rho_k)^{1/2}$. Generally, two iterations are sufficient to reach convergence.

## 2.7 Literature of chapter 2


Amaro-Seoane, P. and Spurzem, R. (2001). Gas in the Central Regions of AGN: The Interstellar Medium and Supermassive Gaseous Objects. In *ASP Conf. Ser. 249: The Central Kiloparsec of Starbursts and AGN: The La Palma Connection*, page 731.

Amaro-Seoane, P. and Spurzem, R. (2004). Dense Gas-Star Systems: Evolution of Supermassive Stars. In *In "Carnegie Observatories Astrophysics Series, Vol. 1: Coevolution of Black Holes and Galaxies," ed. L. C. Ho, Pasadena, USA: Carnegie Observatories, 2003*.

Bettwieser, E. and Spurzem, R. (1986). Anisotropy in stellar dynamics. *A&A*, 161:102–112.

Binney, J. and Tremaine, S. (1987). *Galactic Dynamics*. Princeton University Press.

Castor, J. I. (1972). Radiative Transfer in Spherically Symmetric Flows. *apj*, 178:779–792.

Giersz, M. and Spurzem, R. (1994). Comparing direct *n*-body integration with anisotropic gaseous models of star clusters. *MNRAS*, 269:241.

Henyey, L. G., Wilets, L., Böhm, K. H., Lelevier, R., and Levee, R. D. (1959). A Method for Atomic Computation of Stellar Evolution. *ApJ*, 129:628.

Kippenhahn, R. and Weigert, A. (1994). *Stellar Structure and Evolution*. Springer-Verlag Berlin Heidelberg.

Langbein, T., Fricke, K. J., Spurzem, R., and Yorke, H. W. (1990). Interactions between stars and gas in galactic nuclei. *aa*, 227:333–341.

Lin, D. N. C. and Tremaine, S. (1980). A reinvestigation of the standard model for the dynamics of a massive black hole in a globular cluster. *ApJ*, 242:789–798.

Louis, P. D. and Spurzem, R. (1991). Anisotropic gaseous models for the evolution of star clusters. *MNRAS*, 251:408–426.

Lynden-Bell, D. and Eggleton, P. P. (1980). On the consequences of the gravothermal catastrophe. *MNRAS*, 191:483–498.

Rosenbluth, M. N., MacDonald, W. M., and Judd, D. L. (1957). *Phys. Rev. 2nd Ser.*, 107:1.

Spitzer, L., J. and Saslaw, W. C. (1966). On the evolution of galactic nuclei. *ApJ*, 143:400.

Spitzer, L. (1987). *Dynamical evolution of globular clusters*. Princeton University Press.

Spurzem, R., Berczik, P., Hensler, G., Theis, C., Amaro-Seoane, P., Freitag, M., and Just, A. (2003). Physical Processes in Star-Gas Systems. *ArXiv Astrophysics e-prints*.

Yorke, H. W. (1980). Numerical solution of the equation of radiation transfer in spherical geometry. *aa*, 86:286–294.

# Chapter 3

# Super-massive stars

## 3.1 On the nature and peculiarities of a super-massive gaseous object

ARISING from 1962, we find in the literature one of the first proposals on this topic [1]: Some $10^8$ supernovæ were thought to happen in $10^6$ years; since they were also thought to be the normal galactic source of cosmic rays, we would have found the origin for this strong emission. Nonetheless, this was a too strong requirement for Burbidge and Burbidge (1962), who found the argument not convincing. He proposed the idea that one supernova in a tightly packed set of neighbouring stars could trigger explosions in these. If Burbidge and Burbidge (1962) felt satisfied with such an idea, F. Hoyle and W. A. Fowler could not say the same, for they found it not convincing. To fulfil Burbidge's argument the stars should be so close packed together that they would be *physically in contact*. It was impossible for F. Hoyle and W. A. Fowler to withstand the seduction of the simple idea that at the centres of galaxies star-like objects exist with masses of up to $10^8 M_\odot$ (Hoyle and Fowler, 1963). As regards the stability and/or existence of such an object, they "turn a blind eye". Actually, we have to wait one year to find a deep study on this subject by Chandrasekhar.
F. Hoyle and W. A. Fowler developed their argument with the argument that wholly convective stars could "do the job": Consider an ideal gas with radiation pressure:

$$P = P_{\rm gas} + P_{\rm r} = \frac{\Re}{\mu}\rho T + \frac{a}{3}T^4, \tag{3.1}$$

[1] Part of this chapter was used for Just and Amaro-Seoane (2001), Amaro-Seoane et al. (2002) and Just and Amaro-Seoane (2003)

$P$, $\mu$, $\rho$, and $T$ being total pressure, mean molecular weight, density and temperature; $\Re = k/m_u = 8.315 \times 10^7 \mathrm{erg}/(Kg)$ is the universal gas constant, $k = 1.38 \times 10^{-16} \mathrm{erg}/K$ the Boltzmann constant, $m_u = 1$ amu $= 1.66 \times 10^{-24} g$ the atomic gas unit and $a = 7.565 \times 10^{-15} \mathrm{erg}/(\mathrm{cm}^3 K^4)$ the radiation-density constant. We use here the gas constant with a dimension (energy per $K$ and per *unit mass*); in thermodynamics we usually find that it is energy per $K$ and per mole. Because of that, the molecular weight $\mu$ is dimensionless (instead of $[\mu] = \mathrm{mass}/\mathrm{mole}$). Assume that $\beta = \mathrm{P_{gas}}/\mathrm{P}$ is constant throughout the whole star; thus, we can see in $1-\beta = aT^4/(3P)$ that $\beta =$ constant implies the relation $T^4 \sim P$. Therefore,

$$P = \left(\frac{3\Re^4}{a\mu^4}\right)^{1/3} \left(\frac{1-\beta}{\beta^4}\right)^{1/3} \rho^{4/3}, \tag{3.2}$$

which is a polytropic relation with a polytropic index $n = 3$ for constant $\beta$. The polytropic constant

$$\mathrm{K} = \left(\frac{3\Re^4}{a\mu^4}\right)^{1/3} \left(\frac{1-\beta}{\beta^4}\right)^{1/3}, \tag{3.3}$$

is a free parameter since we can choose $\beta$ in the interval $[0,1]$.
Eddington's quartic equation is

$$\frac{1-\beta}{\mu^4\beta^4} = 3.02 \times 10^{-3} \left(\frac{M}{\mathrm{M}_\odot}\right)^2. \tag{3.4}$$

The left-hand side of the equality becomes smaller in the interval $[0,1]$ when $M$ increases. In other words, the radiation pressure becomes more important the larger the stellar mass is. This means that *SMS*s are dominated by the radiation pressure. As a consequence, the adiabatic gradient $\nabla_{\mathrm{ad}}$ is reduced, (particularly $\nabla_{\mathrm{ad}} \to 1/4$ when $\beta \to 0$, see e.g. Kippenhahn and Weigert 1994) and the star becomes convective with $\nabla = \nabla_{\mathrm{ad}}$. This adiabatic structure requires constant specific entropy $s$. Thanks to the first law of thermodynamics, we have that

$$s = \frac{4aT^3}{3\rho}. \tag{3.5}$$

Constant specific entropy means $\rho \sim T^3$ and from the pressure equation we can see that $P \sim \rho$; therefore $P \sim \rho^{4/3}$, which again means that *SMS*s are polytropes with $n = 3$.
The *SMS*s are star polytropes with a free K, which implies that their mass $M$ can be chosen *arbitrarily*. For each mass, $1-\beta/(\mu^4\beta^4)$ can be obtained and then, Eq. (3.3) gives us the corresponding value of K. But if the mass is given, there still exist an infinite number of models for different radius (in spite of the fact that K is already determined by $M$) since K is independent of $R$. With a specific entropy being constant, we have that the adiabatic polytropic constant $\gamma$ is roughly the local adiabatic index $\Gamma = [d(\ln P)/d(\ln\rho)]_s$.
The *SMS* evolves radiating energy and entropy and, in the case of contemplating rotation, losses also angular momentum via mass shedding. Since the pressure is dominated by radiation, the luminosity of

an *SMS* is close to the Eddington limit,

$$\mathscr{L} = L_{\rm Edd} = \frac{4\pi G c \mathscr{M} m_{\rm p}}{\sigma_{\rm Th}} = 3.4\times10^4\Big(\frac{\mathscr{M}}{\rm M_\odot}\Big)L_\odot, \tag{3.6}$$

where $\mathscr{L}$ is the luminosity of the *SMS* , $m_{\rm p}$ the proton mass and $\sigma_{\rm Th}$ the Thomson cross section.

### 3.1.1 Nuclear energy source

The most important nuclear energy source for *SMS*s is hydrogen burning. We can distinguish between two regimes: For temperatures less than $T \equiv 5\times10^8 K$, hydrogen burns on the standard $\beta$-limited CNO cycle (Fowler, 1965). For temperatures greater than the above-mentioned one, Wallace and Woosley (1981) proved that leak out of the $\beta$-limited CNO cycle can be very important, because of the $^{15}O(\alpha,\gamma)^{19}Ne$ reaction. When we are out of the cycle, we have a flow consisting of radiative proton captures and positron decays which builds up toward the iron peak: this is the so-called rp-process. Wallace and Woosley (1981) proved that when this process operates, it has 200 or 300 times the energy generation rate of the $\beta$-limited CNO cycle. Nevertheless, for masses in excess of a few $10^5\rm M_\odot$, nuclear burning is irrelevant prior to the gravitational instability when we compare the nuclear energy generation rate with the photon luminosity (see e.g. Fowler 1966; Zeldovich and Novikov 1971), and electron-positron annihilation are not important (New and Shapiro, 2001); the creation of electron-positron pairs can be neglected for $M \gtrsim 10^4\rm M_\odot$ (i.e., $T \leq T_{\rm crit} \lesssim 2.5\times10^9 K$) (Bond et al., 1984).

### 3.1.2 Instabilities of radiation-dominated stars

The bulk of the *SMS*s is expected to be convective, thus the entropy is roughly constant. For stars in which the specific entropy is nearly constant, the adiabatic polytropic constant is approximately the local adiabatic index (Chandrasekhar, 1939). The evolution of these objects is a rather complicated subject, for these stars have always a pressure averaged adiabatic index of by $4/3$. In order to keep hydrostatic equilibrium, the central temperature must increase as the star mass rises up. The ratio of gas pressure $P_{\rm g}$ to the total pressure $P = P_{\rm r} + P_{\rm gas}$ (where $P_{\rm r}$ is the radiation pressure) for an index $n = 3$ polytrope is

$$\beta = \frac{P_{\rm g}}{P} \approx \frac{4.3}{\mu}\left(\frac{\mathscr{M}}{\rm M_\odot}\right)^{-1/2}, \tag{3.7}$$

where $\mathscr{M}$ is the mass of the *SMS*. For stars with a huge mass like these objects, the gas pressure is a minor perturbation on the total pressure of the star, $P_{\rm g}$ can only be a minute fraction of the total pressure. The condition for hydrostatic equilibrium can be expressed as a variational principle (Chandrasekhar, 1964; Hoyle and Fowler, 1963); the total energy of the star, which is a function of $\mathscr{M}$, entropy and central density is an extremum. We can thus get the equilibrium mass for a given entropy and central density by extremising this total energy. If we employ a low enough central density, the equilibrium energy will be almost zero, because of the $\gamma \sim 4/3$. The *SMS* will quasi-statically contract, radiating away entropy and increasing the central density while the equilibrium energy decreases. Gravity will

have a minimum due to general relativistic corrections, so that beyond a certain $\rho_{\rm crit}$, energy must be supplied in order to get equilibrium. The *SMS* radiates quasi-statically its entropy away and shrinks to the point where the central density reaches the $\rho_{\rm crit}$ and instability sets in. At this point, the equilibrium energy is stationary, and we have instability, for a second derivative of the total energy of the system is zero. Thus, the *SMS* becomes dynamically unstable and collapse sets in.
The nature of the *SMS*s is such that small effects that are normally negligible in the study of stellar evolution must here be included to determine the stability properties.

- general relativity
- electron-positron pair formation
- rotation
- dissociation of heavy nuclei

In the framework of general relativity, dynamical instability happens before a gaseous mass shrinks to the limiting radius compatible with hydrostatic equilibrium. A star whose structure is determined almost completely by Newtonian gravitation turns out to be unstable because of general relativity. The instability in radiation dominated stars stems from the fact that $\gamma$ is nearly $4/3$; they "are trembling on the verge of instability" (Fowler, 1964). This was first suggested by Chandrasekhar (1964) and Feynman (1963) and first applied to stars by Hoyle and Fowler (1963).
From Chandrasekhar (1964), (post-Newtonian) instability sets in when the radius of the star $\mathscr{R}$ is less than a critical radius $\mathscr{R}^{\rm crit}$. He shows that if the ratio of specific heats $\gamma = C_{\rm p}/C_{\rm v}$ exceeds $4/3$ only by a small amount, then dynamical instability will occur if the mass contract to the radius

$$\mathscr{R}^{\rm crit} = \frac{\mathscr{K}}{\gamma - \frac{4}{3}} \left( \frac{2G\mathscr{M}}{c^2} \right), \tag{3.8}$$

where $\mathscr{K}$ is a constant depending on the density distribution in the configuration and the term between brackets is the Schwarzschild radius of the *SMS*. Chandrasekhar evaluates the $\mathscr{K}$ value for the homogeneous sphere of constant energy density and the polytropes of indices $n = 1,\ 2,\ 3$. The ratio of specific heats $\gamma$ can be shown to be in the limit of high entropy (Chandrasekhar, 1939),

$$\gamma \approx \frac{4}{3} + \frac{\beta}{6} + \mathscr{O}(\beta^2), \tag{3.9}$$

to first order in $\beta$. This means that the radiation-dominated stars have a $\gamma$ close to the value $4/3$ and then they are on the limit of instability. With the last formula and $n = 3$ we can approximate the $\mathscr{R}^{\rm crit}$ by

$$\mathscr{R}^{\rm crit} \approx \frac{6.8}{\beta} \left( \frac{2G\mathscr{M}}{c^2} \right). \tag{3.10}$$

The Schwarzschild radius of the *SMS* is:

$$\frac{2G\mathscr{M}}{c^2} = 10^{-5}\left(\frac{\mathscr{M}}{10^8 \mathrm{M}_\odot}\right)\mathrm{pc}, \tag{3.11}$$

Then, with the $\beta$ formula, we can find out that

$$\mathscr{R}^{\mathrm{crit}} = 0.16\mu\left(\frac{\mathscr{M}}{10^8 \mathrm{M}_\odot}\right)^{3/2}\mathrm{pc}. \tag{3.12}$$

On the other hand, the critical central density for a radiation- dominated, high entropy, index $n = 3$ polytrope is

$$\rho_{\mathrm{crit}} = 2\times 10^{18}\left(\frac{1}{2\mu}\right)^3\left(\frac{\mathscr{M}}{\mathrm{M}_\odot}\right)^{-7/2}\mathrm{g/cm}^3, \tag{3.13}$$

(Fuller et al., 1986). For a higher central density, the nonlinear effects of gravity have a destabilising influence to radial perturbations. The critical central temperature is

$$T_{\mathrm{crit}} = 2.5\times 10^{13}\left(\frac{\mathscr{M}}{\mathrm{M}_\odot}\right)^{-1}K, \tag{3.14}$$

and the corresponding equilibrium energy is

$$E_{\mathrm{crit}} = -3.6\times 10^{54}\mathrm{erg}, \tag{3.15}$$

which is independent of $\mathscr{M}$.

## 3.2 Fencing in the existence zone of an *SMS*

It is interesting to examine the time-scales of *SMS*s in order to know whether or not they are on hydrostatic equilibrium, and so to have a general overview of their possible evolution. The time scale associated with hydrodynamic processes in radiation-dominated stars is

$$\tau_{\mathrm{hyd}} \equiv \frac{1}{\sqrt{24\pi G\rho}} \approx 2\times 10^{-6}\left(\frac{\mathscr{M}}{\mathrm{M}_\odot}\right)^{7/4}\mathrm{s}. \tag{3.16}$$

In order to see a hydrostatic evolution phase, this time scale must be shorter than the modified Kelvin-Helmholtz time, also called “cooling time” or “contracting time” for it is the time-scale which gives us an approximated idea of how long can live the the star from its gravitational energy. In the life of a star there are phases in which this is the main or even the only stellar energy source, and so we say that “the

star evolves on a $\tau_{\rm KH}$". This time is given by

$$\tau_{\rm KH} \approx \frac{|E_{\rm min}|}{L_{\rm Edd}} \approx 3\times 10^{16}\left(\frac{\mathscr{M}}{\rm M_\odot}\right)^{-1}{\rm s}, \tag{3.17}$$

where $L_{\rm Edd}$ is the Eddington luminosity and $E_{\rm min}$ is the value of the total energy of the star at the relativistic or electron-positron pair instability point (Shapiro and Teukolsky, 1983). We find that

$$\tau_{\rm hyd} < \tau_{\rm KH} \iff \mathscr{M} \lesssim 10^8{\rm M_\odot} \tag{3.18}$$

For instance, for a $10^8{\rm M_\odot}$ *SMS*, $\tau_{\rm dyn}\sim 6.33$ yrs and $\tau_{\rm KH}\sim 9.5$ yrs. For times which are comparable to the time-scale we have to take into account the cooling of the *SMS*, since it can determine its evolution. For short times compared to the time-scale ($\tau \ll \tau_{\rm KH}$) we can forget about the cooling when we want to study the state and/or the evolution of the *SMS*. We have to evaluate which process is more effective (which process has a shorter time-scale), either the cooling, the accretion of mass onto the central object or the heating of the *SMS* due to un/confined stars. In such a case, the evolution will not be determined by the cooling, but by the faster processes.

In the case that $\tau_{\rm KH} > \tau_{\rm hyd}$, the cooling is slower than the setting of the hydrodynamical equilibrium and so we get a quasi- hydrostatic *SMS*. At this point there are two completely different aspects which should be studied in detail. The first of them is the state of equilibrium. We have a hydrostatic equilibrium, we consider that we have no cooling and $P_{\rm rad} \gg P_{\rm g}$. The Schwarzschild criterion for dynamical stability says that a star with $\nabla_{\rm rad} > \nabla_{\rm ad}$ (the late being = 4/3, $n = 3$ polytrope) will be unstable, supposing a homogeneous chemical composition of the star, so that $\nabla_\mu = 0$ and the small perturbations will increase until we have a fully convective star. If the equilibrium is stable, we have a contracting *SMS*, but we are close to instability; on the other hand, if it is not stable after the post-Newtonian instability, we have a free-fall collapse, because the radiation pressure grows slower than the gravity force when it contracts. The second aspect with which we have to deal is the quasistationary evolution, which is dominated now by $\tau_{\rm KH}$ and by the slow cooling. Ditto, we have a slow cooling and contracting *SMS* provided that we get such a state of equilibrium after having analysed the foregoing questions. To complete the study we have to know whether the stationary state is stable and how can we describe it.

We can illustrate this situation thanks to the gravitational and total energy ($E_{\rm gr}$, $E_{\rm tot}$), which are

$$E_{\rm gr} = -\frac{3}{2}\frac{G\mathscr{M}^2}{\mathscr{R}} = -1.3\cdot 10^{57}\,\mathscr{M}_8^2\,\mathscr{R}_{\rm pc}^{-1}{\rm erg} \tag{3.19}$$

$$E_{\rm tot} = \frac{3}{2}\beta E_g = -1.5\cdot 10^{54}\,\mathscr{M}_8^{3/2}\,\mathscr{R}_{\rm pc}^{-1}{\rm erg}. \tag{3.20}$$

In these equations, $\mathscr{R}_{\rm pc}$ is the radius of the *SMS* in pc and $\mathscr{M}_8$ its mass in units of $10^8{\rm M_\odot}$. We have also used the fact that

$$\beta = \frac{P_g}{P_g + P_{rad}} = 7.8\cdot 10^{-4}\,\mathscr{M}_8^{-1/2} \tag{3.21}$$

As we already mentioned, the contraction rate of the *SMS*is determined by the Eddington luminosity which, expressed in $\mathscr{M}_8$ (see eq. 3.6), is

$$\mathscr{L}_8 = 1.3 \cdot 10^{46} \mathscr{M}_8 \frac{\text{erg}}{\text{s}} \tag{3.22}$$

Thus, we have a contraction time (Kelvin-Helmholtz time)

$$\tau_{\text{KH}} = \frac{-E_{tot}}{L_{Ed}} = 3.7 M_8^{1/2} R_{pc}^{-1} \text{yr} \tag{3.23}$$

To determine whether a *SMS* can exist or not (from a point of view of the hydrostatic equilibrium), we just have to check for its radius in a $\mathscr{M}$-$\mathscr{R}$ plane. We can define the radius $\mathscr{R}_{\text{ff}}$ at the place where $\tau_{\text{KH}}$ is equal to the free-fall time. In fig. (3.1) the time-scale $\tau_{\text{KH}}$ in which an *SMS*evolves is shown, from right to left. This gives us an up-limit to the limits in the plane for the *SMS*. As for the low-limit, we have to take into account the condition imposed by the post-Newtonian unstability $\mathscr{R}_{\text{pn}}$ or go even "lower" and look for lower masses when nuclear burning at the centre sets in, $\mathscr{R}_{\text{nb}}$. The area where such an object can exist (is stable) starts at $\mathscr{R}_{\text{ff}}$ .When hydrogen burning at the centre sets in at $\mathscr{R}_{\text{nb}}$, or when Post-Newtonian unstabilities triumph over thermal pressure stabilisation, at $\mathscr{R}_{\text{pn}}$, the *SMS*becomes unstable. For masses $\lesssim 5 \cdot 10^4 \text{M}_\odot$, the electron-positron pair instability occurs. The friction time-scale is also plotted ($\tau_{\text{fric}} = 10^5, 10^3, 10^1$ yr from right to left) for a typical star with $v_\star = 1500$ km/s (assuming that 1% of the orbit crosses the inner part of the *SMS*). For radii smaller than the coupling radius $\mathscr{R}_{\text{coupl}}$ such stars are effectively decelerated. Some typical values of $\tau_{\text{fric}}$ for solar type stars are also plotted.

## 3.3 Possible origin of a BH: sequence of *SMS*s

It may be enlightening to distinguish two competing processes to have a first look of the evolution of this physical problem: The contraction (or collapse with re-bounce) of the mixed core with stars that are trapped by friction within the gas and slow down additionally to build a new highly condensed stellar core. This core may re-heat the gas or decouple to build a new core. A core-halo interaction is also possible. The loss-cone stars of the surrounding stellar system heat the core and feed it by means of new trapped stars. This core collapse can be conked for a while until the loss-cone is "empty" (not rigorously speaking, but for the practice we can assume it is empty) or the core becomes too massive.
The friction force of the stars moving through the *SMS* has a dynamical and a geometrical component. For *SMS*s more compact than the coupling radius $\mathscr{R}_{\text{coupl}}$, green line in Fig. (3.1), the typical friction time-scale is shorter than the contraction time of the *SMS*. Thus, stars are effectively decelerated by dynamical friction. As a result, loss-cone stars will be segregated to the centre building a highly concentrated sub-system, which may essentially change the evolution of the *SMS*by enhanced interactions.
The result may be a sequence of *SMS* -stars cores contained one inside the other until the relatively low mass innermost *SMS* initiates hydrogen burning or collapses to a BH "seed". In Fig. (3.2) we give an intuitive scheme for this scenario.

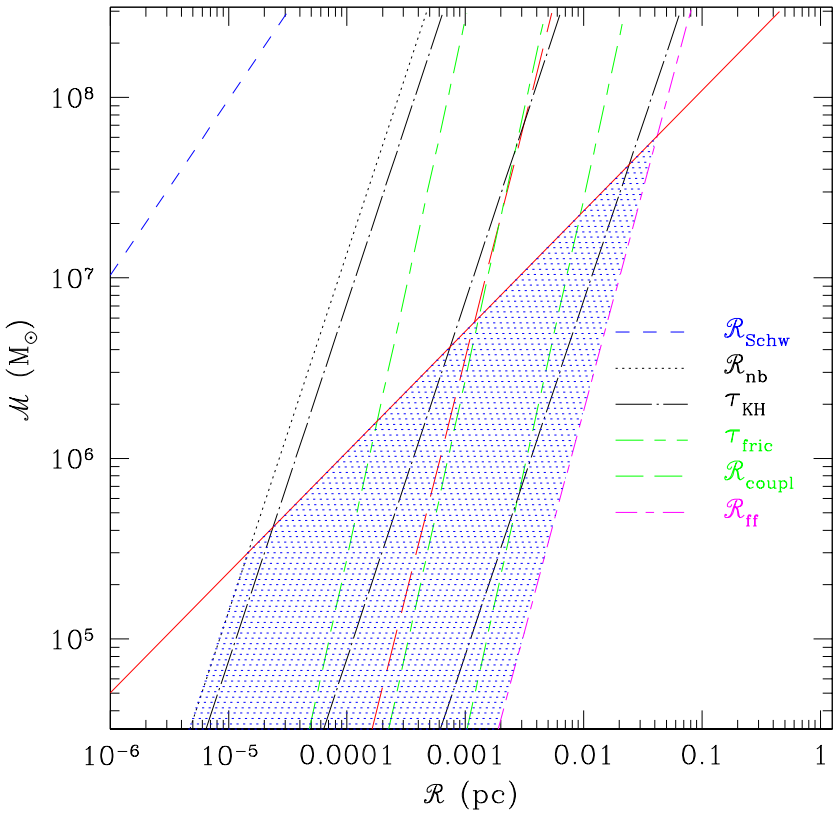


Fig. 3.1: Characteristic radii and time-scales for an *SMS*. The Schwarzschild radius $\mathcal{R}_{\rm Schw}$ is far below the "allowed" region of an *SMS*. The evolutionary tracks are horizontal lines from right to left. The contraction time $\tau_{\rm KH}$ is also displayed in order to show that without re-heating the life time of the *SMS* is at $2 \cdot 10^4$ yr before nuclear burning or the post-Newtonian collapse sets in (see text)

## 3.4 Stabilisation theory

### 3.4.1 The role of rotation

Rotation is likely to play a decisive role in the quasistationary evolution of an *SMS*, as well as in its final collapse. Since *SMS*s are on the verge of stability, rotation can prolongate their equilibrium evolution. The gravitational instability sets in when $\Gamma_{\rm SMS}$ yields a value less than a critical value, which is roughly

$$\Gamma_{\rm SMS} < \Gamma_{\rm crit} \approx \frac{2}{3}\frac{2-5\eta}{1-2\eta} + 1.12\frac{\mathcal{R}_{\rm Schw}}{\mathcal{R}}, \tag{3.24}$$

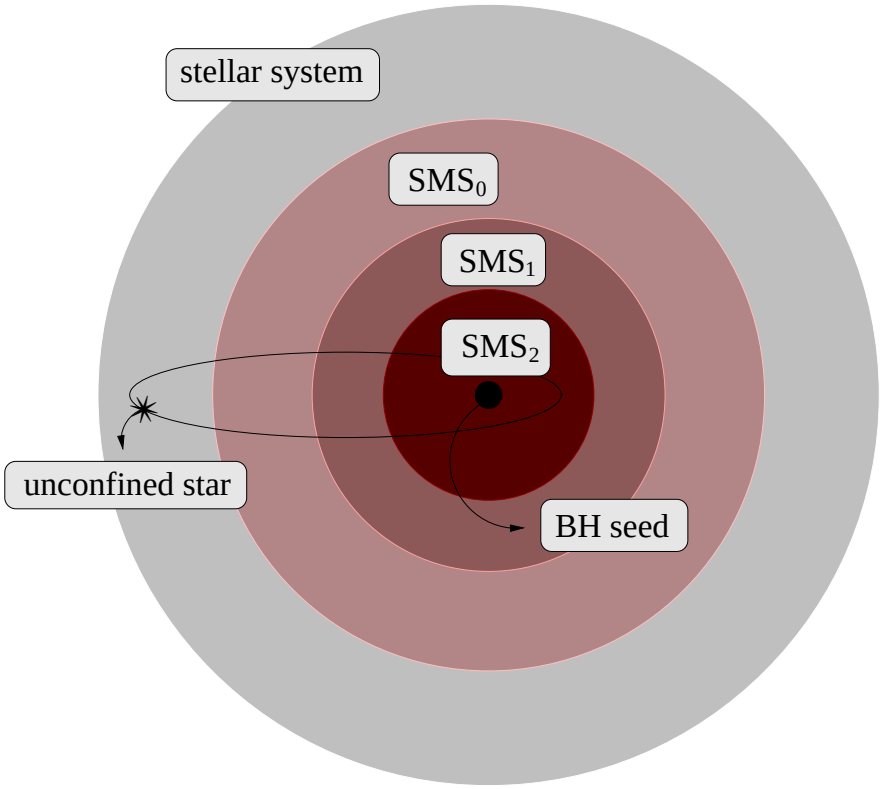


Fig. 3.2: Sequence of *SMS*-stars cores: $SMS_2 \in SMS_1 \in SMS_0$. The non-confined stars which belong to the loss-cone sink on to the central object after a number of crossings, which we call the "trap" number. The innermost *SMS* may collapse to a BH seed

where $\mathscr{R}_{\rm Schw} = 2G\mathscr{M}/c^2$ is the Schwarzschild radius of the star and $\eta = T/|W|$ the ratio of the rotational energy to the gravitational potential energy. For $\eta = 0$, the last equation becomes $\Gamma_{\rm crit} = 4/3 + 1.12\mathscr{R}_{\rm Schw}/\mathscr{R}$ (Misner et al. 1973 and references therein). The adiabatic index grows thus as the radius of the star becomes smaller. Rotation has a stabilising effect and can hold the collapse if

$$\eta > \eta_{\rm crit} \approx \frac{1}{2}\frac{4-3(\Gamma_{\rm SMS}-1.12\mathscr{R}_{\rm Schw}/\mathscr{R})}{5-3(\Gamma_{\rm SMS}-1.12\mathscr{R}_{\rm Schw}/\mathscr{R})} \tag{3.25}$$

Baumgarte and Shapiro (1999b,a) study the effects of rotation on a *SMS* and follow the evolution of these objects up to the dynamical instability and collapse. They find out that ratios like $\mathscr{R}/\mathscr{R}_{\rm Schw}$, $\mathscr{R}/\mathscr{M}$, $T/|W|$ and $Jc/(G\mathscr{M}^2)$ ($T$ is the rotational kinetic energy, $W$ the gravitational potential energy and $J$ the angular momentum) for a maximally and rigidly rotating $n = 3$ polytrope at the onset of radial instability are universal numbers, "key ratios", as they denominate them, which are independent of the

mass, spin, radius or even the history of the star. They are thus universal constants:

$$\left(\frac{T}{|W|}\right)_{\rm crit} \approx 0.009, \left(\frac{Jc}{G\mathscr{M}^2}\right)_{\rm crit} \approx 0.97, \left(\frac{\mathscr{R}_{\rm p}}{\mathscr{R}_{\rm Schw}}\right)_{\rm crit} \approx 214, \tag{3.26}$$

with the polar radius $\mathscr{R}_{\rm p} \approx 2\mathscr{R}_e/3$ ($\mathscr{R}_e$ stands for the equatorial radius). This deformation could be responsible for the reduction of the luminosity by about 36% below the usual Eddington luminosity from a non-rotating *SMS* (Baumgarte and Shapiro, 1999b,a):

$$L_{\rm rot} = 0.639 L_{\rm Edd}. \tag{3.27}$$

Since luminosity determines the timescale (i.e. the mean life) of these objects, rotation seems to be a factor whose importance should be seriously taken into account.
They perform a fully relativistic, numerical calculation and compare it with an analytical treatment, which is in good agreement. They claim that cooling by photon radiation drives the evolution, while the rotating *SMS* loses mass, angular momentum and entropy. Gas pressure may stabilise *SMS*s in the absence of angular momentum (Zeldovich and Novikov, 1971; Shapiro and Teukolsky, 1983), but Baumgarte and Shapiro in their paper maintain that even a small degree of rotation could dominate gas pressure. They analyse also the final collapse of rotating *SMS*s, which might not necessary be a BH. They reckon that the collapse may be inhibited, in the form of a disc and/or bar, or possible fragmenting into several blobs.
The study of the importance of a dark matter background on the stability of an *SMS* has also been done, with the conclusion that although it has stabilising effects, it can be neglected compared with the effects of rotation (Bisnovatyi-Kogan, 1998).
Nevertheless, all the work being performed as regards the stability of *SMS*s in the case that such objects would rotate, and other topics, like the equilibrium and stability of *SMS*s in binary systems assume that the system is an isolated one; namely, *the accretion and heating are assumed to be negligible*.

### 3.4.2 Stabilisation by fluctuations

The density, temperature and velocity fluctuations excited by the stellar component in the gas (Just et al., 1986; Deiss et al., 1990) do not only decelerate the stars by dynamical friction, but there is also a stabilising effect on the gas component, which can be described by an effective $\overline{\beta}$. The diffusion of photons is much faster than the dynamical time scale in the *SMS*. Since the temperature is determined by the radiation field, the perturabations are isothermal as long as the matter is optically thick. For scales smaller than the mean free path $\lambda = 3.3\,10^{-6} M_8^{-1} R_{\rm pc}^3 \rho_c/\rho$ pc, the density fluctuations are adiabatic leading to an enhanced mean thermal pressure. The basic corrections to the unperturbed parameter $\beta_0$ are

$$\overline{\beta} = \beta_0 (1 + K \frac{\langle \rho_1^2 \rangle}{\rho_0^2}) + \beta_{\rm turb} > \beta_0 \tag{3.28}$$

where $\beta_{\text{turb}}$ gives the ratio of turbulent to radiation pressure and $\langle \rho_{=}^2 \rangle$ is the unperturbed density. The scaling constant $K$ and the fluctuations' density $\langle \rho_1^2 \rangle$ must be determined by some fluctuation theory. Using a quasilinear approximation of a mode analysis the perturbations excited by the stars moving through the gas will be estimated to determine the magnitude of the corrections due to the turbulent velocity field and the adiabatic density fluctuations on the stability parameter $\beta_0$. An increase of the effective $\overline{\beta}$ will shift the line for the Post-Newtonian instability to higher masses.

## 3.5 Literature of chapter 3

Amaro-Seoane, P., Spurzem, R., and Just, A. (2002). Super-Massive Stars: Dense Star-Gas Systems. In *Lighthouses of the Universe: The Most Luminous Celestial Objects and Their Use for Cosmology Proceedings of the MPA/ESO/, p. 376*, page 376.

Baumgarte, T. W. and Shapiro, S. L. (1999a). Evolution of Rotating Supermassive Stars to the Onset of Collapse. *apj*, 526:941–952.

Baumgarte, T. W. and Shapiro, S. L. (1999b). Luminosity versus Rotation in a Supermassive Star. *apj*, 526:937–940.

Bisnovatyi-Kogan, G. S. (1998). Stability of Rotating Supermassive Stars in the Presence of a Dark Matter Background. *apj*, 497:559.

Bond, J. R., Arnett, W. D., and Carr, B. J. (1984). The evolution and fate of Very Massive Objects. *apj*, 280:825–847.

Burbidge, E. M. and Burbidge, G. R. (1962). *nat*, 194:367.

Chandrasekhar, S. (1939). *An introduction to the study of stellar structure*. Chicago, Ill., The University of Chicago press [1939].

Chandrasekhar, S. (1964). The Dynamical Instability of Gaseous Masses Approaching the Schwarzschild Limit in General Relativity. *apj*, 140:417.

Deiss, B. M., Just, A., and Kegel, W. H. (1990). Fluctuations of the interstellar medium induced by the stellar system - Mechanical heating and dynamical friction. *aa*, 240:123–136.

Feynman, R. P. (1963). *Feynman lectures on physics - Volume 1*. Reading, Ma.: Addison-Wesley, 1963, edited by Feynman, Richard P.; Leighton, Robert B.; Sands, Matthew.

Fowler, W. A. (1964). Massive Stars, Relativistic Polytropes, and Gravitational Radiation . *Reviews of Modern Physics*, 36:545–554.

Fowler, W. A. (1965). Massive Stars, Relativistic Polytropes, and Gravitational Radiation. In *Quasi-Stellar Sources and Gravitational Collapse*, page 51.

Fowler, W. A. (1966). The Stability of Supermassive Stars. *apj*, 144:180.

Fuller, G. M., Woosley, S. E., and Weaver, T. A. (1986). The evolution of radiation-dominated stars. I - Nonrotating supermassive stars. *apj*, 307:675–686.

Hoyle, F. and Fowler, W. A. (1963). On the nature of strong radio sources. *mnras*, 125:169.

Just, A. and Amaro-Seoane, P. (2001). Gas-star-interaction in Dense Galactic Nuclei. In *Astronomische Gesellschaft Meeting Abstracts*, page 155.

Just, A. and Amaro-Seoane, P. (2003). Stability and Evolution of Supermassive Stars (SMS). *EAS Publications Series, Volume 10, 2003, Galactic and Stellar Dynamics, Proceedings of JENAM 2002, held in Porto, Portugal, 3-6 September, 2002. Edited by C. M. Boily, P. Pastsis, S. Portegies Zwart, R. Spurzem and C. Theis, pp.127.*, 10:127.

Just, A., Kegel, W. H., and Deiss, B. M. (1986). Dynamical friction between the ISM and the system of stars. *aa*, 164:337–341.

Kippenhahn, R. and Weigert, A. (1994). *Stellar Structure and Evolution*. Springer-Verlag Berlin Heidelberg.

Misner, C. W., Thorne, K. S., and Wheeler, J. A. (1973). *Gravitation*. San Francisco: W.H. Freeman and Co., 1973.

New, K. C. B. and Shapiro, S. L. (2001). Evolution of Differentially Rotating Supermassive Stars to the Onset of Bar Instability. *apj*, 548:439–446.

Shapiro, S. L. and Teukolsky, S. A. (1983). *Black holes, white dwarfs, and neutron stars: The physics*

*of compact objects*. Wiley-Interscience.

Wallace, R. K. and Woosley, S. E. (1981). Explosive hydrogen burning. *apjs*, 45:389–420.

Zeldovich, Y. B. and Novikov, I. D. (1971). *Relativistic astrophysics. Vol.1: Stars and relativity*. University of Chicago Press.

# Chapter 4

# A semi-analytical approach to dense gas-star systems

## 4.1 Introduction

DYNAMICS in galactic nuclei of dense stellar systems is the subject to be presented in this chapter [1] for some of the physical configurations we introduced in former sections. It has been often suggested that, in addition to the thermonuclear sources inside the constituent stars, the active phenomena of high-energy emissions occurring at galactic nuclei and quasars could be explained resorting to the idea that a massive dark object is being harboured in the centre of the galaxies (Magorrian et al., 1998).

We will start this discussion facing the black hole star accretion problem in a dense stellar medium in a given time scale. Radii of stars are extremely small ($r_\odot \approx 10^{10}$cm) in comparison with the mean typical distances between stars in astrophysical stellar systems (a typical interstellar distance in our galactic neighbourhood is $\approx 10^{18}$cm). Even though stellar collisions occur seldom, a single star will modify its orbit at random because of the small pushes it receives from stars which pass close by. We can roughly define a certain time required for the stars "to forget their initial orbits" due to two-body, small-angle gravitational encounters, the gravitational tugs of these passing-by stars; this would be one of our timescales of interest, the *relaxation time*.

Then will we follow through the initial problem introducing the concept of *super-massive star*. As a first description of it, a *super-massive star* ($\mathscr{M} \gtrsim 10^4 \mathrm{M}_\odot$, where $\mathscr{M}$ is its mass) is a dense gas cloud located in the centre of dense stellar systems which can be regarded as a general case for the black hole

[1] Part of the work exposed in this chapter was used for Amaro-Seoane and Spurzem (2001a), Amaro-Seoane and Spurzem (2001b) and Amaro-Seoane and Spurzem (2000)

accretion problem.
If the super-massive star scheme embraces the black hole accretion problem, we could think that the most general case is to be analysed first, since it supposedly gives an overview of the general problem. Nevertheless, if we dare to envisage the possibility of doing it upside-down, if we generalise the example and try to extract from it the global concept, it reports us the satisfactory surprise that everything turns out to be clearer after having evaluated the particular case. The most general case becomes pointless if it yields as a result a more difficult understanding of the subject submitted at study.

## 4.2 General concepts

In this section we discuss the consequences from the astrophysical and dynamical point of view of the presence of a black hole (or a massive compact central object, from now onwards just BH) in a dense stellar object in about a relaxation time. We consider the steady-state distribution and consumption of stars orbiting a massive object at the centre of a spherical, stellar system.
The distribution of stars is determined by the relaxation processes associated with gravitational stellar encounters and by the consumption of low angular momentum stars which pass within a small distance of the central mass. Stars whose orbits carry them within the tidal radius $r_t$ of the BH will be tidally disrupted. The *peribarathron* [2] (distance of closest approach to the BH) is determined by the specific orbital angular momentum $L$ and by the BH mass. There are situations in which the stars that have a radially elongated orbit and a low angular momentum pass close by the system centre and interact with the massive central object. In such a situation it is interesting to evaluate the density of those stars whose angular momenta are limited by a superior $L_{\rm min}$; that is, the stars which belong to a defined region in the velocity-space.
Stars at a position $r$ whose velocities are limited by a superior limit $v_{\rm lc}(r)$ and, consequently, with an angular momentum $L < L_{\rm min} = r v_{\rm lc}$, have orbits that will cross the tidal radius of the central BH in their motion. They will be disrupted due to the tidal forces and then they are lost for the stellar system. Such stars are said to belong to the *loss-cone*, since they are lost for the stellar system. The loss-cone is depleted in a crossing time $t_{\rm cross} = r/\sigma$, where $\sigma$ is the 1D velocity dispersion.
The diffusion of stars into this loss-cone has been studied by (Frank and Rees, 1976) and by Lightman and Shapiro (1977). We will talk about a "critical radius" within which stars on orbits with $r \leq r_{\rm crit}$ diffuse. Inside they are swallowed by the BH, after being scattered to low angular momentum *loss-cone* orbits.
If there is a central point mass $\mathscr{M}_\bullet$, such that $\mathscr{M}_\bullet \gg m_\star$, then its potential well will affect the stellar velocity field out to a distance

$$r_{\rm h} = G\mathscr{M}_\bullet/\sigma^2. \tag{4.1}$$

This expression gives us the influence radius of the central object. $G$ is the gravitational constant.
The star gets disrupted whenever the work exerted over the star by the tidal force exceeds its own binding

[2] This word fits quite well the idea of closest approach to this "sinking" hole for it has the meaning of no return. The *barathron* ($\beta\acute{\alpha}\rho\alpha\theta\rho o\nu$) was in the ancient Greece a cliff down to an unreacheable or unseen place where criminals were thrown

energy. If we compute the work exerted over the star by the BH we can get an expression for the tidal radius (see Addendum A of this chapter, section 4.13),

$$r_{\rm t} = \left[\frac{2}{3}(5-n)\frac{\mathscr{M}_\bullet}{m_\star}\right]^{1/3} r_\star, \tag{4.2}$$

where $n$ is the polytropic index of the star, $m_\star$ the mass of the star and $r_\star$ its radius.

## 4.3 Loss-cone phenomena

Frank and Rees (1976) studied how a stationary stellar density profile around a massive star accreting BH looks like. They found that the density profile follows a power-law within the region where the gravity of the massive star dominates the self-gravity of the stars,

$$\rho \propto r^{-7/4}. \tag{4.3}$$

This was followed by intensive numerical studies by other authors (Shapiro and Marchant, 1978; Marchant and Shapiro, 1979, 1980; Shapiro and Teukolsky, 1985) which are all in agreement with the first work of Frank and Rees.
The replenishment of the loss-cone happens thanks to the small-angle gravitational encounters in a timescale which is for the most real stellar systems slower than the dynamical processes.
We have loss-cone effects also in the neighbourhood of a massive central gas-formed object, an *SMS*, see Fig. (4.1). Stars with such orbits enter the gas-formed central object and lose kinetic energy if their density is high enough. Nevertheless, such stars will not disappear from the stellar system just by one crossing of the central object, as it happens for the BH problem. In this scenario the stars lose their energy in each crossing and their orbits come closer and closer to the central object until they are "trapped" in it, their orbits do not extend further than the massive central object radius (confined stars). This process was described qualitatively by Hara (1978), da Costa (1981) and Hagio (1986). Da Costa suggested the name "dissipation-cone". However, we will keep the loss-cone term for it is the most commonly found in the related literature. We have to take into account that the meaning is that of a defined region of the velocity space at the position $r$, even though there is no quick loss.
In Addendum B of this chapter (section 4.14) we derive the following expression for the diffusion angle (the mean deviation of a star orbit in a dynamical time $t_{\rm dyn}$):

$$\theta_{\rm D} \simeq \sqrt{\frac{t_{\rm dyn}}{t_{\rm relax}}}. \tag{4.4}$$

Now we look for a condition at a place $r > r_{\rm h}$ for a star to touch or to cross the influence radius of the central object within a crossing time. For this aim we look now for the amount of stars which reaches the central influence radius with an unperturbed orbit. Unperturbed here means that the star orbit results

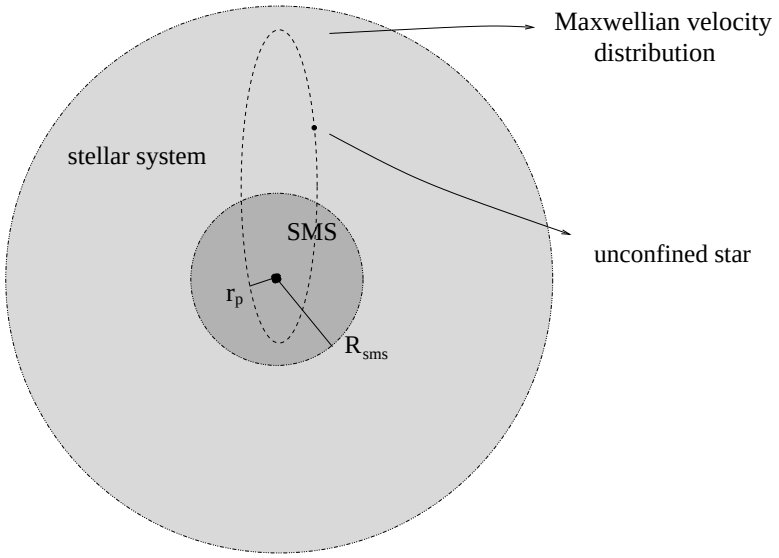


Fig. 4.1: Super-massive star peribarathron radius $r_{\rm p}$

from the influence of the gravitational potential and from that of the rest of the stars and of the central object, and it is not affected by the local, two-body, small- or big-angle gravitational encounters. We envisage then the average part of the gravitational potential, whereas the random component due to the individual behaviour of the stars will be neglected.

To define the loss-cone angle we say that a star belongs to this cone when its distance to the peribarathron (which depends on the orbit we have, i.e., on the energy $E$ and angular momentum) is less or equal to the tidal radius, $r_{\rm p}(E,L) \leq r_{\rm t},\ \theta \leq \theta_{\rm lc}$.

There is a maximum $\theta$ for which the peribarathron radius is less than or equal to the tidal radius. We define this as $\theta_{\rm lc}$ (where the subscript "lc" stands for loss-cone). In Addendum B we derive an expression for it in terms of the influence radius of the central object.

As for the $v_{\rm lc}(r)$, we get its value using angular momentum and energy conservation arguments in Addendum C (section 4.15).

$$v_{\rm lc}(r) = \frac{r_{\rm t}}{\sqrt{r^2 - r_{\rm t}^2}} \cdot \sqrt{2[\phi(r_{\rm t}) - \phi(r)] + v_{\rm r}(r)^2}. \tag{4.5}$$

## 4.4 The critical radius

It is interesting to evaluate a certain radius which Frank and Rees (1976) introduced by defining the ratio $\xi := \theta_{\rm lc}/\theta_{\rm D}$. When $\xi = 1$, then $\theta_{\rm lc} = \theta_{\rm D}$, and this corresponds to a "critical radius", $r_{\rm crit}$, if there is only one radius with this condition. Inside the critical radius (i.e. $\xi > 1$, $\theta_{\rm lc} > \theta_{\rm D}$) stars are removed on a $t_{\rm dyn}$. For larger radii (i.e. $\xi < 1$, $\theta_{\rm lc} < \theta_{\rm D}$) we cannot talk about a "loss-cone" because this $\theta_{\rm D}$ corresponds to

the variation of $\theta$ within a $t_{\rm dyn}$, and this is the required time for the star within the loss-cone to plunge onto the BH if the orbit is unperturbed. The angle variation happens sooner than the required time for stars to sink into the loss-cone. If $\theta_{\rm D} > \theta_{\rm lc}$, loss-cone stars can get in and out of the loss-cone faster than they could reach the central object.

## 4.5 The loss-cone contribution to the heating rate of the gas

Dissipation of the stellar kinetic energy of a star plunging onto the *SMS* and suffering from the drag force leads to a heating of the *SMS*. Another possible consequence of the local star-gas interaction is the formation of massive stars within the cloud due to the accretion of ambient gas (da Costa, 1979). This could increase the supernova rate and be an important source of energy. Here we will assume an equilibrium for the *SMS* for the timescales of interest.

The star distribution will be affected at large radii ($r \gg \mathscr{R}$, $\mathscr{R}$ being the *SMS* radius) by removal of stars in the central regions of a stellar system (Peebles, 1972). A drift of stars occurs in the centre of the stellar system in order to recover the equilibrium. In the special case of having a BH at the centre of the system, processes like tidal disruption lead to the destruction of the star. In this arena we have an outward energy flux created by the sinking of stars via relaxation processes (local, two-body, small-angle gravitational encounters).

When we consider the general case of an *SMS*, the basic picture is the same, but some aspects vary; the removal of stars and the inward transport are due to a different process. The inward flux of energy is produced not only for the local, two-body, small-angle gravitational encounters, but also for dissipative processes. The effective sinking for stars is now related to gas-drag energy dissipation and can involve or not their actual physical destruction. A star moving through the cloud will quickly dissipate energy because of gas drag and then it will sink into the centre of the *SMS*. The main difference between a BH and an *SMS* is basically that the former produces a low-angular momentum star depletion on a crossing time, whereas the dense gas cloud or *SMS* does the same but in a dissipation time.

Since we want to analyse the effects on the dense stellar system arising from the presence of a central gas cloud we have to distinguish between those stars whose orbits are limited to the region where the *SMS* is located (*confined stars*) and those stars in orbits which surpass the radius of the cloud (*unconfined stars*). When we talk about confined stars, the first steps in the evolution are determined by the energy dissipation given by the drag force that the dense gas cloud exerts on the individual stars. Stars lose velocity in their motion inside the cloud, they are slowed down by the gas and therefore they cede heat to the cloud. The slowing down of the stars makes them become a more compact subsystem which will sink down to the centre of the cloud. The system becomes self-gravitating and we have a cusp in the stellar distribution. However, star-star interactions can play a decisive role in this point, since they yield a depletion in the number of confined stars, or we can have direct collisions between them and thus disruption or coalescence. This could avoid that a singularity in the core collapse crops up. We cannot exclude the exchange of mass between individual stars and the gas as another possible way to prevent the singularity, since this can yield the star disruption via stellar wind, or the creation of heavier stars which become a supernova (da Costa, 1979).

The consequent evolution of the confined system will be in part determined by the rate at which surrounding stars outside the gas cloud refill this confined-stars gap. The importance of the core collapse will also be a decisive point for the evolution.
Unconfined stars move on orbits extending larger than the *SMS* radius. However, they can suffer its influence out to a radius within which the presence of the *SMS* is effective. The idea is exactly the same as for the BH, for the *SMS* is a generalisation of the former case

## 4.6 Kinetic energy dissipation

The drag force that the individual stars suffer when they cross the *SMS* is given by the next equation estimated by Bisnovatyi-Kogan and Syunyaev (1972):

$$F_{\rm D} = C_{\rm D} S \rho_{\rm SMS} v_\star^2. \tag{4.6}$$

$C_{\rm D}$ is a numerical parameter of order unity, $\rho_{\rm SMS}$ is the mean density of the gas cloud, $v_\star$ is the velocity of the stars and $S$ is the cross section of the stars, $S = \pi r_\star^2$. In case of a supersonic motion of the star the force $F_{\rm D}$ can be interpreted as caused by the ram pressure (pressure difference) originating at a bow shock in front of the moving star. Due to the physical shock conditions one can show in such a case $C_{\rm D} \approx 4$ (Courant and Friederichs, 1998).
Suppose that the star crosses the *SMS* from one extreme to the opposite, i.e. along its diameter; thus, if $\mathscr{R}$ is the radius of the *SMS*, the stellar energy dissipated during each passage through it is

$$\triangle E_{\rm D} = F_{\rm D} \cdot 2\mathscr{R}. \tag{4.7}$$

The orbits of the stars within $r_{\rm h}$ will be elliptic shaped with one focus at the *SMS* centre. The semi-major orbit axis $a$ will shrink because of the drag force, driving the orbit directly into the *SMS*. The average energy dissipation rate is

$$-\frac{dE}{dt} = \frac{\triangle E_{\rm D}}{T} = \frac{2C_{\rm D}\rho_{\rm SMS}\pi r_\star^2 G\mathscr{M}}{\pi\sqrt{4a^3/G\mathscr{M}}}, \tag{4.8}$$

where $T$ is the period.
In the BH accretion problem the individual stars are doomed to sink in the hole if they belong to the loss-cone, whereas for the *SMS* it depends on the number of passages through the gas cloud. It means that the non-confined star can cross the gas cloud several times until it is trapped. To make this picture clearer we resort to the BH, particularly when we introduced the concept of $\theta_{\rm D}$. In the case of *SMS*,

$$\theta_{\rm D} \approx \sqrt{\frac{n_{\rm trap} \cdot t_{\rm dyn}}{t_{\rm relax}}}. \tag{4.9}$$

We can get the number of necessary passages for the star to be trapped if we write the potential difference

between $r$ and $\mathscr{R}$ (for the BH problem it is $n = 1$),

$$\triangle\phi = G\mathscr{M}m_\star(\frac{1}{r} - \frac{1}{\mathscr{R}}). \tag{4.10}$$

Then, the number of passages is:

$$n_{\rm trap} = |\triangle\phi|/\triangle E_{\rm D}. \tag{4.11}$$

The dissipation of stellar kinetic energy defines a region in phase-space which we will call the loss-cone too, by analogy with the BH accretion problem. We have to recall however, that the star will be blown up by tidal forces and converted into gas by just one passage inside the tidal radius $r_{\rm t}$ for the case of having a BH whereas the number of passages is $n_{\rm trap} > 1$ if we consider the gas cloud situation.

## 4.7 Loss-cone stars velocity field distribution function

It stands to reason that at distances much larger than the *SMS*radius ($r \gg \mathscr{R}$) the star field velocity distribution has a Maxwellian shape:

$$\begin{aligned} f(r,v) = &\quad g(r)\cdot h(v), \\ f(r,v) = &\quad N(r)\cdot\exp(-\frac{v_{\rm r}^2}{2\sigma_{\rm r}^2})\exp(-\frac{v_{\rm t}^2}{2\sigma_{\rm t}^2}) \end{aligned} \tag{4.12}$$

Taking into account that $d^3v = 2\pi v_{\rm t} dv_{\rm r} dv_{\rm t}$, the density is

$$\rho(r) = \int_0^\infty f(r,v)4\pi v^2 dv = \pi\sqrt{\frac{\pi}{2}}N(r)\sigma_{\rm r}\sigma_{\rm t}^2; \tag{4.13}$$

then

$$N(r) = \frac{\rho(r)}{(2\pi)^{3/2}\sigma_{\rm r}\sigma_{\rm t}^2} \tag{4.14}$$

And so get we the normalised field velocity distribution,

$$f(v_{\rm t},v_{\rm r}) = \frac{\rho(r)}{(2\pi)^{3/2}\sigma_{\rm r}\sigma_{\rm t}^2}\exp(-\frac{v_{\rm r}^2}{2\sigma_{\rm r}^2})\exp(-\frac{v_{\rm t}^2}{2\sigma_{\rm t}^2}). \tag{4.15}$$

In order to get the density of stars within the loss-cone we have to compute the following integral:

$$\rho_{\rm lc}(r) = \int_{-v_{\rm r}|_{\rm max}}^{0}\int_{-v_{\rm lc}}^{+v_{\rm lc}} f(v_{\rm r},v_\theta,v_\phi){\rm d}v_{\rm r}dv_\theta dv_\phi. \tag{4.16}$$

Taking into account that ${\rm d}v_\theta dv_\phi = 2\pi v_{\rm t} dv_{\rm t}$ and that $f(r,v) = f(r,-v)$,

$$\rho_{\rm lc}(r) = 4\pi\rho(r)\int_0^{v_{\rm r}|_{\rm max}}{\rm d}v_{\rm r}\int_0^{v_{\rm lc}(r,v_{\rm r})} f(r,v_{\rm r},v_{\rm t})v_{\rm t}{\rm d}v_{\rm t}. \tag{4.17}$$

In this expression, the maximal radial velocity is $v_{\rm r}|_{\rm max} = v_{\rm escape} = \sqrt{2\phi(r)}$ and the potential is the sum of both, the super-massive star and the stellar system potential,

$$\phi(r) = \phi_{\rm SMS}(r) + \phi_{\star}(r). \tag{4.18}$$

The integral happens to be analytical, and it yields the following result:

$$\rho_{\rm lc}(r, v_{\rm r}) = \rho(r) \cdot \{\alpha - \zeta \cdot \beta \cdot \psi\}, \tag{4.19}$$

where

$$\begin{aligned}
\alpha \equiv &\quad \mathrm{erf}(\sqrt{\phi(r)/\sigma_{\rm r}^2}) \\
\beta \equiv &\quad \exp\Big(-\frac{\mathscr{R}^2}{r^2-\mathscr{R}^2}\frac{2\triangle\phi}{\sigma_{\rm t}^2}\Big) \\
\psi \equiv &\quad \mathrm{erf}(\frac{1}{\zeta}\sqrt{\phi(r)/\sigma_{\rm r}^2}) \\
\zeta \equiv &\quad \left(\frac{(r^2-\mathscr{R}^2)\sigma_{\rm t}^2}{(r^2-\mathscr{R}^2)\sigma_{\rm t}^2 + \mathscr{R}^2\sigma_{\rm r}^2}\right)^{1/2} \\
\triangle\phi \equiv &\quad \phi(\mathscr{R}) - \phi(r).
\end{aligned} \tag{4.20}$$

Since we are working with a Gaussian function whose width is $\sigma$, the contributions of velocities $v_{\rm r} > 2\sigma_{\rm r}$ to the total mass are small and therefore negligible. In the practice it means that we can approximate the integral by $v_{\rm r} = 2\sigma_{\rm r}$. In such a situation, the loss-cone adopts an easy geometrical form: an open cylinder in the $-v_{\rm r}$ direction with a radius $v_{\rm lc}$. The resulting integral yields

$$\frac{\rho_{\rm lc}(r)}{\rho(r)} = \left[1 - \exp\left\{-\frac{\mathscr{R}^2}{r^2-\mathscr{R}^2}\frac{2\sigma_{\rm r}^2 + \triangle\phi(r)}{\sigma_{\rm t}^2}\right\}\right] \cdot \mathrm{erf}\left(\sqrt{\frac{\phi(r)}{\sigma_{\rm r}^2}}\right) \tag{4.21}$$

We use for the stellar system a polytrope with $n = 5$, with a compact core and an extended outer envelope (named *Plummer model* after Plummer (1911), since it was first used by him to fit the observed light clusters distributions), which is commonly used for several numerical model computations.
In this model the potential is spherical,

$$\phi = -\frac{G\mathscr{M}_{\star}}{\sqrt{r^2 + r_{\rm c}^2}} \tag{4.22}$$

where $\mathscr{M}_{\star}$ is the system's total mass and $r_{\rm c}$ its core radius.
Thus,

$$\nabla^2\phi = \frac{3GMr_{\rm c}^2}{(r^2 + r_{\rm c}^2)^{5/2}}. \tag{4.23}$$

Then, if we resort to the equation of Poisson, we can find out that this system happens to have the following physical properties:

$$\begin{aligned} \rho_{\rm p}(r) = &\quad \frac{3M}{4\pi r_{\rm c}^3}\left(1+\frac{r^2}{r_{\rm c}^2}\right)^{-5/2}, \\ M_{\rm p}(r) = &\quad M\cdot\frac{r^3/r_{\rm c}^3}{(1+r^2/r_{\rm c}^2)^{3/2}}, \\ v_{\rm p}(r) = &\quad \sqrt{\frac{GM}{6r_{\rm c}}}\left(1+\frac{r^2}{r_{\rm c}^2}\right)^{-1/4}. \end{aligned} \tag{4.24}$$

Thus,

$$\phi(r) = \frac{G\mathscr{M}}{r} + \frac{G\mathscr{M}_\star}{\sqrt{r^2+r_{\rm c}^2}}. \tag{4.25}$$

Therewith, the resulting expression is

$$\frac{\rho_{\rm lc}(r)}{\rho(r)} = (1-\exp A)\cdot\mathrm{erf}(B), \tag{4.26}$$

where

$$\begin{aligned} A \equiv &\quad -\frac{\mathscr{R}^2}{r^2-\mathscr{R}^2}\,\frac{1}{\sigma_{\rm t}^2}(C) \\ B \equiv &\quad \frac{1}{\sigma_{\rm r}}\sqrt{\frac{G\mathscr{M}}{r}+\frac{G\mathscr{M}_\star}{\sqrt{r^2+r_{\rm c}^2}}} \\ C \equiv &\quad 2\sigma_{\rm r}^2+\frac{G\mathscr{M}}{\mathscr{R}}-\frac{G\mathscr{M}}{r}+\frac{G\mathscr{M}_\star}{\sqrt{\mathscr{R}^2+r_{\rm c}^2}}-\frac{G\mathscr{M}_\star}{\sqrt{r^2+r_{\rm c}^2}}. \end{aligned} \tag{4.27}$$

The velocity vectors of all stars which belong to a given (fixed) phase space density $f = f_0 = \mathrm{const}$ shape an ellipsoid whose two tangential and one radial major axes have lenghts equal to the velocity dispersion: $\sigma_\theta = \sigma_\phi$, and $\sigma_{\rm r}$ (Frank and Rees, 1976). If one uses $f_0 = f(\sigma_{\rm r},\sigma_\theta,\sigma_\phi)$, the surface of the ellipsoid $A = \pi\sigma_\theta\sigma_\phi\sigma_{\rm r}$ is a measure for the available velocity space.
A cone of angle $\theta_{\rm lc}$,

$$\theta_{\rm lc} := \arcsin\left(\frac{v_{\rm lc}}{\sigma_{\rm r}}\right), \tag{4.28}$$

cuts out a segment of the foregoing velocity ellipsoid's $A$ surface of corresponding fraction surface $A_{\rm lc}$,

$$A_{\rm lc} \approx \pi\theta_{\rm lc}^2,\ (\theta_{\rm lc} << \pi). \tag{4.29}$$

We can then define the ratio $\Omega' := A_{\rm lc}/A \approx \theta_{\rm lc}^2/4$, which is a measure for the loss-cone size.
With the assumption that $v_{\rm lc}$ does not depend on $v_{\rm r}$ any more and taking into account that with a Schwarzschild-Boltzmann distribution we can reduct the loss-cone momenta to elementary Gaussian

error functions. The quantity

$$\Omega := \frac{\rho_{\rm lc}}{\rho} \tag{4.30}$$

yields in first order

$$\Omega \approx \frac{v_{\rm lc}^2}{4\sigma_\theta^2} \approx \frac{\theta_{\rm lc}^2}{4}. \tag{4.31}$$

This is the connection between the preceding simple picture of the loss-cone and the definition of $\Omega$ in the velocity space: For a Schwarzschild-Boltzmann distribution we can find out that, at first order, $\Omega$ is of the same size as $\Omega'$.

## 4.8 Isotropy and anisotropy in the stellar system

We introduce now an *isotropy ratio* in order to study the different possible situations for the stellar distribution: The tangential velocity dispersion is $\sigma_{\rm t}^2 = \sigma_\phi^2 + \sigma_\theta^2$; in case of isotropy, $\sigma_{\rm r}^2 = \sigma_\phi^2 + \sigma_\theta^2$, then $\sigma_{\rm t}^2 = 2\sigma_{\rm r}^2$.
Now we define the ratio $R := 2\sigma_{\rm r}^2/\sigma_{\rm t}^2$. According to this definition, $R = 1$ for the isotropic case. The corresponding values of $R$ for radial and tangential anisotropy can be obtained bearing in mind that $\sigma^2 = \sigma_{\rm r}^2 + \sigma_{\rm t}^2 = \sigma_{\rm t}^2(R/2+1)$, $\sigma_{\rm t} = \sigma/\sqrt{R/2+1}$ and $\sigma_{\rm r} = \sigma_{\rm t}\cdot\sqrt{R/2}$.
We have the loss-cone star density as a function of the super-massive star radius, $\mathscr{R}$. This does not provide much information, since in principle this radius could have any size; we do not have a criterion for it yet. Instead, what does make sense is to express this loss-cone star density in terms of the super-massive star stability, which is something has been studied in detail (Fuller et al., 1986).
From Chandrasekhar (1964), instability sets in when the radius of the star $\mathscr{R}$ is less than a critical radius $\mathscr{R}^{\rm crit}$. He shows that if the ratio of specific heats $\gamma = C_p/C_v$ exceeds 4/3 only by a small amount, then dynamical instability will occur if the mass contract to the radius $\mathscr{R}^{\rm crit}$

$$\mathscr{R}^{\rm crit} = \frac{K}{\gamma - \frac{4}{3}}\left(\frac{2G\mathscr{M}}{c^2}\right). \tag{4.32}$$

Thus, we introduce the *stability coefficient* $\delta := \mathscr{R}/\mathscr{R}^{\rm crit}$. We just have to substitute $\mathscr{R} = \delta\cdot\mathscr{R}^{\rm crit}$ in the loss-cone star density formula and vary $\delta$ instead of $\mathscr{R}$.

## 4.9 Connection at the influence radius

Since we are interested in the diffusion angle, we now derive two expressions for it, within the influence radius of the *SMS* and outside it. For this aim we look at the dynamical and relaxation time at this radius.

The $\sigma(r)$ varies depending on $r_{\rm h}$.

$\circ$ $r \le r_{\rm h}$:

In this case we assume that the gravitational potential is dominated by the *SMS*. Therefore, the velocity dispersion is:

$$\sigma(r) = \sqrt{\frac{G\mathscr{M}}{r}}; \tag{4.33}$$

This is just an approximation which we make here for simplicity, since we stand on radii $r < r_{\rm h}$. To include $r \ll r_{\rm h}$ we need a better model, which can only be obtained by numerical solution of the equation of Poisson, and this is subject of future work.

$\circ$ $r > r_{\rm h}$:
For radii larger than $r_{\rm h}$ we will use a Plummer model for the velocity dispersion,

$$\sigma(r) = \sqrt{\frac{G\mathscr{M}_\star}{6r_{\rm c}}}\left(1+\frac{r^2}{r_{\rm c}^2}\right)^{-1/4} \tag{4.34}$$

However, we have to match both solutions, within and outside the *SMS* influence radius, for we have to look for a velocity dispersion connection; otherwise we get artificial, non-physical "jumps" in the plots for $r \approx r_{\rm h}$. This can be performed as follows: We add in the velocity dispersion expression a factor $\alpha$,

$$\sigma(r) = \sqrt{\frac{G\mathscr{M}_\star}{6r_{\rm c}}}\frac{\alpha}{(1+r^2/r_{\rm c}^2)^{1/4}}, \tag{4.35}$$

and we ask now for both velocities dispersions to be equal at the influence radius:

$$\sigma(r_{\rm h})|_{r<r_{\rm h}} \equiv \sigma(r_{\rm h})|_{r>r_{\rm h}}. \tag{4.36}$$

We can conclude that $\alpha$ has the following value:

$$\alpha = \sqrt{\frac{6}{r_{\rm h}}\frac{\mathscr{M}}{\mathscr{M}_\star}}\cdot(r_{\rm c}^2+r_{\rm h}^2)^{1/4} \tag{4.37}$$

Note that $\alpha$ is necessary because our velocity dispersion is approximate for $r < r_{\rm h}$, but not for $r \ll r_{\rm h}$. Therefore, the velocity dispersion outside the influence radius is:

$$\sigma(r) = \sqrt{\frac{G\mathscr{M}_s}{r_{\rm c}r_{\rm h}}}\cdot\left[\frac{r_{\rm c}^2}{r_{\rm c}^2+r^2}(r_{\rm c}^2+r_{\rm h}^2)\right]^{1/4}. \tag{4.38}$$

As regards the dynamical time, as we saw in the introduction, $t_{\rm dyn} = r/\sigma_{\rm r}(r)$, is

$$t_{\rm dyn} = \begin{cases} \frac{r^{3/2}}{\sqrt{G\mathscr{M}}} & r \le r_{\rm h} \\ r\sqrt{\frac{r_{\rm h}}{G\mathscr{M}}}\cdot\left(\frac{r^2+r_{\rm c}^2}{r_{\rm h}^2+r_{\rm c}^2}\right)^{1/4} & r > r_{\rm h} \end{cases} \tag{4.39}$$

For the relaxation time we need the density of the stellar system; We already commented that, according

to Frank and Rees (1976) or to Bahcall and Wolf (1976), the density of the spherical stellar system around the central mass should follow a power law of the form $\rho(r) \propto r^{-7/4}$.

$$\rho(r) = \rho_{\rm p}(r_{\rm h}) \cdot \left(\frac{r}{r_{\rm h}}\right)^{-7/4} \tag{4.40}$$

where $\rho_{\rm p}(r_{\rm h})$ is

$$\rho_P(r_{\rm h}) = \frac{3\mathscr{M}_\star}{4\pi r_{\rm c}^3}\left(1+\frac{r_{\rm h}^2}{r_{\rm c}^2}\right)^{-5/2} \tag{4.41}$$

Therefore,

$$\rho(r) = \frac{3\mathscr{M}_\star}{4\pi r_{\rm c}^3}\left(1+\frac{r_{\rm h}^2}{r_{\rm c}^2}\right)^{-5/2}\left(\frac{r}{r_{\rm h}}\right)^{-7/4} \tag{4.42}$$

Thus, the final expression for the relaxation time in such a system is

$$t_{\rm relax} = \begin{cases} \frac{3\sqrt{\pi}r_{\rm c}^3}{4\mathscr{M}_\star \ln(\gamma N)}\left(\frac{G\mathscr{M}}{r}\right)^{3/2}\left(\frac{r}{r_{\rm h}}\right)^{7/4}\left(1+\frac{r_{\rm h}^2}{r_{\rm c}^2}\right)^{5/2} & r \le r_{\rm h} \\ \frac{3\sqrt{\pi}r_{\rm c}^3}{4\mathscr{M}_\star \ln(\gamma N)}\left(\frac{G\mathscr{M}}{r_{\rm c}r_{\rm h}}\right)^{3/2}\left(1+\frac{r^2}{r_{\rm c}^2}\right)^{5/2}\left[\frac{r_{\rm c}^2}{r^2+r_{\rm c}^2}(r_{\rm c}^2+r_{\rm h}^2)\right]^{3/4} & r > r_{\rm h} \end{cases} \tag{4.43}$$

These expressions enable us to get the value for $\theta_{\rm D}$; we can get $\theta_{\rm lc}$ thanks to $\Omega$, $\theta_{\rm lc} \approx 2\sqrt{\Omega}$. Then we plot them altogether to find out at what radius do they cross, since we are looking for the critical radius, $r = r_{\rm crit} \iff \theta_{\rm lc} = \theta_{\rm D}$.

## 4.10 Mass accretion rates

The rate of stars plunging onto the central *SMS* is given by two different formulæ, depending on whether or not there is a crossing point for the $\theta_{\rm lc}$, $\theta_{\rm D}$- plot against the radius, *a critical radius*. If we find that the curves happen to cross, the mass accretion rate $\dot{\mathscr{M}}_\bullet$ has the expression $\dot{\mathscr{M}}_\bullet = \mathscr{M}_\star(r_{\rm h})/t_{\rm relax}(r_{\rm h})$ because the loss-cone will be depleted in a relaxation time, and the mass to take into account is that which lays within the critical radius. On the other hand, if there is no crossing point, this means that the loss-cone in not empty and in this situation we have to employ a rather different expression, we have to resort to the loss-cone star density expression to get the mass being accreted into the *SMS*. In this case the timescale of interest is the dynamical time, $\dot{\mathscr{M}}_\bullet = \Omega(r)\mathscr{M}_\star(r)/t_{\rm dyn}(r)$.

It may be asserted, nevertheless, that this formula is not completely correct because it is based on the stationary model, which supposes an empty loss-cone in the first case and a full loss-cone in the second case. We have to generalise it by means of a "diffusion" model (see chapter 5). We introduce the concept of the *filling degree* K of the loss-cone as follows: Let us conjecture that $f$ is the unperturbed velocity distribution. If the loss-cone is empty and angular momentum diffusion is neglected, then $f = 0$ inside the loss-cone and $f$ remains unchanged elsewhere in velocity space. Actually, this distribution function will have a continuous transition from nearly unperturbed values at large angular momenta towards a partially depleted value inside the loss-cone. We approximate this by a distribution function $f$ having a sudden jump just at the value $L_{\rm min} = m_\star v_{\rm lc}$ from an unperturbed value $f_0$, $f = K \cdot f_0$, with $0 \le K \le 1$.

Since we work with the hypothesis that some kind of stationary state is to be established in the limit $t \to \infty$, the filling degree is the result of calculating this limit,

$$k_\infty := \lim_{t\to\infty} K(t) = \frac{t_{\rm out}}{P_{\rm lc}\, t_{\rm in}\chi} = \tag{4.44}$$

$$\left(\frac{\theta_{\rm D}^2}{\theta_{\rm lc}^2}\right)\cdot\frac{1}{P_{\rm lc}\chi},$$

where

$$\chi \equiv 1 + \frac{t_{\rm out}}{P_{\rm lc} t_{\rm in}} = 1 + \frac{4\theta_{\rm D}^2}{P_{\rm lc}\theta_{\rm lc}^2}. \tag{4.45}$$

Therefore,

$$k_\infty = \frac{\nu(1+\nu)}{1+\nu(1+\nu)}. \tag{4.46}$$

In this expression $\nu \equiv \theta_{\rm D}^2/\theta_{\rm lc}^2$. Then we have to multiply the accretion rates by this filling degree $k_\infty$. The stellar mass within and outside the influence radius is

$$M(r, r_{\rm min})|_{r<r_{\rm h}} = \lim_{r_{\rm min}\to 0} 4\pi \int_{r_{\rm min}}^{r} \rho(r') r'^2 dr' = \tag{4.47}$$

$$\lim_{r_{\rm min}\to 0} 4\pi\rho(r_{\rm h})\cdot r_{\rm h}^{7/4}\int_{r_{\rm min}}^{r} r'^{\,1/4} dr' =$$

$$\lim_{r_{\rm min}\to 0} 4\pi\rho(r_{\rm h})\cdot r_{\rm h}^{7/4}\left[\frac{4}{5} r'^{\,5/4}\right]_{r_{\rm min}}^{r} =$$

$$\frac{16\pi}{5}\rho(r_{\rm h})\, r_{\rm h}^3\left(\frac{r}{r_{\rm h}}\right)^{5/4},$$

$$M(r)|_{r>r_{\rm h}} = M(r_{\rm h})|_{r<r_{\rm h}} + 4\pi\int_{r_{\rm h}}^{r}\rho(r')r'^2 dr' \tag{4.48}$$

$$= \frac{16\pi}{5}\rho(r_{\rm h})\, r_{\rm h}^3 + 4\pi\frac{\mathscr{M}_\star}{r_{\rm c}^3}\left[\frac{r^3}{\left(1+r^2/r_{\rm c}^2\right)^{3/2}} - \frac{r_{\rm h}^3}{\left(1+r_{\rm h}^2/r_{\rm c}^2\right)^{3/2}}\right].$$

To get the total heating rates, we just have to compute the value of

$$L_{\rm heat,\ all} = \left(\frac{\dot{\mathscr{M}}_\bullet}{m_\star}\right)\cdot E_{\rm heat,\ 1\star}, \tag{4.49}$$

where $E_{\rm heat,\ 1\star}$ is the heating for one star (during one crossing).

## 4.11 Heating rates: An esteem

In this section we analyse the interaction rate of stars with the *SMS* by varying the parameters introduced in the former sections, namely $\delta$, the core radius $r_c$, the total stellar mass and the super-massive star mass itself. We suppose that the stars which conform the stellar system are solar-type stars. For all the plots we extend the radii down to 1.001 times the *SMS* radius, because we would run into a snag if we extended it within the *SMS* radius, since the proportions $\sigma^2 \propto 1/r$ and $\rho \propto r^{-7/4}$ would be wrong and the loss-cone star density and therefore the loss-cone angle has been obtained considering a Maxwell-Boltzmann distribution. It would also be an error of the problem conception itself, because we are studying the non-confined stars and the loss-cone, and its definition does not make any sense for radii less than the $\mathscr{R}$. This explains the first inequality in $\mathscr{R} < r_h < r_c$, which is an exigency that we must follow unfailingly because, otherwise, the Plummer model, which we use for the stellar system, would not be a suitable solution for it in the case that $r_h < r_c$ is not satisfied. However, what we demand here is not a requirement of the physics of the problem, but a condition for the method being employed to solve it. Situations in which $r_h < \mathscr{R}$ or $r_h > r_c$ have to be solved numerically for the equation of Poisson and the velocity distributions.

In order to estimate the heating rates for a single star crossing the *SMS* we have to plot out the mass accretion rate of this central massive object in the case that we have no crossing point for the loss-cone and diffusion angle curves, whereas if we have a critical radius we will have to compute the total stellar mass and dynamical time at this value.

In Fig. (4.2) we plot the velocity dispersion against the radius for a $10^3 M_\odot$ *SMS*. We observe a typical power law of $\propto r^{-1/2}$ within the influence radius -which we represent by a vertical dashed line for all cases- because we have a cusp on velocities in this interval of radii. We have a nearly constant velocity for later radii which lie in the section of values close to the core radius. Then the velocity dispersion decays. The length of this nearly constant velocity section as well as the slope for the decay depends on the galactic nuclei in the galaxy.

Regarding Fig. (4.3), we show the loss-cone normalised density difference between the isotropic and radially anisotropic cases for a $10^7 M_\odot$ *SMS*. In this plot we can observe a bigger number of stars being accreted into the *SMS* for the radially anisotropic case,since a radial orbit means a lower angular momentum and thus it is more probable that the star sinks into the central object, and vice-versa for a tangential orbit, Fig. (4.4).

As regards the loss-cone and diffusion angle plots, we examine two different cases in Figs.(4.5) and (4.6): a $10^4 M_\odot$ and a $10^7 M_\odot$ *SMS*. One may observe that for the first one we find a critical radius, whereas for the latter one the curves do not intersect. It is also interesting to find out which angle is bigger and where, since for a $\theta_{lc} \gg \theta_D$ we have an almost empty loss-cone, because it is quickly depleted and the stars replenish it very slowly; the opposite case, $\theta_{lc} \ll \theta_D$, implies that the loss-cone is full.

We get a maximum $\dot{\mathscr{M}}_\bullet$ at about a core radius in the mass accretion rates plot for a $10^7 M_\odot$ *SMS*, because the biggest contribution of stars being accreted into the *SMS* lies at this radius. Fig. (4.7) shows an irregularity at the influence radius, because the loss-cone and diffusion angle plots show us that the former happens to be always bigger than this one and thus we have to apply the approximation

commented in the foregoing section.
When we look at the $\dot{\mathscr{M}}_\bullet$ for the $10^3 M_\odot$ and $10^4 M_\odot$ *SMS*s, we obtain that for the $10^3 M_\odot$: $\dot{\mathscr{M}}_\bullet|_{\rm iso} = 1.75\times10^{-13}\ M_\odot/{\rm yr}$, $\dot{\mathscr{M}}_\bullet|_{\rm tan} = 1.66\times10^{-13}\ M_\odot/{\rm yr}$, $\dot{\mathscr{M}}_\bullet|_{\rm rad} = 1.97\times10^{-13}\ M_\odot/{\rm yr}$. Where the subscript "iso" stands for isotropy, "rad" for radial anisotropy and "tan" for tangential anisotropy.
The case of $10^4 M_\odot$ is similar to the last one. For the $10^7 M_\odot$ *SMS*, we will select the $\dot{\mathscr{M}}_\bullet$ corresponding to the core radius, since the most important contribution is reached there: $\dot{\mathscr{M}}_\bullet|_{\rm core} = 10^{-2}\ M_\odot/{\rm yr}$. To get the heating rates of these non-confined stars, we just have to compute

$$\dot{E} = \left(\frac{\dot{\mathscr{M}}_\bullet}{M_\odot}\right)\pi r_\star^2 \rho_{sms} v_\star^2 \cdot 2\mathscr{R}/t_{\rm cross}, \tag{4.50}$$

where $v_\star^2 = G\mathscr{M}/\mathscr{R}$, $t_{\rm cross} = 2\mathscr{R}/v_\star$, $\rho_{\rm SMS} = \mathscr{M}/(\frac{4\pi}{3}\mathscr{R}^3)$. For the *SMS* we have supposed, as a first approximation, a constant density.
The corresponding $\mathscr{R}$'s are:

$\mathscr{R}_{10^3} = 2.5\times10^{-9}$ pc
$\mathscr{R}_{10^4} = 8\times10^{-8}$ pc
$\mathscr{R}_{10^7} = 2.5\times10^{-2}$ pc,
where $\mathscr{R}_{10^i}$ stands for the $10^i M_\odot$ *SMS* radius.

The luminosities are:

$L_{10^3}/L_\odot = 6.2\times10^3$
$L_{10^4}/L_\odot = 1.17\times10^4$
$L_{10^7}/L_\odot = 5.6\times10^5$,
idem $L_{10^i}$ $10^i M_\odot$ *SMS* luminosity. It is not a surprise that these luminosities are not sufficient to support quasar luminosities, which was known before. We confirm however the earlier result by Langbein et al. (1990) with our more detailed, but stationary loss-cone model, that the luminosities are large enough to prevent for some time the relativistic collapse of a *SMS* in a galactic centre; that was called the quasi-pile stage by Hara (1978).
In the case of a confined star, the heating rate can be obtained in a much simpler way. We just have to assume that the star is on a circular orbit at $r \approx \mathscr{R}$, then its velocity is

$$v_{\rm circ}^2 = \frac{G\mathscr{M}}{\mathscr{R}}, \tag{4.51}$$

the orbital time is

$$t = \frac{2\pi\mathscr{R}}{v_{\rm circ}} = 2\pi\sqrt{\frac{\mathscr{R}^3}{G\mathscr{M}}}. \tag{4.52}$$

Regarding to the drag force, $F_{\rm D} = C_{\rm D}\pi r_\star^2 \rho_g v_{\rm circ}$, where $\rho_g = \mathscr{M}/(\frac{4\pi}{3}\mathscr{R}^3)$ is the average density. The heating by one star will be

$$E_{\rm heating}|_{\rm conf} = F_{\rm D}\cdot 2\pi\mathscr{R} \tag{4.53}$$

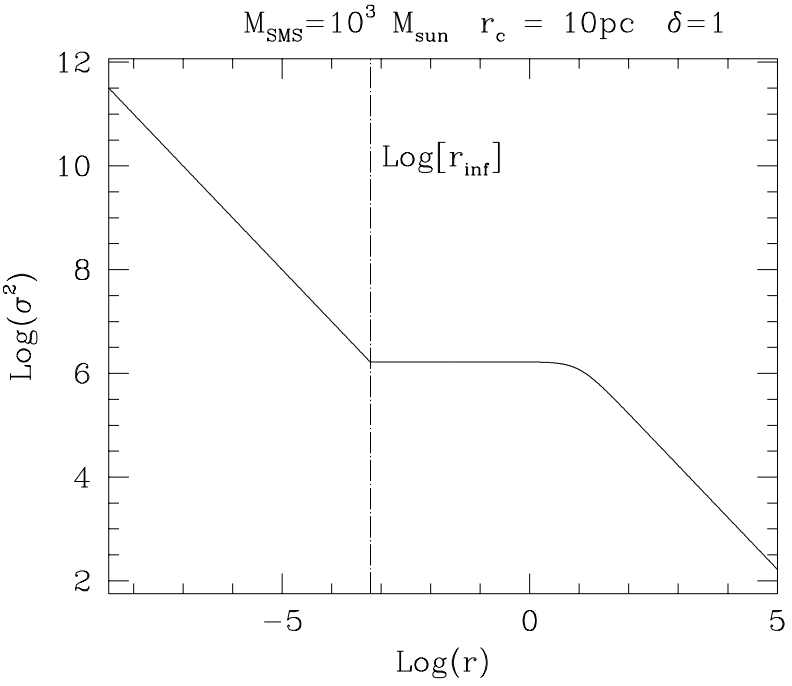


Fig. 4.2: The velocity units are $(m/s)^2$ and $r$ is expressed in pc. The influence radius is located at $6 \cdot 10^{-4}$pc. We show its logarithm in the plot with a vertical dashed line. The central velocity dispersion (the velocity dispersion at the influence radius) is $\sigma_{\text{central}} = \sqrt{G\mathscr{M}_\star/(6r_\text{c})} = 84$ km/s. $\text{M}_{\text{SMS}}$ stands for $\mathscr{M}$

The number of stars in the *SMS*is given by

$$N_\star = \frac{4\pi}{3}\rho(\mathscr{R})\mathscr{R}^3, \tag{4.54}$$

where $\rho(\mathscr{R}) = \rho(r_\text{h})(\mathscr{R}/r_\text{h})^{-7/4}$. Therewith, the heating by confined stars is

$$E_{\text{heating, conf}} = N_\star \cdot F_\text{D} \cdot 2\pi\mathscr{R}. \tag{4.55}$$

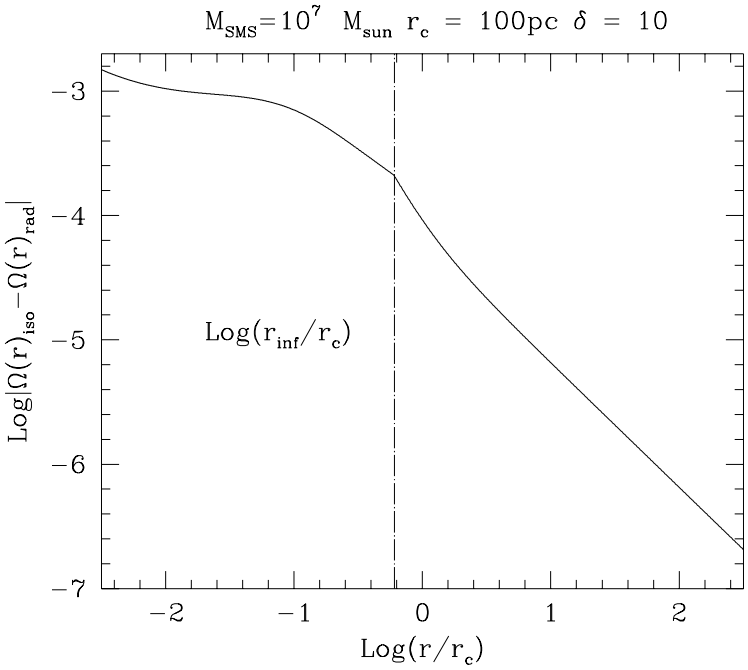


Fig. 4.3: $\Omega(r) := \rho_{\rm lc}(r)/\rho(r)$ decays with the distance to the *SMS*. We have divided the radius by the core radius in order to normalise it. A bigger number of stars plunge on to the *SMS* for the radially anisotropic case

## 4.12 Discussion of the results

We have revisited the classical loss-cone semi-analytic theory invented by Frank and Rees (1976) for star accretion onto central super-massive black holes in galactic nuclei and star clusters and extended by da Costa (1981) for the case of stars on radial orbits being trapped by star-gas interactions in a central super-massive star-gas system. In Langbein et al. (1990) such model was included in time-dependent, spherically symmetric models of star-gas systems in galactic nuclei. Though highly idealized, we think that such configurations are still worth a study to understand the physical processes at work in the early formation phase of massive galaxies with formation of central black holes. Notions such as the critical radius in the classical work, where the loss-cone star accretion becomes important and flattens out the cusp density profile turn out naturally in our model without any ad hoc assumptions. While in this

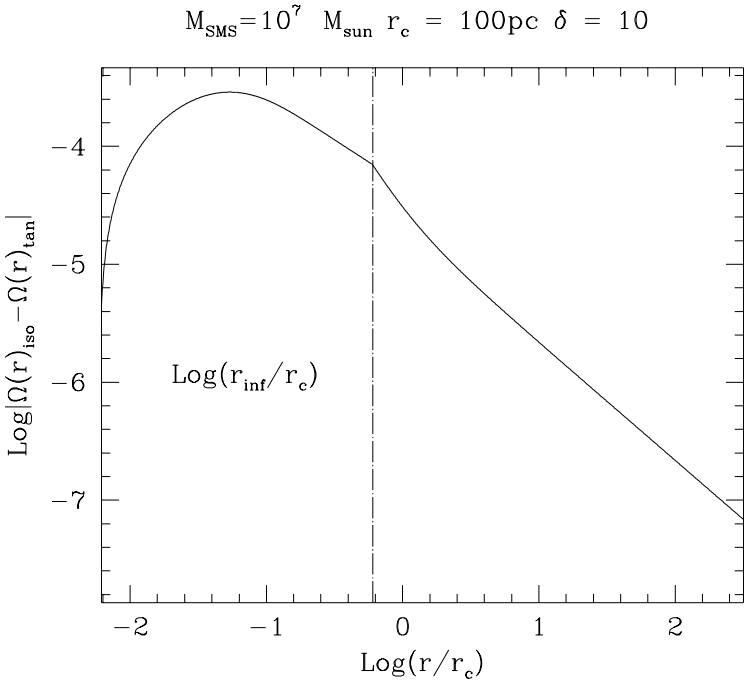


Fig. 4.4: The same as for Fig. (4.3) but for the tangentially anisotropic case and a lower number of stars

research note we keep the stellar background system fixed and develop the old ideas in an up-to-date form, one should include them into a self-consistent dynamical model of relaxing star clusters with central black hole. Recent dramatic improvements of the observational situation and the demography of black holes in nuclei demand such progress in dynamical modelling, which is yet surprisingly poor (Richstone et al., 1998). It is clear that in a proper cosmological context many complications occur for simplified modelling: the whole system is embedded in a collisionless dark halo with disputed central density profile, it is non-stationary due to a sequence of merger events in hierarchical structure formation, with the possible formation of binary or multiple black holes and perturbations of various kinds will even cause a single black hole not to be fixed in the centre. Despite of all that have begun our work at the point where we think present (astro)physical understanding and modelling comes to its limits, and this is the case for a spherical dense large $N$ star cluster, suffering from relaxation and star accretion around a fixed massive black hole.

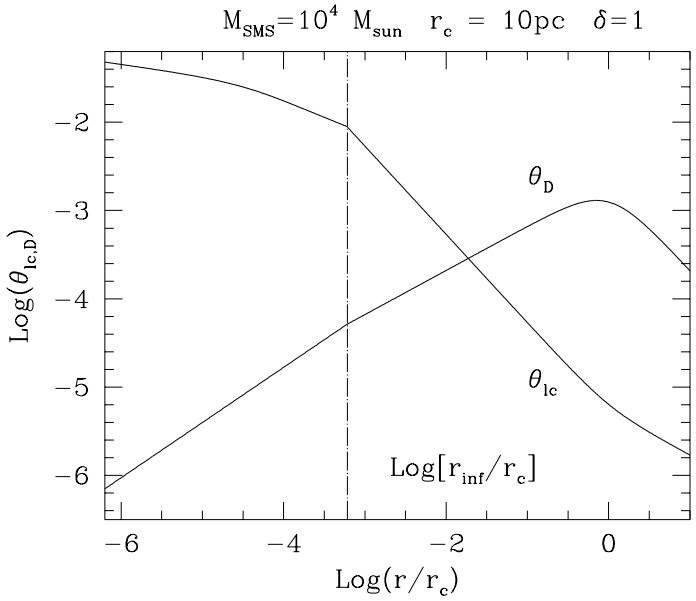


Fig. 4.5: $\theta_{\rm lc} = 2 \cdot \sqrt{\Omega(r)}$, $\theta_{\rm D} = \sqrt{t_{\rm dyn}/t_{\rm relax}}$. For this mass the two curves cross at the critical radius. For radii smaller than that, the loss-cone angle is bigger than the diffusion angle, and this implies that the loss-cone is empty. From the $r_{\rm crit}$ onwards it is no longer empty, for $\theta_{\rm D} > \theta_{\rm lc}$. With the crossing point we can work out the accretion rate and find out the differences depending on whether we consider an isotropic situation for the stellar velocity distribution function or an anisotropic one, distinguishing between a radial or tangential anisotropy. If we set this case against the $10^3 {\rm M}_\odot$ we do not find big differences

## 4.13 Addendum A: The tidal radius

When the stars approach the BH they experience strong tidal forces which may be violent enough to blow up the star. The star gets disrupted whenever the work exerted over the star by the tidal force exceeds its own binding energy, (all energies are per unit mass):

$$E_{\rm bind} = \alpha \frac{G m_\star}{r_\star},\ \alpha = \frac{3}{5-n} \tag{4.56}$$

where $n$ is the polytropic index (Chandrasekhar, 1942).

$$(F_1 - F_2) 2 r_\star = \alpha \frac{G m_\star}{r_\star} \tag{4.57}$$

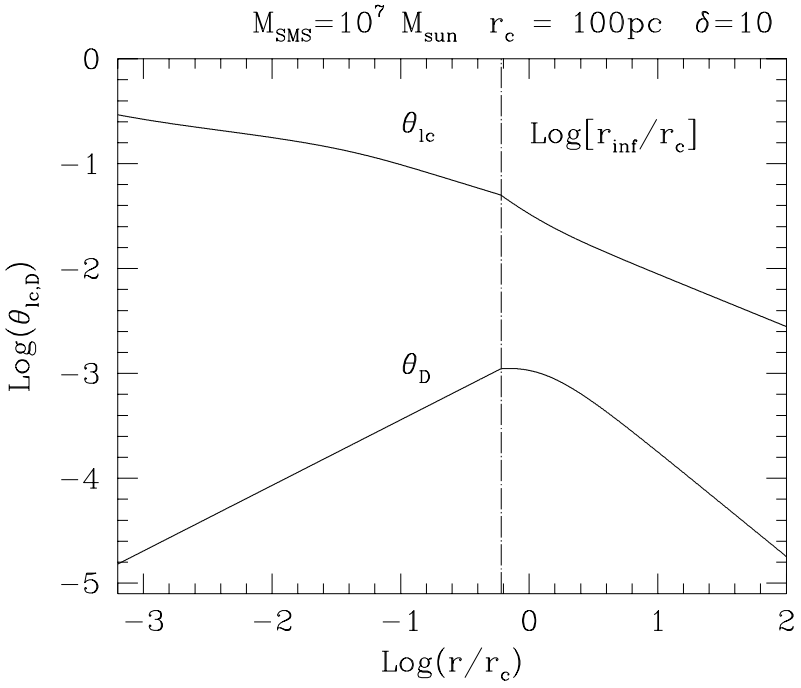


Fig. 4.6: For higher masses, such as $10^7 M_\odot$, the loss-cone is empty. We get no critical radius

$$F_1 = \frac{G\mathscr{M}_\bullet}{(r_t - r_\star)^2},\ F_2 = \frac{G\mathscr{M}_\bullet}{(r_t + r_\star)^2}. \tag{4.58}$$

Considering $r_\star \ll r_t$, we can approximate the expressions:

$$\begin{aligned} \tfrac{1}{(r_t - r_\star)^2} &\approx \frac{1}{r_t^2} + \frac{2r_\star}{r_t^3} \\ \tfrac{1}{(r_t + r_\star)^2} &\approx \frac{1}{r_t^2} - \frac{2r_\star}{r_t^3}; \end{aligned} \tag{4.59}$$

then,

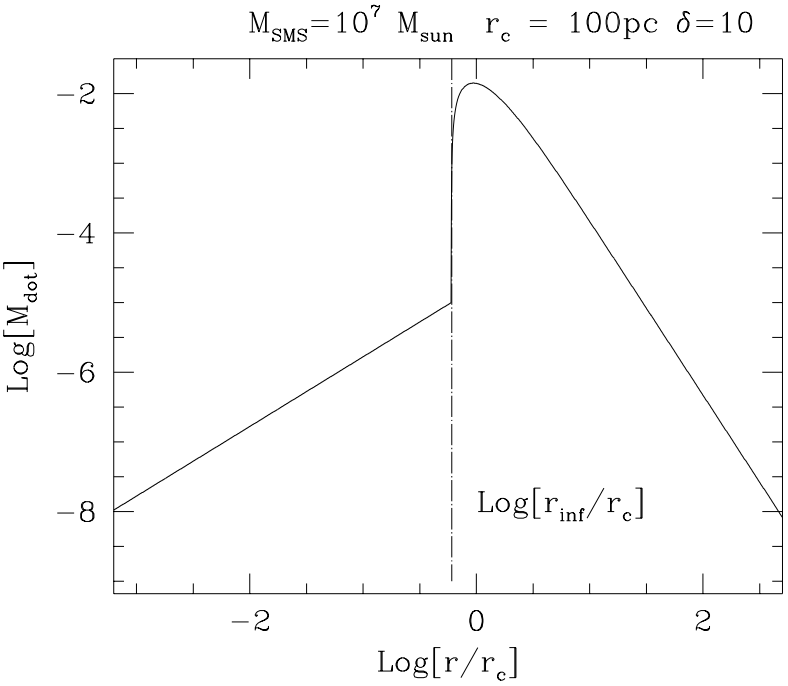


Fig. 4.7: The "jump" is due to the approximation we made in order to get the accretion rates. The maximum is reached at a distance which corresponds to the core radius

$$r_{\rm tidal} = \left[\frac{2}{3}(5-n)\frac{\mathscr{M}_\bullet}{m_\star}\right]^{1/3} r_\star. \tag{4.60}$$

For solar-type stars it is (considering a $n = 3$ polytrope)

$$r_{\rm t} \simeq 1.4 \times 10^{11}\left(\frac{\mathscr{M}_\bullet}{M_\odot}\right)^{1/3} \text{cm}. \tag{4.61}$$

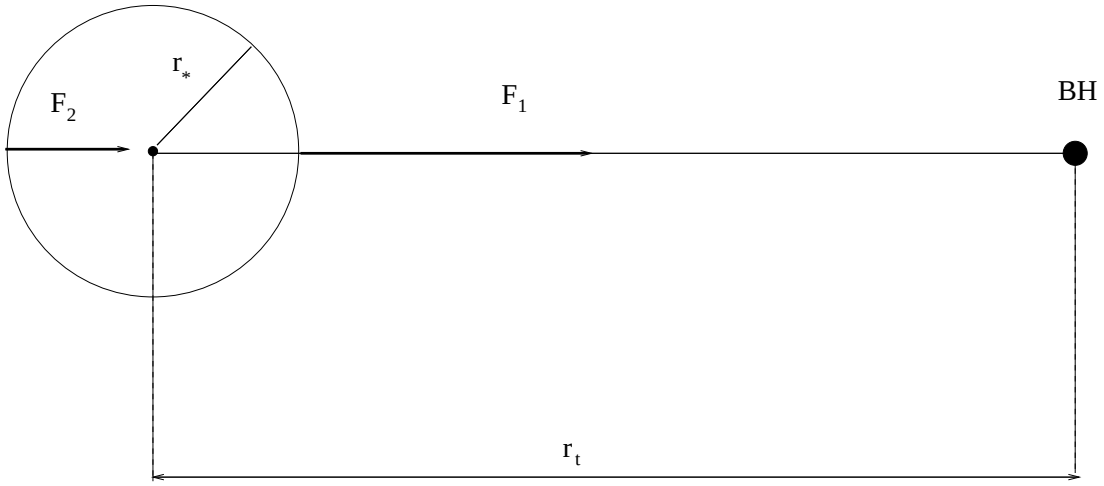


Fig. 4.8: Decomposition of the tidal forces over a star

## 4.14 Addendum B: The difussion and loss-cone angles

### 4.14.1 Definition of the difussion angle $\theta_{\rm D}$

The relaxation time is the required time for $\triangle v_\perp^2/v_\perp^2 \simeq 1$ (i.e. the change in the perpendicular velocity component is of the same order as the perpendicular velocity component itself);

$$\triangle v_\perp^2 = n_{\rm relax}\cdot\delta v_\perp^2,\ \triangle v_\perp^2/v_\perp^2 = 1 = \frac{n_{\rm relax}\cdot\delta v_\perp^2}{v_\perp^2} \tag{4.62}$$

$$t_{\rm relax} = n_{\rm relax}\cdot t_{\rm dyn} = \left(\frac{v_\perp^2}{\delta v_\perp^2}\right)\cdot t_{\rm dyn}, \tag{4.63}$$

where $n_{\rm relax}$ is the numbers of crossings for $\triangle v_\perp^2/v_\perp^2 \simeq 1$. This conforms the definition of the relaxation time, $\triangle v_\perp^2/v_\perp^2 = t/t_{\rm relax}$ (Binney and Tremaine, 1987).
If we consider that $\theta_{\rm D}$ is very small,

$$\sin\theta_{\rm D} \simeq \frac{\delta v_\perp}{v} \simeq \theta_{\rm D};\ t_{\rm relax} \simeq \frac{t_{\rm dyn}}{\theta_{\rm D}^2} \tag{4.64}$$

$$\theta_{\rm D} \simeq \sqrt{\frac{t_{\rm dyn}}{t_{\rm relax}}}. \tag{4.65}$$

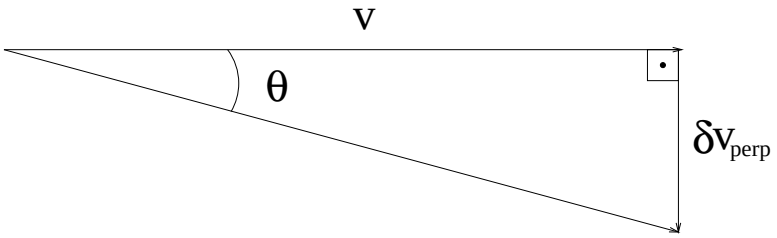


Fig. 4.9: Definition of angle $\theta$

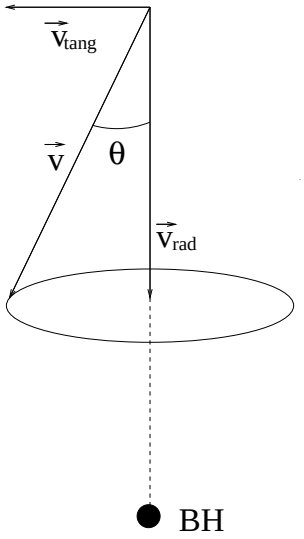


Fig. 4.10: Definition of angle $\theta_{\rm lc}$

### 4.14.2 Definition of the loss-cone angle $\theta_{\rm lc}$

We suppose that the central object with mass $\mathscr{M}_\bullet$ has an influence radius $r_{\rm h}$. To define this radius we say that a star will interact with the central object only when $r \leq r_{\rm h}$. Then we look for a condition at a place $r > r_{\rm h}$ for a star to touch or to cross the influence radius of the central object within a crossing time $t_{\rm cross} = r/\sigma_{\rm r}$.
As we saw in the text, the condition that defines this angle is the following:

$$r_{\rm p}(E,L) \leq r_{\rm t},\ \theta \leq \theta_{\rm lc}. \tag{4.66}$$

$$\sin\theta = \frac{v_{\rm t}}{v},\ \theta \ll 1;\ \Longrightarrow \theta \simeq \frac{v_{\rm t}}{v} = \frac{L/r}{v}. \tag{4.67}$$

Where $L = r v_{\rm t}$ is the specific angular momentum.
Now we derive an expression for this angle in terms of the influence radius:

• $r \leq r_{\rm h}$

In this region the star moves under the BH potential influence, then

$$\sigma(r) \approx \sqrt{\frac{G\mathscr{M}_\bullet}{r}} = \sqrt{\frac{G\mathscr{M}_\bullet}{R_{\rm h}}}\sqrt{\frac{R_{\rm h}}{r}} = \sigma(R_{\rm h}) \cdot \sqrt{R_{\rm h}/r} = \sigma_c \cdot \sqrt{R_{\rm h}/r}, \tag{4.68}$$

since $\sigma_c^2 \equiv G\mathscr{M}_\bullet/R_{\rm h}$.
The typical velocity of the orbit is $< v^2 > \simeq 3\sigma^3$, where the factor three stands for the three directions in the space. Since $\sigma$ means the one- dimensional dispersion, we have to take into account the dispersion of the velocity in each direction. Then,

$$< v > \simeq \sqrt{3}\sigma_c\sqrt{r_{\rm h}/r}. \tag{4.69}$$

Finally, we obtain the loss-cone angle,

$$\theta_{\rm lc} = \sqrt{\frac{2}{3}\frac{r_{\rm t}}{r}}. \tag{4.70}$$

• $r \geq r_{\rm h}$

We can consider that the velocity dispersion is more or less constant from this $r_{\rm h}$ onwards, $v \approx \sqrt{3}\sigma_c$,

$$\theta_{\rm lc} = \frac{\sqrt{2G\mathscr{M}_\bullet r_{\rm t}}}{\sqrt{3}r\sigma_c};\ \sigma_c = \sqrt{G\mathscr{M}_\bullet/r_{\rm h}}. \tag{4.71}$$

The angle is

$$\theta_{\rm lc} \approx \sqrt{\frac{2}{3}r_{\rm t}r_{\rm h}}/r. \tag{4.72}$$

## 4.15 Addendum C: The loss-cone velocity

We derive the $v_{\rm lc}(r)$ using angular momentum and energy conservation arguments. We just have to evaluate it at a general radius $r$ and at the tidal radius $r_{\rm t}$, where the tangential velocity is maximal and the radial velocity cancels (see Fig.4.11).
• general radius:

$$\begin{aligned} E(r) = &\quad \phi(r) - \frac{v_{\rm tg}(r)^2}{2} - \frac{v_{\rm r}(r)^2}{2} \\ L(r) = &\quad r v_{tg}(r) \end{aligned} \tag{4.73}$$

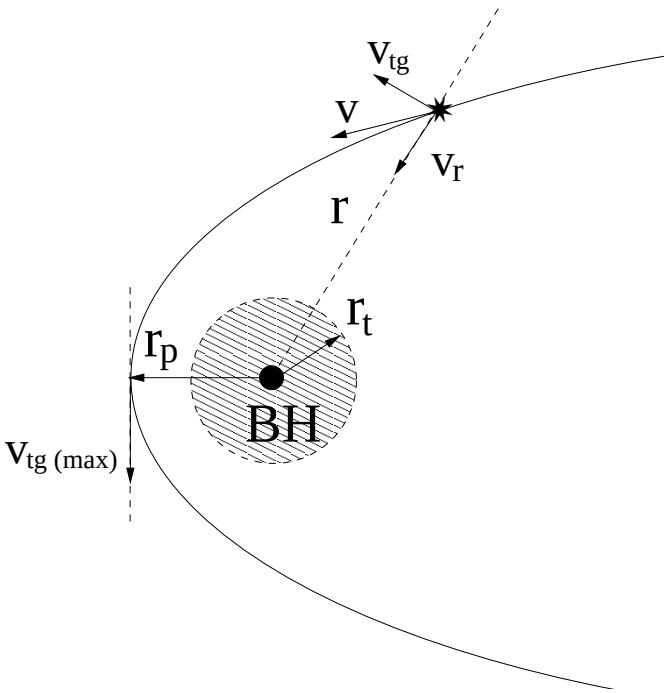


Fig. 4.11: Definition of the *peribarathron* as the distance of closest approximation of the star in its orbit to the BH. In this point the radial component of the velocity of the star cancels and the tangential component is maximum. In the figure "$r_{\rm p}$" stands for the peribarathron radius and "$r_{\rm t}$" for the tidal radius

• tidal radius:

$$\begin{aligned} E(r_{\rm t}) = &\quad \phi(r_{\rm t}) - \frac{v_{tg}(r_{\rm t})^2}{2} \\ L(r_{\rm t}) = &\quad r_{\rm t} v_{tg}(r_{\rm t}), \end{aligned} \tag{4.74}$$

from the momentum conservation and the fact that $v_{\rm r}(r_{\rm t}) = 0$ we get that:

$$v_{\rm tg}(r_{\rm t}) = \frac{r}{r_{\rm t}} \cdot v_{\rm tg}(r). \tag{4.75}$$

Idem energy, and using the last result,

$$\phi(r) - \frac{v_{tg}(r)^2}{2} - \frac{v_{\rm r}(r)^2}{2} = \phi(r_{\rm t}) - \frac{r^2}{2r_{\rm t}^2} \cdot v_{tg}(r)^2. \tag{4.76}$$

Then we get the tangential velocity of the stars in terms of r; namely, the loss-cone velocity:

$$v_{\rm lc}(r) = \frac{r_{\rm t}}{\sqrt{r^2 - r_{\rm t}^2}} \cdot \sqrt{2[\phi(r_{\rm t}) - \phi(r)] + v_{\rm r}(r)^2}. \tag{4.77}$$

Therewith, the angular momentum is

$$\begin{aligned} L(r_{\rm t}) = \quad & r_{\rm t} \cdot v_{\rm tg}(r)|_{\rm max} = r_{\rm t} \cdot \frac{r}{r_{\rm t}} v_{\rm tg}(r) = \\ r \cdot v_{\rm tg}(r) \quad & = r \cdot \frac{r_{\rm t}}{\sqrt{r^2 - r_{\rm t}^2}} \sqrt{2\triangle\phi + v_{\rm r}(r)^2}, \end{aligned} \tag{4.78}$$

where

$$\triangle\phi \equiv \phi(r_{\rm t}) - \phi(r) = \frac{G\mathscr{M}_\bullet}{r_{\rm t}} + \phi_\star(r_{\rm t}) - \frac{G\mathscr{M}_\bullet}{r} - \phi_\star(r) \tag{4.79}$$

If we use the fact that

$$r \gg r_{\rm t} \Rightarrow \frac{G\mathscr{M}_\bullet}{r_{\rm t}} \gg \left( \frac{G\mathscr{M}_\bullet}{r} + \phi_\star(r) \right) = \phi(r) \tag{4.80}$$

Also it is

$$\frac{G\mathscr{M}_\bullet}{r_{\rm t}} \gg \phi_\star(r_{\rm t}), \text{ since } \mathscr{M}_\bullet \gg \mathscr{M}_\star(r_{\rm t}) \tag{4.81}$$

thus,

$$v_{\rm lc}(r) \approx \frac{r_{\rm t}}{r} \sqrt{\frac{2G\mathscr{M}_\bullet}{r_{\rm t}}}. \tag{4.82}$$

If we use now the fact that

$$\sigma_{\rm r}(r) = \sigma_{\rm r}(r_{\rm t}) \cdot \left( \frac{r}{r_{\rm t}} \right)^{-1/2} = \sqrt{\frac{G\mathscr{M}_\bullet}{r_{\rm t}}} \cdot \left( \frac{r}{r_{\rm t}} \right)^{-1/2} \tag{4.83}$$

$$\Rightarrow \sqrt{\frac{G\mathscr{M}_\bullet}{r_{\rm t}}} = \sigma_{\rm r}(r) \cdot \left( \frac{r}{r_{\rm t}} \right)^{-1/2} \tag{4.84}$$

It is then in fair approximation

$$v_{\rm lc}(r) \approx \frac{r_{\rm t}}{r} \sqrt{\frac{2G\mathscr{M}_\bullet}{r_{\rm t}}} \approx \sigma_{\rm r}(r) \cdot \left( \frac{r_{\rm t}}{r} \right)^{1/2}. \tag{4.85}$$

## 4.16 Literature of chapter 4


Amaro-Seoane, P. and Spurzem, R. (2000). The Loss-Cone Problem in Dense Nuclei Revisited. In *Astronomische Gesellschaft Meeting Abstracts*.

Amaro-Seoane, P. and Spurzem, R. (2001a). The loss-cone problem in dense nuclei. *MNRAS*, 327:995–1003.

Amaro-Seoane, P. and Spurzem, R. (2001b). The Loss-Cone Star Contribution to the Heating Rate of a Supermassive Star. In *Stellar Dynamics: from Classic to Modern*, page 444.

Bahcall, J. N. and Wolf, R. A. (1976). Star distribution around a massive black hole in a globular cluster. *ApJ*, 209:214–232.

Binney, J. and Tremaine, S. (1987). *Galactic Dynamics*. Princeton University Press.

Bisnovatyi-Kogan, G. S. and Syunyaev, R. A. (1972). Quasars and the Nuclei of Galaxies: A Single Object or a Star Cluster? *Soviet Astronomy*, 16:204.

Chandrasekhar, S. (1942). Principles of stellar dynamics. *Physical Sciences Data*.

Chandrasekhar, S. (1964). The Dynamical Instability of Gaseous Masses Approaching the Schwarzschild Limit in General Relativity. *apj*, 140:417.

Courant, R. and Friederichs, K. O. (1998). Supersonic flow and shock waves. In Heidelberg, S.-V. B., editor, *Applied Mathematical Sciencies*, volume 21.

da Costa, L. N. (1979). Thesis. Harvard University, American Doctoral Dissertations.

da Costa, L. N. (1981). Star distribution in the presence of a massive central gas cloud. *MNRAS*, 195:869–880.

Frank, J. and Rees, M. J. (1976). Effects of massive central black holes on dense stellar systems. *MNRAS*, 176:633–647.

Fuller, G. M., Woosley, S. E., and Weaver, T. A. (1986). The evolution of radiation-dominated stars. I - Nonrotating supermassive stars. *apj*, 307:675–686.

Hagio, F. (1986). Effects of viscous drag on a slowly rotating supermassive star due to an embedded stellar system. *pasj*, 38:111–120.

Hara, T. (1978). Evolution of a super-massive star in a dense stellar system. *Progress of Th. Phys.*, 60:711–723.

Langbein, T., Fricke, K. J., Spurzem, R., and Yorke, H. W. (1990). Interactions between stars and gas in galactic nuclei. *aa*, 227:333–341.

Lightman, A. P. and Shapiro, S. L. (1977). The distribution and consumption rate of stars around a massive, collapsed object. *ApJ*, 211:244–262.

Magorrian, J., Tremaine, S., Richstone, D., Bender, R., Bower, G., Dressler, A., Faber, S. M., Gebhardt, K., Green, R., Grillmair, C., Kormendy, J., and Lauer, T. (1998). The Demography of Massive Dark Objects in Galaxy Centers. *AJ*, 115:2285–2305.

Marchant, A. B. and Shapiro, S. L. (1979). Star clusters containing massive, central black holes. II - self-consistent potentials. *ApJ*, 234:317–328.

Marchant, A. B. and Shapiro, S. L. (1980). Star clusters containing massive, central black holes. III - evolution calculations. *ApJ*, 239:685–704.

Peebles, P. J. E. (1972). Star distribution near a collapsed object. *ApJ*, 178:371–376.

Plummer, H. C. (1911). On the problem of distribution in globular star clusters. *MNRAS*, 71:460.

Richstone, D., Ajhar, E. A., Bender, R., Bower, G., Dressler, A., Faber, S. M., Filippenko, A. V., Gebhardt, K., Green, R., Ho, L. C., Kormendy, J., Lauer, T. R., Magorrian, J., and Tremaine, S.

(1998). Supermassive black holes and the evolution of galaxies. *nat*, 395:A14+.

Shapiro, S. L. and Marchant, A. B. (1978). Star clusters containing massive, central black holes - monte carlo simulations in two-dimensional phase space. *ApJ*, 225:603–624.

Shapiro, S. L. and Teukolsky, S. A. (1985). The collapse of dense star clusters to supermassive black holes - the origin of quasars and agns. *ApJ Lett.*, 292:41–44.

# Chapter 5

# A diffusion model for accretion of stars

VIEWING the problem of the joint evolution of a spherical star cluster with a central BH making feasible anisotropy, we shall introduce in these pages [1] the simulation method to follow to analyse such a scenario. This procedure, as we exposed in former chapters, is based on moments of the Boltzmann equation with relaxation. The cluster is modelled like a self-gravitating, conducting gas sphere, according to the methods presented in Louis and Spurzem (1991) and Giersz and Spurzem (1994). These models improved earlier gas models of Bettwieser (1983) and Heggie (1984). Much as the structure of the numerical method is for the sake of computational efficiency on account of physical accuracy, it allows for all the most important physical ingredients that may carry out a role in the evolution of a spherical cluster. These include, among others, self-gravity, two-body relaxation, stellar evolution, collisions, binary stars etc and, undoubtedly, the interaction with a central BH and the role of a mass spectrum. The specific advantage of the so-called "gaseous model" to other simulations methods (see chapter 2 for a description) is that the simulations are comparatively much faster, since they are grounded on numerical integration of a relatively small set of partial differential equations with just one spatial variable, the radius $r$. In addition, all quantities of interest are accessible as smooth functions of $r$ and time and this allows one to investigate in detail clean-cut aspects of the dynamics without being hindered by the important numerical noise particle-based methods ($N$–body and Monte Carlo) suffer from.

In this chapter we concentrate on the simplest version of the gaseous model which includes the interaction between a central BH and its host cluster. In particular, we assume that all stars are sun-like, neglect stellar evolution, direct collisions between stars and the role of binary stars. Also, the only interaction between BH and the stellar system is tidal disruptions (besides the BH's contribution to the gravitational field), and we undertake that the BH stays fixed at the centre of the cluster. While admittedly

[1] We employed some of the results of this chapter for Amaro-Seoane et al. (2004) and Spurzem et al. (2003)

very simplified, we reckon this idealised situation warrants consideration. First, it helps us to establish that the gaseous model is also able to treat more complex situations in phase space than self-gravitating star clusters, such as those caused by loss-cone accretion and a central BH; second, experience with the gaseous model and other methods showed us how intricate the interplay between various physical effects can become during the evolution of clusters and so we feel compelled to first consider the simplest models to develop a robust understanding of the mechanisms at play.
The structure of this chapter is as follows: In section 5.1 we explain the physics of the problem. In 2.2 we introduce briefly the various analytical and numerical methods used so far to investigate spherical clusters with central BH and summarise their key results. In section 5.2 we give a description of the theoretical diffusion model. Section 5.4 is devoted to results obtained in a first set of simulations. Finally, in 5.5, we draw conclusions about this first use of this new code version and present what our future work with it will likely consist of.

## 5.1 Loss-cone accretion on to massive BHs

### 5.1.1 Previous theoretical and numerical studies

If we arrange numerical methods for stellar dynamics in order of validity and both increasing the spatial resolution and decreasing the required computational time, we can distinguish four general classes. The most direct approach is the so-called *N*–body method (Aarseth, 1999a,b; Spurzem, 1999). Monte Carlo codes are also particle-based, but rely on the assumptions that the system is spherically symmetric and in dynamical equilibrium and treat the relaxation in the Fokker-Planck approximation (see 3.2) (Freitag and Benz 2004; Fregeau et al. 2003; Freitag and Benz 2001; Giersz and Spurzem 2003; Giersz 1998; Joshi et al. 2001). Ensuingly, we have the two-dimensional numerical direct solutions of the Fokker-Planck equation (Takahashi, 1997, 1996, 1995), and the gaseous models. The idea of this model goes back to Hachisu et al. (1978) and Lynden-Bell and Eggleton (1980), who first proposed to treat the two-body relaxation as a transport process like in a conducting plasma. They had been developed further by Bettwieser (1983); Bettwieser and Sugimoto (1984); Heggie (1984); Heggie and Ramamani (1989). Their present form, published in Louis and Spurzem (1991); Giersz and Spurzem (1994); Spurzem and Takahashi (1995) improves the detailed form of the conductivities in order to yield high accuracy (for comparison with *N*–body) and correct multi-mass models. This point has been made already in Spurzem (1992).
Peebles (1972); Shapiro and Lightman (1976) and especially Frank and Rees (1976) and Bahcall and Wolf (1976) addressed the problem of a stationary stellar density profile around a massive star accreting BH. They found that, under certain conditions, the density profile $\rho \propto r^{-7/4}$ is established in the region where the BH's gravitational potential well dominates the self-gravity of the stars [2].
The problem of a star cluster with a massive central star-accreting BH has been widely coped with Fokker-Planck numerical models. This approach was useful in order to test the solidness of the method

[2]We must mention here the legwork done twelve years before this analysis by Gurevich (1964), since he got an analogous solution for the distribution of electrons in the vicinity of a positively charged Coulomb centre.

to reproduce the $\rho \propto r^{-7/4}$ stationary density profile, since loss-cone accretion disturbs such a density cusp (Ozernoi and Reinhardt, 1978). The authors show that the stationary density profile follows from their stellar-dynamical equation of heat transfer by scaling arguments which are analogous to those given in Shapiro and Lightman (1976).

### 5.1.2 The diffusion model

We can express the tidal radius in terms of the internal stellar structure re-writing Eq. (4.60),

$$r_{\rm t} \propto \left( \frac{\mathscr{M}_\bullet}{x_{\rm b} \pi \bar{\rho}} \right)^{1/3}, \tag{5.1}$$

where $\mathscr{M}_\bullet$ denotes the mass of the central BH, $\bar{\rho}$ the mean stellar internal density, $n$ is the polytropic index (stars are supposed to be polytropes) and $x_{\rm b}$ is a parameter proportional to the gravitational binding energy of the star that describes effects of the internal stellar structure. We assume that a star is disrupted by tidal forces when it crosses the tidal radius. The free parameter $\varepsilon_{\rm eff}$ (accretion efficiency) determines the mass fraction of the gaseous debris being accreted on to the central BH ($\varepsilon_{\rm eff} = 1$ corresponds to 100% efficiency).

There are two concurrent processes driving stars towards the tidal radius; namely the *energy diffusion* and the *loss-cone accretion*. In the first case, stars on nearly circular orbits lose energy by distant gravitational encounters with other stars and in the process their orbits get closer and closer to the central BH. The associated energy diffusion time-scale can be identified with the local stellar-dynamical relaxation time, Eq. (1.1), but generalised for anisotropy as in Bettwieser (1983),

$$t_{\rm relax} = \frac{9}{16\sqrt{\pi}} \frac{\sigma_{\rm r}(\sigma_{\rm t}^2/2)}{G^2 m_\star \rho_\star(r) \ln \Lambda}. \tag{5.2}$$

Here $\sigma_{\rm r}$, $\sigma_{\rm t}$ are the radial and tangential velocity dispersions (in case of isotropy $2\sigma_{\rm r}^2 = \sigma_{\rm t}^2$), $\rho_\star(r)$ is the mean stellar mass density, $N$ the total particle number, $G$ the gravitational constant, $m_\star$ the individual stellar mass and

$$\ln \Lambda \equiv \ln (p_{\rm max}/p_0) = \ln (\gamma N) \tag{5.3}$$

is the Coulomb logarithm. We set $\gamma = 0.11$ (Giersz and Heggie, 1994). In this expression $p_{\rm max}$ is an upper limit of $p$, the *impact parameter*; $p_0$ is the value of $p$ that corresponds to an encounter of angle $\psi = \pi/4$, where $\psi = (\pi - \xi)/2$ if $\xi$ is defined to be the *deflection angle* of the encounter (Spitzer, 1987). In the vicinity of the BH ($r < r_{\rm h}$, see Sec. 5.3), one should be aware that $\Lambda \approx \mathscr{M}_\bullet/m_\star$ (Bahcall and Wolf, 1976; Lightman and Shapiro, 1977) but, for simplification, here we shall use Eq. 5.3 (strictely speaking only valid at distances $r > r_{\rm h}$) everywhere.

For a more detailed discussion of the energy diffusion process and its description in the context of the moment model see Bettwieser and Spurzem (1986).

As regards the second process, the *loss-cone accretion*, stars moving on radially elongated orbits are

destroyed by tidal forces when they enter the tidal radius $r_t$. A star will belong to the loss-cone when its *peribarathron* (distance of closest approach to the BH, see Fig.4.11) is less than or equal to the tidal radius $r_t$, provided that its orbit is not disturbed by encounters. Thus, the loss-cone can be defined as that part of stellar velocity space at radius $r$, which is given by

$$|v_t| < v_{lc}(r) = \frac{r_t}{\sqrt{r^2 - r_t^2}} \cdot \sqrt{2[\phi(r_t) - \phi(r)] + v_r(r)^2} \tag{5.4}$$

(see Eq. 4.77). In the last formula $v_r$, $v_t$ are the radial and tangential velocity of a star and

$$\phi(r_t) - \phi(r) = \frac{G\mathscr{M}_\bullet}{r_t} + \phi_\star(r_t) - \frac{G\mathscr{M}_\bullet}{r} - \phi_\star(r) \tag{5.5}$$

At distances $r \gg r_t$ we can approximate this expression taking into account that $G\mathscr{M}_\bullet/r_t \gg \phi(r)$ and $\phi(r_t)$ (see Eq. 4.85).

For a deeper analysis on loss-cone phenomena see chapter 4.

Similar to da Costa (1981), we define two time-scales: $t_{out}$ to account for the depletion of the loss-cone and $t_{in}$ for its replenishment. For a BH, $t_{out}$ is equivalent to one crossing time, since it is assumed that a star is destroyed by just one crossing of the tidal radius. In chapter 4 we mentioned that in the special case that the central object is a super-massive star, $t_{out} = n t_{cross}$. Here $n > 1$ is the number of passages until a star is trapped in the central object.

The loss-cone is replenished by distant gravitational encounters that change the angular momentum vectors of the stars. To estimate $t_{in}$, we make the assumption that random gravitational encounters thermalise the whole velocity space at some given radius $r$ after a time-scale of the order of $t_{relax}$. As a first approximation, the fraction $\Omega$ of the three-dimensional velocity space is re-populated within a time-scale

$$t_{in} = \Omega t_{relax} \tag{5.6}$$

where

$$\Omega := \int_{lc} f d^3v \Big/ \int_{\infty} f d^3v; \tag{5.7}$$

the subscript $\infty$ denotes an integration over the velocity space as a whole, and the subscript *lc* means that the integration over the loss-cone part of the velocity space is given by Eq. (5.4). As a matter of fact, $\Omega$ can be envisaged as the fraction of the surface of a velocity ellipsoid which is cut out by the loss-cone. Close to the tidal radius $r_t$, and for appreciable amounts of stellar-dynamical velocity dispersion anisotropies, our method describes the loss-cone size $\Omega$ more exactly than those given by (Frank and Rees, 1976; da Costa, 1981). On the other hand, their models can be "recovered" in the limit of $r \gg r_t$ and isotropy, $2\sigma_r^2 \approx \sigma_t^2$ (denoted as the "small loss-cone approximation"), where

$$\Omega \approx v_{lc}^2/\sigma_t^2 \approx r_t/r. \tag{5.8}$$

This is equivalent to their definition of $\theta_{lc}$ if $\Omega = \theta_{lc}^2/4$ is adopted.

Where the loss-cone effects can be neglected, a Schwarzschild-Boltzmann type distribution function can be assumed,

$$f \propto \exp\Big(-\frac{(v_r - \langle v_r \rangle)^2}{2\sigma_{\rm r}^2} - \frac{v_t^2}{\sigma_{\rm t}^2}\Big). \tag{5.9}$$

Third order moments of the velocity distribution that represent the stellar-dynamical energy flux do not alter such a distribution function significantly (Bettwieser and Sugimoto, 1985).
An important quantity is the *critical radius* $r_{\rm crit}$. Let $\theta_{\rm D}^2$ be the average quadratic deflection angle produced by relaxation during $t_{\rm out}$ ($= t_{\rm cross}$ here),

$$\theta_{\rm D}^2 = \frac{t_{\rm out}}{t_{\rm relax}}. \tag{5.10}$$

Then, by definition,

$$\theta_{\rm lc}(r_{\rm crit}) = \theta_{\rm D}(r_{\rm crit}), \tag{5.11}$$

which is equivalent to $t_{\rm out}(r_{\rm crit}) = 4t_{\rm in}(r_{\rm crit})$. For most clusters where such a radius can be defined, $\theta_{\rm lc} > \theta_{\rm D}$ inside $r_{\rm crit}$ while the opposite holds outside. This means that, at large radii, relaxation is efficient enough to make stars diffuse into and out of loss cone orbits over a time scale $t_{\rm out}$ so that the distribution function is not appreciably depleted in the loss cone. Conversely, deep inside $r_{\rm crit}$, the loss cone orbits are essentially empty and the flux of stars into this domain of phase-space (and into the BH) can be treated as a diffusive process because the size of one individual step of the velocity random walk process, $\theta_{\rm D}$, is (much) smaller that the characteristic size of the problem, $\theta_{\rm lc}$.
Note that a critical radius does not necessarily exist (see chapter 4). For instance, if one assumes that gravity of the BH dominates the stellar self-gravitation and that the density profile follows a power-law, $\rho \propto r^{-\alpha}$, one has $\theta_{\rm lc}^2 \propto r^{-1}$, $\theta_{\rm D}^2 \propto r^{3-\alpha}$ and a critical radius would not exist for $\alpha > 4$.
Now we want to generalise the stationary model (see chapter4), which assumes an empty loss-cone within $r_{\rm crit}$ and a full loss-cone elsewhere, by means of a simple "diffusion" model, which is derived from the above considerations; this means that the filling degree of the loss-cone $K$ can be continuously estimated within its limiting values,

$$K \in [0,1]. \tag{5.12}$$

Let $f$ be the unperturbed velocity distribution (without loss-cone accretion); if the loss-cone is empty and we neglect the angular momentum diffusion, $f = 0$ inside the loss-cone (and unchanged elsewhere in the velocity space). In point of fact, $f$ will have a continuous transition from nearly unperturbed values at large angular momenta to a partially depleted value within the loss-cone. This value is determined by the ratio of $t_{\rm in}$ and $t_{\rm out}$. Such a smooth transition of the distribution function given as a function of angular momentum $f(J)$ has been derived from self-consistent models of angular momentum diffusion (e.g. Cohn and Kulsrud 1978 or Marchant and Shapiro 1980). We approximate $f(J)$ by a distribution function that has a sudden jump just at the value $J_{\rm min} = m_\star v_{\rm lc}$ from an unperturbed value $f_0$ given by the moment equations (assuming a Schwarzschild-Boltzmann distribution) to the constant lowered value

$$f = K f_0, \text{ with } 0 \leq K \leq 1 \tag{5.13}$$

within the loss-cone (i.e. $J < J_{\rm min}$ or $|v_t| < v_{\rm lc}$). This implies that, as means to compute the mean mass density of loss-cone stars, we have to calculate the integral

$$\rho_{\rm lc} = \int_{\rm lc} K\, f_0\, d^3v. \tag{5.14}$$

And then, accordant with the definition of $\Omega$,

$$\rho_{\rm lc,full} = \rho\, \Omega, \tag{5.15}$$

in the case that we have a full loss-cone.
In regard to the radial and tangential stellar velocity dispersions in the loss-cone $\sigma_{{\rm lc},r}$ and $\sigma_{{\rm lc},t}$, we can compute them using second moments integrated over the loss-cone part of velocity space. As for the definition of the quantities $E_r$ and $E_t$ used in Sect. 3,

$$\begin{aligned} \sigma^2_{{\rm lc},r} &= E_r\, \sigma^2_{\rm r}, \\ \sigma^2_{{\rm lc},t} &= E_t\, \sigma^2_{\rm t}, \end{aligned} \tag{5.16}$$

in the small loss-cone approximation we have that $E_r \approx 1$ and $E_t \ll 1$.
The arguments about the time-scales that have led us to the derivation of $t_{\rm in}$ and $t_{\rm out}$ guide us also to the following *diffusion equation* for the time evolution of the spatial density $\rho_{\rm lc} = K\rho\,\Omega$ of loss-cone stars:

$$\frac{d\rho_{\rm lc}}{dt} = -\frac{\rho_{\rm lc} P_{\rm lc}}{t_{\rm out}} + \frac{\rho\,\Omega - \rho_{\rm lc}}{t_{\rm in}}. \tag{5.17}$$

In this equation, the second term on the right hand is the refilling term due to relaxation.
As we assume relaxation is due to a large number of small-angle deflections and can thus be seen as a diffusive process in velocity space, the probability $P(\theta)$ that a star is scattered in an angle $\theta$ in a time $t_{\rm out}$ is

$$P(\theta) = \frac{2}{\sqrt{\pi}\,\theta_D} \exp\left(-\theta^2/\theta_D^2\right), \tag{5.18}$$

The distribution is normalised to one,

$$\int_0^\infty P(\theta)\, d\theta = 1 \tag{5.19}$$

and has the property that its mean square value is $\theta_D^2$. A star remains in the loss-cone during a time $t_{\rm out}$ if its RMS diffusion angle is smaller than the loss-cone angle $\theta_{lc}$. The probability for this to happen is

$$P_{lc} = \int_0^{\theta_{lc}} P(\theta)\, d\theta = {\rm erf}(\sqrt{4 t_{\rm in}/t_{\rm out}}). \tag{5.20}$$

In the case that a star is unperturbed by the rest of the stellar system, it will sink on to the central BH in a time $t_{\rm out}$. Actually, this is a somehow simplified description of the physical process, for part of the loss-cone stars will be scattered out of it before they slump. The required time for this event is $t_{\rm in}$, since in this time-scale the angular momentum vector will change (due to distant encounters) on an amount that is comparable with the size of the loss-cone in the angular momentum space. For this reason we have introduced the quantity $P_{\rm lc}$ in Eq. (5.17).
Bluntly speaking, the *effective* time-scale that describes the loss-cone depletion allowing for perturbation due to angular momentum diffusion is

$$t_{\rm out,\,eff} = t_{\rm out}/P_{\rm lc}. \tag{5.21}$$

As a matter of fact, this definition ensures us that far outside of the critical radius the loss-cone depletes in a time that grows infinitely, as it is physically expected. In the regime where $r \ll r_{\rm crit}$, $P_{\rm lc}$ tends asymptotically to 1 and to 0 where $r \gg r_{\rm crit}$, passing through a transition zone at $r = r_{\rm crit}$.
We can consider Eq. (5.17) as an ordinary differential equation for $K = \rho_{\rm lc}/(\rho\,\Omega)$ if we assume that the stellar density and the loss-cone size are time-independent. Transport phenomena can be neglected, for they are related to the relaxation time, and $t_{\rm relax} \gg t_{\rm in}, t_{\rm out}$. Bearing this in mind we can get an analytical solution $K(t)$ for the differential equation with the initial condition that $K(t)|_{t_0} = K_0$,

$$K(t) = K_0 \exp\Big(-\frac{P_{\rm lc}\,\xi\,(t-t_0)}{t_{\rm out}}\Big) + \frac{t_{\rm out}}{P_{\rm lc}\,t_{\rm in}\,\xi}\cdot\left(1-\exp\Big(-\frac{P_{\rm lc}\,\xi\,(t-t_0)}{t_{\rm out}}\Big)\right). \tag{5.22}$$

In the last equation we have defined $\xi$ for legibility reasons as follows,

$$\xi := 1 + (t_{\rm out}/P_{\rm lc}\,t_{\rm in}). \tag{5.23}$$

For $r = r_{\rm crit}$, with $t_{\rm in} = t_{\rm out}$, the stationary filling degree of the loss-cone turns out to be

$$K_\infty := \lim_{t\to\infty} K(t) = \frac{1}{2}. \tag{5.24}$$

Note that Milosavljević and Merritt (2003) recently gave a detailed summary of loss-cone effects. They derived expressions for non-equilibrium configurations. They employ a rather different treatment for the diffusion since they tackle the problem of binary BHs scattering.

## 5.2 Inclusion of the central BH in the system

In this subsection we discuss the way we cope with the loss-cone in our approach. For this aim we accept the following:

1. The system has central ($r = 0$) fixed BH

2. Stars are totally destroyed when they enter $r_{\rm t}$

3. Gas is completely and immediately accreted on to the BH

As regards the first point, one should mention that the role of brownian motion of the central BH can be important; as a matter of fact, for a cluster with core radius $R_{\rm core}$, equipartition predicts a wandering radius $R_{\rm wan}$ of order

$$R_{\rm wan} \approx R_{\rm core}\sqrt{M_\star/\mathscr{M}_\bullet}, \tag{5.25}$$

which is larger than the tidal disruption radius for BHs less massive than $10^9 M_\odot$ if the core radius is 1 pc (Bahcall and Wolf, 1976; Lin and Tremaine, 1980; Chatterjee et al., 2002). The wandering of a MBH at the centre of a cuspy cluster has been simulated by Dorband et al. (2003) with a $N$-body code allowing $N = 10^6$. They find that RMS velocity of the quickly reaches equipartition with the stars but do not comment on the wandering radius. In Addendum A, at the end of this chapter (section 5.6), we present a simple estimate suggesting that, in a cusp $\rho \propto r^{-\alpha}$, the wandering radius may be much reduced, $R_{\rm wan} \propto a(m_\star/\mathscr{M}_\bullet)^{1/(2-\alpha)}$, where a is typical length scale for the central parts of the cluster. For $\alpha \geq 1.5$, one would then expect $R_{\rm wan}$ to be smaller than $R_{\rm t}$ for black holes as light as $2000\,{\rm M}_\odot$, but this arguments neglects the flattening of the density profile due to loss-cone accretion. Further $N$-body simulations are clearly required to settle the question and, in particular, if $R_{\rm wan}$ is larger than $R_{\rm t}$, to establish the effect of the motion of the MBH on disruption rates, which can be either increased or decreased (Magorrian and Tremaine, 1999).

We arrogate that at any sphere of radius $r$ the transport of loss-cone stars in the time-scale $t_{\rm out,eff}$ towards the centre happens instantaneously compared with the time step used for the time evolution.

Hence, the local density "loss" at $r$ is

$$\left(\frac{\delta\rho}{\delta {\rm t}}\right)_{\rm lc} = -\frac{\rho_{\rm lc} P_{\rm lc}}{t_{\rm out}}; \tag{5.26}$$

with $\rho_{\rm lc} = K\Omega\rho$.

This corresponds to a local energy *loss* [3] of

$$\begin{aligned}\left(\frac{\delta\rho\,\sigma_{\rm r}^2}{\delta t}\right)_{\rm lc} &= -\left(\frac{\delta\rho}{\delta t}\right)_{\rm lc}\cdot\left(E_r\,\sigma_{\rm r}^2 + u^2\right)\\ \left(\frac{\delta\rho\,\sigma_{\rm t}^2}{\delta t}\right)_{\rm lc} &= -\left(\frac{\delta\rho}{\delta t}\right)_{\rm lc} E_t\,\sigma_{\rm t}^2.\end{aligned} \tag{5.27}$$

$E_r$ and $E_t$ are worked out integrating over the velocity distribution part that corresponds to the loss-cone with the approximation $u \ll \sigma_{\rm r}$ and $v_{\rm lc} \ll \sigma_{\rm t}$,

[3] By *loss* we mean here transport of mass and kinetic energy toward the central BH, for it is lost for the stellar system.

$$\begin{aligned} E_r &\approx 1 \\ E_t &\approx v_{\rm lc}^2/\sigma_{\rm t}^2 \ll 1 \end{aligned} \tag{5.28}$$

Thereupon, the mass accretion rate of the central BH can be calculated as

$$\dot{M} = -\varepsilon_{\rm eff} \int_{r_{\rm t}}^{R_{\rm tot}} \left(\frac{\delta\rho}{\delta t}\right)_{\rm lc} 4\pi r^2 dr. \tag{5.29}$$

Here $R_{\rm tot}$ stands for the total radius of the stellar system. The accretion efficiency has been set throughout our calculations to $\varepsilon_{\rm eff} = 1$; for a discussion on different $\varepsilon_{\rm eff}$-values see Marchant and Shapiro (1980). The complete set of Eqs. (2.22) including the local accretion terms of the type $(\delta/\delta t)_{\rm lc}$ for energy diffusion and loss-cone accretion are solved implicitly. For every time step the mass of the BH and the filling degree $K$ of the loss-cone are brought up to the new state of the system. The time step is chosen in order to keep the maximum changes of the variables below 5% .
For the model calculation we have utilised for the boundary conditions that at the outer limit, $R_{\rm tot} = 10^4$ pc, we impose $u = F = 0$ and $M_{\rm r} = M_{\rm tot}$. No stellar evaporation is allowed. At the centre, the usual boundary conditions for the gaseous model are $u = M_{\rm r} = F = 0$ but the central point $r_1 = 0$ is not explicitly used when there is a BH, for obvious reasons. Instead, one imposes that all quantities vary as power-laws, $\mathrm{d}\ln x/\mathrm{d}\ln r = C^{\rm st}$ inside the first non-zero radius of the discretisation mesh, $r_2 = 1.7\times10^{-6}$pc (see chapter 2).

## 5.3 Units and useful quantities

The units used in the computations correspond to the so-called $N$-body unit system, in which $G = 1$, the total initial mass of the stellar cluster is 1 and its initial total energy is $-1/2$ (Hénon, 1971; Heggie and Mathieu, 1986). For the simulations presented here, the initial cluster structure corresponds to the Plummer model whose density profile is $\rho(r) = \rho_0\left(1+(r/R_{\rm Pl})^2\right)^{-5/2}$, where $R_{\rm Pl}$ is the Plummer scaling length. For such a model the $N$-body length unit is $\mathscr{U}_{\rm l} = 16/(3\pi)\,R_{\rm Pl}$.
In the situations considered here, the evolution of the cluster is driven by 2-body relaxation. Therefore, a natural time scale is the (initial) *half-mass relaxation time*. We use the definition of Spitzer (1987),

$$T_{\rm rh}(0) = \frac{0.138N}{\ln\Lambda}\left(\frac{R_{1/2}^3}{G\mathscr{M}_{\rm cl}}\right)^{1/2}. \tag{5.30}$$

For a Plummer model, the half-mass radius is $R_{1/2} = 0.769\,\mathscr{U}_{\rm l} = 1.305\,R_{\rm Pl}$. $\mathscr{M}_{\rm cl}$ is the total stellar mass. For a cluster containing a central BH, an important quantity is the *influence radius*, enclosing the central region inside of which the gravitational influence of the BH dominates over the self-gravity of the stellar cluster. The usual definition is $r_{\rm h} = G\mathscr{M}_\bullet/\sigma_0^2$, where $\sigma_0$ is the velocity dispersion in the cluster at a large distance from the BH. As the latter quantity is only well defined for a cluster with an extended core, we

use here the alternate and approximate definition $M_{\rm r}(r_{\rm h}) = \mathscr{M}_\bullet$, i.e. $r_{\rm h}$ is the radius of that encloses a total stellar mass equal to the mass of the BH.

## 5.4 Results

We study the evolution of a stellar cluster with a so-called "seed BH" at its centre. We consider two possible configurations for the stellar system; one of a total mass of $M_{\rm tot} = 10^5 {\rm M}_\odot$ and another of $10^6 {\rm M}_\odot$. For the initial BH mass, we have chosen $\mathscr{M}_\bullet(0) = 50 {\rm M}_\odot$ and $500 {\rm M}_\odot$ and we model it as a Plummer of $R_{\rm Pl} = 1$pc. Even though it would be more realistic to set the efficiency parameter $\varepsilon_{\rm eff} = 1/2$, we choose here $\varepsilon_{\rm eff} = 1$ for historical reasons. Nonetheless, here we study additionally the influence of a variation of the stellar structure parameter $x_b$, since it influences the tidal radius and hence the accretion rates (see Eq. 4.60). For this intent we compare case a ($x_b = 1$) with another one in which we choose the value $x_b = 2$ (case b). As regards the physical meaning, the stars of case b have twice as much internal binding energy than case a.

The cluster evolves during its pre-collapse phase up to a maximum central density from which the energy input due to star accretion near the tidal radius becomes sufficient in order to halt and reverse the core collapse. Immediately afterwards, the post-collapse evolution starts. At the beginning of the re-expansion phase, the BH significantly grows to several $10^3$ solar masses. Thereon, a slow further expansion and growth of the BH follow.

In Fig. 5.1, we follow the evolution of the mass of a central BH in a globular cluster of $10^5$ stars of $1\,{\rm M}_\odot$. Panel (a) shows the mass of the BH as function of time. On panel (b), we present the accretion rate on to the BH, i.e. its growth rate. For $\mathscr{M}_{\rm bh}(0) = 50\,{\rm M}_\odot$, the early cluster's evolution is unaffected by the presence of the BH which starts growing suddenly at the moment of deep core collapse, around $T \simeq 14.5\,T_{\rm rh}(0)$. In Fig. 5.2 we follow the same evolution for the case of a stellar cluster of $10^6$ stars.

From Figs. (5.1) and (5.2) we can see that the differences between the cases a, b and c are nearly negligible after core collapse. In general, the structure of the cluster at late times is nearly independent of $\mathscr{M}_\bullet(0)$ and $x_{\rm b}$. From these plots we can infer that this occurs since core collapse leads to higher densities if the initial BH mass is smaller and thus the integrated accreted stellar mass increases.

We exhibit the evolution of the structure of the cluster for case a with $10^5$ stars in Fig. 5.3. With dotted lines we plot various Lagrangian radii, for mass fractions ranging between $10^{-3}\,\%$ (which formally corresponds to only one star) to $90\,\%$. Only the mass still in the stellar component at a given time is taken into account. Moreover, the evolution of the influence radius (solid line, defined as the radius enclosing a stellar mass equal to the BH mass) and critical radius (dashed line) are shown, so that one can infer the percentage of the stellar mass embodied within them at a certain moment. For late time, one obtains self-similar evolution with size increasing like $R \propto T^{2/3}$, as expected for a system in which the central object has a small mass and the energy production is confined to a small central volume. (Hénon, 1965; Shapiro, 1977; McMillan et al., 1981; Goodman, 1984). We consider too the case of a $10^6$ stars in Fig. 5.4, for which the $R \propto T^{2/3}$ expansion is a poor approximation because, at late times, the BH comprises of order $40\,\%$ of the system mass.

We observe in Fig. 5.5 that for the evolved post-collapse model the spatial profile of the stellar density

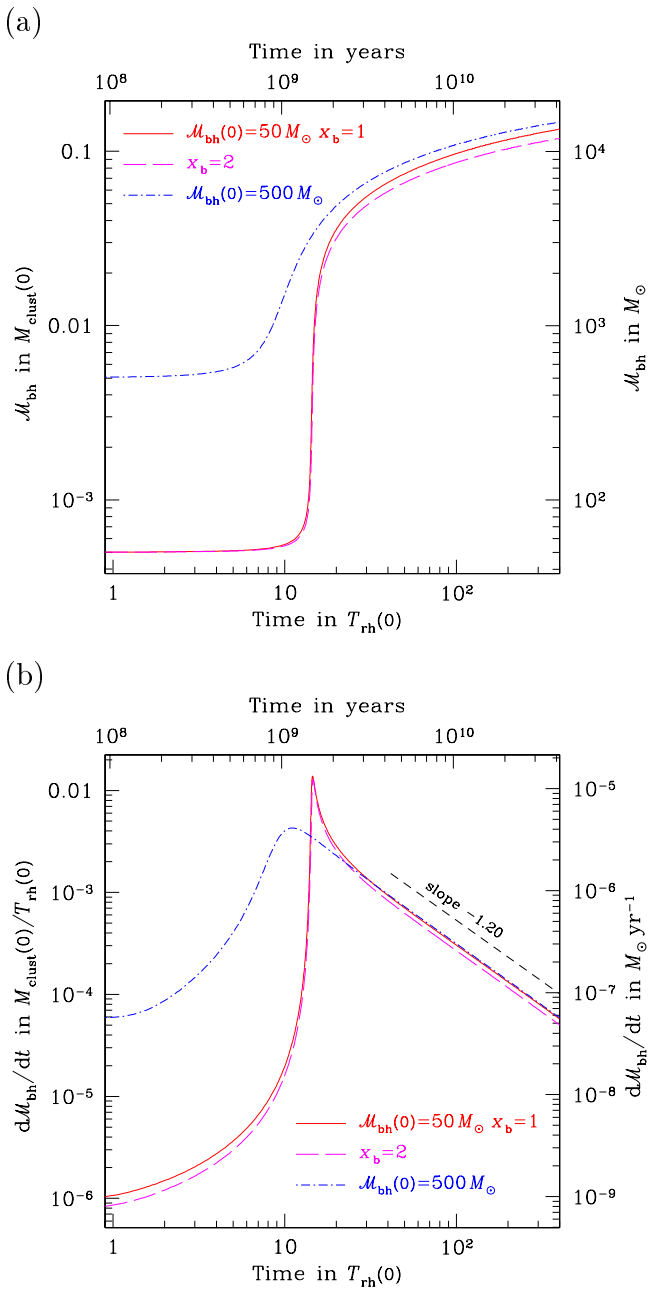


Fig. 5.1: Evolution of the mass of a central BH in a globular cluster of $10^5$ stars of $1\mathrm{M}_\odot$. We considered three cases. In case a (solid line), the initial BH mass is $\mathscr{M}_\bullet(0)=50\mathrm{M}_\odot$ and $x_b=1$, case b (dashes) has the same initial BH mass but $x_b=2$ while case c (dash-dot) corresponds to $\mathscr{M}_\bullet(0)=500\mathrm{M}_\odot$ and $x_b=1$. An accretion efficiency of $\varepsilon_{\rm eff}=1$ is assumed. Panel (a) shows the mass of the BH as function of time and panel (b) the accretion rate on to the BH. At late times, the mass of the central BH increases like $\dot{\mathscr{M}}_\bullet \propto T^{-1.2}$ as predicted by simple scaling arguments (see text)

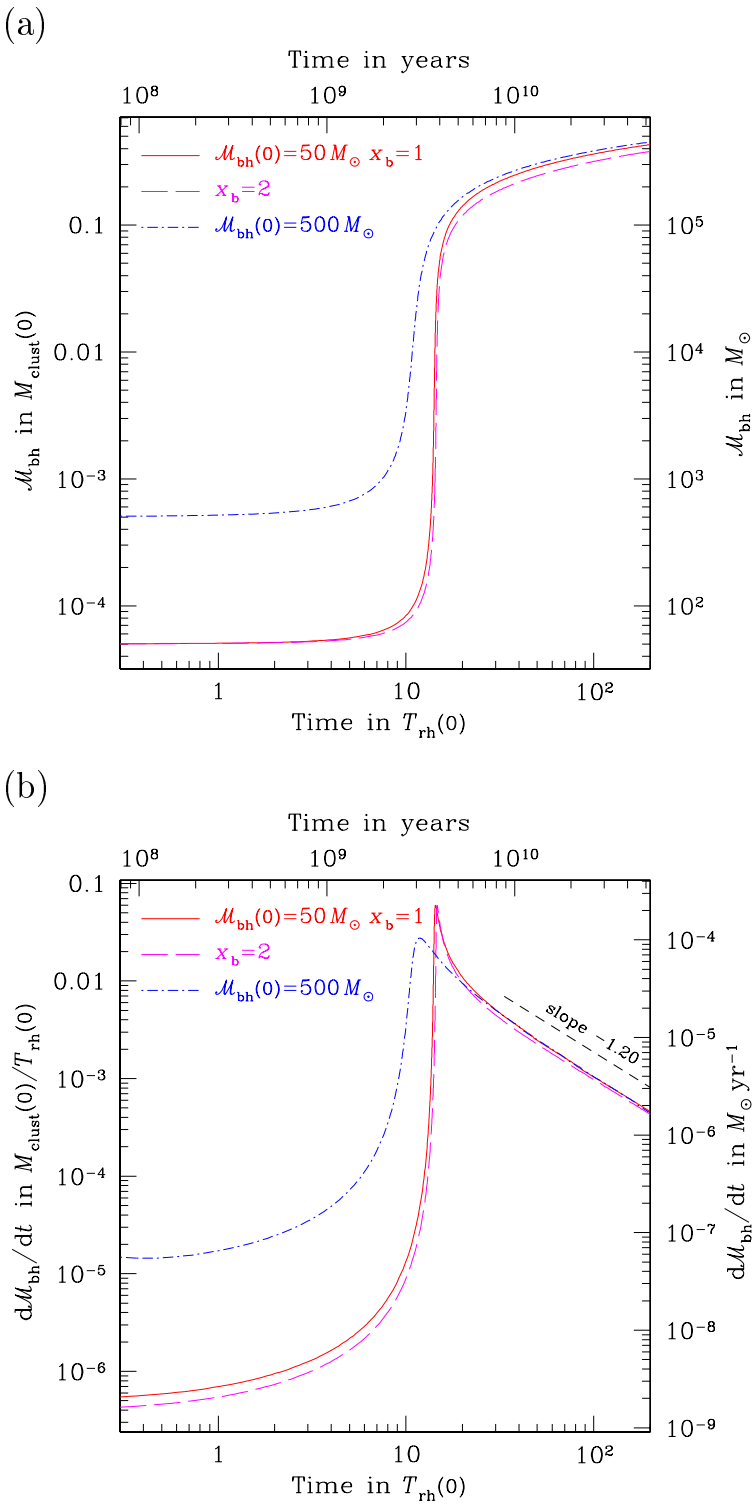


Fig. 5.2: Same as Fig. 5.1 but for a cluster of $10^6$ stars with the same size ($R_P = 1$pc).

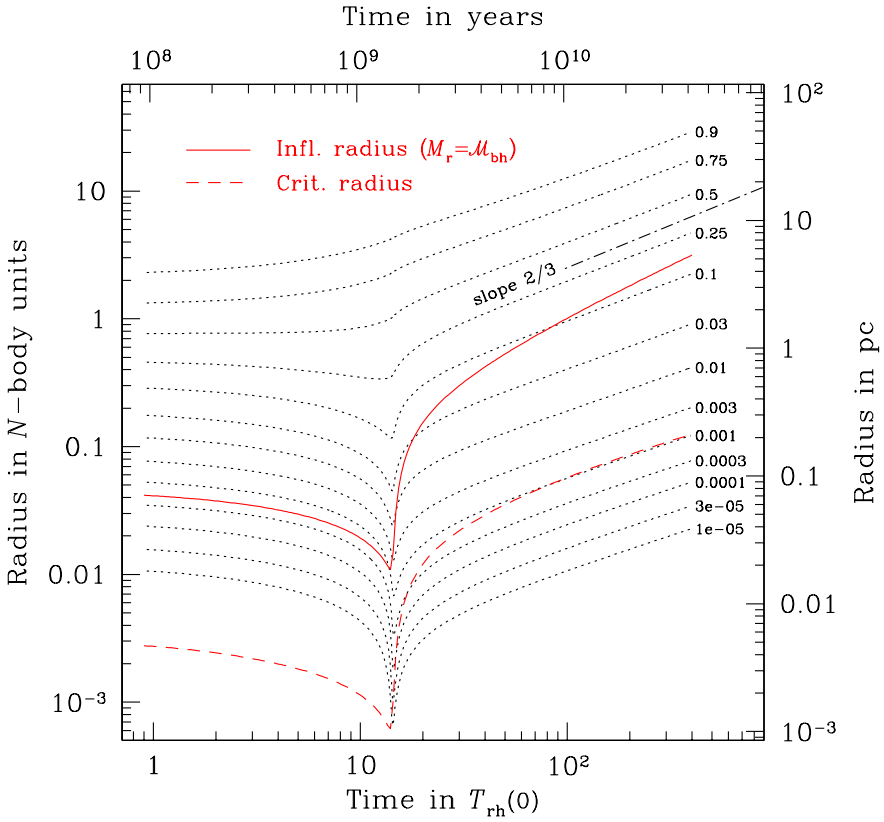


Fig. 5.3: Evolution of the radii of spheres enclosing the indicated fraction of the total mass, Lagrangian radii, for case a. The mass fractions range from $10^{-3}$ % to 90 %. The influence and critical radius are displayed (solid and broken line). See text for further explanation.

has a power law slope of $\rho \propto r^{-7/4}$ in the region $r_{\rm crit} < r < r_{\rm h}$, where $r_{\rm h}$ is the influence radius. The density profile flattens for $r < r_{\rm crit}$ due to the effective loss-cone accretion. For the same post-collapse moment we display the surface density for case a in Fig. 5.8.

Arguments based on constant accretion rate lead to the result that one should expect a stellar density profile proportional to $r^{-1/2}$ inside $r_{\rm crit}$. If one takes Eq. (5.17) and considers that $\dot{M} = C^{\rm st}$, we get that

$$\frac{d\rho_{\rm lc}}{dt} \propto r^{-\alpha-5/2}. \tag{5.31}$$

Where we have assumed that $P_{\rm lc} \approx 1$, $\rho \propto r^{-\alpha}$ and suppose that the gravity of the BH totally dominates this region, so that we have a Keplerian profile, $\sigma \propto r^{-1/2}$. We have also taken into account the fact that $t_{\rm dyn} = r/\sigma$. Thus,

$$\dot{M} = r^{1/2-\alpha}. \tag{5.32}$$

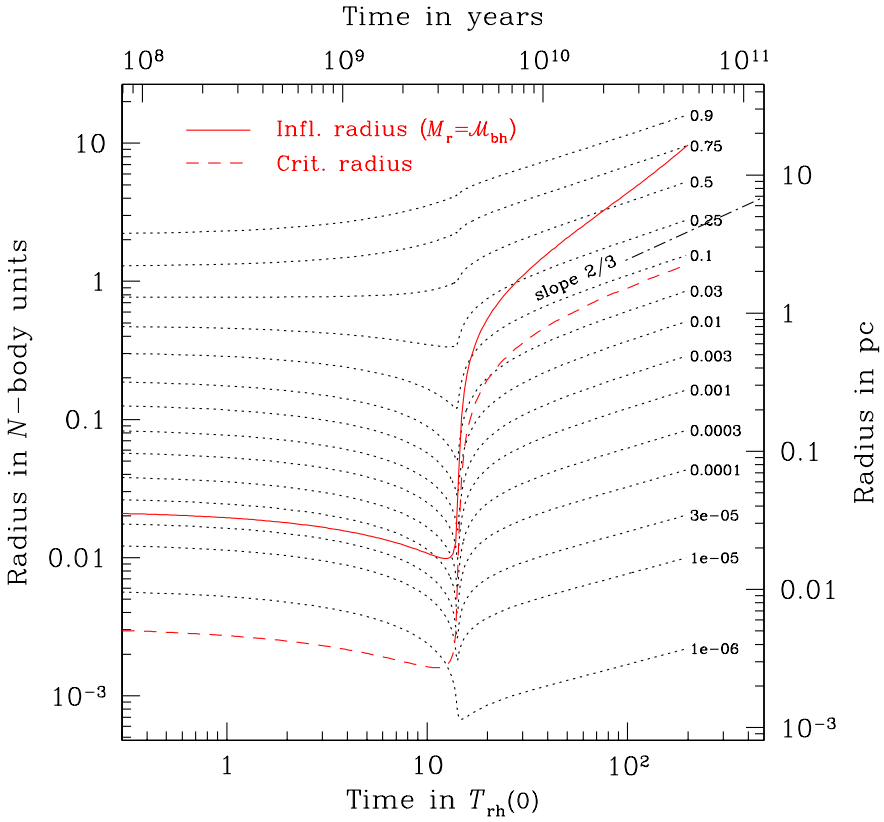


Fig. 5.4: Same as Fig. 5.3 but for a cluster of $10^6$ stars.

Whence, $\alpha = -1/2$.
Another possible way to derive this result is based on the Eq. (4-137) of Binney and Tremaine (1987),

$$\rho(r) = 4\pi \int_0^{\psi} f(\varepsilon)\sqrt{2(\psi-\varepsilon)}d\varepsilon \tag{5.33}$$

In this equation $\psi := -\phi + \phi_0$ and $\varepsilon := -E + \phi_0$, where $\phi_0$ is a constant that makes $f > 0$ for $\varepsilon > 0$ and $f = 0$ for $\varepsilon \leq 0$. If we assume that f ($\varepsilon$)=0 for $\varepsilon > \varepsilon_0$ (where $\varepsilon_0$ is around $r_{crit}$) and consider that we are in the region where $r \ll r_{crit}$, $\psi = G\mathcal{M}_\bullet/r \gg \varepsilon$ and then, from

$$\rho(r) \approx 4\pi\sqrt{2\psi} \int_0^{\psi_{\varepsilon_0}} f(\varepsilon)d\varepsilon \tag{5.34}$$

one can conclude that $\rho(r) \propto r^{-1/2}$.
Nevertheless, none of these derivations can be applied to the interpretation of our results, since it would contradict the basis of our model's idea. We cannot expect this "classical" result in our results, since it

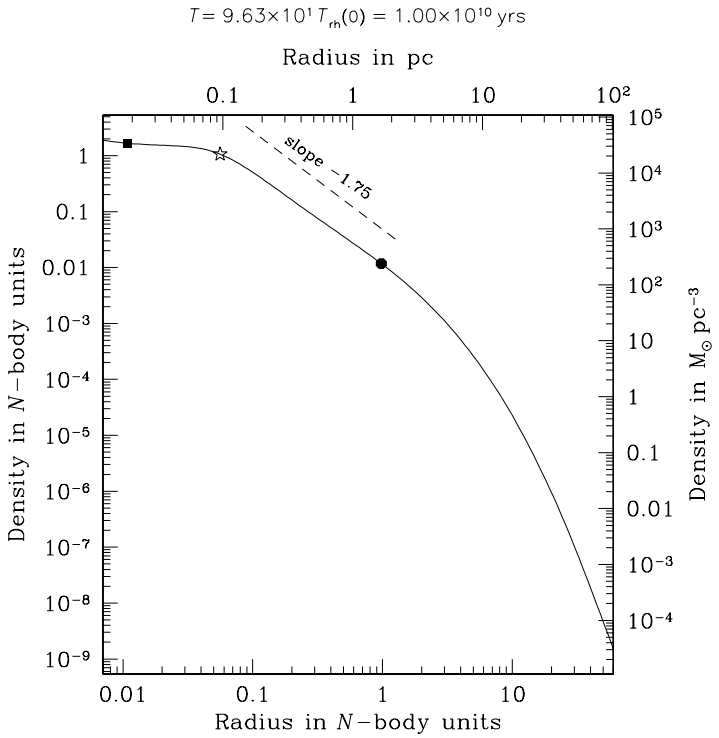


Fig. 5.5: Density profile for a $10^5 M_\odot$ globular cluster with $\mathscr{M}_{\rm bh}(0) = 50 M_\odot$ (case a) at 10 Gyrs. The round dot indicates the influence radius ($M_r = \mathscr{M}_{\rm bh}$), the star the critical radius and the square the radius below which the description of the cluster as a continuum loses significance because the enclosed mass is smaller than $1 M_\odot$. As expected, for the zone between the critical and influence radii, the density profile closely reassembles a power-law of exponent $-7/4$. At that stage, the structure of case c ($\mathscr{M}_{\rm bh}(0) = 500 M_\odot$) is extremely similar. We can see that from the "1-star" radius onwards the slope of the curve shows a tendence to increase. This is due to the fact that the loss-cone size is artificially limited for stability purposes. On the other hand, the slope comprised between the critical radius and the 1-star radius is consistent with the arguments given in the work of Lightman and Shapiro (1977) (see text for further explanation).

would imply that the filling degree $K$ is constant in the region where $P_{\rm lc} \approx 1$ ($r \ll r_{\rm crit}$ see Fig. 5.12), which is not the case at all.

As a matter of fact, one does not know a priori which kind of slope one will have in this region. It is rather an initial condition that we introduce and it is totally disconnected with our diffusion model. We could bargain for such a slope in the case that we just have stars that come from unbound orbits and fall on to the central BH disappearing immediately from the stellar system. In the model presented here, we have also stars with bounded orbits around the BH that will perturbe the slope of $\alpha = -1/2$. Lightman and Shapiro (1977) proved that within $r_{\rm crit}$, according to their Eq. (71) (where they assume $\Omega \ll 1$, small loss-cone), $\alpha$ will continously vary from 1.75 to $-\infty$.

Regarding the three dimensional velocity dispersion, in Fig. 5.6 we can see coming a slope of -1/2 at

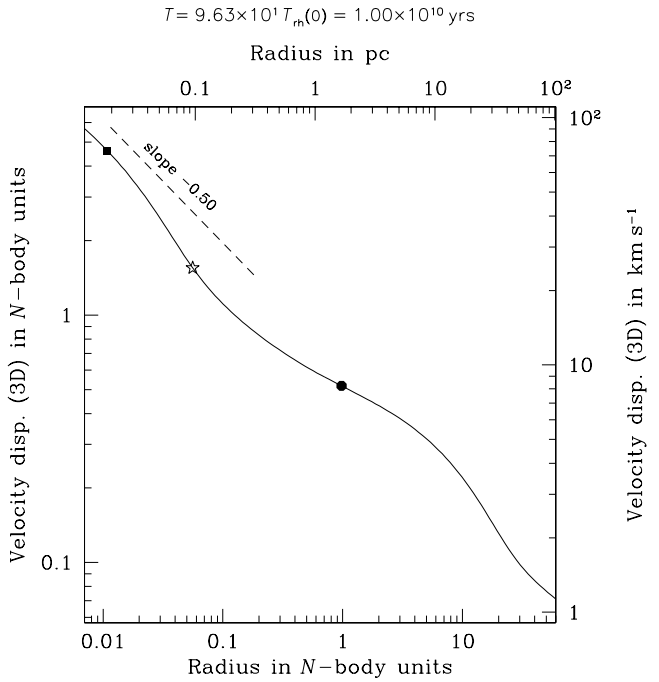


Fig. 5.6: Profile of the three-dimensional velocity dispersion for the same case and time as Fig. 5.5. See text for comments.

the inner region; but extending below the one-star radius does not make much sense. A slope of -1/2 is what one would expect from Kepler's third law and a simple application of Jeans equation, with the assumptions that (1) dynamical equilibrium holds, (2) the gravity is dominated by the central BH, (3) the density follows a pure power-law and (4) the anisotropy $\sigma_t/\sigma_r$, is constant, indeed predicts $\sigma \propto r^{-1/2}$. At the end of this chapter, in Addendum B (section 5.7) , we show that the Jeans equation for stationary equilibrium actually describes the central regions of the cluster quite well. The reason why the velocity dispersion does not follow closely the "Keplerian" profile has to do with the fact that none of assumptions (2)-(4) exactly holds all the way from the influence radius inward.

Figures 5.9 and 5.8 give the plots of the projected density and velocity dispersions for the late post-collapse model. See Addendum C (section 5.8).

The effects of anisotropy are studied in Fig. 5.7, where we can see that the external parts of the cluster are dominated by radial orbits. Inside the critical radius (indicated by a star symbol), one notices a slight tangential anisotropy, an effect of the depletion of loss-cone orbits. At large radii, the velocity distribution tends to isotropy as an effect of the outer bounding condition imposed at $10^4$ pc.

The effects of anisotropy in the stellar system can also be seen in Fig. 5.9, where we plot the components along the line of sight $\sigma_{\rm LOS}$ (solid line) and on the sky ("proper motions"). The latter is decomposed into the radial direction (i.e. towards/away from the position of the cluster's centre) component, $\sigma_{\rm PM,r}$

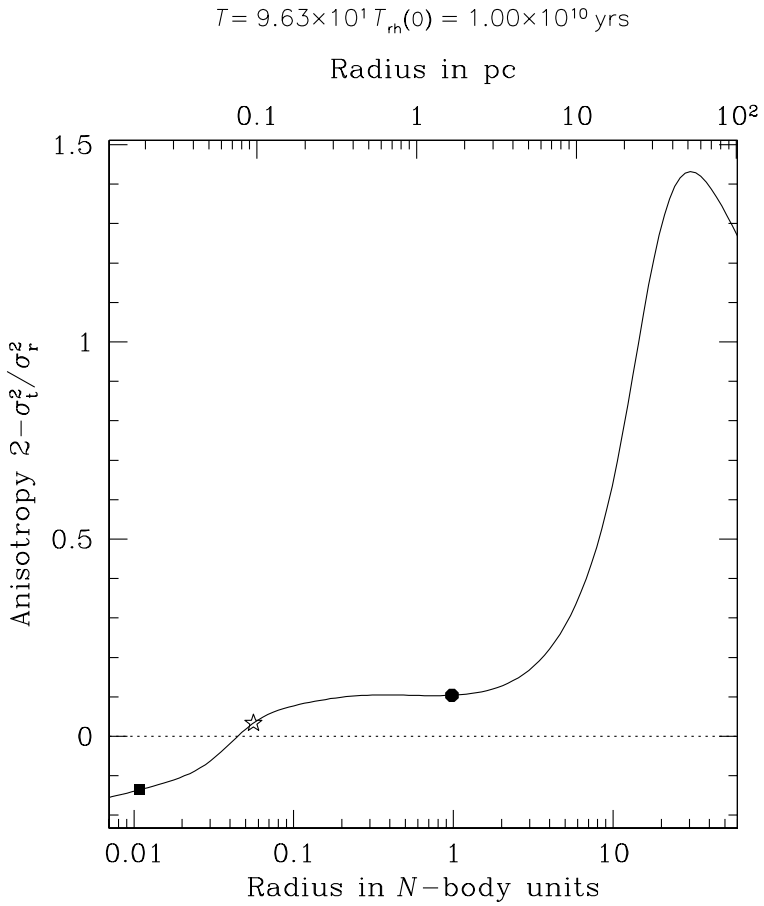


Fig. 5.7: Profile of the anisotropy parameter for the same case and time as Fig. 5.5. The decrease of at the border is an artefact of the inappropriate boundary condition. An outer boundary with radial anisotropy should be open, but here we enforce the adiabatic wall. If one "opens" the wall, but it would be at the expense of the stability of the program. All this does affect only a very small fraction of the total mass.

(dashes) and the tangential component, $\sigma_{PM,t}$ (dash-dot). Note that the radial anisotropy in the outskirts of the cluster reveals itself as a radial "proper motion" dispersion slightly larger than the other components. For an isotropic velocity dispersion, all three components would be equal. Despite loss-cone effects, there is no measurable anisotropy at the centre.

The loss-cone induced anisotropy could be detected only if one could select the stars that are known to be spatially close to the centre (and not only in projection) as would be feasible these stars happened to be of a particular population. An interesting possibility that we'll soon investigate with multi-mass models is the concentration at the centre of more massive stars, i.e. mass segregation.

Note that some anisotropy has been detected among the stars orbiting the central massive black hole of

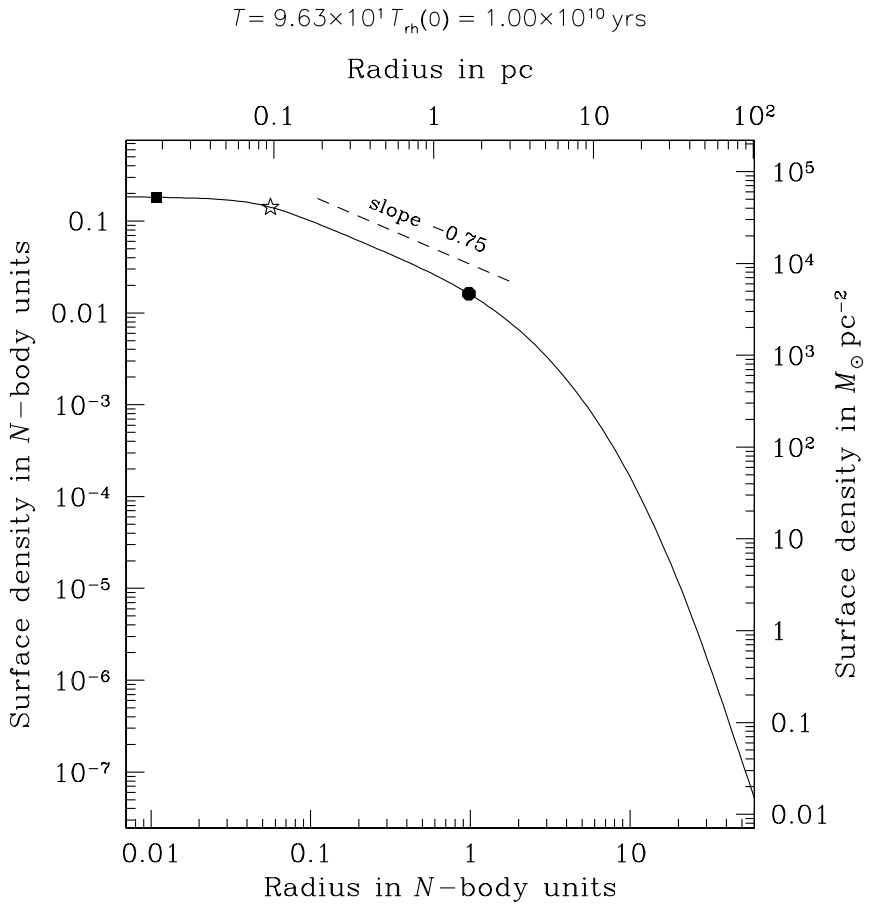


Fig. 5.8: Projected density for the same case and time as Fig. 5.5. In the interval between $r_{\rm h}$ and $r_{\rm crit}$ we get a slope of $-3/4$, as expected.

the Milky Way, Sgr A$^*$, at distances closer than 1, i.e. 0.04 pc which is well inside the critical radius ($> 1$ pc) (Schödel et al., 2003). However, the detected anisotropy is in the radial direction rather than tangential. It is probably not connected to loss-cone effects but to particular history of these seemingly very young stars (Ghez et al., 2003) which remains a puzzle.

In Fig. 5.12 the diffusion model is layed out for the loss-cone as evaluated in previous sections. We evaluate a model close to the post-collapse moment analysed in the other plots. We depict here the loss-cone filling factor $K$ (upper panel), the loss-cone and diffusion angles $\theta_D$ and $\theta_{\rm lc}$ (middle panel) and the local contributions to the total loss-cone star accretion rate (lower panel). Our diffusion model reproduce well the picture of Frank and Rees (1976): the critical radius is defined by $\theta_D = \theta_{\rm lc}$ and coincides with the radius where the local contribution to the loss-cone accretion rate has its peak value. These two angles are connected to the time-scales $t_{\rm in}$ and $t_{\rm out}$, $\theta_D^2 \propto t_{\rm out}/t_{\rm relax}$ and $\theta_{\rm lc}^2 \propto t_{\rm in}/t_{\rm relax}$. The figures show that

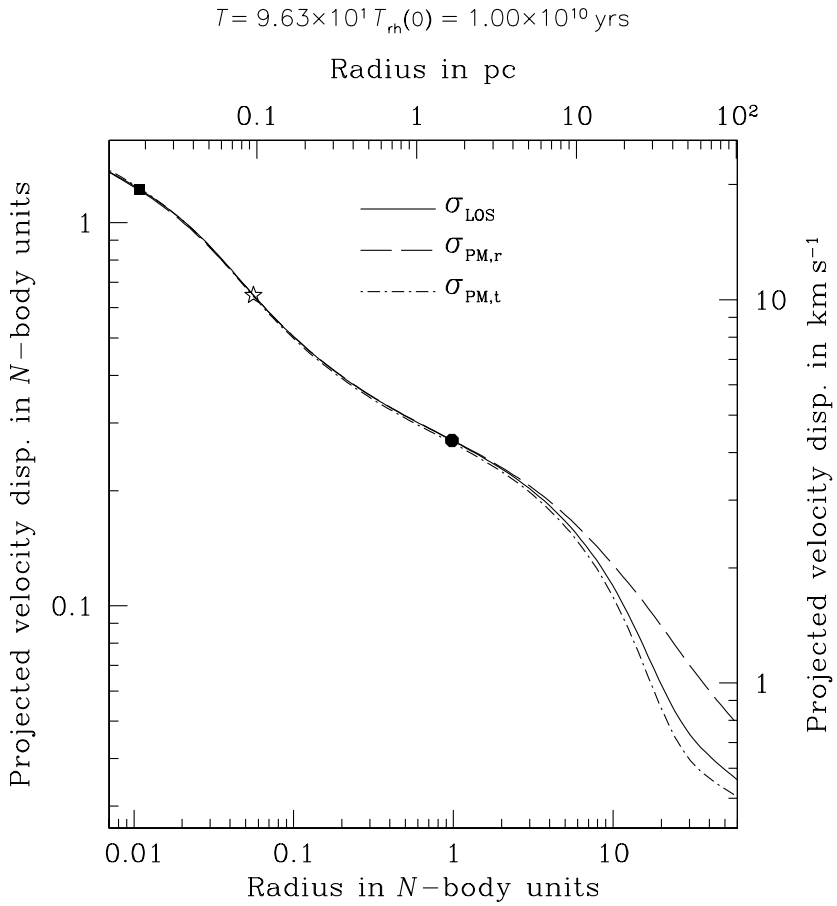


Fig. 5.9: Projected velocity dispersions for the same case and time as Fig. 5.5. The line of sight component is represented with a solid line and the proper motion component with a dashed one for the radial and dashed-dot for the tangential contribution.

the maximum contribution to the mass accretion rate stems at the radius where $\theta_D = \theta_{lc}$. Consistently, Frank and Rees (1976) estimated the total mass accretion rate as $\dot{M}_\bullet \propto \rho(r_{crit})\, r_{crit}^3 / t_{relax}(r_{crit})$.
The dependence of loss-cone accretion rate on time during the late re-expansion phase can be estimated through simple scaling laws. One starts with the relation of Frank and Rees (1976) mentioned above,

$$\dot{M}_\bullet \simeq \frac{\rho(r_{crit})\, r_{crit}^3}{t_{relax}(r_{crit})}, \tag{5.35}$$

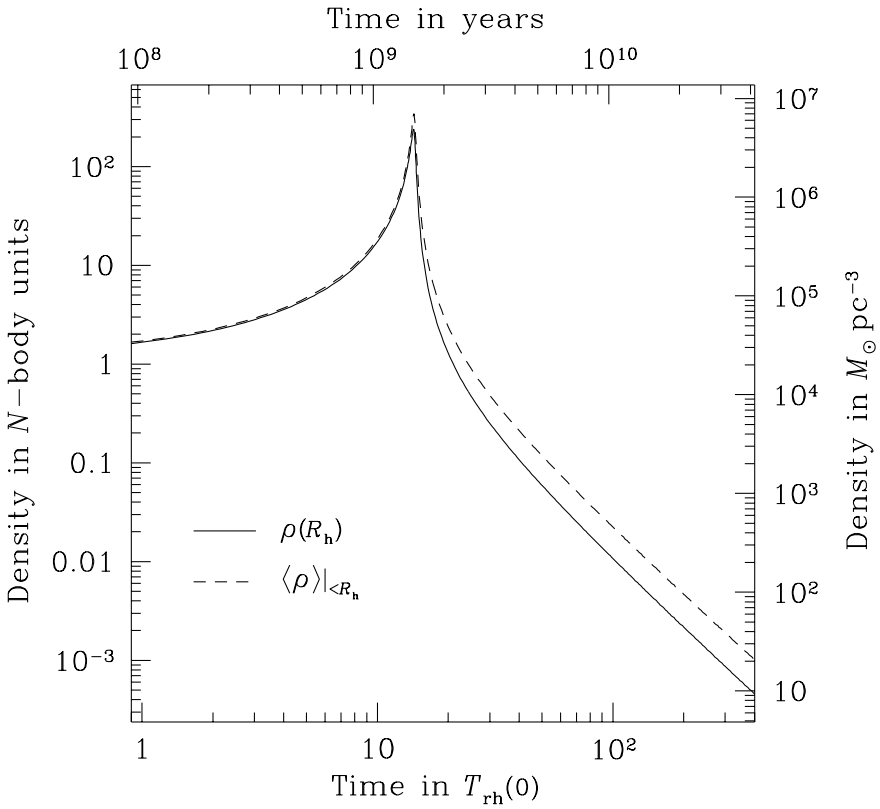


Fig. 5.10: Evolution of the stellar density in the central region for our model with $10^5$ stars and $\mathscr{M}_{\rm bh}(0) = 50\,{\rm M}_\odot$ (case a). The solid line depicts the density at the influence radius $R_{\rm h}$. The dashed line shows the average density *within* $R_{\rm h}$.

and the definition of the critical radius,

$$\begin{aligned} \theta^2_{\rm lc}(r_{\rm crit}) &= \theta^2_{\rm D}(r_{\rm crit}) \\ \Rightarrow \frac{r_{\rm t}}{r_{\rm crit}} &\simeq \frac{t_{\rm cross}(r_{\rm crit})}{t_{\rm relax}(r_{\rm crit})}. \end{aligned} \tag{5.36}$$

One substitutes the following relations into Eq. 5.36,

$$\begin{aligned} r_{\rm t} &\propto \mathscr{M}_\bullet^{1/3}, \\ t_{\rm cross}(r) &\propto \frac{r^{3/2}}{\mathscr{M}_\bullet^{1/2}}, \\ t_{\rm relax}(r) &\propto \frac{\sigma(r)^3}{n(r)} \propto \frac{\mathscr{M}_\bullet^{3/2}}{r^{3/2} n(r)}, \end{aligned} \tag{5.37}$$

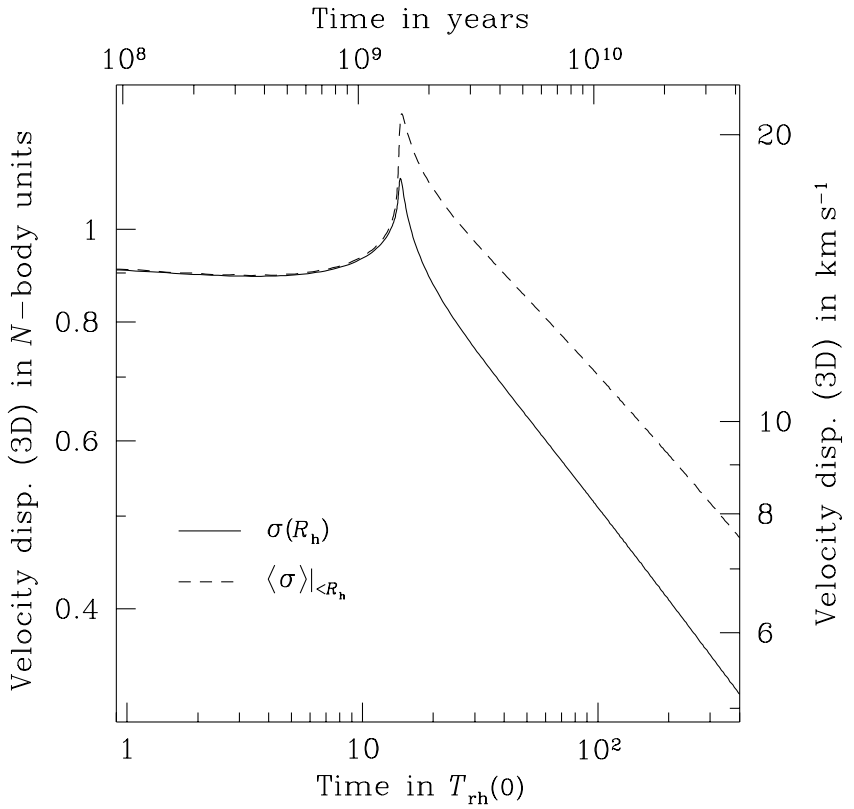


Fig. 5.11: Same as Fig. 5.10 but for the three dimensional velocity dispersion.

where we have made use of the fact that the potential is dominated by the BH in the region of interest ($r_{\rm crit} < r_{\rm h}$). Finally one needs the dependence of the density of stars on time and radius, $n(r,T)$. We have seen that, to a good approximation, the re-expansion of the cluster is homologous with Lagrange radii expanding like $R \propto T^{2/3}$. In the region between $r_{\rm crit}$ and $r_{\rm h}$, the density profile resembles a power-law cusp; hence, a general self-similar evolution can be described by

$$n(r,T) = n_0(T)\left(\frac{r}{r_0(T)}\right)^{-\alpha}, \tag{5.38}$$

where $r_0$ is some Lagrange radius. Hence, from conservation of mass inside $r_0$,

$$n(r,T) \propto T^{\frac{2\alpha-6}{3}} r^{-\alpha}. \tag{5.39}$$

Combining relations 5.36, 5.37 and 5.39, one finds

$$r_{\rm crit} \propto \mathscr{M}_\bullet^{\frac{7}{3(4-\alpha)}} T^{\frac{2(3-\alpha)}{3(4-\alpha)}} \tag{5.40}$$

and, inserting this into Eq. 5.35,

$$\dot{\mathscr{M}}_\bullet \propto \mathscr{M}_\bullet^{\frac{27-19\alpha}{6(4-\alpha)}} T^{\frac{7(\alpha-3)}{3(4-\alpha)}}, \tag{5.41}$$

which, by integration, yields

$$\mathscr{M}_\bullet \propto T^{\frac{2(4\alpha-9)}{13\alpha-3}}, \tag{5.42}$$

$$\dot{\mathscr{M}}_\bullet \propto T^{\frac{-5(\alpha-3)}{13\alpha-3}}. \tag{5.43}$$

For $\alpha = 7/4$, which is appropriate here (again because $r_{\rm crit} < r_{\rm h}$), the exponent in the last relation turns out to be $-95/79 \simeq -1.20$, in remarkable agreement with figures 5.1b and 5.2b.

## 5.5 Discussion

We have presented in this chapter a method to follow the evolution of a spherical stellar cluster with a central accreting BH in a fully self-consistent manner concerning the spatial resolution. As regards the velocity space, we use a simplified model based on ideas of Frank and Rees (1976) in order to describe the behaviour of the distribution function inside and outside the loss-cone by a simple diffusion equation. This numerical method is an extension of the "gaseous model" which has been successfully applied to a variety of aspects of the evolution of globular clusters without central BH (Spurzem and Takahashi, 1995; Spurzem and Aarseth, 1996; Giersz and Spurzem, 2000, 2003; Deiters and Spurzem, 2001, amongst others). With this new version, the simulation of galactic nuclei is also feasible.
In addition to an explanation of the physical and numerical principles underlying our approach, we have concentrated on a few simple test computations, aimed at checking the proper behaviour of the code. We considered a system where all stars are and remain single, have the same mass, stellar evolution and collisions are neglected and a seed central BH is allowed to grow by accreting stellar matter through tidal disruptions. The present version of the code already allows for a (discretised) stellar mass spectrum and stellar evolution and we are in the process of including stellar collisions because they are thought to dominate over tidal disruption in most galactic nuclei, as far as accretion on to the BH is concerned (David et al., 1987a,b; Murphy et al., 1991; Freitag and Benz, 2002). In a subsequent chapter, we shall increase complexity and realism one step further and consider systems with a mass spectrum. Using both this gaseous code and the Monte Carlo algorithm (Freitag and Benz, 2001, 2002), we will investigate the role of mass segregation around a massive black hole (Amaro-Seoane, Freitag & Spurzem, in preparation), a mechanism which may have important observational consequences as it probably affects the structure of the central cluster of the Milky Way (Morris, 1993; Miralda-Escudé and Gould, 2000; Freitag, 2003b,a; Pfahl and Loeb, 2003) and impacts rates of tidal disruptions and capture of compact

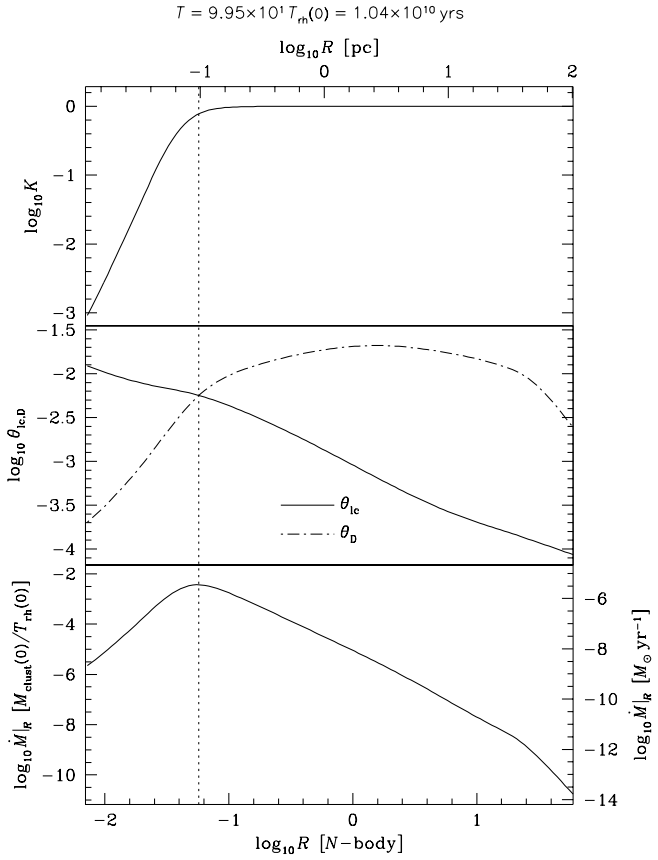


Fig. 5.12: In this triple diagram we evince the dependence on radius of the mass accretion rate, the loss-cone and diffusion angle which are related to the filling and depletion time-scales of the loss-cone (see text) and the filling factor $K$. The critical radius is defined by the condition $\theta_D = \theta_{\rm lc}$ (broken line).

stars by emission of gravitational waves in dense galactic nuclei (Magorrian and Tremaine, 1999; Syer and Ulmer, 1999; Sigurdsson, 2003, and references therein).

Unfortunately, the literature has relatively little to offer to check our models. The most robust predictions are probably the analytical and semi-analytical analysis for the regime where the gravity of the BH dominates and the Fokker-Planck treatment of relaxation holds (Bahcall and Wolf, 1976; Shapiro and Lightman, 1976; Lightman and Shapiro, 1977; Cohn and Kulsrud, 1978). The most important feature of these solutions is that, provided the system is well relaxed and one stands beyond the critical radius (inside of which loss-cone effects complicate the picture), a cuspy density distribution is established, $\rho \propto r^{-\alpha}$ with $\alpha = 7/4$. Our code nicely agrees with this prediction.

Concerning the evolution of the system, we first note that, initially, the cluster follows the usual and well understood route to core-collapse. That the gaseous model can successfully simulate this phase has

been clearly established in previous works (Giersz and Spurzem, 1994; Spurzem and Aarseth, 1996). When the core has become dense enough, the BH starts growing quite suddenly. As it accretes stars that are deeply bound, i.e. with very negative energies, the BH creates a outward flux of energy and allows the cluster to re-expand. As long as the source of energy is centrally concentrated and that the mass of the BH remains relatively slow, one expect the re-expansion to become self-similar, a regime during which the size of the cluster increases like $R \propto T^{2/3}$ (Hénon, 1965; Shapiro, 1977; McMillan et al., 1981; Goodman, 1984, among others). This is again well reproduced by the gaseous model. Solving the Fokker-Planck equation with a Monte Carlo method, Marchant and Shapiro (1980) and Duncan and Shapiro (1982) have realised a series of simulations of single-mass globular clusters with a central BH. Because their resolution was quite low and because they used "initial" conditions difficult to implement (in most of their runs the central BH is not present initially but introduced at some instant during deep collapse), we do not attempt a quantitative comparison with their results. An added difficulty is that we do not include tidal truncation of the cluster. However, an important finding of Marchant and Shapiro (1980) is reproduced by our computations, namely that the initial mass of the seed black hole has little effect on the post-collapse evolution, provided it represents only a small fraction of cluster mass. In particular, the BH mass at late times converges to the same value which only depends on the size and mass of the cluster. We note that such convergence was also obtained with the Monte Carlo algorithm and that a comparison between results obtained with that code and an early version of the program described here was presented in Freitag and Benz (2002). More comparisons between the two methods are planned (Amaro-Seoane, Freitag & Spurzem, in preparation).

Here one has to mention that the energy input of the BH star accretion causes a "temperature" increase in the central region which is followed by a thermal expansion. Therefore, the system is a normal thermal system with positive specific heat in contrast to the cores of self-gravitating systems, where the energy input due to binary hardening causes a core expansion and decrease of temperature (Bettwieser and Sugimoto, 1984). Afterwards, an inversion in the radial temperature profile follows and the expansion is a reverse gravothermal instability (Spurzem, 1991). Since our system is dominated by external gravitation in the centre we cannot expect such a behaviour. Furthermore, as the central BH grows irreversibly, it continues accreting stars in spite of the re-expansion and continuous decrease of the density of stars. Hence, a second core collapse is impossible and oscillations of the central cluster density do not occur.

Among the aspects of our results that require further investigation, we mention the shape of the density profile inside the critical radius. Although the well known $\rho \propto r^{-7/4}$ Bahcall-Wolf solution only strictly applies for $r_{\rm crit} < r < r_{\rm h}$, this cusp extends inward nearly down to the tidal disruption radius in the stationary models of Marchant and Shapiro (1979), which also include loss-cone physics. This result is in disagreement with the analysis of Dokuchaev and Ozernoi (1977) (see also Ozernoi and Reinhardt 1978) which predicted $\rho \propto r^{-1/2}$ in this region. As shown on Fig. 5.5, we obtain an even stronger flattening of the density law inside $r_{\rm crit}$. At the present time it is unknown to us which solution, if any, is the correct one. A possibility to be considered is that this a consequence of the truncation of the moment equations to the second order. In other words, in regions where the loss-cone is significantly depleted, representing the velocity distribution by a simple dispersion ellipsoid and using the velocity dispersion to determine an "effective" loss-cone aperture (Eq. 4.85) is clearly quite a strong approximation. This

may impact the density distribution as the system adjusts its central structure to produce the heating rate required by the overall expansion.
Fortunately, numerical inaccuracies at very small radii are unlikely to affect the overall structure and evolution of the cluster because the loss-cone accretion physics are essentially determined by the conditions at the critical radius, not in the immediate vicinity of the BH.

## 5.6 Addendum A: MBH wandering in a cuspy cluster.

Here we present a simple estimate of the wandering radius $R_{\rm wan}$ of a MBH embeded in a stellar cluster whose density posseses a power-law cusp in the inner regions. We assume that, were it not for the effect of the MBH itself, the stellar cluster would be described by an eta-model (Dehnen, 1993; Tremaine et al., 1994) with enclosed stellar mass

$$\mathscr{M}_*(r) = \mathscr{M}_{\rm cl}\left(\frac{r/a}{1+r/a}\right)^{\eta}, \tag{5.44}$$

where $\mathscr{M}_{\rm cl}$ is the total mass in stars and $a$ the break radius. For $r \ll a$, the density is $\rho \propto r^{-\alpha}$ with $\alpha = 3-\eta$. Inside $R_{\rm wan}$, the MBH strongly perturbates stellar orbits and we suppose the density is rendered more or less constant. Hence, the potential felt by the MBH is approximately harmonic,

$$\Phi(r) = \Phi_0 + \frac{1}{2}\omega^2 r^2 \ \text{, with } \omega^2 = \frac{G\mathscr{M}_*(R_{\rm wan})}{R_{\rm wan}^3}. \tag{5.45}$$

For a harmonic oscillator, the RMS amplitude of the oscillations in velocity and space are linked to each other,

$$V_{\rm RMS}^2 = \omega^2 R_{\rm RMS}^2 \approx \omega R_{\rm wan}^2 = \frac{G\mathscr{M}_*(R_{\rm wan})}{R_{\rm wan}}. \tag{5.46}$$

Dorband et al. (2003) have verified with $N$-body simulations that equipartition of kinetic energy between the MBH and the stars is established, at least in the case of $\eta = 1.5$. Namely,

$$\mathscr{M}_\bullet V_{\rm RMS}^2 \simeq m_*\sigma^2, \tag{5.47}$$

where $\sigma$ is the stellar velocity dispersion at $r = a$. For $\eta = 1.5$ (Tremaine et al., 1994),

$$\sigma^2 \simeq 0.1\frac{G\mathscr{M}_{\rm cl}}{a}. \tag{5.48}$$

Finally, assuming $R_{\rm wan} \ll a$ and, hence, $\mathscr{M}_*(R_{\rm wan}) \simeq \mathscr{M}_{\rm cl}\,(R_{\rm wan}/a)^{\eta}$ and combining equations 5.46, 5.47 and 5.48, we obtain

$$R_{\rm wan} \approx 0.01a\left(\frac{m_*}{\mathscr{M}_\bullet}\right)^2 \ \text{ for } \eta = 1.5 \tag{5.49}$$

and

$$R_{\rm wan} \propto a \left( \frac{m_*}{\mathscr{M}_\bullet} \right)^{1/(\eta-1)} \tag{5.50}$$

for general eta-models.

## 5.7 Addendum B: Velocity dispersion in the central regions

In the region dominated by the central BH, one may expect a "Keplerian" profile for the velocity dispersion, $\sigma \propto r^{-1/2}$. However, in Sec. 5.4, we have seen that in our standard model ($10^5$ stars, case a this relation does not really apply where expected, i.e. between the "1-star" and the influence radius. Here we show that the spherical Jeans equation for a system in dynamical equilibrium is nevertheless obeyed. In spherical symmetry the assumption of dynamical equilibrium (or stationarity) amounts to $u = \langle v_{\rm r} \rangle \equiv 0$. We note that the gaseous model can cope with $u \neq 0$. On the other hand, for a system whose evolution is driven by relaxation, one expects $\sigma_{\rm r,t} \gg u$. The Jeans equation then reads (Binney and Tremaine 1987, Eq. 4-55)

$$GM_{\rm r} = -r\sigma_{\rm r}^2 \left( \frac{{\rm d}\ln n}{{\rm d}\ln r} + \frac{{\rm d}\ln \sigma_{\rm r}^2}{{\rm d}\ln r} + 2\beta \right). \tag{5.51}$$

$M_{\rm r}$ is the mass enclosed by the radius $r$, $n$ the number density of stars and $2\beta = 2 - \sigma_t^2/\sigma_r^2$ is the anisotropy parameter; other quantities have been defined previously. One sees easily that if $M_{\rm r} \equiv \mathscr{M}_\bullet$ and the first and third term in the brackets are both constant, $\sigma \propto r^{-1/2}$ at small $r$. But, as figures 5.13 and 5.14 demonstrate, none of these assumptions exactly applies in the range of radius under consideration. Consequently, we do not get a clean Keplerian velocity profile although (or *because*) Eq. 5.51 is satisfied. Finally, we mention that our models with $10^6$ and $10^7$ stars (and same initial size) exhibit a Keplerian velocity cusp outside the 1-star radius, during their post-collapse evolution. This is partly due to the relatively more massive black hole (larger influence radius) and partly to the much smaller 1-star radius.

## 5.8 Addendum C: Projected velocity dispersions

For the Figures 5.9 and 5.8 we have integrated the density along the z-axis for the projection,

$$\begin{aligned} \Sigma(r) &= \int_{z=0}^{z=R_{\rm max}} \rho(\sqrt{r^2+z^2})\, dz = \\ & 2\int_{\rm r}^{z=R_{\rm max}} \rho(R) \frac{R}{\sqrt{R^2-r^2}}\, dR \end{aligned} \tag{5.52}$$

If one observes the cluster along the z-axis, the contributions to the projected velocity dispersions are as indicated in Fig. 5.15. We have that $R = \sqrt{r^2+z^2}$ and $\sigma_\theta = \sigma_\phi = \sigma_{\rm t}$, where the subscript t stands for tangential. We can reckon that

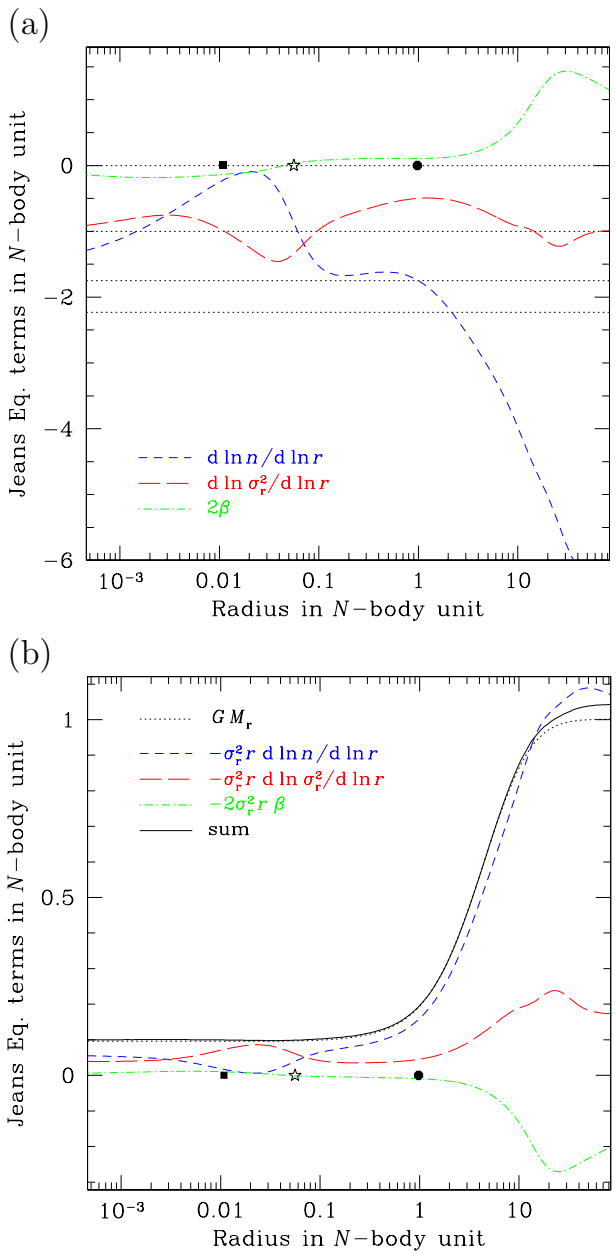


Fig. 5.13: Check of stationary Jeans equation for our "standard" model ($10^5$ stars, case a) at $T = 10\,Gyrs$ (same model and time as Fig. 5.6). Panel (a) depicts the logarithmic derivatives of the stellar density $n$ and radial component of the velocity dispersion well as the anisotropy parameter, $2\beta = 2 - \sigma_t^2/\sigma_r^2$. Horizontal lines corresponding to values of 0, $-1$, $-1.75$ and $-2.23$ are present to guide the eye. In particular, the "Keplerian" velocity profile is $\mathrm{d}\ln\sigma_r^2/\mathrm{d}\ln r \equiv -1$. The round dot indicates the influence radius, the star the critical radius and the square the "1-star" radius. On panel (b), we plot the three terms of the right side of the stationary Jeans equation and check that their sum is (nearly) equal to the left side term, i.e. $GM_\mathrm{r}$.

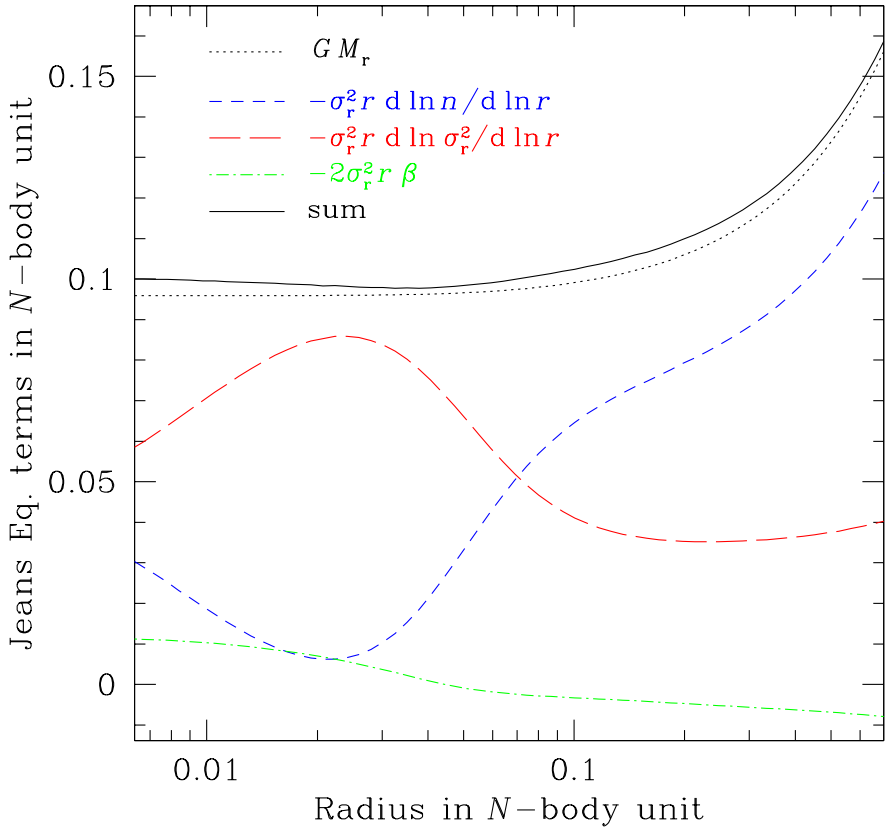


Fig. 5.14: Blow-up of panel (b) of Fig. 5.13 for the region between the 1-star and the influence radius.

$$\sigma_z^2 = \sigma_R^2 \cos^2\theta + \tilde{\sigma}_t^2 \sin^2\theta$$
$$\sigma_r^2 = \sigma_R^2 \sin^2\theta + \tilde{\sigma}_t^2 \cos^2\theta, \tag{5.53}$$

where we have defined $\tilde{\sigma}_t^2 \equiv \sigma_t^2/2$, to be consistent with the notation used until now.
In Fig. 5.15 we can see that $\sigma_z$ contributes to $\sigma_{LOS}$, $\sigma_r$ to $\sigma_{pm,r}$ and $\tilde{\sigma}_t^2$ to $\sigma_{pm,t}$.
Thus, we obtain the projected velocity dispersions,

$$\sigma_{LOS}^2(r) = \frac{2}{\Sigma(R)} \int_{z=0}^{R_{max}} (\sigma_R^2(R)\cos^2\theta + \tilde{\sigma}_t^2(R)\sin^2\theta)\rho(R)\,dz =$$
$$\frac{2}{\Sigma(R)} \int_{z=0}^{R_{max}} (\frac{z^2}{R^2}(\sigma_R^2(R) - \tilde{\sigma}_t^2(R)) + \tilde{\sigma}_t^2(R))\rho(R)\,dz$$

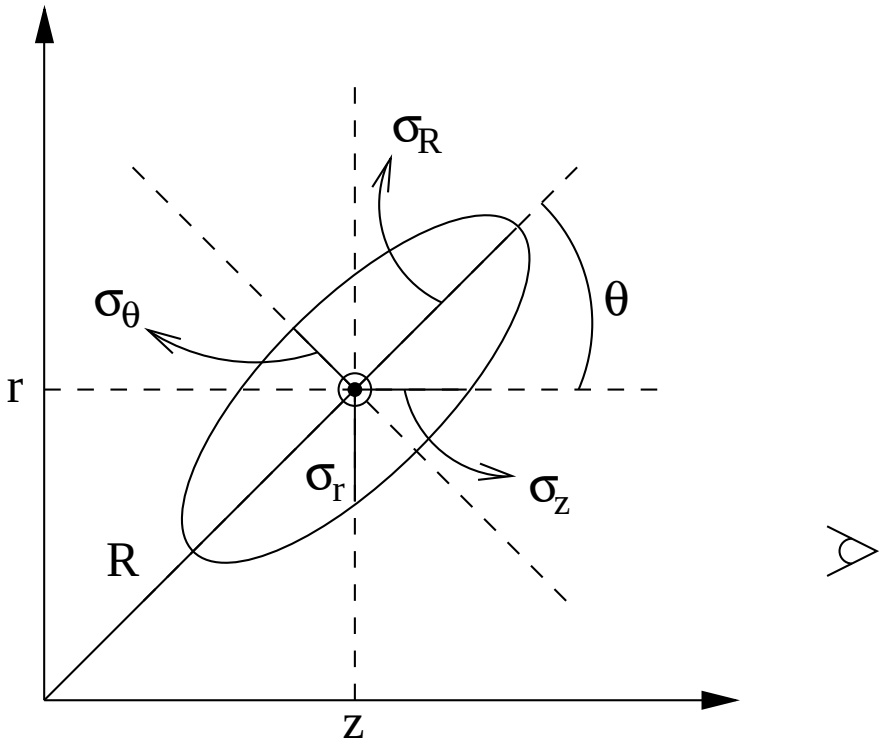


Fig. 5.15: Different contributions to the projected velocity dispersions. The semi-major axis of the ellipsoid perpendicular to the page corresponds to $\sigma_\mathrm{t} = \sigma_\phi$.

$$\sigma^2_{\mathrm{pm,r}}(r) = \frac{2}{\Sigma(R)} \int_{z=0}^{R_\mathrm{max}} (\sigma^2_\mathrm{R}(R) \sin^2\theta + \tilde{\sigma}^2_\mathrm{t}(R) \cos^2\theta) \rho(R)\, dz =$$
$$\frac{2}{\Sigma(R)} \int_{z=0}^{R_\mathrm{max}} (\frac{z^2}{R^2}(\tilde{\sigma}^2_\mathrm{t}(R) - \sigma^2_\mathrm{R}(R)) + \sigma^2_\mathrm{R}(R)) \rho(R)\, dz$$

$$\sigma^2_{\mathrm{pm,t}}(r) = \frac{2}{\Sigma(R)} \int_{z=0}^{R_\mathrm{max}} \tilde{\sigma}^2_\mathrm{t}(R) \rho(R)\, dz, \tag{5.54}$$

since $\sin^2\theta = r^2/R^2 = 1 - \cos^2\theta$ and $\cos^2\theta = z^2/R^2$.

## 5.9 Literature of chapter 5


Aarseth, S. J. (1999a). From NBODY1 to NBODY6: The Growth of an Industry. *PASP*, 111:1333–1346.

Aarseth, S. J. (1999b). Star Cluster Simulations: the State of the Art. *Celestial Mechanics and Dynamical Astronomy*, 73:127–137.

Amaro-Seoane, P., Freitag, M., and Spurzem, R. (2004). Accretion of stars on to a massive black hole: A realistic diffusion model and numerical studies. *mn*.

Bahcall, J. N. and Wolf, R. A. (1976). Star distribution around a massive black hole in a globular cluster. *ApJ*, 209:214–232.

Bettwieser, E. (1983). A numerical method for the study of the gravothermal instability in star clusters. *MNRAS*, 203:811–831.

Bettwieser, E. and Spurzem, R. (1986). Anisotropy in stellar dynamics. *A&A*, 161:102–112.

Bettwieser, E. and Sugimoto, D. (1984). Post-collapse evolution and gravothermal oscillation of globular clusters. *MNRAS*, 208:493–509.

Bettwieser, E. and Sugimoto, D. (1985). Gravitational n-body problem and the validity of concepts of the gas model. *MNRAS*, 212:189–195.

Binney, J. and Tremaine, S. (1987). *Galactic Dynamics*. Princeton University Press.

Chatterjee, P., Hernquist, L., and Loeb, A. (2002). Dynamics of a Massive Black Hole at the Center of a Dense Stellar System. *ApJ*, 572:371–381.

Cohn, H. and Kulsrud, R. M. (1978). The stellar distribution around a black hole - numerical integration of the fokker-planck equation. *ApJ*, 226:1087–1108.

da Costa, L. N. (1981). Star distribution in the presence of a massive central gas cloud. *MNRAS*, 195:869–880.

David, L. P., Durisen, R. H., and Cohn, H. N. (1987a). The evolution of active galactic nuclei. i - models without stellar evolution. *ApJ*, 313:556–575.

David, L. P., Durisen, R. H., and Cohn, H. N. (1987b). The evolution of active galactic nuclei. II - models with stellar evolution. *ApJ*, 316:505–516.

Dehnen, W. (1993). A Family of Potential-Density Pairs for Spherical Galaxies and Bulges. *MNRAS*, 265:250.

Deiters, S. and Spurzem, R. (2001). Multi-mass Gaseous Models of Globular Clusters with Stellar Evolution. In *ASP Conf. Ser. 228: Dynamics of Star Clusters and the Milky Way*, page 416.

Dokuchaev, V. I. and Ozernoi, L. M. (1977). Distribution of stars in the vicinity of a massive black hole. *Sov. Astron. Lett.*, 3:112–114.

Dorband, E. N., Hemsendorf, M., and Merritt, D. (2003). Systolic and hyper-systolic algorithms for the gravitational N-body problem, with an application to Brownian motion. *Journal of Computational Physics*, 185:484–511.

Duncan, M. J. and Shapiro, S. L. (1982). Star clusters containing massive, central black holes. IV - galactic tidal fields. *ApJ*, 253:921–938.

Frank, J. and Rees, M. J. (1976). Effects of massive central black holes on dense stellar systems. *MNRAS*, 176:633–647.

Fregeau, J. M., Gürkan, M. A., Joshi, K. J., and Rasio, F. A. (2003). Monte Carlo Simulations of Globular Cluster Evolution. III. Primordial Binary Interactions. *ApJ*, 593:772–787.

Freitag, M. (2003a). Captures of stars by a massive black hole: Investigations in numerical stellar dynamics. to appear in the proceedings of “The Astrophysics of Gravitational Wave Sources”, astro-

ph/0306064.
Freitag, M. (2003b). Gravitational waves from stars orbiting the Sagittarius A* black hole. *ApJ Lett.*, 583:21–24.
Freitag, M. and Benz, W. (2001). A new monte carlo code for star cluster simulations: I. relaxation. *A&A*, 375:711–738.
Freitag, M. and Benz, W. (2002). A new monte carlo code for star cluster simulations: II. central black hole and stellar collisions. *A&A*, 394:345–374.
Freitag, M. and Benz, W. (2004). A comprehensive set of simulations of high-velocity collisions between main sequence stars. submitted to MNRAS, astro-ph/0403621.
Ghez, A. M., Duchêne, G., Matthews, K., Hornstein, S. D., Tanner, A., Larkin, J., Morris, M., Becklin, E. E., Salim, S., Kremenek, T., Thompson, D., Soifer, B. T., Neugebauer, G., and McLean, I. (2003). The First Measurement of Spectral Lines in a Short-Period Star Bound to the Galaxy's Central Black Hole: A Paradox of Youth. *ApJ Lett.*, 586:L127–L131.
Giersz, M. (1998). Monte carlo simulations of star clusters - i. first results. *MNRAS*, 298:1239–1248.
Giersz, M. and Heggie, D. C. (1994). Statistics of N-Body Simulations - Part Two - Equal Masses after Core Collapse. *MNRAS*, 270:298.
Giersz, M. and Spurzem, R. (1994). Comparing direct *n*-body integration with anisotropic gaseous models of star clusters. *MNRAS*, 269:241.
Giersz, M. and Spurzem, R. (2000). A stochastic monte carlo approach to model real star cluster evolution - II. self-consistent models and primordial binaries. *MNRAS*, 317:581.
Giersz, M. and Spurzem, R. (2003). A stochastic Monte Carlo approach to modelling real star cluster evolution - III. Direct integration of three- and four-body interactions. *MNRAS*, 343:781–795.
Goodman, J. (1984). Homologous evolution of stellar systems after core collapse. *ApJ*, 280:298–312.
Gurevich, A. (1964). Instability of the disturbed zone in the vicinity of a charged body in plasma. *Geomag. Aeronom.*, 4:247–255.
Hénon, M. (1965). Sur l'évolution dynamique des amas globulaires. II. Amas isol&eacute. *Annales d'Astrophysique*, 28:62.
Hachisu, I., Nakada, Y., Nomoto, K., and Sugimoto, D. (1978). Post-collapse evolution of a gaseous cluster model. *Prog. Theor. Phys. 60, 393*, 393:60.
Heggie, D. C. (1984). Post-collapse evolution of a gaseous cluster model. *MNRAS*, 206:179–195.
Heggie, D. C. and Mathieu, R. D. (1986). Standardised units and time scales. In Hut, P. and McMillan, S. L. W., editors, *The Use of Supercomputers in Stellar Dynamics*, page 233. Springer-Verlag.
Heggie, D. C. and Ramamani, N. (1989). Evolution of star clusters after core collapse. 237:757–783.
Hénon, M. (1971). Monte carlo models of star clusters. *Ap&SS*, 13:284–299.
Joshi, K. J., Nave, C. P., and Rasio, F. A. (2001). Monte Carlo Simulations of Globular Cluster Evolution. II. Mass Spectra, Stellar Evolution, and Lifetimes in the Galaxy. *ApJ*, 550:691–702.
Lightman, A. P. and Shapiro, S. L. (1977). The distribution and consumption rate of stars around a massive, collapsed object. *ApJ*, 211:244–262.
Lin, D. N. C. and Tremaine, S. (1980). A reinvestigation of the standard model for the dynamics of a massive black hole in a globular cluster. *ApJ*, 242:789–798.
Louis, P. D. and Spurzem, R. (1991). Anisotropic gaseous models for the evolution of star clusters. *MNRAS*, 251:408–426.
Lynden-Bell, D. and Eggleton, P. P. (1980). On the consequences of the gravothermal catastrophe. *MNRAS*, 191:483–498.
Magorrian, J. and Tremaine, S. (1999). Rates of tidal disruption of stars by massive central black holes. *MNRAS*, 309:447–460.
Marchant, A. B. and Shapiro, S. L. (1979). Star clusters containing massive, central black holes. II -

self-consistent potentials. *ApJ*, 234:317–328.
Marchant, A. B. and Shapiro, S. L. (1980). Star clusters containing massive, central black holes. III - evolution calculations. *ApJ*, 239:685–704.
McMillan, S. L. W., Lightman, A. P., and Cohn, H. (1981). Luminosity evolution of quasars and active galaxies - theoretical models of the evolving mass supply rate. *ApJ*, 251:436–445.
Milosavljević, M. and Merritt, D. (2003). Long-Term Evolution of Massive Black Hole Binaries. *ApJ*, 596:860–878.
Miralda-Escudé, J. and Gould, A. (2000). A cluster of black holes at the galactic center. *ApJ*, 545:847–853.
Morris, M. (1993). Massive star formation near the Galactic center and the fate of the stellar remnants. *ApJ*, 408:496–506.
Murphy, B. W., Cohn, H. N., and Durisen, R. H. (1991). Dynamical and luminosity evolution of active galactic nuclei - models with a mass spectrum. *ApJ*, 370:60–77.
Ozernoi, L. M. and Reinhardt, M. (1978). Massive black holes in nuclei of galaxies and quasars. *A&AS*, 59:171–192.
Peebles, P. J. E. (1972). Star distribution near a collapsed object. *ApJ*, 178:371–376.
Pfahl, E. and Loeb, A. (2003). Probing the Spacetime Around Sgr A* with Radio Pulsars. *ArXiv Astrophysics e-prints*.
Schödel, R., Ott, T., Genzel, R., Eckart, A., Mouawad, N., and Alexander, T. (2003). Stellar Dynamics in the Central Arcsecond of Our Galaxy. *ApJ*, 596:1015–1034.
Shapiro, S. L. (1977). The dissolution of globular clusters containing massive black holes. *ApJ*, 217:281–286.
Shapiro, S. L. and Lightman, A. P. (1976). The distribution of stars around a massive black hole. *Nat*, 262:743–745.
Sigurdsson, S. (2003). The loss cone: past, present and future. *Classical and Quantum Gravity*, 20:45.
Spitzer, L. (1987). *Dynamical evolution of globular clusters*. Princeton University Press.
Spurzem, R. (1991). Gravothermal instability of anisotropic self-gravitating gas spheres - Singular equilibrium solution. *MNRAS*, 252:177–189.
Spurzem, R. (1992). Evolution of stars and gas in galactic nuclei. In *Reviews of Modern Astronomy*, volume 5, pages 161–173.
Spurzem, R. (1999). Direct *n*-body simulations. *Journal of Computational and Applied Mathematics*, 109:407–432.
Spurzem, R. and Aarseth, S. J. (1996). Direct collisional simulation of 100000 particles past core collapse. *MNRAS*, 282:19.
Spurzem, R., Berczik, P., Hensler, G., Theis, C., Amaro-Seoane, P., Freitag, M., and Just, A. (2003). Physical Processes in Star-Gas Systems. *ArXiv Astrophysics e-prints*.
Spurzem, R. and Takahashi, K. (1995). Comparison between fokker-planck and gaseous models of star clusters in the multi-mass case revisited. *MNRAS*, 272:772–784.
Syer, D. and Ulmer, A. (1999). Tidal disruption rates of stars in observed galaxies. *MNRAS*, 306:35–42.
Takahashi, K. (1995). Fokker-planck models of star clusters with anisotropic velocity distributions i. pre-collapse evolution. *PASJ*, 47:561–573.
Takahashi, K. (1996). Fokker-planck models of star clusters with anisotropic velocity distributions II. post-collapse evolution. *PASJ*, 48:691–700.
Takahashi, K. (1997). Fokker-planck models of star clusters with anisotropic velocity distributions III. multi-mass clusters. *PASJ*, 49:547–560.
Tremaine, S., Richstone, D. O., Byun, Y., Dressler, A., Faber, S. M., Grillmair, C., Kormendy, J., and Lauer, T. R. (1994). A family of models for spherical stellar systems. *AJ*, 107:634–644.

# Chapter 6

# Multi-components clusters with/out a central BH: Mass segregation

## 6.1 An academic exercise: Mass segregation in two mass-component clusters

SINCE we have arduously examined the idealised situation for a stellar cluster in which all stars possess the same mass in order to subject to scrutiny our model, we have morally the right to extend the analysis a further step. Here we tackle with more realistic configurations in which the stellar system is splitted into various components [1]. The second integer number immediately after one is two and so will we first extend, cautious and wary as we are, our models to two-components star clusters. The initial motivation for the study of such physical systems was the better resemblance to real clusters. The processes that one-component clusters bring about is nowadays well understood and has been plenteously studied by different authors to check for the goodness of their approaches. New features of these systems' behaviour arise when we consider a stellar system in which masses are divided into two groups. Depending on how the system taken into consideration is configurated will we exclude *dynamical equilibrium* (here it is meant that the system is not stable on dynamical time-scales) or equipartition of different components kinetic energies is not allowed (*thermal equilibrium*).
Spitzer (1969) gave the analysis an initial shove with his study. For some clusters it seemed impossible to find a configuration in which they enjoy dynamical and thermal equilibrium altogether. The

[1] This chapter is part of present work and will be published like Freitag, Amaro-Seoane and Spurzem (2004). Some part of it has been employed for Khalisi, Amaro-Seoane and Spurzem (2004) -submitted to MNRAS- and an initial concept was employed for Amaro-Seoane and Spurzem (2003)

heavy component sink into the centre because they cede kinetic energy to the light one when reaching equipartition. The process will carry on until equipartition is fully gained on and the heavy component self-gravity moves out in the core. In the most of the cases, equipartition happens to be impossible, because the subsystem of massive stars will undergo core collapse before equipartiton is reached. Anon, a *gravothermal collapse* will happen upon this component and, as a result, a small dense core of heavies is formed (Spitzer, 1969; Lightman and Fall, 1978). This gravothermal contraction is a product of negative heat capacity, a typical property of gravitationally bound systems (Elson et al., 1987).

Disparate authors have addressed the problem of thermal and dynamical equilibrium in such systems, from recent direct $N$-body simulations (Portegies Zwart and McMillan, 2000) and Monte Carlo simulations (Watters et al., 2000) to direct integration of the Fokker-Planck equation (Inagaki and Wiyanto, 1984; Kim et al., 1998) including Monte Carlo approaches to the numerical integration of this equation (Spitzer and Hart, 1971). For a general and complete overview of the historical evolution of two-stars stellar components, see Watters et al. (2000) and references therein.

If we do not have any energy source in the cluster and stars do not collide (physically), the contraction carries on self-similarly indefinitely; in such a case, one says that the system undergoes *core-collapse*. This phenomenon has been observed in a big number of works using different methods (Hénon, 1973; Hénon, 1975; Spitzer and Shull, 1975; Cohn, 1980; Marchant and Shapiro, 1980; Stodołkiewicz, 1982; Takahashi, 1993; Giersz and Heggie, 1994; Takahashi, 1995; Spurzem and Aarseth, 1996; Makino, 1996; Quinlan, 1996; Drukier et al., 1999; Joshi et al., 2000, etc) Core collapse is not just a characteristic of multi-mass systems, but has been also observed in single mass analysis.

Spitzer (1969) gave the analytical criterion to determine whether a two-component system has achieved energy equipartition. According to his analysis, energy equipartition between the light and heavy component exists if

$$S := \left(\frac{\mathscr{M}_{\rm h}}{\mathscr{M}_{\rm l}}\right)\left(\frac{m_{\rm h}}{m_{\rm l}}\right)^{3/2} < 0.16 \tag{6.1}$$

Where $\mathscr{M}_{\rm l}$ and $\mathscr{M}_{\rm h}$ are the total numbers of light and heavy components, respectively. More recent numerical calculations (Watters et al., 2000) have settled this criterion to $\Lambda$,

$$\Lambda := \left(\frac{\mathscr{M}_{\rm h}}{\mathscr{M}_{\rm l}}\right)\left(\frac{m_{\rm h}}{m_{\rm l}}\right)^{2.4} < 0.16 \tag{6.2}$$

When we modify the ratio $\mathscr{M}_{\rm max}/\mathscr{M}$, the time required to reach core-collapse is different. In a cluster with, for instance, a broad Salpeter IMF between $[0.2\,{\rm M}_\odot, 120\,{\rm M}_\odot]$ core-collapse takes place after $\lesssim 0.1\,t_{\rm rh}(0)$, whereas for a single-mass Plummer model it occurs after $\gtrsim 10\,t_{\rm rh}(0)$ (this example was taken from the Monte Carlo-based calculations of Gürkan et al. 2004)

There is an ample evidence for mass-segregation in observed clusters. McCaughrean and Stauffer (1994) Hillenbrand and Hartmann (1998) provided a new deep infrared observations of the Trapezium cluster in Orion that clearly show the mass segregation in the system, with the highest mass stars segregated into the centre of the cluster. To test whether there is evidence for more general mass segregation, they show in Fig. (6.1) cumulative distributions with radius of stars contained within different mass intervals. They

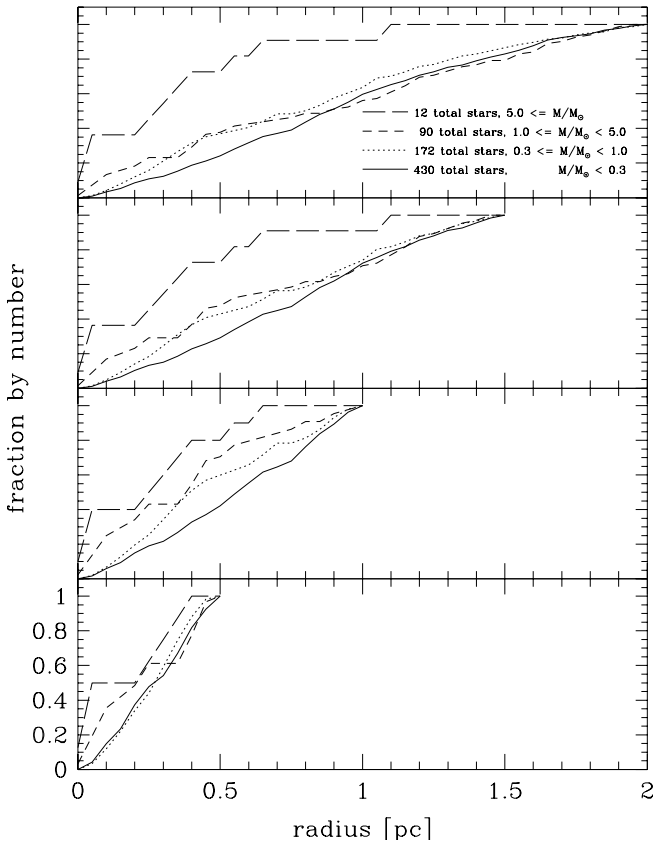


Fig. 6.1: In this plot by Hillenbrand and Hartmann (1998) we have a clear-cut evidence for mass-segregation of stars more massive than 5 $M_\odot$ (long-dashed lines) toward the cluster centre and some evidence for general mass segregation persisting down to 1-2 $M_\odot$ in the Orion Nebula cluster. The cumulative radial distributions of source counts over different mass intervals are shown. To clarify the sensitivity of the cumulative plots to the outer radius they have shown here four panels with four different limiting radii

include in the plot four different panels in order to manifest the sensitivity to the limiting radius. They find that, inside 1.0 pc, general mass segregation appears to be established in the cluster, with stars of masses less than 0.3, 0.3-1.0, 1.0-5.0, and greater than 5 $M_\odot$ progressively more centrally concentrated with increasing mass.

At this point, the question looms up whether for very young clusters mass segregation is due to relaxation, like in our models, or rather it reflects the fact that massive stars are formed preferentially towards the centre of the cluster, as some models predict.

Raboud and Mermilliod (1998) study the radial structure of Praesepe and of the very young open cluster NGC 6231. There they find evidence for mass segregation among the cluster members and between binaries and single stars. They put it down to the greater average mass of the multiple systems. In

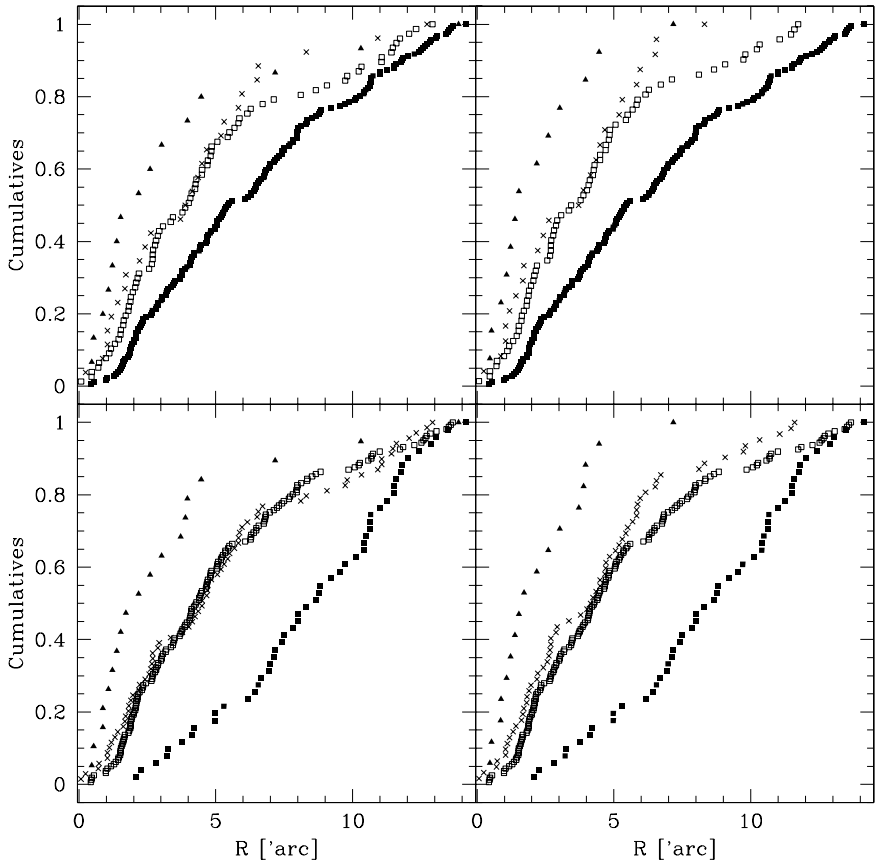


Fig. 6.2: Mass segregation in NGC 623 for two mass interval sets. The two left panels include all sample stars, whereas the right ones do not include the 9 bright stars of the cluster corona. For the two top figures $M < 5\mathrm{M}_{\odot}$ (filled squares), $M \in [5, 10[\mathrm{M}_{\odot}$ (open squares), $M \in [10, 20[\mathrm{M}_{\odot}$ (crosses) and $M \geq 20\mathrm{M}_{\odot}$ (triangles). For the two bottom figures, $M < 2.5\mathrm{M}_{\odot}$ (filled squares), $M \in [2.5, 6.3[\mathrm{M}_{\odot}$ (open squares), $M \in [6.3, 15.8[\mathrm{M}_{\odot}$ (crosses) and $M \geq 15.8\mathrm{M}_{\odot}$ (triangles)

Fig. (6.2) of Raboud and Mermilliod (1998) again we have clear evidence for mass segregation in NGC 6231. In the two first panels the mass intervals are set in a different way to those in the bottom.
The two left-hand panels include the 9 bright stars of the cluster Corona, while the right hand two diagrams do not. The manifestation of mass segregation for massive stars (triangles) is clearly nailed down, whereas for stars with masses $\in [5, 20]\,\mathrm{M}_{\odot}$ are spatially well mixed (open squares and crosses); i.e., mass segregation is not yet established over a rather large mass interval. This population is more concentrated than the lower-mass population (here shown with filled squares). They make out from this Fig. (6.2) that only a dozen, bright, massive, mainly binary stars are well concentrated toward the cluster centre.

It seems therefore interesting to set out for multi-mass models with the two-component ones as a starting point to take care of, since it is well-studied and we have robust observational proofs of this phenomenon. On the other hand, observations do not tell us whether mass segregation is due to relaxation. For this aim, and as the title of this section indicates, we have performed here a somehow homiletic but in any case interesting exercise in order to make an acid test of the gaseous model. In less than three days we performed a whole set of $10^4$ simulations for two-component models. We define two parameters now that describe the physics of the system,

$$q := \mathscr{M}_{\rm h}/\mathscr{M}\,,\ \mu := m_{\rm h}/m_{\rm l} \tag{6.3}$$

In this definition, $\mathscr{M}$ is the total mass of the system, $\mathscr{M}_{\rm h}$ the total mass in heavies and $m_{\rm h,l}$ the mass of one heavy (light) star.
If $\zeta \equiv 1-q$, we have let $\zeta$ vary from $10^{-4}$ to $9.99\cdot 10^{-1}$. For each $\zeta$ value, we let $\mu$ vary between 1.03 and $10^3$.
The values for $q$ are regularly distributed in $\log(\zeta)$. For $\zeta \approx 1$ we have added a series of values in $\log(\zeta-1)$. The mean particle mass is $1\,{\rm M}_\odot$ and the total mass $10^6\,{\rm M}_\odot$, but this has not importance for our study, because the physics of the system is ruled by relaxation and therefore the only relevant thing is the relaxation time. If we are using Fokker-Planck or half-relaxation units, we can always extend the physics to any other system containing more particles (if only relaxation is on play). As a matter of fact, one relates the $N$-body units to Fokker-Planck units as follows:

$$\mathscr{U}_{\rm FP} = \mathscr{U}_{\rm NB}\cdot \mathscr{N}_\star/\ln(\gamma\cdot\mathscr{N}_\star) \tag{6.4}$$

Therefore, the relation between FP- and $N$-body- time units is

$$\mathscr{U}_{\rm FP}|_{\rm time} = \mathscr{U}_{\rm NB}|_{\rm time}\cdot \mathscr{N}_\star/\ln(\gamma\cdot\mathscr{N}_\star) \tag{6.5}$$

In order to be able to compare our results with $N$-body, this relation is very useful. The mean mass is therefore just a normalisation. What really determines the dynamics of the system are the mass ratios, $q$ and $\mu$.
In Fig. (6.3) we show the whole $(q,\mu)$-parameter space in a plot where the time at which the core-collapse begins is also included. The green zone corresponds to the quasi single-mass case. In the red zone we have the largest difference between masses and blue is an intermediate case.
In Fig. (6.4) we show collapse times for clusters models with two mass components normalised to the single-mass core-collapse time $T_{\rm cc}$(s.s.) for different values of $\mu$. The initial clusters are Plummer spheres without segregation. The collapse times are displayed as a function of the mass fraction of the heavy component in the cluster. When compared to single-mass component systems, we see that the core-collapse time is accelerated notably for a wide range of the heavy component $\mathscr{M}_{\rm h}$ ($M_2$). Even a small number of heavies accelerate the core-collapse time.
It is really interesting to compare the capacity of our approach by comparing the results of this set of simulations to the $N$-body calculations of star clusters with two-mass components performed by Khalisi

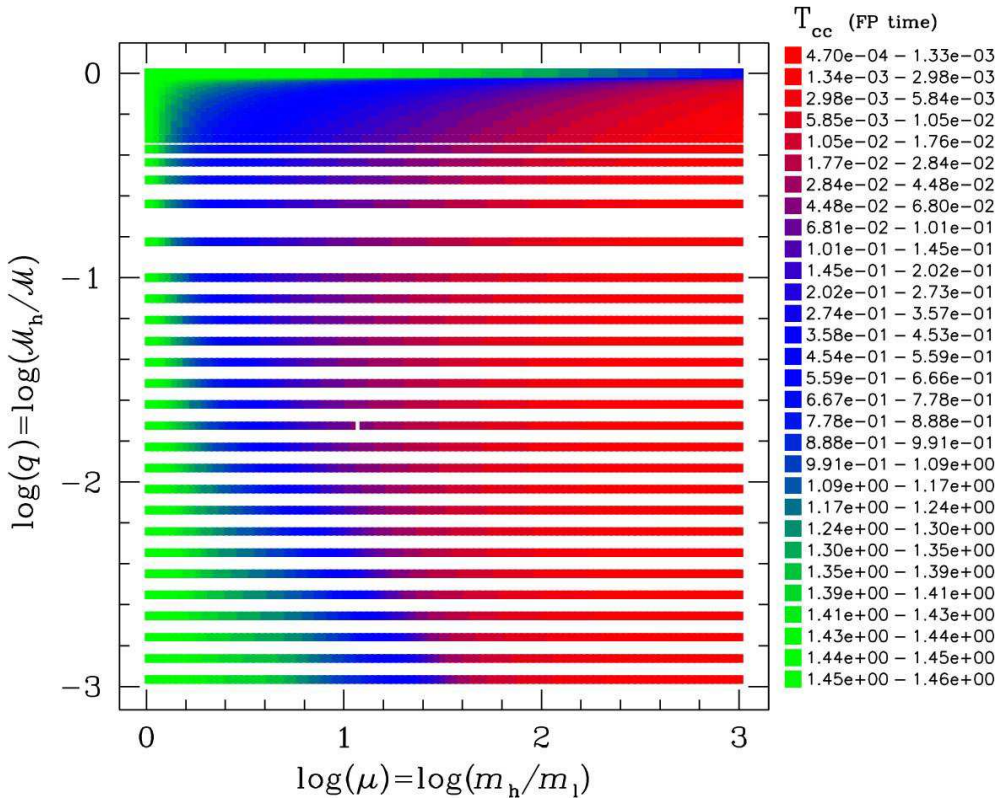


Fig. 6.3: Parameter space for the set of $10^4$ simulations. Here $t_{\rm end}$ stands for the core collapse time and is expressed in FP units (see text); time at which the simulation ended. $q$ and $\mu$ are plotted logarithmically.

(2002) during the completition of his doctoral thesis. For this aim, we plot the evolution of the average mass in Lagrangian shells of the cluster from the averaged mass in Lagrangian *spheres* containing the following mass percentages $[0-1]$, $[2-5]$, $[10-20]$, $[40-50]$, $[75-95]$ %, among others, to be able to compare with the results of Khalisi. These are the comprised volume between two Lagrangian radii, which contain a fixed mass fraction of the bound stars in the system.

We have calculated the average mass as follows: If $M_{\rm r}^{(\rm i)}$ is the total mass for the component i comprised at the radius r and $\bar{m}_\star^{(\rm i)}$ is the average mass for this component within that radius, we can find out what is the value of $\bar{m}_\star^{(\rm i;i+1)}$ (the average mass between $\bar{m}_\star^{(\rm i)}$ and $\bar{m}_\star^{(\rm i+1)}$) knowing $M_{\rm r}^{(\rm i)}$, $M_{\rm r}^{(\rm i+1)}$, $\bar{m}_\star^{(\rm i)}$ and $\bar{m}_\star^{(\rm i+1)}$. This is schematically shown in Fig. (6.5). Indeed,

$$M_{\rm r}^{(\rm i+1)} = N_{\rm r}^{(\rm i)} \cdot \bar{m}_\star^{(\rm i)} + N_{\rm r}^{(\rm i;i+1)} \cdot \bar{m}_\star^{(\rm i;i+1)} = N_{\rm r}^{(\rm i+1)} \cdot \bar{m}_\star^{(\rm i+1)}. \tag{6.6}$$

Since

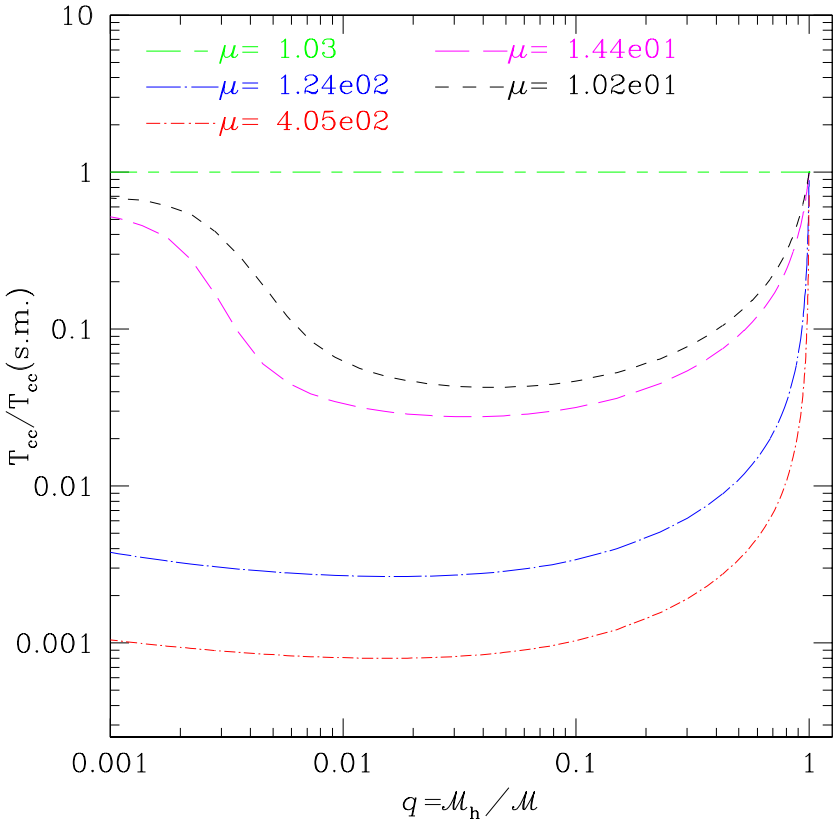


Fig. 6.4: Core-collapse time for different values of $q$ and $\mu$

$$N_r^{(i+1)} = N_r^{(i)} + N_r^{(i;i+1)}, \tag{6.7}$$

where

$$N_r^{(i)} = \frac{M_r^{(i)}}{\bar{m}_\star^{(i)}} \tag{6.8}$$

we have that, from Eq. (6.6),

$$\bar{m}_\star^{(i;i+1)} = \frac{M_r^{(i+1)} - M_r^{(i)}}{M_r^{(i+1)}/\bar{m}_\star^{(i+1)} - M_r^{(i)}/\bar{m}_\star^{(i)}} \tag{6.9}$$

We show in Figs. (6.6) and (6.7) we show the curves corresponding to the values shown in table 6.1.

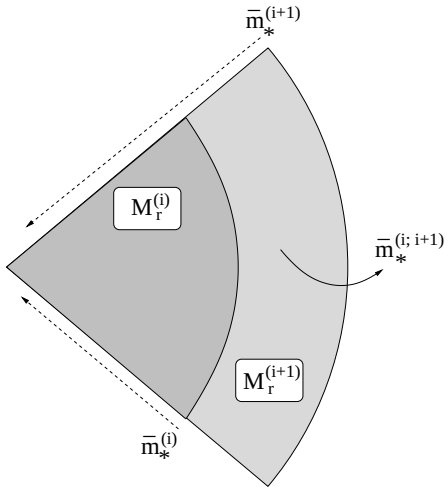


Fig. 6.5: Average mass in Lagrangian shells from averaged mass in Lagrangian spheres

| $\mu$ in Khalisi (2002) | $\mu$ in this work |
|---|---|
| 1.25 | 1.27 |
| 1.5 | 1.56 |
| 2 | 2.06 |
| 3 | 2.92 |
| 5 | 5.09 |
| 10 | 10.2 |

Table 6.1: Different $\mu$ values used in the *N*-body calculations and in our models for Fig. (6.6)

We have followed in the curves the evolution of the system until a deep collapse of the system. They show the evolution until the most massive component dominates the centre.

In order to compare our plots with those of Khalisi (2002), one should look in his diagrams in the region *during* core contraction. At this point, we can observe in Fig. (6.6) a self-similarity after core-collapse (Giersz and Heggie, 1996). Binaries are responsible for interrupting core-collapse and driving core re-expansion in the *N*-body simulations. The flattening in the *N*-body plots at the moment of core-collapse is due to the binary energy generation. This means that we can only compare the steep rise, but not the saturation.

For instance, in the second plot of the *N*-body set (second column on the top), we have to look at the point in which the average mass of the *N*-body system is about 1.20 in the $0-1\%$ shell. This establishes the limit until which we can really compare the behaviour as given by both methods. Our simulations yield a very similar evolution until that point. The gaseous model behaves (it clearly shows the tendency) like *N*-body.

From Eq. (6.5), we get that the conversion factor is the same; namely, for $\gamma = 0.11$, $\ln(\gamma \cdot \mathscr{N}_\star)/\mathscr{N}_\star =$

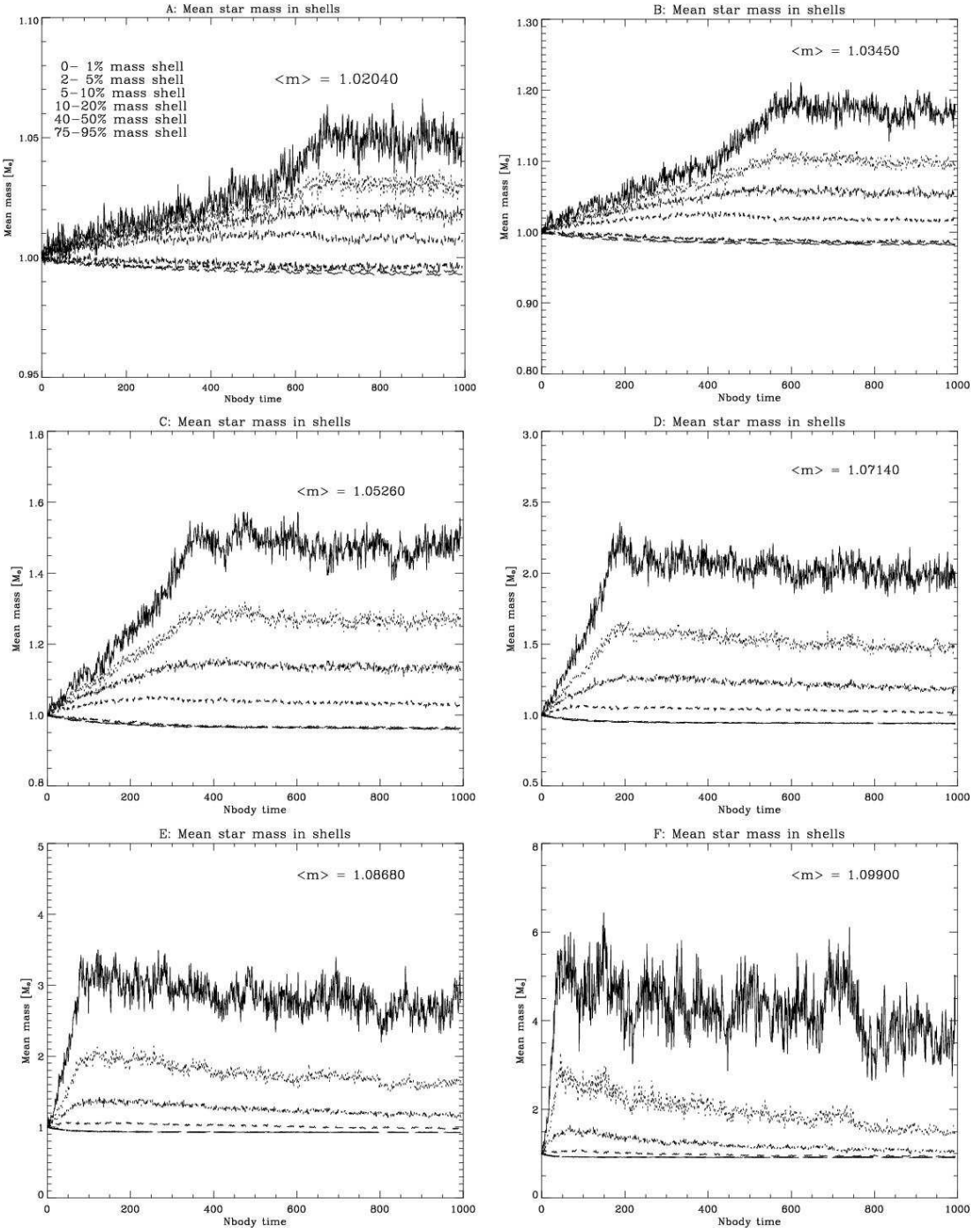


Fig. 6.6: Average Lagrangian radii shells for the $N$-body models of Khalisi (2002) (see text for further explanation)

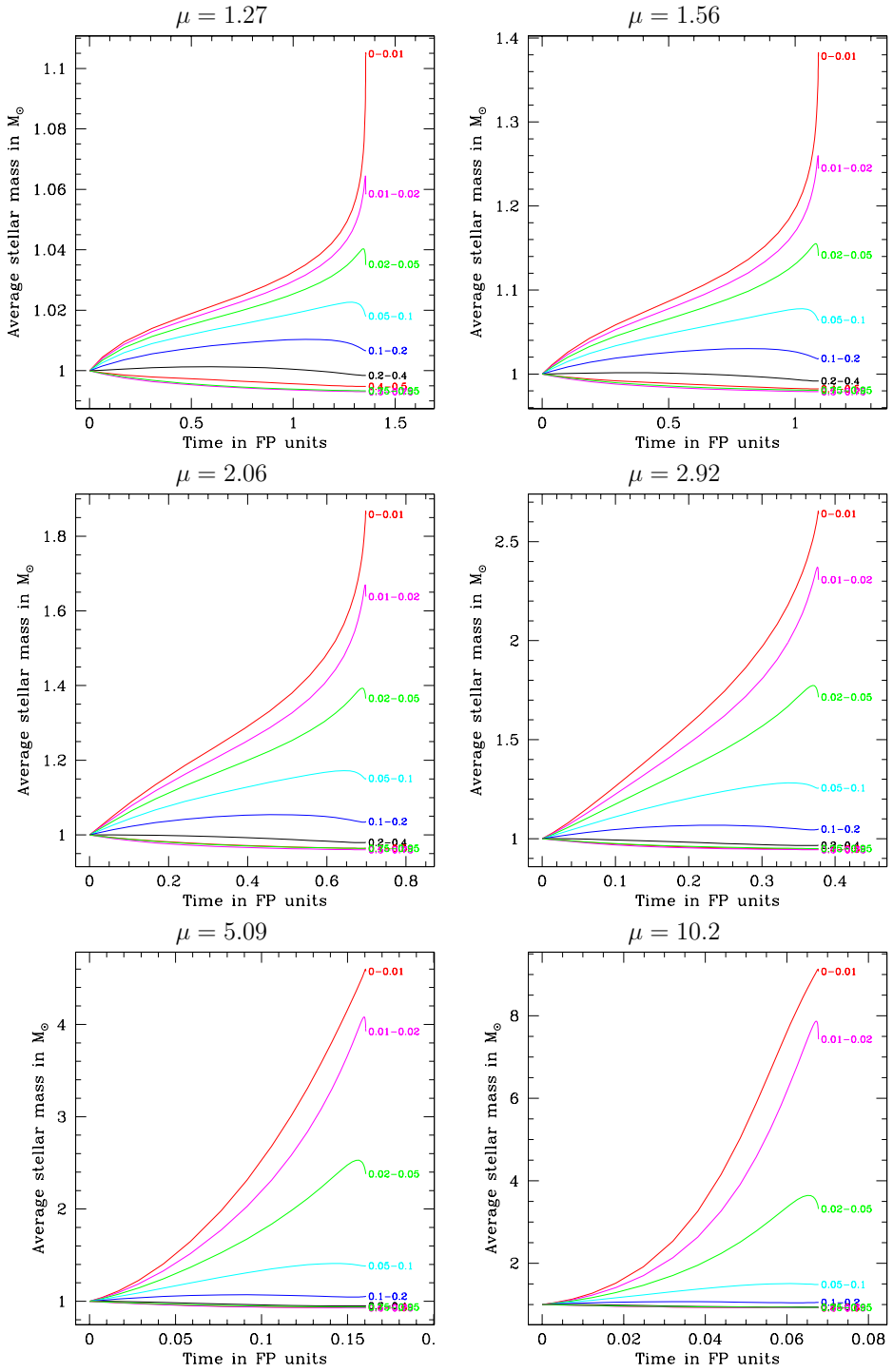


Fig. 6.7: Average Lagrangian radii shells for our models, equivalents to those of Fig. (6.6)

0.0022. On the other hand, the value of $\gamma$ is not so well defined and depends on the cluster's mass spectrum (Hénon, 1975). This means that potentially it is not the same for the different models. For a broader mass spectrum, $\gamma$ is about 0.01 and, unfortunately, in the case of having a small particle number, it will definitively make an important difference despite the "smoothing" effect of the logarithm, viz $\ln(\gamma \cdot \mathscr{N}_\star)/\mathscr{N}_\star = 0.0013$. Thus, in order to be able to compare the different models, one should consider $\gamma$ as a free parameter ranging between 0.01 to 0.2 and look for the best fit for the most of the cases. On the other hand, we must bear in mind that the *N*-body simulations of Khalisi (2002) do not go in deep core collapse and, so, the moment at which the core radius reaches a minimum is not the same as for our model. To sum up, we cannot really exactly say until which point we can compare, because the core collapse time will be different.

## 6.2 Clusters with a broader ($> 2$) mass spectrum *without* a BH

So as to be able to interpret observations of young stellar clusters extending to a larger number of mass components, it is of paramount relevance to understand the physics behind clusters without a central BH first. It has been shown that for a cluster with a realistic IMF, equipartition cannot be reached, for the most massive stars build a subsystem in the cluster's centre as the process of segregation goes on thanks to the kinetic energy transfer to the light mass components until the cluster undergoes core collapse (Spitzer, 1969; Inagaki and Wiyanto, 1984; Inagaki and Saslaw, 1985).
Whereas the case in which the BH ensconces itself at the centre of the host cluster is more attractive from the dynamical point of view, one should study, in a first step, more simple models.
In this section we want, thus, to go a step further and evaluate stellar clusters with a broad mass function (MF hereafter). We study those clusters for which the relaxation time is short enough, because this will lead the most massive stars to the centre of the system due to mass segregation before they have time to leave the main sequence (MS). In this scenario, we can consider that stellar evolution plays no role; stars did not have time to start evolving. The configuration is similar to that of Gürkan et al. (2004), but they employ a rather different approach based on a Monte Carlo code, using the ideas of Hénon (1973) that allows one to study various aspects of the stellar dynamics of a dense stellar cluster with our without a central MBH. Our scheme, although being less realistic than MC codes (and *N*-body ones) and unable, in its present version, to account for collision has the advantage, as already mentioned in fore-going sections, of being much faster to run, and providing data that has no numerical noise. It captures the essential features of the physical systems considered in our analysis.

### 6.2.1 Mass segregation in realistic clusters

One of the first questions we should dope out is up to how many components one should take into consideration when performing our calculations. Since the computational time becomes larger and larger when adding more and more components to the system, we should first find out what is a realistic number of components in our case. For this end we performed different computations with different number of stellar components.

For the simulations shown here, the initial cluster models are Plummer models with a Salpeter MF

$$\frac{dN_\star}{dM_\star} \propto M_\star^{-\alpha} \tag{6.10}$$

between 0.2 and 120 $M_\odot$. In this equation $\alpha$ takes $\alpha = 2.35$ (Salpeter). There is no initial mass segregation.

The discretisation of the mass components has been done as follows:

$$\log(M_{\rm comp}|_i) = \log(M_{\rm min}) + \log\left(\frac{M_{\rm max}}{M_{\rm min}}\right) \cdot \left(\frac{i}{N_{\rm comp+1}}\right)^{\delta} \tag{6.11}$$

In this equation $\delta$ is the discretisation exponent. If $\delta > 1$ we have more bins at low mass; for $\delta < 1$, we have more bins at high mass. I.e., $\delta$ allows one to put more discretised mass components at low masses ($\delta > 1$) or at high masses ($\delta < 1$), $\delta$=1 gives the logarithmical equal spacing. $M_{\rm max,\,min}$ are, respectively, the maximum and minimum individual stellar masses for the components. For all simulations the number of mass bins has been typically set to 15. We have chosen a Plummer model by default and the models have $10^6$ stars. The model radius by default is $R_{\rm Pl} = 1$ pc. The default initial mass function is a Salpeter.

In Fig. (6.8) we show the Lagrangian radii for ten different models and look for main dynamical characteristics of the system's behaviour, the core collapse time, the Lagrangian radii containing 90, 70, 50, 20, 10, 3, 1, 0.3, 0.1, $3\cdot10^{-2}$, $10^{-2}$, $3\cdot10^{-3}$ and $10^{-3}$ % of the stellar mass.

In this plot, $N_{\rm comp}$ stands for the mass spectrum different components number. For $N_{\rm comp} = 6$ we have performed three simulations varying the $\delta$ parameter between 1.0 (equal logarithmic spacing of components), 0.75 (more massive components) and 0.5 (even more). For $N_{\rm comp} = 12$ we have performed one only simulation (with $\delta = 1$, by default); for the $N_{\rm comp} = 20$ case we have repeated the same procedure as with six components, the last but one that we have chosen is $N_{\rm comp} = 20$ and, in this case, we studied two grid resolutions, $N_{\rm sh} = 200$ (the default value) and 400 grid points, in order to check whether this could influence the results (see chapter 2). To finish with, a big simulation with $N_{\rm comp} = 50$ was performed and included in the analysis. Whereas we can see an important difference between models of 6 and 12 components, we see that the global behaviour from 12 components onwards is very similar. Therefore, unless indicated, we choose 15 components in our study in this section, since a higher number would not contribute anything essential.

To see this in more detail, in Fig. (6.9) we show the Lagrangian radii for each stellar mass $m_i$ and the corresponding mass fraction $f_m$ for the 25 and 15 components simulations. Again, we cannot see any substantial difference between the 25 and 15 cases.

Taking the last arguments into account, we have done an analysis of mass segregation in multi-mass models with more than two stellar components without BH. In Figs. (6.10) and (6.11), we show in the evolution of a stellar cluster of 15 components (in colours); $m$ is the mass (in $M_\odot$) of the stars in each component and $f_m$ the corresponding fraction of the total mass. In the upper box we have the density profile, where the solid black line represents the total density; below, we have the average total mass for the system. We show different moments of the system. At $T = 0$ we have the initial model, which duly

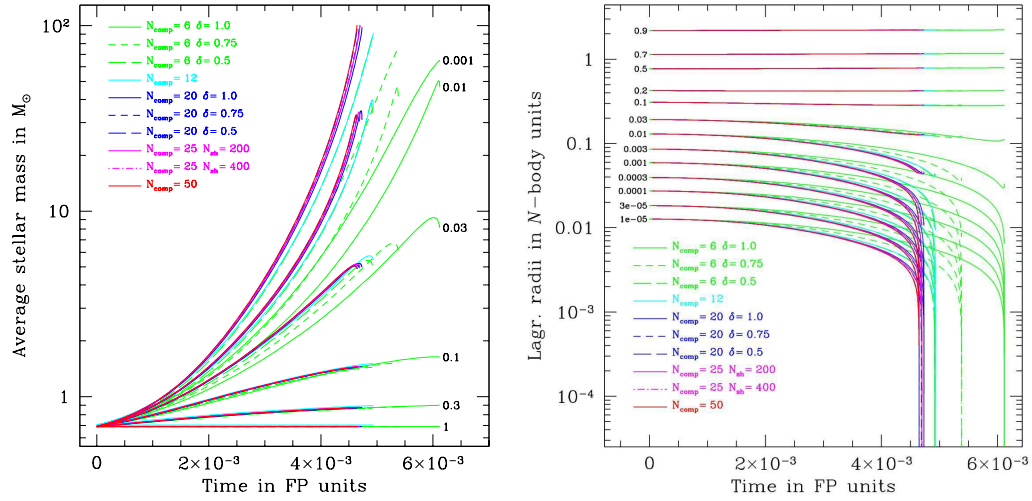


Fig. 6.8: Lagrangian radii and average stellar mass for 10 models with different mass spectrum (see text)

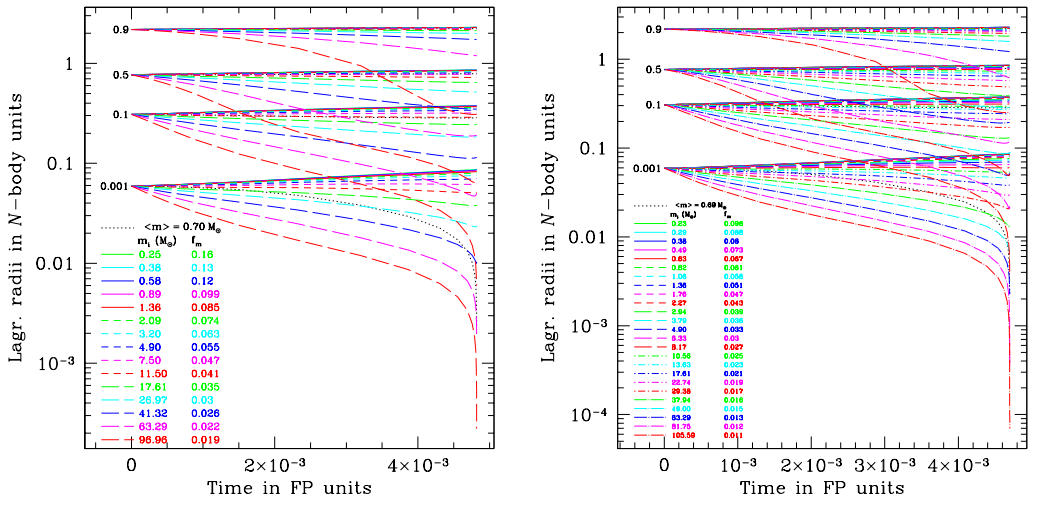


Fig. 6.9: Lagrangian radii for each stellar mass $m_i$ in the cases of 25 and 15 mass components

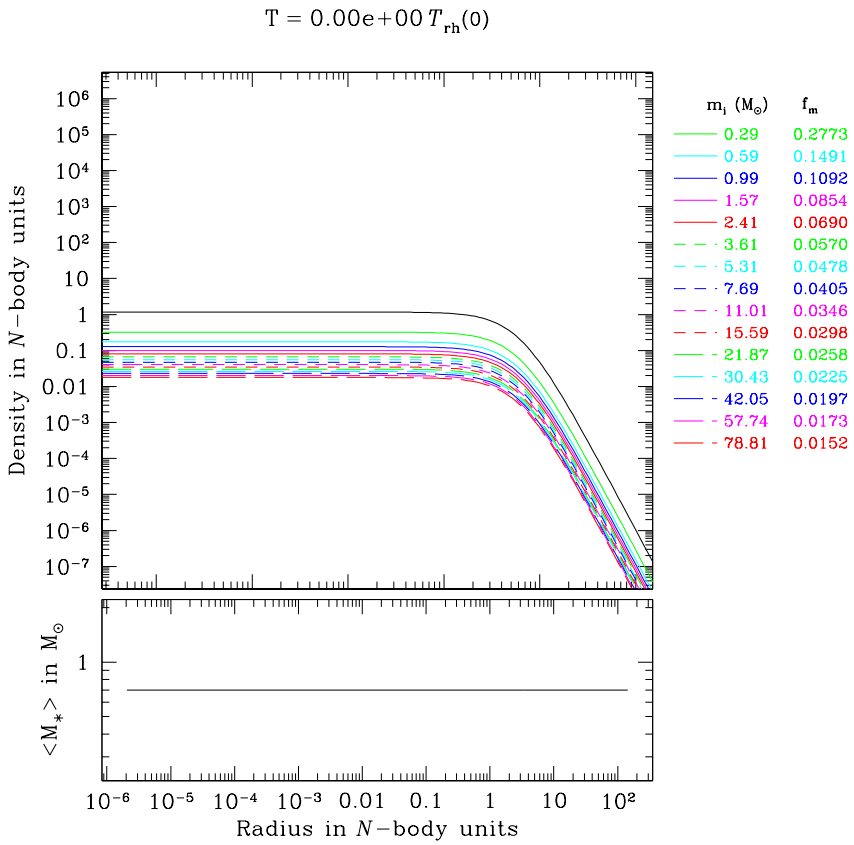


Fig. 6.10: Initial density profile for a stellar cluster with 15 components (upper panel) in $N$-body units and average total stellar mass in $M_\odot$ (lower panel)

shows no mass segregation. As time elapses, at $T = 5.30 \cdot 10^{-2}\, T_{\rm rh}(0)$, we observe how mass segregation has fragmented the initial configuration; the heavy components have sunken into the central regions of the stellar cluster and, thus, risen the mean average mass. The outer parts of the system start losing their heavy stars quickly and, consequently, their density profile retrogresses. This becomes more acute for later times at $T = 6.75 \cdot 10^{-2}\, T_{\rm rh}(0)$, as the right plots of Fig. (6.11) show. In these plots and, more markedly in the right panel of density profile, we can observe a depletion at intermediate radius.

### 6.2.2 Core-collapse evolution

Gürkan et al. (2004) shown that for a broad MF –which can be a Salpeter or a Kroupa–, mass segregation produces a core-collapse of the system that happens very fast. For clusters of moderate initial concentration, they find that this is in about 10 % of the $T_{\rm rh}(0)$, the initial half-mass relaxation time (i.e.

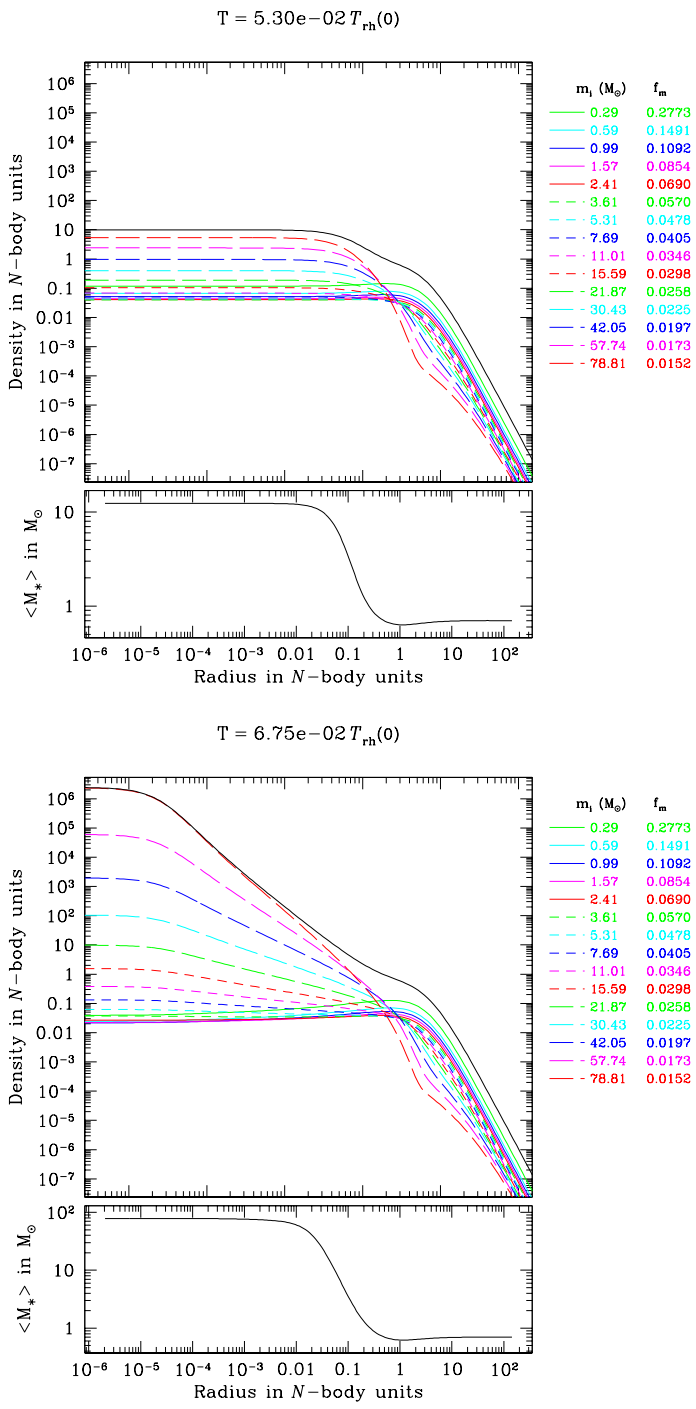


Fig. 6.11: Same situation as in Fig. (6.10) but at later times. See text for explanations.

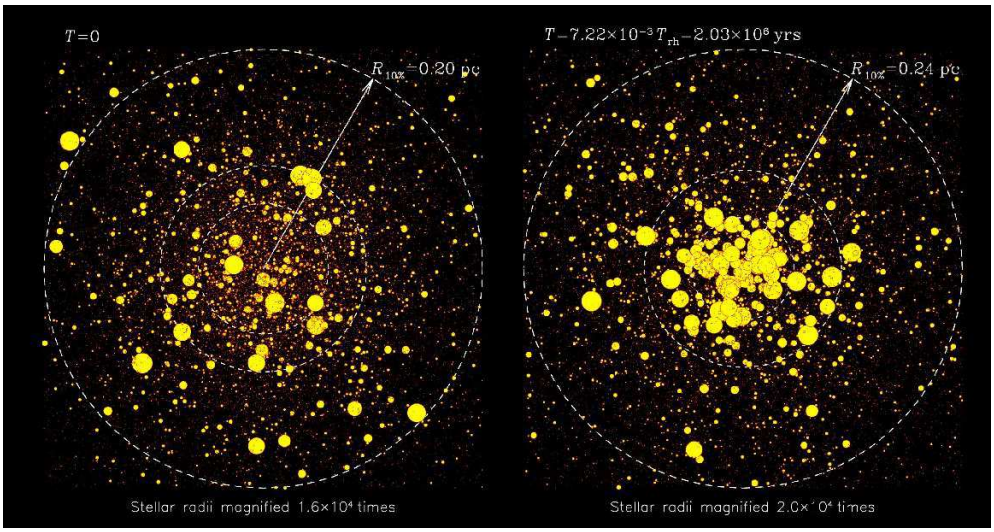


Fig. 6.12: Illustration of core-collapse in multi-mass systems treated with a Monte Carlo approach (courtesy of M. Freitag)

the half-relaxation time that the cluster had when time started, at $t = 0$). A good and clear illustration of this is Fig. (6.12) and Fig. (6.13). In the former one, on the left panel we have the initial configuration of the system. On the right one, we have the cluster at the moment of core-collapse. In the figure, all stars within a slice containing the centre has been depicted. On the other hand, this does not represent a real physical system, because all stars' radii have been magnified (see bottom of each panel). The dashed circles represent spheres containing 1, 3 and 10 % of the total cluster mass (from the centre). We can clearly see how the massive, large stars are segregated towards the centre. In Fig. (6.13), we show the core-collapse evolution of a multi-mass stellar cluster simulated with the gaseous model. As usual, $m$ is the mass (in $M_\odot$) of the stars in each component and $f_m$ the corresponding fraction of the total mass. On the left panel we display the time evolution of the central density for a model in which we have employed 15 individual mass components. The total density is given by the dotted line. On the right panel we have the evolution of the central velocity dispersions. The dotted black line shows the mass-averaged value

$$\bar{\sigma}^2 = \sqrt{\frac{\sum_{i=1}^{15} m_i\,\sigma_i^2}{\bar{m}}}. \tag{6.12}$$

$N$-body units are used for the $y$-axes.

One notes that, during core collapse, the central regions of the cluster become completely dominated by the most massive stars. But, contrary to the case of single-mass clusters, the central velocity dispersion *decreases* [2] (see Fig. 6.13).

[2] Priv. comm. M. Freitag

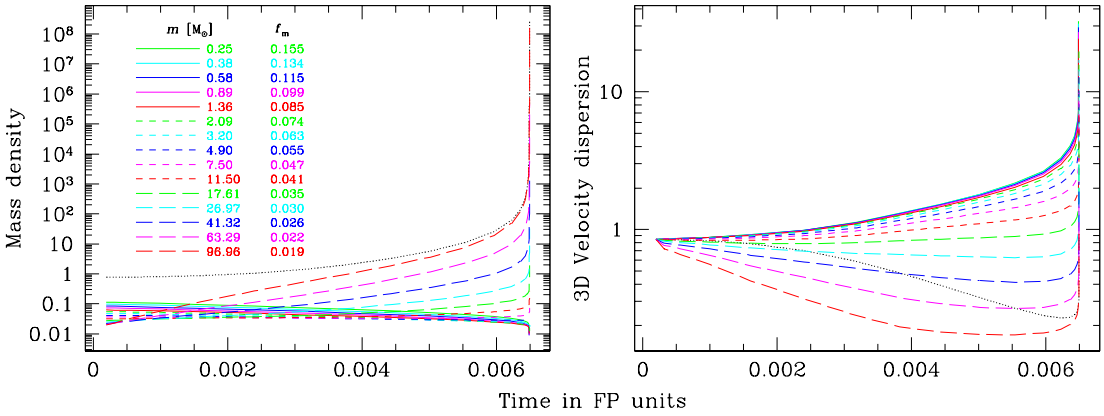


Fig. 6.13: Evolution of the central density and 3*D*-velocity dispersion in a model with 15 components (see text for further explanations)

## 6.3 Clusters with a broader mass spectrum *with* a BH

The logical next step to the systems studied in previous sections is that of a multi-mass component cluster harbouring a central seed BH that grows due to stellar accretion.
In this final section we extend our analysis to systems for which we use an evolved mass function of an age of about 10 Gyr. We consider a mass spectrum with stellar remnants. We employ a Kroupa IMF (Kroupa et al., 1993; Kroupa, 2001) with Mzams[3] from 0.1 to $120\,M_\odot$ with the turn-off mass of $1\,M_\odot$. We have chosen the following values for the exponent according to the mass interval,

$$\alpha = \begin{cases} 1.3, & 0.008 \leq m_\star/M_\odot < 0.5 \\ 2.2, & 0.5 \leq m_\star/M_\odot < 1 \\ 2.7, & 1 \leq m_\star/M_\odot \leq 120. \end{cases} \tag{6.13}$$

And with the following component's distribution,

- Main sequence stars of $0.1 - 1\,M_\odot$ ($\sim 7$ components)
- White dwarves of $\sim 0.6\,M_\odot$ (1 component)
- Neutron stars of $\sim 1.4\,M_\odot$ (1 component)
- Stellar black holes of $\sim 10 M_\odot$ (1 component)

The defined IMF evolves and gives us at later times an evolved populations with compact remnants. This means that main sequence stars can transform into white dwarves, neutron stars or stellar black holes according to their masses. If $m_{\rm MS}$ is the mass of a MS star, we have defined the following mass ranges for the evolution into compact remnants:

[3]The zero age main sequence (ZAMS) corresponds to the position of stars in the Hertzsprung-Russell diagram where stars begin hydrogen fusion.

**White dwarves** in the range of $1 \leq m_{\rm MS}/{\rm M}_{\odot} < 8$

**Neutron stars** for masses $8 \leq m_{\rm MS}/{\rm M}_{\odot} < 30$

**Stellar black holes** for bigger masses, $\geq 30{\rm M}_{\odot}$

As we already mentioned, we put at the centre a seed BH whose initial mass is of $50\,{\rm M}_{\odot}$. The initial model for the cluster is a Plummer sphere with a Plummer radius $R_{\rm Pl} = 1$ pc. The total number of stars in the system is $\mathscr{N}_{\rm cl} = 10^6$.

The presence of a small fraction of stellar remnants may greatly affect the evolution of the cluster and growth of the BH because they segregate to the centre from which they expel MS stars but, being compact cannot be tidally disrupted. This kind of evolution is shown in Figs. (6.14) and (6.15).

Fig. (6.14) shows us the time evolution of different Lagrange radii with $0.1, 10, 50, 80\,\%$ of the mass of each component. Here the core collapse happens at about $T = 0.18\,T_{\rm rh}(0)$. The henceforth re-opening out is due BH accretion.

In Fig. (6.15), we plot the density profiles of the system before and after the post-collapse phase. We can see that the slope of $\rho \propto R^{-7/4}$ on account of the cusp of stellar BHs that has formed around the central BH. We can see how the different components redistribute in the process. We can see how the BH dominates the dynamics at the centre.

We can study how the system evolves from the point of view of the distribution of kinetic energies between the different components of the clusters during the process of mass segregation.

In Fig. (6.16) we show the evolution of the "temperature" of the system, defined as the mean kinetic energy per star divided by the global mean mass (in order to have a "temperature" expressed in square velocity units).

In this plot we show the core collapse situation corresponding to Figs. (6.14) and (6.15): We consider a 10 component cluster with the characteristics explained before. The mean temperature is defined like $\sum n_{\rm i} \cdot T_{\rm i} / \sum n_i$, where $n_{\rm i}$ is the numerical local density for component i. This corresponds to the mean kinetic energy per star. We can see in the plot that it is about the same as the heaviest component in the inner regions, even though one could think that segregation should not have set in in the beginning. This is due to the fact that the moment does not correspond to exactly the initial moment, $T = 0$. On the right, we can already see how the mean central temperature moves back (solid black line) and the most massive component (dashed red line) increases. For later times, the kinetic energies of the different components rise at the inner part of the cluster and the most massive one approaches the sum of all of them. This is even more evident in the last plot, where all components' temperatures have sunken except for the corresponding to the most massive one. At the exterior zones, the mean temperature is much lower than the most heavy component because the system did not have evolution towards equipartition and, so, the velocity dispersion $\sigma_{\rm v}$ of the heavy components is the same that the other's component velocity dispersion but their kinetic energy is much larger (in terms of mass).

At the current moment we are tackling with these and another configurations, but we have to first resolve the problem of BH growth and grid resolution, because as the BH grows, the grid gets too close to the centre. This problem is being now studied to carry on with new calculations from the cluster re-expansion onwards caused by the BH growth.

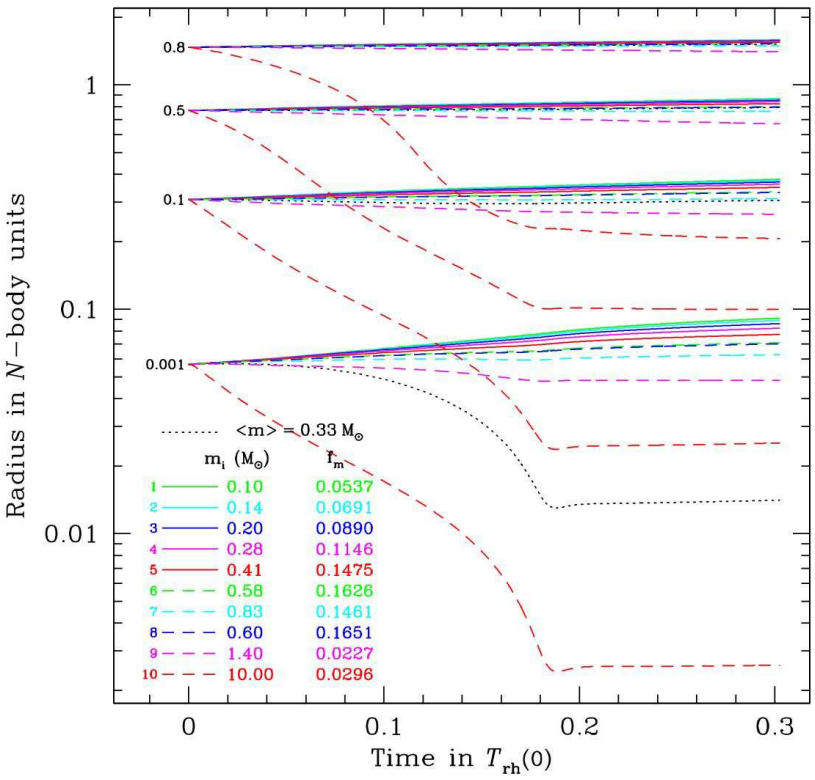


Fig. 6.14: Lagrange radii evolution for a 10 components calculation with a seed BH and stellar remnants

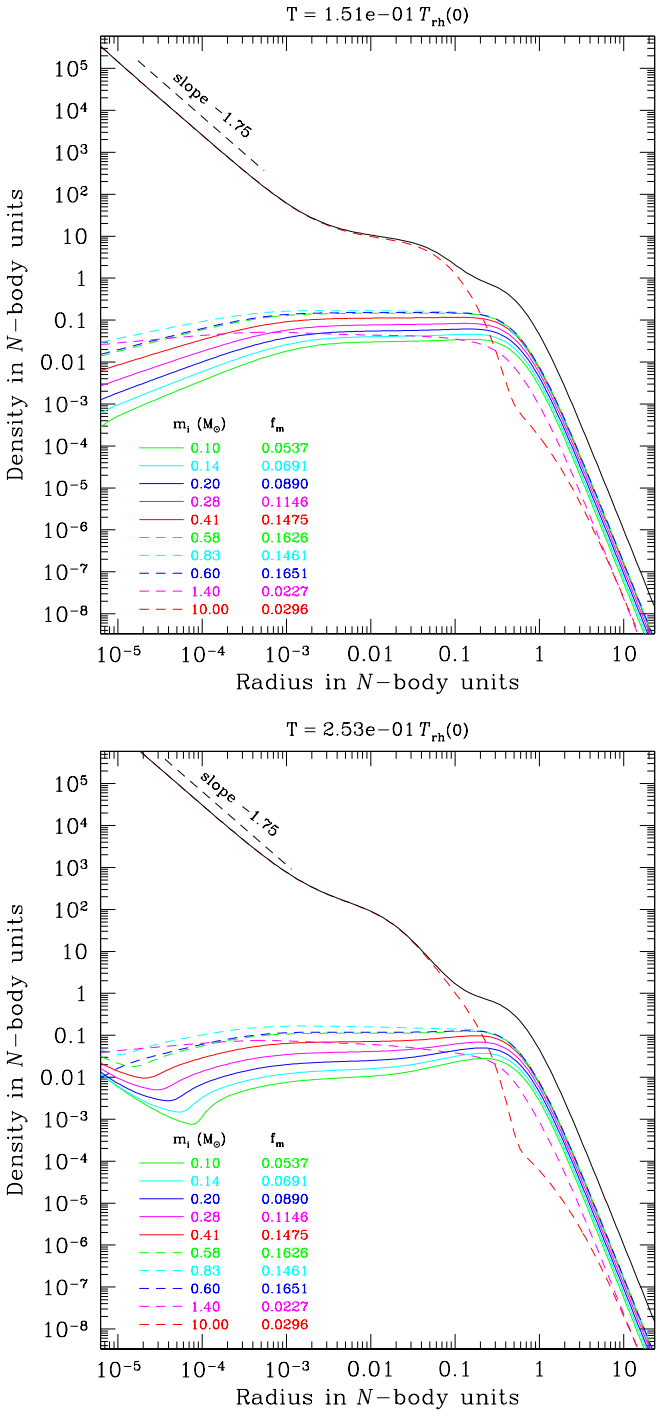


Fig. 6.15: Density profiles in a multi-mass system with seed BH before and after core-collapse (see text)

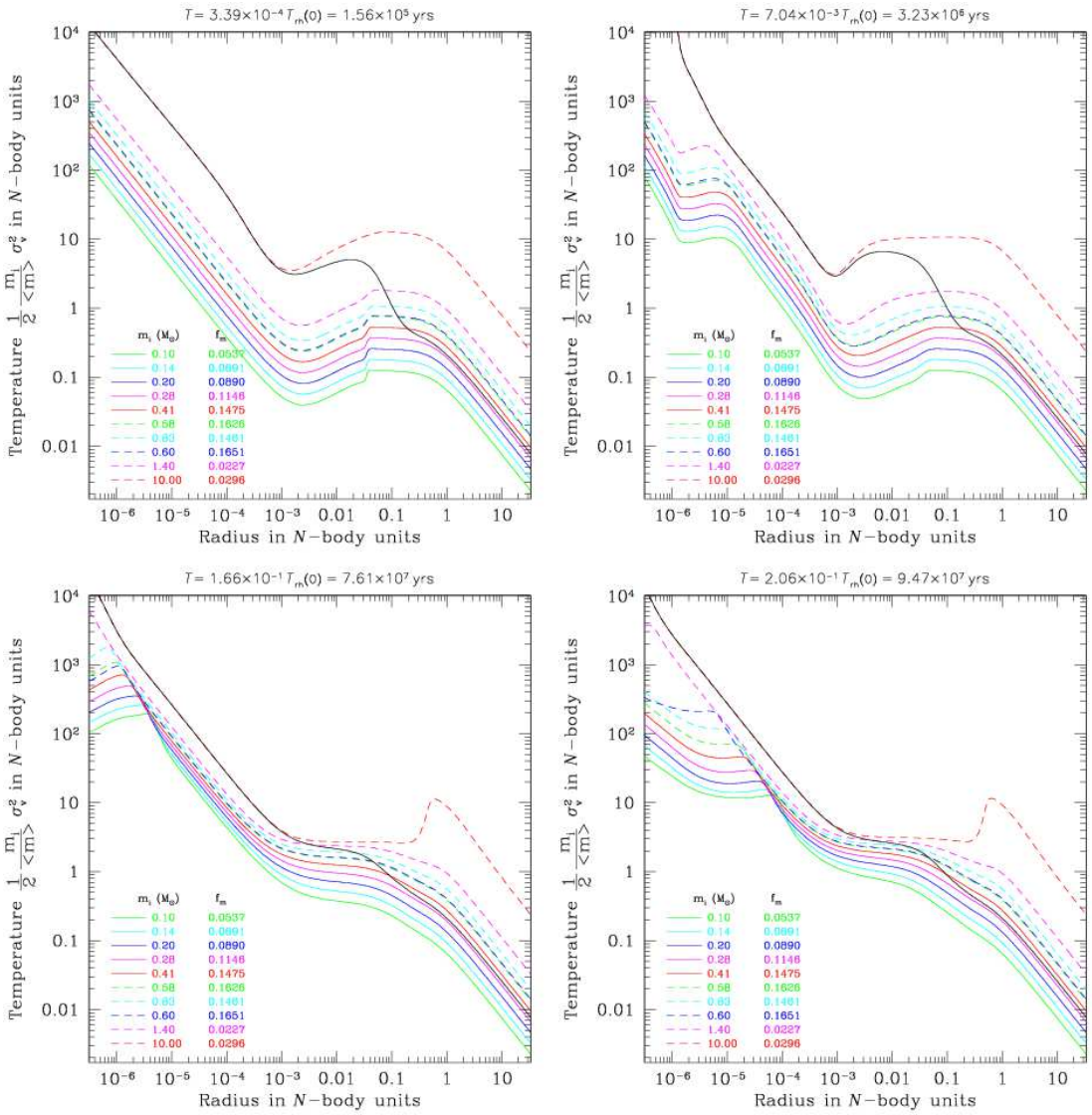


Fig. 6.16: Different moments in the evolution of the cluster's temperature for a 10 stellar components system with a seed BH

## 6.4 Literature of chapter 6

Amaro-Seoane, P. and Spurzem (2003). The anisotropic gaseous model 'Spedi' : A tool to study the formation and growth of black holes in galactic nuclei. *In "The formation and early evolution of galaxies", workshop held in Irsee, Germany,* [4].

Cohn, H. (1980). Late core collapse in star clusters and the gravothermal instability. *ApJ*, 242:765–771.

Drukier, G. A., Cohn, H. N., Lugger, P. M., and Yong, H. (1999). Anisotropic fokker-planck models for the evolution of globular star clusters: The core-halo connection. *ApJ*, 518:233–245.

Elson, R., Hut, P., and Inagaki, S. (1987). Dynamical evolution of globular clusters. *araa*, 25:565–601.

Gürkan, M. A., Freitag, M., and Rasio, F. A. (2004). Formation of Massive Black Holes in Dense Star Clusters. I. Mass Segregation and Core Collapse. *apj*, 604:632–652.

Giersz, M. and Heggie, D. C. (1994). Statistics of n-body simulations - part two - equal masses after core collapse. *MNRAS*, 270:298.

Giersz, M. and Heggie, D. C. (1996). Statistics of *n*-body simulations - III. unequal masses. *MNRAS*, 279:1037–1056.

Hénon, M. (1973). Collisional dynamics of spherical stellar systems. In Martinet, L. and Mayor, M., editors, *Dynamical structure and evolution of stellar systems, Lectures of the 3rd Advanced Course of the Swiss Society for Astronomy and Astrophysics (SSAA)*, pages 183–260.

Hénon, M. (1975). Two recent developments concerning the monte carlo method. In Hayli, A., editor, *IAU Symp. 69: Dynamics of Stellar Systems*, page 133.

Hillenbrand, L. A. and Hartmann, L. W. (1998). A Preliminary Study of the Orion Nebula Cluster Structure and Dynamics. *apj*, 492:540.

Inagaki, S. and Saslaw, W. C. (1985). Equipartition in multicomponent gravitational systems. *ApJ*, 292:339–347.

Inagaki, S. and Wiyanto, P. (1984). On equipartition of kinetic energies in two-component star clusters. *PASJ*, 36:391–402.

Joshi, K. J., Rasio, F. A., and Portegies Zwart, S. (2000). Monte carlo simulations of globular cluster evolution. i. method and test calculations. *ApJ*, 540:969–982.

Khalisi, E. (2002). Equipartition and mass segregation: Simulations of star clusters with two-mass components. *Doctoral dissertation. Ruperto-Carola University of Heidelberg, Germany* [5], 349.

Kim, S. S., Lee, H. M., and Goodman, J. (1998). Two-Component Fokker-Planck Models for the Evolution of Isolated Globular Clusters. *apj*, 495:786.

Kroupa, P. (2001). On the variation of the initial mass function. *mnras*, 322:231–246.

Kroupa, P., Tout, C. A., and Gilmore, G. (1993). The distribution of low-mass stars in the Galactic disc. *mnras*, 262:545–587.

Lightman, A. P. and Fall, S. M. (1978). An approximate theory for the core collapse of two-component gravitating systems. *apj*, 221:567–579.

Makino, J. (1996). Postcollapse evolution of globular clusters. *ApJ*, 471:796.

Marchant, A. B. and Shapiro, S. L. (1980). Star clusters containing massive, central black holes. III - evolution calculations. *ApJ*, 239:685–704.

McCaughrean, M. J. and Stauffer, J. R. (1994). High resolution near-infrared imaging of the trapezium: A stellar census. *AJ*, 108:1382–1397.

[4] Available at `http://www.mpia-hd.mpg.de/GALAXIES/CADIS/irsee2003/PROCEEDINGS/Amaro-Seoane.pdf`

[5] Idem `http://www.ub.uni-heidelberg.de/archiv/3096`

Portegies Zwart, S. F. and McMillan, S. L. W. (2000). Black Hole Mergers in the Universe. *apjl*, 528:L17–L20.

Quinlan, G. D. (1996). The time-scale for core collapse in spherical star clusters. *New Astronomy*, 1:255–270.

Raboud, D. and Mermilliod, J.-C. (1998). Evolution of mass segregation in open clusters: some observational evidences. *aa*, 333:897–909.

Spitzer, L. and Shull, J. M. (1975). Random gravitational encounters and the evolution of spherical systems. VI - plummer's model. *ApJ*, 200:339–342.

Spitzer, L. J. (1969). Equipartition and the formation of compact nuclei in spherical stellar systems. *ApJ Lett.*, 158:139.

Spitzer, L. J. and Hart, M. H. (1971). Random gravitational encounters and the evolution of spherical systems. II. models. *ApJ*, 166:483.

Spurzem, R. and Aarseth, S. J. (1996). Direct collisional simulation of 100000 particles past core collapse. *MNRAS*, 282:19.

Stodołkiewicz, J. S. (1982). Dynamical evolution of globular clusters. i. *Acta Astron.*, 32:63–91.

Takahashi, K. (1993). A new powerful method for solving the orbit-averaged fokker-planck equation regarding stellar dynamics. *PASJ*, 45:233–242.

Takahashi, K. (1995). Fokker-planck models of star clusters with anisotropic velocity distributions i. pre-collapse evolution. *PASJ*, 47:561–573.

Watters, W. A., Joshi, K. J., and Rasio, F. A. (2000). Thermal and dynamical equilibrium in two-component star clusters. *ApJ*, 539:331–341.

# Agraïments, Danksagung

Heidelberg is a little city in the south of Germany. It has a nice old bridge, a romantic castle, a very concurred old town and -I was told- a couple of native inhabitants. I spent in this city about five years of my life, and I daresay they were the most intesive ones. A lot of things happened. “For instance”, I got to know Sabine after one and a half weeks of my arrival. Very soon we started *the* relationship that would conduct us in a inavoidably retoric way to marriage.
If somebody asked me to tell the first thing that comes to my mind when I think about these years, I would answer the following...

> sabine bridge potatoes kitchen Schwalbe Jorge Mayer Ärger fill de sa mare Francine Vienna bridge cold cold cold cold mountains sauerkraut Frank Wixenpa’aslocas wine Oberseminar hin und her fahren Wien cold cold cold Hauptstraße Emil potato Mike Deiters 4| [|n4 g3nd m3$ r4r374 Teeminar teaminar teminable @Weberstraße 13 Sant Petersburg Masha Sergei Russian Russian Mahos Tilemahos Vienna Sabine Gerhabt-Hauptmann Straße Mutter Umzug moving moving CRACK oh my goodness that was my back Basel Alfonso shop buy smoke Dante Inferno work work woman in pink tracksuit yellow umbrella Nickel Nickel what for und viele iuius for a long while escape go back to Spain and walk walk walk in the night Danzigerstraße John Lucie tinto Sabine is back al·leluia per què peta borinot turbi (A) anxious -xit anxiety dean- and uprooting syndrome quatsch better cold dark night Vienna Russian Sprachlabor Marc Russian Silke Eva Marion work work Marc wark Mork Russian workian Freitag Blödsinn in der Küche paper light see end pictures marriage vacherin gluant Marc’s supermongo subroutines again Dante Inferno but smoothed end

This section cannot be short at all because I am in hock to a lot of people. I cannot help feeling very grateful to them and they deserve it. On the other hand, being a social animal, as only a genetically galician but in València born person can be, it would be a crass error and an unpardonable insult not to talk about the friends I made during these years.

First of all, I would like to thank here my advisor, **Rainer Spurzem**, for giving me the opportunity of coming to Germany to do a Ph.D. He encouraged me always when things were not working as they should (a bad habit of the process of becoming a doctor, according to a lot of people). He and **Andreas Just** treated me as if I had been in the group for years from the very beginning.

The French-speaking commonwealth, **Marc Freitag** and **Francine Leeuwin**, carried out a very important role during these years... I daresay Marc is responsible for me becoming a scientist, if you happen

to have any complaint, please refer to him. They gave me also something much more valuable than their help, namely their friendship. I am very grateful to both of them for a lot of things... Francine, for instance, introduced me into the wonderful world of french spirits (I am *not* talking about the agent or subject of vital and spiritual functions, whether spiritual or material). It helped a lot to survive the absolutely sun-less winter evenings of Heidelberg after a long full working day. I got to know Marc when he visited our group in Heidelberg in March 2001. I felt as if we had been friends since always from the very first beer at the Markt Stübel (a place which we haunted later). When he moved to Heidelberg we became inseparable and even neighbours. Among innumerable things, Marc made me rediscover Édika in his full splendour. It would not be an exaggeration at all to say that both of them, Marc and Francine, have become a part of my family (in its full southern meaning).

Elaborating on nice people, I have to mention here two very nice aussies, Bruce and Sheila... I mean **John** and **Lucie Benz** (née Chapman), who made me feel "at home" from the very beginning. Everything began with a red wine, carried on with tinto and jamón (pata negra, of course) and finished with two marriages, theirs (on next Saturday, by the way) and mine.

As regards the *Kersche* community, it is a must to say how nice it was for me to share a place in the Kirchheim community with our fellow-beings **Eva**, **Marion**, **Silke** and -inevitably- Marc. The iberians would not be happy if I forgot them here and so I have to address a few words to my two favourite tableland people, **Jorge Peñarrubia**, *el Doctor Xungalín*, compañero infatigable de diversas peripecias acontecidas en el consuetudinario devenir, por no llamarlo divagar, del instituto (léase cocina, broncas diversas con el aparato administrativo ariense, puerta corrediza y un sinfín más de cosas) and el lobo mesetario **David López** and parienta, **Elise Schieck**, for his spirituous southern chocolate, republican ideas and swedish food. And here I cannot -I must not- forget **Pablo González**, *Polito*, den entspanntesten Canario der Welt, for his natural sedateness, papas arrugadas con mojo rojo (y verde) and ron canario.

Respect to the ARI people, **Gernot Burkhardt**'s predisposition to make any kind of favour I asked for nicely surprised me everytime. He supported us, Jorge and me, in our little "domestic" conflicts at the Institute and was always very friendly to us. Somebody like he can make you see things in a different way when you start as a newbie and have to confront difficulties and people who are not as nice as he is. **Christoph Eichhorn**, **Kristin Warnick**, **Chingis Omarov**, **Toshio Tsuchiya**, **Eliani Ardi**, **Ikbal Aryfanto**, **José Fiestas**, **Emil Khalisi**, **Michael Fellhauer**, **Stefan Deiters**, **Andreas Ernst**, **Patrick Glaschke**, **Pavel Kroupa** and **Christian Boily** were very cordial and amiable to me during my stay at ARI.

**Ernst Pendl**, *Eanstl*, bin i dångba fia dem Våda sei Dochda Sabine und seine Begeisterung für Astronomie. Im Kosmos umanaundstrawanzn... per aspera ad astra. – Heast! geh gibtsn des å, Spania de wos Weanerisch kennan! But yes, there are, and I am one. Då håb i eams einegsåt, net!

Ich weiß **Christine** ob der nach einer Woche meines Daseins in Deutschland geschlossenen Bekanntschaft zu ihrer Nachfahrin sehr zu schätzen.

**Margaret Mehls**, *Margarita* war immer äußerst liebenswürdig zu mir in der Weberstraße 13 (Aussenstelle vom ARI). Es macht einen riesengroßen Unterschied, ob deine "Nachbarn" (eigentlich Mitbewohner, nachdem ich fast den ganzen Tag hier bin) nett sind oder nicht. In ihrem Falle (und in dem von Herrn Mehls, selbstredend) sollte man eigentlich eher über Herzlichkeit als Nettigkeit reden.

**Matt Bonner** em va ajudar amb l'Anglès de la petita introducció que vaig fer, car se'm feia molt envitricollat de traduir l'Homer i les meues paraules a la seua vernacla saxona. Ell, habituat com està a

traduir coses al Català per a `Debian`, ho féu en un tres i no-res i, el millor, perquè sí, sense conèixer-me de quasi res, només del fòrum de traducció. Amb persones com *Mateu Bonet* (com a ell li agrada que li diguen), hom pot creure que es pot recuperar les esperances. No vaig gosar de demanar ningú de Micro$oft. Sóc optimista, però no tant.

Going back a bit in history, just over a couple of years, when I was studying at the Universty of València, **Vicent Martínez Sancho** played a decisive role in a lot a different aspects of my education. He not only managed to unfailingly wake up in all his students an enthusiastic interest for the subjects he teaches, but also won our trust and affection. Besides Physics, he taught us how to tackle with life, which is a much more difficult subject. Putting it into his words, "Ésser dotat per a les matemàtiques no té cap mèrit. Car mèrit ve de meritum, del participi de merere 'merèixer'. És això, una qualitat natural... Com el beneit del cabàs del meu poble, que fa trucs molt enginyosos amb un palet. El que faces amb la teua vida, com l'enfoques i quin tipus d'ésser humà esdevingues, això sí que *mereix*". His concern and attentiveness for culture (understood in all its broad meaning) influenced, *influences*, me until now.

Cuando, en los últimos días de la redacción de la tesis, me puse a repasar estas páginas, me di cuenta de que el nombre de mi madre no aparecía en ninguna de ellas. ¿Me había olvidado de ella? ¡¿ De mi madre?! No era posible. En ese momento, en que estaba pensando (contecimiento extraordinario), me di cuenta de que había sido porque para mí es tan evidente todo lo que le debo -que es, eso, todo- y lo mucho que la quiero -que es un muchísimo mucheante mucheado- que, de hecho, el nombre, no es importante. Lo que sí es importante es todo lo que ella me ha aportado y aporta en la vida. Gracias, ***Luisa***.

Über Dich brauche ich wenig zu sagen, **Sabine**, denn es ist nicht nur für mich, sondern für alle klar, wie sehr ich Dich liebe. Wir haben ein ganzes Leben vor uns, das gerade anfängt.

3́$ gl4̀ g'4$í g4l 3$m3nd4̀ 3l n0m d3l($) $4ny0($) **Els Etsus**: 3rr|gu|, 3rm|[| | 3rb3r3 d'b4n|4 b3r d0d 3r g0n r0dll1 g4'n$ h4m b1rd4d 4gu3$d$ 4ny$.

G0n d|-D-4rl!!! ----1 (sorry for that, but it was *also* a must).

**Buuu**$_{\mathbf{auuf}}$ I think this is really the end. I do not know what else I could tell you, after 161 pages of wanton hullabaloo... Now it is time to have a carajillo... Let me pythonise it...


This work was written with LaTeX (what else?) and processed with a Debian Sid– based system, VINDOBONA